GEOLOGIC, VEGETATIVE AND CLIMATIC CONTROLS ON COUPLED HYDROLOGIC PROCESSES IN A COMPLEX RIVER BASIN: LESSONS LEARNED FROM A FULLY INTEGRATED HYDROLOGIC MODEL

By

VIBHAVA SRIVASTAVA

A DISSERTATION PRESENTED TO THE GRADUATE SCHOOL
OF THE UNIVERSITY OF FLORIDA IN PARTIAL FULFILLMENT
OF THE REQUIREMENTS FOR THE DEGREE OF
DOCTOR OF PHILOSOPHY

UNIVERSITY OF FLORIDA

2013

To my family

ACKNOWLEDGEMENTS

First and foremost I would like to thank GOD for everything that led to the fulfillment of all that a student can desire – passion for research, a knowledgeable nice and perfect advisor, supportive family and friends. It has been a long journey during which I learnt valuable life lessons on perseverance, passion, and people. I am lucky to have Dr. Wendy Graham as my Doctoral research advisor. I don't know if I can thank her enough for her patience, advice, and time amongst many other things. She taught me three most valuable lessons that I will live with for the rest of my life. First, work on things that you feel passionate about. Second, never give up. Third, you need love and support of all the people in your personal and professional life to succeed. Dr. Graham Thanks for everything!

I am grateful to the members of my graduate committee Dr. Rafael Munoz Carpena, Dr. Jonathan Martin, Dr. Matthew Cohen, Dr. Michael Annable, and Dr. Reed Maxwell for their valuable time and interest in completing this research. Their timely advice and input helped to improve the quality of this research. Special thanks to Dr. Carpena for inspiring new ideas and never letting me settle for less.

I don't have enough words to express gratitude towards my parents, Vivekanand and Sarita, and my sister Smita. If it was not for their encouragement and support I would have never made it to the United States. Their love and blessings kept me going when things got tough during my stay in the USA.

I am lucky to have a friend in my wife, Richa, who has been there for me throughout my research. She inspires me with her sincerity and passion towards her work and with her perseverance. I am grateful to her for being there, listening to me when I got frustrated, cheering me up in bad times, praying for me when I struggled,

and for unconditionally loving me. My love and hugs to my son Parth whose smiles gave me endurance to take on all the challenges of the past three years.

I am grateful to my Water Institute Family, Kathleen, Lisette, SyeWoon, Rob, Mary, Jason, and Wes for all the moral support and love that they have extended to me. Big thanks to Kathleen for working tirelessly to collect and manage all the data needed for my research.

During my student life, I met several awesome people. Many have since become good friends and are an integral part of my life. I extend my gratitude to Sumit Sen and Madhukar Varshney who have been like elder brothers to me. Thanks for your patience and advice during our long phone conversations. Thanks to Shailey for your words of encouragement and for being there for me and my family when we needed you. Thanks to Purushottum for standing by me during the most difficult days of my life. Thanks to Rob deRooij for accompanying me on countless coffee breaks and long discussions on personal and professional issues.

At last I would like to thanks everyone who I have not mentioned above and who have been helpful to me during my time at the University of Florida.

TABLE OF CONTENTS

Page

LIST OF TABLES

LIST OF FIGURES

Abstract of Dissertation Presented to the Graduate School
of the University of Florida in Partial Fulfillment of the
Requirements for the Degree of Doctor of Philosophy

GEOLOGIC, VEGETATIVE AND CLIMATIC CONTROLS ON COUPLED HYDROLOGIC PROCESSES IN A COMPLEX RIVER BASIN: LESSONS LEARNED FROM A FULLY INTEGRATED HYDROLOGIC MODEL

By

Vibhava Srivastava

August 2013

Chair: Wendy D. Graham
Major: Agricultural and Biological Engineering

This dissertation documents the first implementation of an integrated transient 3D surface water-groundwater-land surface process model, ParFlow.CLM, to evaluate the interacting geologic, climatic and vegetative controls on water budget components and streamflow generation processes over the Santa Fe River Basin in North Central Florida. Model predictions indicate that evapotranspiration (ET) is the most important water balance component in the basin comprising 77% of rainfall. Geologic conditions and vegetative properties were found to exert primary control on the spatial variability of streamflow generation processes in the basin through their influence on the balance between rainfall, ET, runoff and infiltration processes. Climatic variability was found to provide primary control on the temporal variability of streamflow generation processes.

Model predictions indicate that in the upper basin more than 95% of streamflow is generated by recent near-stream rainfall. In contrast, in the lower basin the majority of streamflow is contributed by the Upper Floridan Aquifer, with the fraction of subsurface flow averaging approximately 77% at the outlet of basin. A global sensitivity analysis of

the model revealed that the permeability of the Intermediate Aquifer System is the most influential factor driving hydrologic response throughout the SFRB.

Particle tracking experiments predicted that the median age of streamflow in the upper basin ranges from approximately 1 day at the peak of storm hydrographs to approximately 7 days at the end of stormflow recession, with travel time distributions that vary over time but are generally well-fit with log-normal distributions at the peak of the storm hydrograph. The median age of subsurface contributions to streamflow in the lower portion of the basin was predicted to be approximately 17 years, and the travel time distribution for the subsurface contribution is well-fit by a gamma distribution showing fractal properties that do not vary significantly over time. The fraction of new stormwater versus old groundwater in the streamflow in the unconfined region, and thus the shape of the total streamflow travel time distribution, varies as a function antecedent conditions, storm magnitude, time during the storm, and assumptions regarding the contrast in hydraulic conductivity between high permeability zones and the porous matrix.

CHAPTER 1
INTRODUCTION

Increased pressure on water resources, due to expanding urban areas and a growing population, has raised the concern about the sustainability of water resources and the proper functioning of ecosystems dependent on these resources. This has increased the demand for robust predictive tools that can help water managers and policy makers with current and future water management decisions in large basins which are comprised of a complex mix of natural and urban environments.

All hydrological systems consists of three major flow domains namely, the atmosphere, the surface and the subsurface which are interconnected with continuous exchange of water between them (Furman, 2008). However, due to disparity in temporal and spatial scales associated with the flow processes within each domain the three domains are commonly modeled as separate entities. As such modeling is focused on one flow domain and the remaining two domains are simplified and applied as boundary conditions, resulting in incomplete representation of actual physical processes by the models (Furman, 2008).

Hydrological processes such as runoff, subsurface flow (both saturated and unsaturated), and evapotranspiration losses co-vary in space and time (Huntington and Niswonger, 2012). Therefore, it is imperative to use hydrological models which facilitate integration of all hydrological processes when modeling objectives are geared towards exploring their behavior and interactions at various space and time scales under varying physical settings as well as possible future land-use, water-use and climatic conditions. (e.g. Huntington and Niswonger, 2012; Bolger et al., 2011; Goderniaux et al., 2009).

Although the first blueprint for an integrated hydrologic model was outlined in the year 1969 (Freeze and Harlan, 1969), it was not until recently that significant advances were made towards the development of sophisticated, robust hydrological models that exploit advanced parallel computational capabilities and represent the surface-subsurface-near land surface hydrologic processes in a seamlessly integrated and physically plausible manner (e.g. ParFlow (Ashby and Falgout, 1996; Kollet and Maxwell, 2008a; Kollet and Maxwell, 2006), InHm (VanderKwaak, 1999), MODHMS (Panday and Huyakorn, 2004), HydroGeoSphere (Therrien et al., 2010)). Past applications of these fully integrated models have been mostly limited to studying controls over rainfall-runoff generation for hillslopes or small catchments (area ~ 10^0 - 10^1 km^2 e.g. Jones et al., 2006). A few applications of these fully integrated models have involved simulation of hydrologic behavior of medium to large scale watersheds (area ~ 10^2 km^2 e.g. Kollet and Maxwell, 2008; Bolger et al., 2011; Ferguson and Maxwell, 2010). Modeling studies explicitly simulating evapotranspiration or land surface processes in the modeling framework have rarely been reported (e.g. Kollet and Maxwell, 2008; Li et al., 2008; Goderniaux et al., 2009).

The application of fully integrated models to understand surface-groundwater interactions and controls over river water source mixing dynamics in large river basins is still in its infancy. Although there have been studies on integrated model applications to understand surface-groundwater dynamics in idealized test cases (e.g. Frei et al., 2009), applications over real large basins are rare (e.g. Huntington and Niswonger, 2012; Werner et al., 2006). Huntington and Niswonger (2012) used the GSFLOW model to understand the linkage between snowmelt timing and surface water – groundwater

interactions in a 54 km^2 watershed at eastern Sierra Nevada. Werner et al. (2006) used MODHMS to identify river reaches receiving groundwater influx and spatio-temporal characteristics of groundwater-surface flow dynamics in the ~420 km^2 Pioneer Valley, Australia. There remains a need for studies which can test the capabilities of fully integrated models at even larger (area ~10^3 km^2) and more complex river basins covering multiple geologic formulations with spatio-temporally varying connectivity between surface water and groundwater flow systems.

The Santa Fe River Basin (SFRB) in North Central Florida provides an ideal test bed to study controls over coupled surface-subsurface processes and more specifically surface-groundwater interactions in large river basins. This basin offers a complex mix of hydro-geomorphic conditions which makes it an ideal setting to study and characterize important river flow producing mechanisms and their interactions under varying geological, and physiographic settings. Depending upon the combination of geology, physiography, and land cover, the sources of river water and their mixing dynamics change dramatically along the entire length of the Santa Fe River. In the upper two thirds of the basin, hydrologic processes are dominated by surface runoff and surficial stores (wetlands and lakes) which is reflected in high variability in the flow regime, and low dissolved mineral contents (Ritorto et al., 2009; Bailly-Comte et al., 2011; Bailly-Comte et al., 2010; Moore et al., 2009). In the lower one third of the basin direct mixing between surface and ground water occurs and there are virtually no stream networks feeding the river. The SFRB is a well instrumented basin with various state and federal government agencies collecting hydrologic and water quality data at daily to monthly temporal scales and it has also been the focus of numerous field scale

studies. Thus there is a wealth of information available which can be used to develop and validate hydrologic models.

This dissertation documents the implementation of a fully integrated 3D surface water-groundwater-land surface process modeling platform, ParFlow.CLM, to evaluate the interacting geologic, climatic and vegetative controls on streamflow generation processes in a complex eogenetic karst basin in North Central Florida. The model predictions were benchmarked against observations and used to understand hydrologic functioning of the basin, river water sources origins, travels times and mixing dynamics throughout the basin. The Parflow.CLM model developed for the SFRB significantly improves over the existing steady state groundwater modeling platforms available for the region. Findings of the study are presented in the next three chapters, each of which meets requirements for independent publication in the peer reviewed scientific literature including background, study area and data, methodology, results, and summary. The key research questions addressed in this dissertation are:

1. What are the major water budget components in the basin and how do they vary in space and time? How do surface and subsurface water contributions to streamflow vary along the river?
2. What Parflow.CLM parameters are ET, groundwater level, streamflow, and subsurface contributions to streamflow most sensitive to? How does parametric sensitivity, and interaction among sensitive parameters, vary across the basin?
3. How do streamflow sources, flow paths and travel times vary along the river and between base flow and storm events? What processes and parameters exert primary control on travel time distributions?

Chapter 2 documents the development and application of a three-dimensional, fully integrated transient modeling platform, ParFlow.CLM, for the SFRB. The model was used to evaluate the interacting geologic, climatic and vegetative controls on streamflow generation processes and spatiotemporal water budget components over

the basin. Results of this study underscore the usefulness of combining end member mixing model results with integrated hydrologic models to identify sources of model error while simulating surface water – groundwater interactions. This study provides the first implementation of a fully integrated transient modeling platform in the region, which is important in light of the important current issues of declines in aquifer and streamflows and nutrient enrichment of surface and groundwater throughout the study area. Chapter 3 documents a global sensitivity analysis (GSA) experiment designed to investigate the sensitivity of predictions from ParFlow.CLM to uncertainties in a wide range of parameters governing the coupled surface, subsurface and land-atmosphere processes. This application highlights the efficiency of using the Morris method of GSA to understand interactions among coupled non-linear surface-groundwater-land atmosphere processes, to identify variables most relevant for hydrologic process of interest, to understand interactions among these variables, and to identify those parameters which contribute highest uncertainty to model predictions. The result of the Morris GSA was successful in identifying spatial and temporal variability among the dominant hydrological processes and sensitive parameters for this large complex basin. The findings demonstrate important nonlinear interactions among geologic, soil and vegetation properties on land-atmosphere, surface and subsurface processes across large scales. Moreover, based on our findings it can be concluded that any future sensitivity and uncertainty analysis on the model should account for spatial variability in the parameter values within the contrasting hydro-geologic regions of the basin.

Chapter 4 documents results from the application of Slim-Fast, a fully coupled surface-subsurface particle tracking scheme in conjunction with ParFlow.CLM, to the

SFRB to identify dominant sources of river water, their travel time, flow paths and mixing dynamics under varying hydrologic conditions. The results of particle tracking experiments identify first order controls over river water sources origins, flowpaths, and travel times and how these controls, and associated source water dynamics vary with space and time.

The final chapter of this dissertation presents a summary of the findings of this study along with some general conclusions. Based on the findings of this study recommendations are made for future research needed to build on the research presented in this dissertation.

CHAPTER 2
GEOLOGIC AND CLIMATIC CONTROLS ON STREAMFLOW GENERATION PROCESSES IN A COMPLEX EOGENETIC KARST BASIN

2.1 Background

Streamflow at any given location and time is comprised of surface and subsurface contributions from various sources. The ability to identify the factors controlling these contributions is key to successfully understand the stores, fluxes, flowpaths and travel times of water and solutes through hydrologic systems. Hydrological processes are highly non-linear and interactive making it difficult to predict the emergent behavior of the system under alternative external stressors. Representation of these coupled processes in an integrated physical model provides an efficient way to explore their behavior and interactions at various space and time scales under varying physical settings as well as possible future land-use, water-use and climatic conditions (VanderKwaak and Loague, 2001; Loague et al., 2005; Maxwell and Miller, 2005; Li et al., 2008; Jones et al., 2008; Sudicky et al., 2008). For example, Bolger et al. (2011) developed a fully integrated surface-subsurface HydroGeosphere model to study historic hydrologic conditions in the San Joaquin Valley in California. Model simulations helped understand evapotranspiration (ET) losses and associated root zone processes in the vadose zone as well as surface water – groundwater interactions along the rivers and within wetlands areas during historic and pre-development conditions. Goderniaux et al. (2009) developed a fully integrated surface-subsurface HydroGeosphere model for the Geer Basin in eastern Belgium to study impacts of climate change on groundwater resources. The integrated flow simulations indicated potential for significant reductions in groundwater levels and surface water flow rates in the basin by the year 2080. Sudicky et al. (2008) developed a fully

integrated InHM model for the Laurel Creek watershed in southern Ontario, Canada. The model was used to understand the transport of surficial contaminants through the fully integrated surface-subsurface environment of the basin for a variety of precipitation patterns.

In addition to physical modeling, data-driven approaches such as end member mixing analyses (EMMA; Hooper et al., 1990; Christophersen and Hooper, 1992) which use natural and/or isotopic tracers offer alternative ways to explore the hydrological functioning of natural systems under varying hydrogeological settings. For example, Banks et al. (2011) analyzed time series of hydrologic data such as river flow, groundwater elevation, rainfall; water chemistry data such as temperature, electric conductivity, pH, total dissolved solids; stable isotope data along with tracer-based techniques to understand spatiotemporal connectivity between surface and groundwater in Rocky River catchment in South Australia. They found that the connection between surface and groundwater varied along the length of the river and was affected by hydrogeological and hydroclimatic conditions within the basin. Capell et al. (2011) used multivariate tracer analysis to study dominant runoff generation processes in two contrasting geological regions within the North-Esk catchment, north east Scotland. Results showed a contrast in major sources of streamflow water with near-surface processes dominant in uplands and groundwater fed baseflow dominant in lower parts of the catchment. Although effective for exploration and to gain system insight, the data-driven nature of these techniques limits their effectiveness as predictive tools.

In recent years there have been an increasing number of studies that have used data-driven approaches within a physical modeling framework as additional diagnostic

tests for testing the representation of hydrologic process within simplistic models for small basins. For example, Seibert and McDonnell (2002) used “process knowledge” or “soft data” based numeric criteria such as new water contribution to peak runoff and reservoir volumes to improve the internal consistency and performance of a conceptual three box model for the ~3.8ha Maimai basin, in New Zealand. They concluded that the use of the soft data in addition to the hard data including runoff and groundwater elevation significantly improved their model’s performance and reduced parameter uncertainty. McMillan et al. (2011) demonstrated the use of available rainfall, flow and soil moisture data for parameter estimation as well as identification of more scientifically defensible model structures for the ~0.25 km^2 Satellite Right subcatchment of the Mahurangi river basin, New Zealand. Werner et al. (2006) used field observations with an integrated model, MODHMS, to identify river reaches receiving groundwater influx in the ~420 km^2 Pioneer Valley, Australia. However, they did not investigate the spatio-temporal characteristics of the groundwater-surface water flow dynamics in the basin.

In this study we use a fully integrated 3D surface water-groundwater-land surface model, ParFlow.CLM (Maxwell and Miller, 2005; Kollet and Maxwell, 2008a; Kollet and Maxwell, 2006) to evaluate the interacting geologic, climatic and vegetative controls on streamflow generation processes in a complex 3700 km^2 eogenetic karst basin in North Central Florida. The period of study, January 1, 2000 through December 31, 2008 was selected to include diverse climatological conditions spanning several extreme events. For instance year 2004 was an extremely wet period during which four hurricanes and a tropical storm crossed the state of Florida causing flooding over much of the study area. Conversely, years 2006 - 2007 were one of the driest periods ever recorded for the

basin and were followed by relatively wet conditions as a result of a tropical storm which occurred in September 2008. In addition to traditional model evaluation criterion, such as comparing field observations to model simulated streamflow and groundwater elevations, we evaluate the model's predictions of surface-groundwater interactions over space and time using EMMA that we performed using observed specific conductivity (SC) differences among surface and subsurface water sources throughout the domain.

After benchmarking ParFlow.CLM's performance against field observations, we used the model to address following questions about integrated hydrologic processes in this complex regional river basin; (1) how do spatiotemporal patterns of surface water: groundwater streamflow fractions vary throughout the basin; (2) how do geology, land cover and climatic variability interact to control surface water - groundwater interactions in the basin, and (3) how do geology, land cover and climatic variability control spatiotemporal patterns of major hydrologic water budget components such as ET and groundwater recharge in the basin.

2.2 Santa Fe River Basin – Physical System and Conceptual Model

The 3700 km^2 Santa Fe River Basin (SFRB) consists of two distinct yet linked hydrogeologic units (Figure 2-1): the upper confined region (CR) and the lower unconfined region (UR) which are separated by a topographic break known as the Cody Escarpment (CE). The climate of the SFRB is warm and humid with mean annual precipitation of 1356 mm, receiving most of its rain from mid-may through mid-October. The rainy season is followed by a cool, dry period from mid-October through mid-February and a moderately cool, wet period from mid-February through mid-May characterized by periodic extra-tropical fronts. The basin experiences rare/episodic

extreme events in form of hurricanes, and seasonal and multi annual events caused by the El-Nino Southern Oscillations (ENSO) phenomenon.

In the upper two-thirds of the SFRB the Surficial Aquifer System (SAS) is a perched aquifer separated from the regional Upper Floridan Aquifer System (UFAS) by the presence of a low hydraulic conductivity Intermediate Aquifer System (IAS; Water resources associates, 2007) composed of Hawthorne clays (Figure 2-2A). Major soils covering the CR are classified as poorly or very poorly drained with very low vertical hydraulic conductivity resulting in low infiltration (Arthur et al., 2005). Stream networks, lakes and swamp systems are well developed in the region (Upchurch, 2007). The abundance of swamps, wetlands, forests, and poorly drained soil result in high water table conditions even during extended dry periods.

The CE is formed by marine, fluvial and karst related erosion of the Hawthorn clay which makes up the IAS (Upchurch, 2007). The SAS is generally absent in this region and the IAS, if present, is in the form of local clay rich strata (Upchurch, 2007). The soil types are a mix of poor or well drained depending on location. The CE is characterized by the presence of numerous sinkholes, sinking streams, siphons, springs and other karst features which have the potential to rapidly recharge the UFAS (Upchurch, 2007). During baseflow conditions the upper Santa Fe River (SFR) is captured in its entirety by the SFR Sink (hereafter referred to as the sink) in the CE region. The river emerges from the SFR Rise (hereafter referred to as the rise), located approximately 6 km downstream of the sink, as a first order magnitude spring. Hydrological behavior of the river in the transition zone is highly dynamic with no flow entering the sink during extreme drought conditions and with a portion of the river

occasionally bypassing the sink as overland flow to the lower SFR during large flood events.

In lower third of the SFRB both the SAS and the IAS are absent and the UFAS system becomes an unconfined aquifer, with a thin overlying sand layer and direct exchange with surface water in the river channels. Major soils covering the UR region are classified as well or excessively well drained with high hydraulic conductivity resulting in high infiltration rates and virtually no surface runoff (Arthur et al., 2005). Thus rainfall in excess of ET rapidly moves through the vadose zone to the UFA, which feeds the river via series of springs and diffuse groundwater discharge. The UFA in this region is known to have major conduits creating internal subsurface drainage networks connected to the main river (Figure 2-2B), some of which extend beyond the topographic boundary of the basin (Upchurch, 2007; Upchurch et al., 2008; Meyer et al., 2008). In contrast to teleogenetic karst systems that have low intergranular porosity, because they have undergone deep burial and alterations, eogenetic karst systems that exist in Florida have not undergone deep burial and have retained their higher matrix porosity (Vacher and Mylroie, 2002; Florea and Vacher, 2007). As such primary matrix porosity in the SFRB plays an important role in water storage, flow through the subsurface environment, and exchange with the river system.

2.3 Methods

2.3.1 River Source Water Mixing Dynamics: End Member Mixing Analyses

During low flow conditions continuously flowing rivers typically receive baseflow contributions from the subsurface environment which helps sustain their flow. Because of their origin and age, the hydrologic modeling literature often refers to these baseflow subsurface contributions as “old” or “pre-event” water (e.g. Desmarais and Rojstaczer,

2002). River source water characteristics change during storm events when rain water, commonly referred to as “new” or “event” water (e.g. Desmarais and Rojstaczer, 2002) typically dominates the river hydrographs. In this study our goal is to understand factors controlling streamflow generation processes in the SFRB, including “new” surface water contributions originating in the upper CR of the domain and “old” subsurface contributions from the UFAS.

Many hydrologic studies have used SC of water as a natural tracer in hydrograph separation analysis (Nakamura, 1971; Pilgrim et al., 1979; Matsubayashi et al., 1993; Cox et al., 2007). Hooper et al. (1990) and Christophersen and Hooper (1992) detail the mathematical basis and assumptions of EMMA for source water identification. For brevity, in this paper we provide a brief description of the method, equations used and information pertinent to application of the method in the SFRB.

Rain water in the SFRB is known to have low ionic concentration and therefore, low SC (Ritorto et al., 2009). In contrast water in the subsurface environment of UFAS, because of continuous dissolution of surrounding matrix, has higher ionic concentration and therefore high SC (Langston et al., 2012). Given that SC values representative of “new” surface water and “old” groundwater can be approximated from field observations, the fraction of “old” groundwater contributions in total streamflow (Eq. (2-3)) can be approximated by solving binary mass balance Eqs. (2-1) and (2-2) (Desmarais and Rojstaczer, 2002).

$$SW + GW = 1 \tag{2-1}$$

$$SC_{SW}\, SW + SC_{GW}\, GW = SC_{river} \tag{2-2}$$

$$GW = 1 - \frac{(SC_{GW} - SC_{river})}{(SC_{GW} - SC_{SW})} \quad (2\text{-}3)$$

Where SW and GW, respectively, represents the fraction of "new" surface water and "old" groundwater present in streamflow at a given location and time. SC_{SW}, SC_{GW}, SC_{river} represent the SC values for "new" surface water, "old" groundwater, and SFR water, respectively.

SC measurements at station 1500 in the CR (Figure 2-1) during high streamflow conditions caused by hurricanes in October 2004 were used to represent SC_{SW} values (0.07 ms/cm) in Eqs. (2-2), and (2-3). This value was chosen to represent SC value for "new" surface water because during this period all the river channels (both in CR and UR) were flooded with rain water received from four hurricanes that passed through the study area over very short time. The SC measurements in the SFR during the peak of October 2004 storm event ranged from 0.07 ms/cm (at stations 1000, 1500) to 0.1 ms/cm (at station 2800). To account for known effects of local variations in geology on variability in ionic concentration of "old" ground water (Gulley et al., 2012) we used separate estimates of "old" ground water SC for each UR river locations. This approach of using independent end member estimates for distinct locations has been previously used successfully to account for soil and aquifer heterogeneity (e.g. Soulsby and Dunn, 2003). For each UR river location, SC values corresponding to lowest five percentile flow values were averaged, to represent SC_{GW}. The SC end member values thus calculated for SC_{GW} at stations 1975, 2500, 2800, respectively, were 0.47, 0.39, and 0.37 ms/cm. All the above mentioned calculations used discrete (monthly) SC measurements obtained from the Suwannee River Water Management District

(SRWMD) to calculate surface and groundwater fractions at stations 1975, 2500 and 2800 over the entire duration of this study.

2.3.2 Integrated 3D Model – ParFlow.CLM

We used ParFlow to simulate the 3D integrated surface water – groundwater system in the SFRB. Full details on model physics and how the surface and subsurface components are integrated can be found elsewhere (Ashby and Falgout, 1996; Jones and Woodward, 2001; Kollet and Maxwell, 2006). In this section we present a brief summary of equations used by the model.

To simulate flow through variably saturated subsurface environment, ParFlow solves the 3D Richards equation using a cell-centered finite difference scheme in space and an implicit Euler scheme in time. Overland flow is simulated using 2D Kinematic wave equation and Manning's equation. Surface and subsurface equations are integrated using a free surface overland flow boundary condition (Eqs. (2-4), (2-5), and (2-6)).

$$S_S S_w(\psi_p)\frac{\partial \psi_p}{\partial t} + \phi\frac{\partial S_w(\psi_p)}{\partial t} = \nabla.[k(x)\, k_r(\psi_p)\nabla(\psi_p - z)] + q_s \tag{2-4}$$

$$-k(x)\, k_r(\psi_o)\nabla(\psi_o - z) = \frac{\partial \|\psi_o, 0)\|}{\partial t} - \nabla\cdot\vec{\upsilon}\|\psi_o, 0\| - q_r(x) \tag{2-5}$$

$$\upsilon_x = \frac{\sqrt{S_{f,x}}}{n}\psi_o^{2/3} \qquad \upsilon_y = \frac{\sqrt{S_{f,y}}}{n}\psi_o^{2/3} \tag{2-6}$$

Where ψ_p is the subsurface pressure head [L]; $S_w(\psi_p)$ is the degree of saturation [-] represented as function of ψ_p as defined by van Genuchten model (Van Genuchten, 1980); S_s is the specific storage [L^{-1}]; ϕ is the porosity [-]; k(x) is saturated hydraulic conductivity [LT^{-1}]; k_r is the relative permeability as a function of subsurface pressure

head[-]; z is depth below the land surface [L]; q_s is a general source/sink term [T^{-1}]; q_r represents rainfall and evaporative fluxes [LT^{-1}]; ||A,B|| indicates the greater of A and B; $S_{f,x}$ and $S_{f,y}$ are the friction slopes in x and y direction [-]; n is the Manning's coefficient [$TL^{-1/3}$]; an **v** is the depth averaged velocity vector of surface runoff [LT^{-1}]; ψ_o in Eqs. (2-5) and (2-6) is the pressure head or water ponding depth at the land surface [L].

ParFlow.CLM incorporates a modified version of the Common Land Model (CLM ; Dai et al., 2003) into ParFlow to simulate near land surface energy and water balance. CLM simulates evaporation losses from the ground surface and vegetation canopy; transpiration losses from plants; snow accumulation and melt processes; and latent, sensible, and ground heat fluxes (Kollet and Maxwell, 2008a). Near land surface – atmospheric fluxes are calculated as a function of atmospheric variables that CLM requires as input (precipitation, air temperature, pressure, wind speed, specific humidity, and solar radiation) and soil moisture calculated by ParFlow. Details of equations used to simulate various water and energy fluxes in CLM and coupling of the two models are provided elsewhere (Maxwell and Miller, 2005; Kollet et al., 2009; Kollet and Maxwell, 2008a); however, equations relevant to work presented here are summarized in the following.

At any given land surface location, the available net radiation (given by sum of both short and long wave radiations) is dissipated through the sum of latent, sensible, and soil heat fluxes:

$$R_n(\theta) = LE(\theta) + H(\theta) + G(\theta) \tag{2-7}$$

where R_n is net radiation at the land surface (W/m^2); LE is latent heat (W/m^2), H is sensible heat flux (W/m^2), and G is the ground heat flux (W/m^2). The energy balance

at the land surface is coupled to water balance in the subsurface environment through the soil moisture content at or close to ground surface (θ; kg/kg). Each of the terms on the right hand side of Eq. (2-7) are independently calculated by CLM using atmospheric forcing, soil, vegetation characteristics, and soil moisture provided by ParFlow. LE is calculated as:

$$LE = L_v E \tag{2-8}$$

$$E = E_c + E_g \tag{2-9}$$

where, L_v is latent heat of evaporation (J/kg) and E is the sum of evaporative fluxes from the foliage (E_c (kg/m^{2}s), if vegetation is present) and ground E_g (kg/m^{2}s). Evaporative fluxes from the ground are calculated as:

$$E_g = \rho_a \frac{(q_g - q_a)}{r_d} \tag{2-10}$$

Where ρ_a is the intrinsic density of air (kg/m^3); q_g is the air specific humidity at the ground surface (kg/kg); q_a is the air specific humidity at reference height z_q obtained from atmospheric forcing (kg/kg); r_d is the aerodynamics resistance at z_q (s/m). Evaporative fluxes from the foliage are estimated as the sum of evaporative flux from wet foliage E_w (kg/m^{2}s) and total transpiration flux E_{tr} (kg/m^{2}s) from the root zone cells:

$$E_c = E_w + E_{tr} * \sum f_{root,j*} \tag{2-11}$$

$$E_w = \sigma_f L_{SAI} [1 - \delta(E_f^{pot})(1 - \tilde{L}_w)] E_f^{pot} \tag{2-12}$$

$$E_{tr} = \sigma_f L_{SAI} \delta(E_f^{pot}) L_d \frac{r_b}{(r_b + r_s)} \tag{2-13}$$

Where $f_{root,j*}$ is effective root fraction in root zone layer j

$$f_{root,j^*} = \frac{f_{root,j}\, w_{LT}[j]}{\sum f_{root,i}\, w_{LT}[i]} \quad (2\text{-}14)$$

$$w_{LT}[i] = \frac{\theta_i - \theta_{wp}}{\theta_{fc} - \theta_{wp}} \quad (2\text{-}15)$$

$$f_{root,j} = 1 - 0.5[\exp(-az) + \exp(-bz)] \quad (2\text{-}16)$$

Where σ_f is the vegetation fraction (-); L_{SAI} is the stem plus leaf area index (-); δ is the step function (one for positive and zero for zero and negative arguments); E_f^{pot} is the potential evaporation from wet foliage (kg/m^{2}s); $\tilde{L}_w$ is the wetted fraction of the canopy (-); L_d is the dry fraction of foliage surface (-); r_b is the conductance of heat and vapor flux from leaves (s/m); and r_s is the stomatal resistance (s/m). θ_i, θ_{fc}, and θ_{wp}, respectively, are soil moisture content in layer i, moisture content at field capacity, and permanent wilting point; $f_{root,j}$ is root fraction parameter which varies exponentially with the depth from land surface z (-) in root zone layer j; a and b are coefficients dependent upon vegetation type. In ParFlow.CLM the term q_s in subsurface mass balance equation (Eq. (4)) is expressed as

$$q_s = LE(\theta) + q_g(\theta) \quad (2\text{-}17)$$

Where q_g (s^{-1}) is the flux of water infiltrating at the land surface after accounting for precipitation, canopy throughfall, and/or surface runoff.

2.3.2.1 Model setup, parameterization and initialization

In this study ParFlow.CLM was developed for a domain that extends beyond the SFRB topographic boundaries in order to include major springsheds that are thought to provide subsurface flow to the river in the UR of the basin (Meyer et al., 2008; Upchurch et al., 2008). The bottom of the domain was set at 70 m below mean sea level to

include the top of the active subsurface zone believed to contribute flow to the SFR. A lateral discretization ($\Delta x = \Delta y$) of 1500 m and vertical discretization (Δz) of 1 m was used to discretize the domain resulting in 56x50x150 cells, in x, y, and z dimensions, respectively. Thus the domain included a total of 420,000 rectilinear elements covering a total land surface area of 6300 km^2 (Figure 2-1). The land surface elevation in the domain ranges from 4 m to 74 m above mean sea level, resulting in a maximum domain depth of 144m.

A 10 meter (m) resolution digital elevation model (DEM) dataset obtained from the United States Geological Survey (USGS) was resampled to a resolution of 1500 m using bilinear interpolation approximation in the Spatial Analyst Module in ArcInfo (Figure 2-3 A). The main channels, as represented by the National Hydrography Dataset (NHD), were incised into the DEM by setting the bottom elevation of the channels equal to the elevations used in a HECRAS model previously developed for the region (Water resources associates, 2007) and personal communication Clay Coarsey, (SRWMD, 2012). Manning's surface roughness coefficients (n) needed for ParFlow were taken from the n values assigned to the channels in the existing HECRAS model (Water resources associates, 2007) and personal communication Clay Coarsey, (SRWMD, 2012), with the same values assigned to the channels and the floodplains by region (see Table 2-1). In the CR the n value approximately corresponds to that of channel with heavy brush and timber (Chow et al., 1988). In the UR the value corresponds to something between a clean straight and clean winding channel (Chow et al., 1988).

Information regarding the spatial extent and depths of the SAS, IAS and UFAS in the region were taken from maps available from the Floridan Aquifer Vulnerability Assessment (FAVA) conducted by the Florida Geological Survey (FGS; Arthur et al., 2005). These maps were available at resolutions ranging from 30m to 390m and were all resampled to resolution of 1500 m using bilinear interpolation approximation in the Spatial Analyst Module in ArcInfo. Where conflicts arose between the USGS DEM used to define the land surface and the top elevations, horizontal extents and thicknesses of the SAS and IAS obtained from FAVA, it was assumed that SAS occupied at least the top 8 meters below the USGS defined land surface over the region where the IAS was mapped. The resulting geological representation is shown in Figure 2-2A.

The UFAS is known to have networks of conduits in the UR and CE regions of the domain. A digital map of the approximate locations of these conduits was obtained from (Meyer et al., 2008) who compiled their best estimates of conduit locations based on results of dye tracer studies, groundwater chemistry and potentiometric surface measurements in the domain (Figure 2-2B). All the conduits were assumed to be 10m in height and to occur between depths of 5 m to 15 m below mean sea level, based on previous field investigations (Langston et al., 2012). Since ParFlow does not contain algorithms for turbulent conduit flow, conduits were represented as high hydraulic conductivity zones in this study. This assumption should be reasonable given the goal of the study to estimate controls on regional variability of streamflow generation processes and water budget components over a large river basin and the resulting, relatively coarse 1500 m horizontal discretization of the model. Finer discretization and more accurate representation of turbulent conduit flow processes would be required to

investigate smaller scale interactions (i.e. on the order of meters to 10s of meters) between the river, conduits and surrounding karst matrix. The subsurface environment was assumed to be isotropic and homogeneous within each aquifer type (SAS, IAS, UFAS, conduits). The effective aquifer properties for each type were estimated based on literature values from previous modeling, observational and experimental studies in the region and are summarized in Table 2-1.

A 30 m resolution digital map depicting land cover in the domain for was obtained from the Florida Fish and Wildlife Conservation Commission for the year 2003 (Figure 2-3 B). These data were resampled to 1500 m resolution using the nearest neighbor interpolation approximation in the Spatial Analyst Module in ArcInfo. The domain was initially described by 22 different land cover categories. Land cover categories were merged/reclassified into nine distinct land cover types (i.e. evergreen needleleaf forests (31%), grasslands (14%), open shrublands (13%), permanent wetland (13%), mixed forests (11%), urban areas (8%), croplands (4%), barren or sparsly vegetated (3%), and water bodies (2%)) to correspond to the vegetation types included in ParFlow.CLM default vegetation property database, which follow the standard of the International Geosphere-Biosphere Program (IGBP Running et al., 1994).

Spatially distributed climatic forcing data obtained from the North American Land Data Assimilation System (NLDAS; Cosgrove et al., 2003) were used to drive the model. The NLDAS dataset is available at an hourly temporal resolution and at a spatial resolution of 12 km x 12 km. The forcing data was spatially resampled to a resolution of 1500 m by using a bilinear interpolation approximation.

To initialize ParFlow requires estimation of the initial pressure distribution throughout the domain. The May 2002 UFAS potentiometric surface map published by the SRWMD was used as the initial condition in the UFAS. This is closest date to the beginning of the study period for which a potentiometric surface map was available. For the SAS and IAS no groundwater elevation maps were available. Therefore, to initialize the model the water table in the SAS was set at a depth equal to 10% of total SAS thickness (i.e. SAS was 90% saturated everywhere in the CR), and the IAS was assumed to be in hydrostatic equilibrium with the UFAS. Constant pressure boundary conditions equal to the initial conditions were applied along all lateral domain boundaries. A no flux boundary condition was applied to the domain bottom and an overland flow boundary condition was applied at the land surface.

To minimize the influence of initial condition assumptions the model was spun up by repeatedly simulating the entire 9 year study period (of 2000 through 2008) using the spatially distributed NLDAS forcing data until a quasi dynamic equilibrium was reached, i.e. until the difference between the beginning and ending subsurface water storage (over the 9 year period run) dropped to less than <0.05 % of average subsurface storage and the simulated streamflow and groundwater elevations time series at multiple locations across the domain showed minimal visual difference between two consecutive 9 year runs. These criteria were met by the end of the second 9 year simulation period, thus all the model results presented in this paper are the model results obtained from round 3 of model spinup.

2.3.2.2 Estimating surface water and groundwater contributions to streamflow using ParFlow.CLM

The groundwater fraction of flow at a given river location on a given day includes the subsurface contribution that the location receives from its entire upstream contributing area on that day. A portion of this contribution is received at upstream channel locations which then travels downstream as channel flow and a portion is received as local subsurface contribution. In this study we approximated instantaneous daily subsurface flow at a particular river location as the sum of subsurface flow contributions received over the entire upstream river reaches on that day. The subsurface flow to/from each channel cell was calculated using the saturated hydraulic conductivity and hydraulic head gradients provided by ParFlow at each river cell in the Richards equation on daily basis. This methodology neglects travel time within the stream channel, which may have some impact on instantaneous comparisons with the EMMA, but should not affect event-scale, monthly, seasonal or annual subsurface contribution estimates.

2.3.2.3 Benchmarking ParFlow.CLM

The adequacy of model simulated regional surface and subsurface flow processes within the domain was tested using traditional benchmarks including comparison of measured and model simulated daily streamflow and groundwater surface elevations, at multiple locations across the study domain (Figure 2-1). In addition comparison between ParFlow.CLM simulated and EMMA estimated groundwater flow contributions at multiple river locations was used to evaluate the accuracy of model simulated groundwater surface water interactions under varying hydrologic conditions. Daily streamflow data were obtained from the USGS and

SRMWD, daily groundwater elevation data were obtained from the SRWMD, and monthly SC measurements were obtained from the SRWMD. The extreme climate variability (e.g. hurricanes in 2004 versus historic droughts in 2007) during the study period allows testing of the robustness of the model under highly variable hydrologic conditions.

It should be noted that results presented in this paper were obtained without formal model calibration. Rather than optimally fitting a model structure and parameters to a calibration dataset, we aimed to develop a model that incorporates physically plausible hydrological characteristics of the domain, based on best known existing information, and to use this model to 1) test our conceptual model of the hydrologic functioning of the basin, 2) gain improved insights about the interactions of coupled hydrologic processes in the basin, and 3) to determine where additional field experiments may be needed to refine both the conceptual and numerical models of the basin.

2.4 Results and Discussion

2.4.1 Streamflow

Measured and simulated flow hydrographs at 5 locations along the SFR and 1 location on New River (station 1000 in Figure 2-1), a major tributary to SFR, were compared to evaluate ParFlow.CLM flow predictions (Figure 2-4). Stations 1000 and 1500 are located within the CR of the domain, Station 1898 is located along the CE, and Stations 1975, 2500 and 2800 are located within the UR of the domain (Figure 2-1).

Model simulated streamflow at all CR and CE locations showed good agreement with measured data during both low and high flow conditions (Figure 2-4 stations 1000, 1500, 1898). Timing and peaks of hydrographs were accurately simulated by the model

at all locations with very few exceptions. ParFlow.CLM underpredicted flow during a major event in middle of year 2003-2004 at station 1000; however comparison of the hydrographs at other confined locations during same time period indicates that the poor performance at the given location might be attributed to inadequate representation of rainfall around station 1000.

In general model predictions at all UR stations showed reasonable agreement with measured data during high flow conditions (Figure 2-4 stations 1975, 2500, 2800). At station 1975, the model consistently simulated higher than observed streamflow during peaks of storm events. This is likely due to the model's coarse spatial resolution which cannot simulate small-scale short duration interactions between conduits and the porous matrix that are known to occur in the region between station 1898 and 1975. Nevertheless, the model adequately simulated the transition from high to low flow conditions at 1975. At stations 2500 and 2800 in the UR the model adequately simulated the timing and peaks of storm events but consistently underpredicted streamflow during the end of the falling limbs of storm hydrographs. Thus the model, as currently configured, is missing a transient source of groundwater to the streams in the UR. This could be due to the constant fixed pressure head boundary conditions applied at the lateral boundaries of the domain which may result in some loss of groundwater from the domain during high rainfall periods, or inaccuracies associated with the extent and thickness of the IAS, and the location of the CE boundary, which could result in less water infiltrating into the UFAS in the upper portions of the UR.

2.4.2 Groundwater Elevation

ParFlow.CLM simulated groundwater elevation in the UFAS were evaluated at six CR locations (wells E1 through E6 in Figure 2-1) and three UR locations (wells E7

through E9 in Figure 2-1). With exceptions of wells E3, E7, and E8 the model simulated groundwater surface elevations were in good agreement with field observations (Figure 2-5). Both measured and model simulated groundwater elevation at all CR wells show smooth annual variations corresponding to slow rise and fall of regional groundwater surface in response to wet and dry hydrologic periods. In contrast, both measured and simulated groundwater elevation at all unconfined well locations indicate direct response to individual rain events as well as smoother annual variations corresponding to the slow rise and fall of regional groundwater surface in response to wet and dry hydrologic periods.

Well E3 and E8 are close to the CE and therefore highly sensitive to the degree of confinement and extent of karstification along the CE, which are uncertain. Due to their locations these wells are expected to show greater response (as compared to well confined well locations) to large storm events. However the piezometric head at these locations is always higher than observed and showed even more response to storm events than measured data. We hypothesize that the difference between the model simulated and measured elevations at these location is due to uncertainty in extent of confinement and conduit locations in this area and perhaps the coarse resolution of the model.

Well E7 is located in a physiographic region known as Wacassassa Flats (Figure 2-1). It is assumed that there are remnants of the IAS in this region, which causes the observed local piezometric surface high in the region. However these IAS remnants are not mapped in the FGS aquifer datasets used in this study, in fact there is no published information on thickness of IAS in this region. Therefore we did not include them in the

conceptual model underlying ParFlow. As a result the model was unable to capture the observed significant rise in the potentiometric surface in Wacassassa Flats after storm events and showed marginal rise in groundwater elevation in response to rise in regional groundwater surface rise. These results, as well as those for wells E3 and E8 underscore the need for more accurate, spatially explicit hydrogeologic characterization of the region.

In addition to model evaluation of groundwater elevations at point locations we evaluated the model simulated regional UFAS response to wet and dry hydrologic conditions resulting from extreme climate events. Here we present the piezometric surface of the UFAS during wet conditions caused by hurricanes in year 2004 (Figure 2-6 A, B, and C) and during extremely dry conditions in years 2006 and 2007 (Figure 2-6 D, E, and F). In general the piezometric surface shows regional flow from east to west, with the river draining the UFAS in the UR. The transient effects of rainfall on UFAS groundwater elevations are visible during peaks of hurricanes in year 2004 as well as tropical storm Fay in year 2008 (Figure 2-6 B and F). The effect is most prominent around high hydraulic conductivity zones, representative of conduits that breach the IAS in the CR, in the northwest portion of the domain. It is less prominent around high hydraulic conductivity zones representative of conduits in the UR in the south central part of the domain, and is not visible in the well confined western portion of the basin. January 2005, a few months after the end of the 2004 hurricane season, shows smoothing of the regional piezometric surface, but the piezometric head around the high hydraulic conductivity zones is still significantly elevated compared to the pre-hurricane condition. These observations suggest that high hydraulic conductivity zones in the

UFAS provide hotspots for rapid transport of water and surficial contaminants into the regional groundwater system during large storm events, particularly where they breach the IAS. Comparison of Figures 2-6 D and E shows that as the drought conditions extended during 2006-2007 the river drained water from regions further away, extending into the CR.

2.4.3 Surface Versus Subsurface Contributions to Streamflow

Comparison of measured versus predicted ratios of total daily subsurface flow to total streamflow was used as an additional diagnostic test of the adequacy of the conceptual model and parameterization underlying ParFlow.CLM over a range of hydrologic conditions. As shown in Figure 2-7, river reaches upstream of station 1898 receive no significant contributions from the subsurface, indicating rainfall and near stream overland flow to be the dominant source of streamflow in the CR of the domain. At station 1898 the river shows a net loss of stream flow to the subsurface during storm events as streamflow generated from surface processes in the CR is lost to the UFAS through high conductivity breaches in the IAS beneath the river channel. Thereafter, each downstream station in the UR (1975 through 2800) shows a consistent gain in subsurface flow contribution. Streamflow at all gages in the UR shows an immediate decrease in subsurface contributions immediately after the onset of largest storm events, as the surface pulse of storm flow passes and hydraulic gradients from the local UFAS to the stream are reduced. This is followed by an extended period of elevated subsurface contributions from the UFAS to the river after the storm. Table 2-2 summarizes the net annual gain/loss of subsurface flow at various river locations. Note that for station 1898 at the CE, values represent the total gain/loss in all river cells upstream of that gage location, whereas for the remaining UR stations the values

represent total gain/loss of subsurface flow downstream of station 1898. The negative values of subsurface flow contributions for station 1898 indicate that in all years except 2006 the river shows a net loss of surface water generated in the CR to the subsurface environment.

Figure 2-8 compares the ratio of EMMA estimated (using SC measurements and observed streamflow) and ParFlow.CLM predicted groundwater to total streamflow ratios at the three UR river locations. This figure indicates that the model accurately simulates both the timing and magnitude of the surface to groundwater mixing ratio response to storms at these stations. Results show dominance of “new” surface water components from the CR during peaks of all storm events and dominance of “old” groundwater contributions from the UFAS during low flow conditions. Subsurface contributions decline during storm events due to both the high volume of streamflow coming off the CR as a result of the storms and the reduction of the hydraulic gradient towards the river as the surface water pulse passes. Both of these mechanisms are accurately represented by ParFlow.CLM, for example see prominent drop in subsurface flow contributions during 2004 hurricanes in Figure 2-7 and corresponding drop in groundwater to total streamflow ratio in Figure 2-8. Note that at station 1975, directly downstream of the CE, groundwater to total streamflow ratios are significantly underestimated by ParFlow during low flow periods. However during these periods total streamflow is extremely low (See Figures 2-4 and 2-9) making the groundwater to surface water ratio highly sensitive to small errors.

Figure 2-9 shows observed and model simulated streamflow, along with total subsurface flow contributions as estimated by EMMA and simulated by ParFlow, at

three UR locations for two different periods: 2002-2003 (a wet year 2003 following an equally wet year 2002; see total annual rainfall in Table 2-3) and 2007-2008 (a wet year 2008 following two dry years 2006 - 2007). These results show that ParFlow more accurately simulates both total streamflow response to storm events, and groundwater contributions to streamflow, after dry antecedent conditions (2008) than after wet antecedent conditions (2003), particularly for stations 2500 and 2800. Comparison with EMMA results indicate that ParFlow underestimates groundwater contribution to streamflow, especially when wet years follow wet years. This suggests an underestimate of interannual storage in the UFAS system, with unrealistic losses either occurring across the southwestern domain boundary or by ET (rather than recharge to the UFAS) in the transition region between the CR and UR where the extent, thickness and hydraulic conductivity of the IAS is highly uncertain.

2.4.4 Analysis of Water Budget Components for the SFRB

Use of fully integrated models makes it possible to elucidate significant spatiotemporal patterns in coupled near land surface energy and hydrologic processes and resulting water balance components. In this section we present annual (Table 2-3) and monthly averaged water balance components (rainfall, ET, runoff, surface storage (St_s) and subsurface storage (St_{ss}), Figure 2-10) integrated over the study domain and compare them to commonly reported values for the study area wherever possible.

Average annual rainfall received by the domain during the study period (January 2000 through December 2008) was 1253 mm as compared to the 1356 mm long term average annual rainfall reported for the study area (Schneider et al., 2008). The average annual ET loss simulated by ParFlow.CLM was 982 mm (78% of applied rainfall) as compared to long term average annual ET losses of 1041 mm (77% of

rainfall as estimated by (Schneider et al., 2008)). Thus ParFlow.CLM accurately simulates average ET fluxes from the domain, the most important water balance component after rainfall.

Monthly averaged values for all water balance components for the domain are shown in Figure 2-10. A negative value in the figure indicates water loss from the domain and a positive value indicates water gain in the domain. Averaged monthly rainfall follows a bimodal pattern with highest rainfall occurring during months of March and June, and 57% of the rainfall occurring during the months of June through September. Average monthly ET losses were highest during summer months (peaking during the month of July) and lowest during winter months of December – January. In general the rainfall and ET patterns during the simulation period are consistent with long term trend reported for the basin (e.g. Tripathi, 2006).

Runoff, St_s, St_{ss}, and groundwater recharge all show a strong dependence on seasonal and interannual variability in rainfall and ET patterns over the basin (Figure 2-10; Table 2-3). In general St_s and runoff from the domain outlet followed the rainfall pattern with wet months (e.g. months of August and September) and wet years (e.g. 2004 and 2005) showing an overall increase in St_s and higher runoff losses in response to higher rainfall over the domain. Patterns in St_{ss} indicate higher recharge during months of June through August in response to higher rainfall rates, despite higher ET losses. Net discharge from the subsurface occurs during periods of rainfall deficit in April-May and October and November (i.e. when ET > rainfall).

Annual water balance components, summarized in Table 2-3, show a strong influence of interannual climate variability, with loss of St_s and St_{ss} from the domain

during dry years (2000, 2001, 2006, 2007) and gain of St_s and St_{ss} in the domain during wet years (2002, 2004, 2005, and 2008). It is interesting to note the dependence of water balance dynamics on antecedent conditions. Year 2005, a wet year following a wet year, showed a smaller gain in St_{ss}, and more runoff and ET losses compared to year 2004 which received similar amount of rainfall. Thus the high antecedent St_{ss} conditions at the beginning of 2005 resulted in higher runoff and ET losses. Similarly year 2003 (an average rainfall year following an average rainfall year) showed more runoff and ET losses as compared to year 2002 (an average year following a dry year) resulting in very small net gain of storage in the domain. In contrast years such as 2002 and 2008 which followed dry conditions showed a net gain in St_{ss} and smaller runoff and ET losses compared to 2003 which received similar amount of rainfall but followed an average rainfall year.

2.4.5 Geological Control Over Spatial Pattern of Monthly ET Losses and Subsurface Recharge

Spatial distribution of average monthly ET losses from the domain and average monthly groundwater recharge (net change in St_{ss}) are shown in Figures 2-11 and 2-12, respectively. High ET losses and low groundwater recharge occur in the CR where the presence of a confining unit and relatively low hydraulic conductivity result in a high water table and poorly drained conditions. In contrast the absence of the confining layer over the UFAS and the presence of high hydraulic conductivity zones (i. e. conduits) in the UR create lower water tables and a well drained subsurface environment. Thus the contrast in the geology between the two regions strongly controls the balance between ET and groundwater recharge, which in turn controls streamflow generation

mechanisms, i.e. dominance of surface flow in the CR and dominance subsurface flow in the UR.

Monthly variations in climate modulate the water balance components, but do not alter the sharp contrast between the two geologic regimes. The months of June through September receive more rainfall than ET losses and showed a net subsurface recharge (Figures 2-10 and 2-12). Consistently higher recharge in the UR than in the CR during these summer months occurs due to drainage of subsurface storage by the highly permeable UFAS to river. During April-May and October-November ET losses equal or exceed rainfall inputs and thus groundwater discharge to the river results in a loss of storage from the subsurface.

2.4.6 Vegetation and Geological Control Over Water Table Depth and ET Dynamics

In addition to geologic controls on energy and hydrologic feedbacks between land surface and atmosphere (through control on water table depth), vegetation also plays an important role (Kollet and Maxwell, 2008a). Figure 2-13 A shows the relationship between averaged daily water table depths (WTD) from land surface and averaged daily ET loss for each land surface cell in the model domain. Blue and red circles, respectively, are cells in the CR and UR of the basin. As discussed in section 4.5, the shallower WTD in the CR results in higher ET losses as compared to the UR. Similar to results presented by (Kollet and Maxwell, 2008a) we observe a strong dependency between ET losses and WTD up to an approximate critical WTD of 5 m. Beyond this critical depth ET losses become independent of WTD and are limited to withdrawal from moisture available in the unsaturated subsurface environment. Figure 2-13 B shows that landcover exerts a secondary control on ET and WTD, with grass

lands showing the lowest ET losses and forests and wetlands showing the highest ET losses. These findings illustrate a strong link between potential changes in anthropogenic activities (via changes in land cover) to changes in the most significant component in the water balance for the basin i.e. ET losses.

2.5 Summary and Conclusions

ParFlow.CLM, an integrated 3D surface water-groundwater-land surface hydrologic model, was used to evaluate the interacting geologic, climatic and vegetative controls on streamflow generation processes and spatiotemporal water budget components over a large, complex eogenetic karst basin in North Central Florida. Comparison to field observations throughout the basin showed that the model successfully simulated the spatial and temporal dynamics of streamflow, ET fluxes and groundwater elevations throughout the domain, across extreme hydrologic conditions and without any formal model calibration.

Results of this study indicate that geologic heterogeneity exerts primary control on streamflow generation processes in this basin through its influence on water table depth and ET fluxes. In the upper basin, where the regional karst aquifer is overlain by a thick confining layer, a persistent high surficial water table results in high ET and low groundwater recharge. Low topographic relief and relatively low surficial aquifer hydraulic conductivity result in both low surface and low subsurface connectivity of the larger watershed with the streams in the upper basin despite the high water table. Thus streamflow is episodic, with more than 95% generated by recent near-stream rainfall that temporarily raises the water table above the land surface near stream channels, and virtually no inter-event subsurface baseflow. In the lower basin, where the karst aquifer is unconfined, deeper water tables result in lower ET and higher groundwater

recharge. There is little surface connectivity between the watershed and streams in the lower basin and thus virtually all surface contributions to streamflow originate in the upper confined basin. However the high karst aquifer hydraulic conductivity results in extensive subsurface connectivity with the streams in the lower basin. As a result the majority of the streamflow in the lower basin is subsurface flow originating as diffuse infiltration through the epikarst, with the fraction of subsurface flow increasing from 52% in the upper portion of the UR to 77% at the outlet of basin.

Climatic variability was found to provide a secondary control on streamflow generation processes, resulting in significant seasonal and interannual variability in both the timing and sources of streamflow. In the upper confined basin stream flow occurs primarily as a result of extra-tropical cold fronts in the spring and tropical storms in the fall when ET fluxes are relatively low. Persistent summer streamflow only occurs in the confined basin when consecutive years of above average rainfall result in water storage in the region in excess of high summer evapotranspirative demand. In the lower basin the fraction of surface flow (i.e. flow contribution from the upper basin) ranges from 12% in late spring (May) to 55% in early spring and fall (March and September), and ranges from an annual average of 52% during periods of consecutive wet years to 23% during periods of consecutive dry years.

The ratio of surface water – groundwater contributions to streamflow estimated from EMMA were used to test the surface water - ground water dynamics simulated by ParFlow.CLM. Results indicated that the model accurately simulated both the timing and magnitude of the surface to groundwater mixing ratio response to storms at all UR stations. The model accurately simulated the dominant fraction of “new” surface water

during peaks of all storm events and the dominant fraction of “old” groundwater contributions from the UFAS during low flow conditions. However comparison of total surface water – groundwater contributions to streamflow estimated from EMMA to those simulated by ParFlow.CLM revealed that ParFlow consistently underestimates groundwater contribution to streamflow after wet antecedent hydrologic conditions. We hypothesize that is due to underprediction of interannual storage in the UFAS system, caused by errors in the representation of the extent, thickness and hydraulic conductivity of the IAS in both the Cody Escarpment and Wacassassa Flats regions of the domain.

These results underscore the usefulness of combining integrated hydrologic modeling with insights from data-driven EMMA to develop a quantitative, predictive understanding of surface water – groundwater flow dynamics within a complex eogenetic karst basin, and to indicate where additional field measurements may be necessary to refine geologic heterogeneity and to improve numerical model predictions. To the best of our knowledge this is the first time EMMA based hydrograph separation results have been used to evaluate the transient and spatially distributed river source water mixing dynamics simulated by a fully integrated hydrologic model for such a large and complex basin. In the next phase of this research we will use global sensitivity/uncertainty analyses (Saltelli et al., 2005) to confirm key model processes and parameters governing model prediction errors identified in this study. Data assimilation techniques such as Generalized Likelihood Uncertainty Analysis (Beven, 1993) or Ensemble Kalman Filtering (Graham and McLaughlin, 1991) will then be used

with new high frequency groundwater level, streamflow, and specific conductivity data taken at key locations in the basin to improve model parameters and predictions.

The fully integrated ParFlow.CLM model presented here represents a baseline scenario that provides a strong basis to quantitatively predict the impacts of major changes in landuse (e.g. wetlands and forests cleared for agricultural or urban development), water use and climate on stores, fluxes, flowpaths and travel times of water in the SFRB. These predictions are essential to inform holistic land and water resource planning in the region in order to provide reliable water supply for human uses as well environmental flows that are protective of aquatic ecosystems. Furthermore accurate predictions of surface versus groundwater contributions to streamflow will allow prediction of transport and transformations of ecologically relevant solutes such as carbon, nitrogen and phosphorus in the spring and river systems in the region.

Table 2-1. Summary of ParFlow input variables and their relevant source of information.

ID	Region	Parameter	Base Case	Reference
1	SAS[i]	porosity (-)	0.42	Rawls et al., 1982
2	SAS	hydraulic conductivity (m/hr)	0.83	averaged from Meyer et al. 2008
3	SAS	specific storage (-)	1.00E-04	default for the model
4	SAS	Vgalpha[vi] (m^{-1})	2.7	Meyer and Taira 2001
5	SAS	Vgn[vii] (-)	2	Meyer and Taira 2001
6	IAS[ii]	porosity (-)	0.39	Rawls et al., 1982
7	IAS	hydraulic conductivity (m/hr)	1.00E-09	extrapolated lowest value from Meyer et al. 20008
8	IAS	specific storage (-)	1.00E-04	default for the model
9	IAS	Vgalpha (m^{-1})	2.7	Meyer and Taira 2001
10	IAS	Vgn (-)	2	Meyer and Taira 2001
11	UFAS[iii]	porosity (-)	0.3	Langston et al. 2012
12	UFAS	hydraulic conductivity (m/hr)	9	averaged from Meyer et al. 2008
13	UFAS	specific storage (-)	1.00E-04	default for the model
14	UFAS	Vgalpha (m^{-1})	2.7	Meyer and Taira 2001
15	UFAS	Vgn (-)	2	Meyer and Taira 2001
16	Conduit	porosity (-)	0.3	same as UFL porosity
17	Conduit	hydraulic conductivity (m/hr)	270	two order of magnitude higher than UFL permeability
18	Conduit	specific storage (-)	1.00E-04	default for the model
19	CR[iv]	mannings n ($hr/m^{1/3}$)	6.14E-05	WRA 2007
20	UR[v]	mannings n ($hr/m^{1/3}$)	2.15E-05	WRA 2007

[i]SAS = Surficial Aquifer System

[ii]IAS = Intermediate Aquifer System

[iii]UFAS = Upper Floridan Aquifer System

[iv]CR = Confined Region

[v]UR = Unconfined Region

[vi]Vgalpha = Van Genuchten alpha

[vii]Vgn = Van Genuchten n

Table 2-2. Subsurface flow contributions as percent of total streamflow at river locations downstream of Cody Escarpment (CE).

Year	USGS 1898	USGS 1975	USGS 2500	USGS 2800
2000	-2	75	100	91
2001	-13	71	98	89
2002	-12	61	91	85
2003	-3	30	52	60
2004	-2	29	53	60
2005	-1	33	55	63
2006	2	49	76	77
2007	-6	75	99	91
2008	-7	46	73	75
Average	-5	52	77	77

Table 2-3. Annual total of major water balance components for the SFRB.

Flux/volume (mm)	2000	2001	2002	2003	2004	2005	2006	2007	2008
∆ Surface storage	-14	-8	18	22	47	46	-13	-11	14
∆ Subsurface storage	-105	-16	128	3	116	23	-216	-22	72
Surface runoff	-108	-103	-104	-197	-190	-213	-147	-107	-140
Rainfall	1029	1090	1321	1388	1523	1514	1011	1087	1314
Evapotanspiration	-953	-932	-986	-1021	-1020	-1058	-966	-925	-977
Subsurface boundary flow	-87	-79	-84	-146	-150	-174	-125	-88	-110

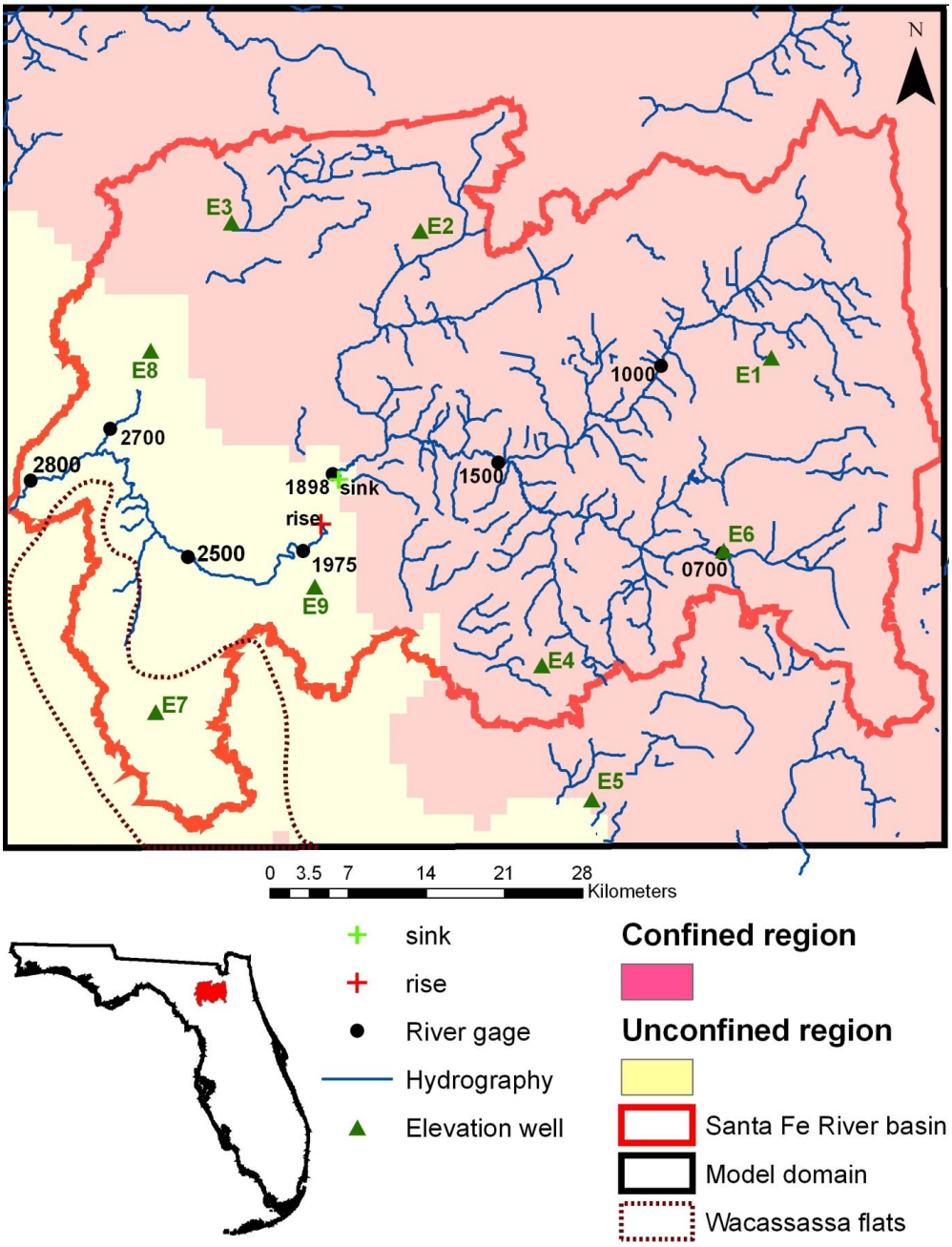

Figure 2-1. Map of the model domain. Also shown are the extents of the Santa Fe River Basin, locations of the river channels, monitoring wells, USGS stream gages and major hydrogeological regions in basin.

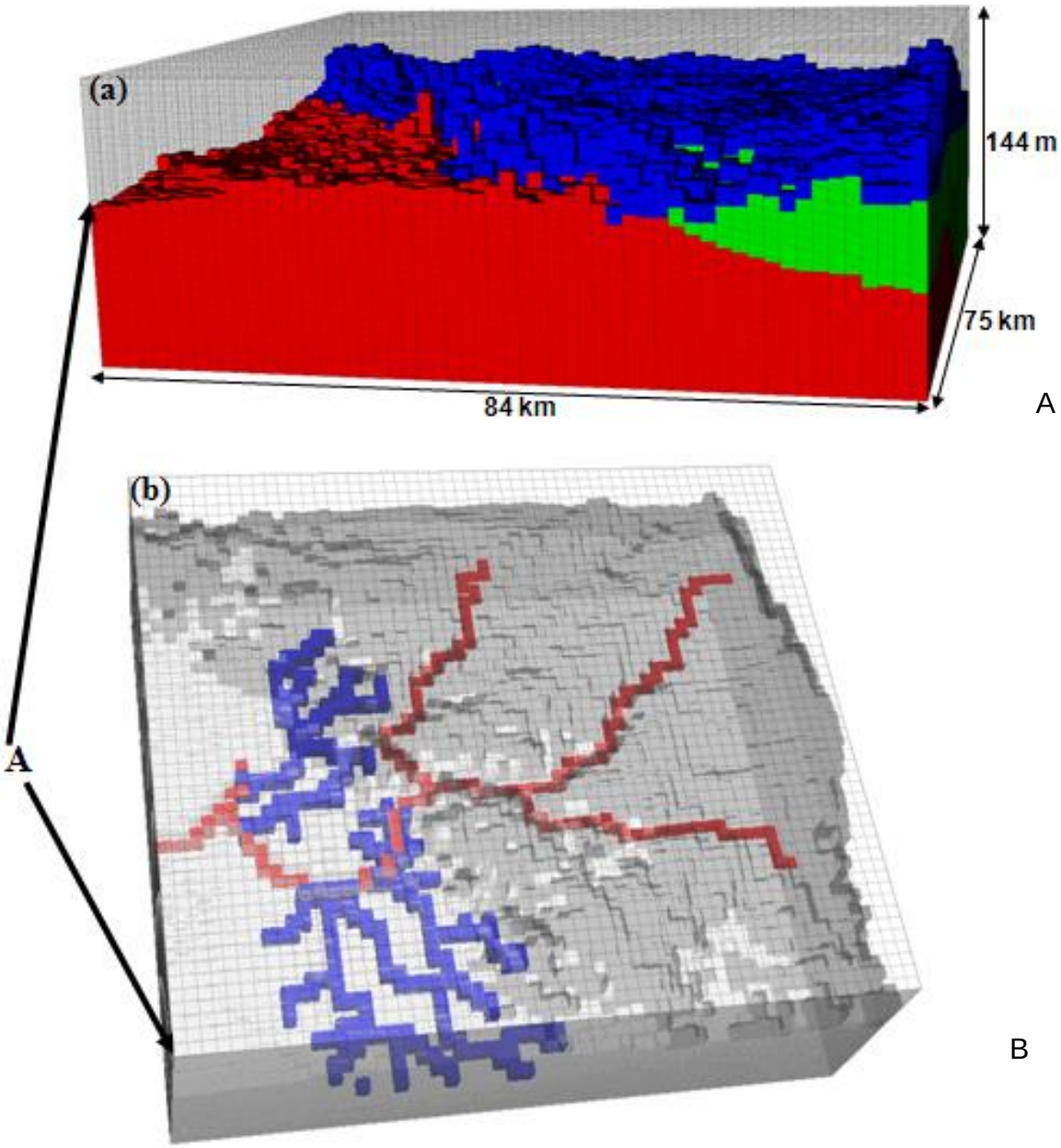

Figure 2-2. 3D mesh used to define the domain. A) the extent of the three major hydrogeological regions based on Floridan Aquifer Vulnerability Assessment (FAVA) dataset within the mesh along with their indicator variables, Surficial Aquifer System – blue region, Intermediate Aquifer System – green region, and Upper Floridan Aquifer System – red region. B) Locations of high hydraulic conductivity zones (blue cells) and main channels (red cells).

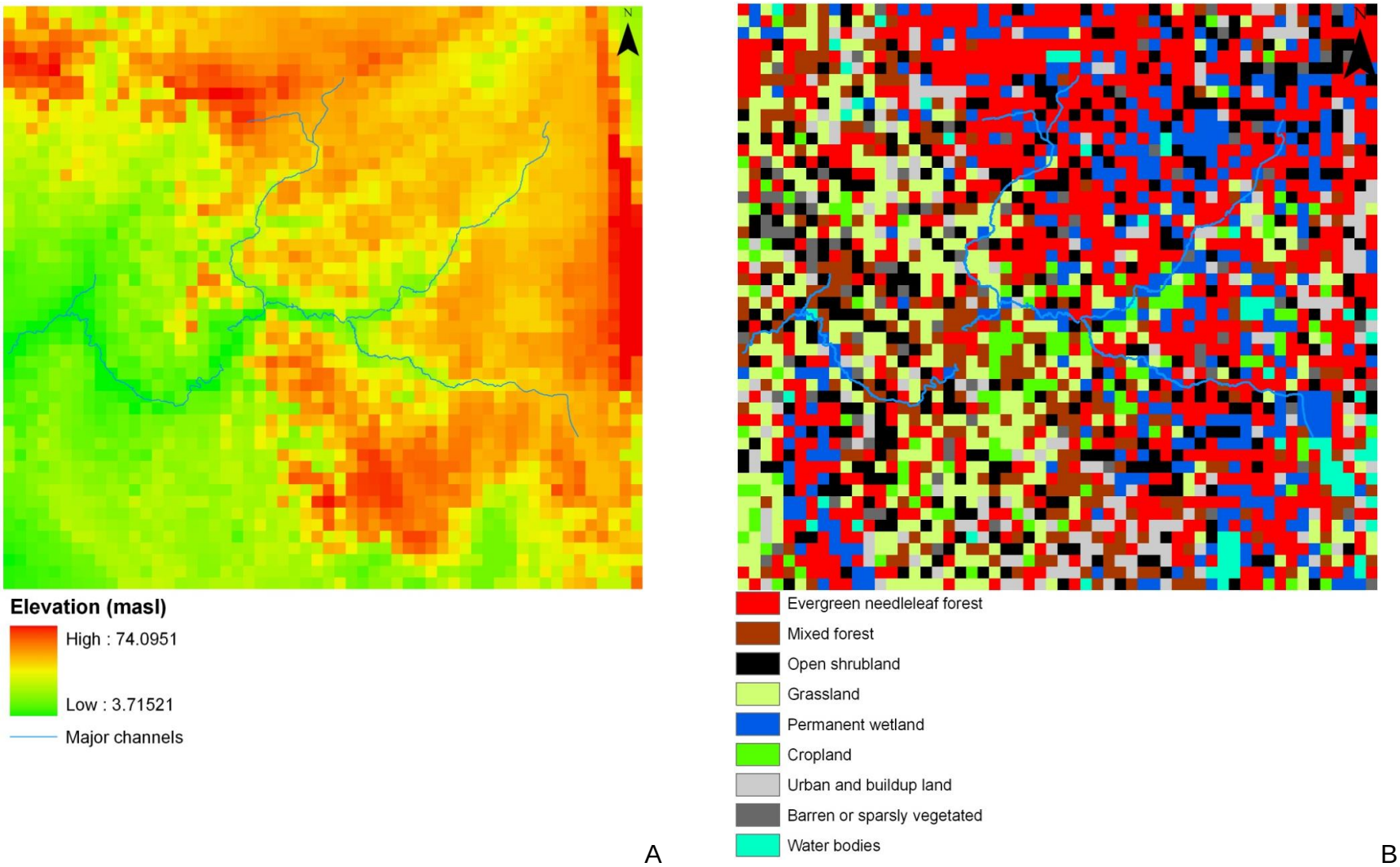

Figure 2-3. Spatial distribution of land surface properties over the SFRB. A) Elevation. B) Major landuse classes.

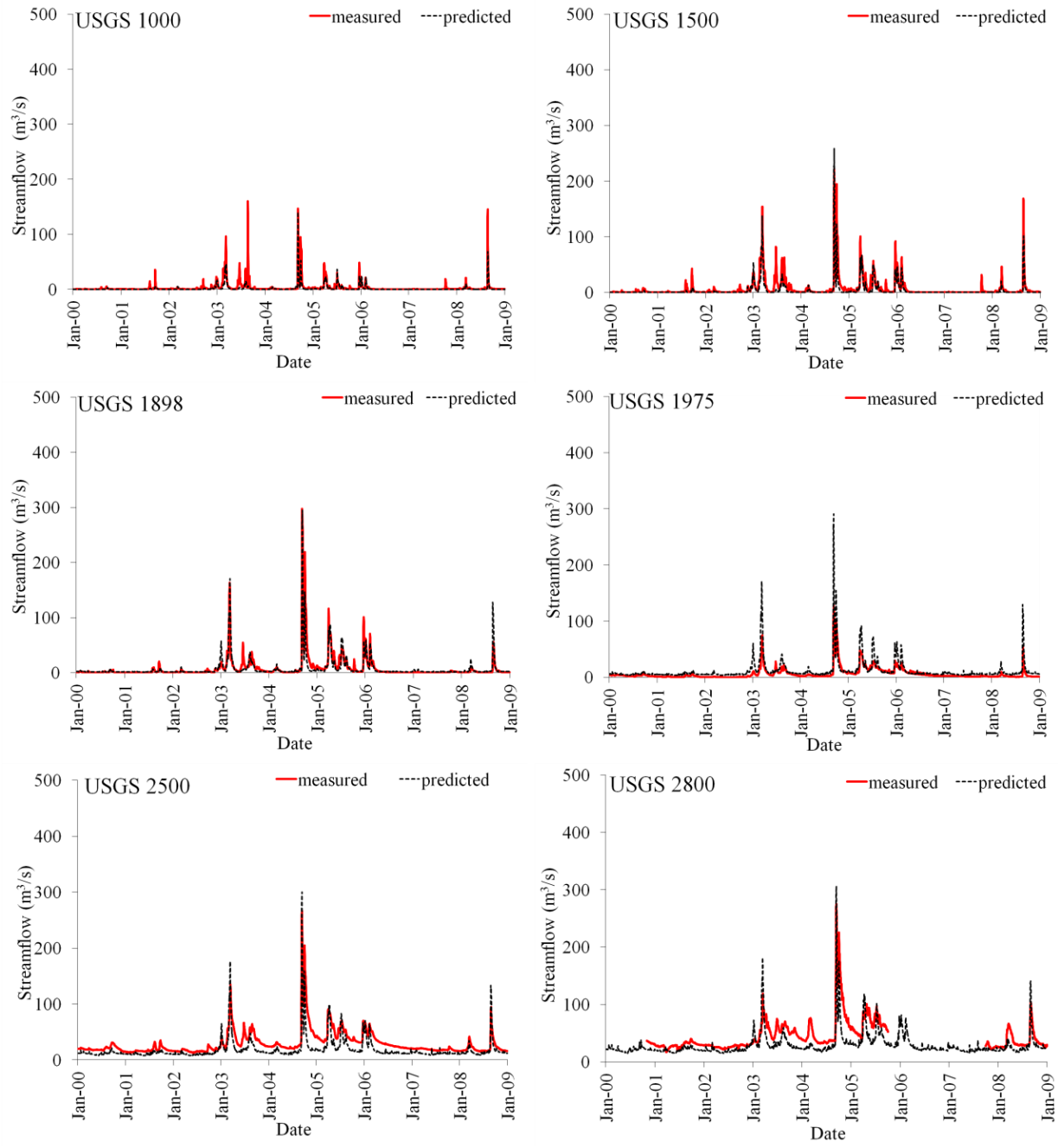

Figure 2-4. Comparison of observed and model predicted daily streamflow measurements at various streamgage locations across the domain.

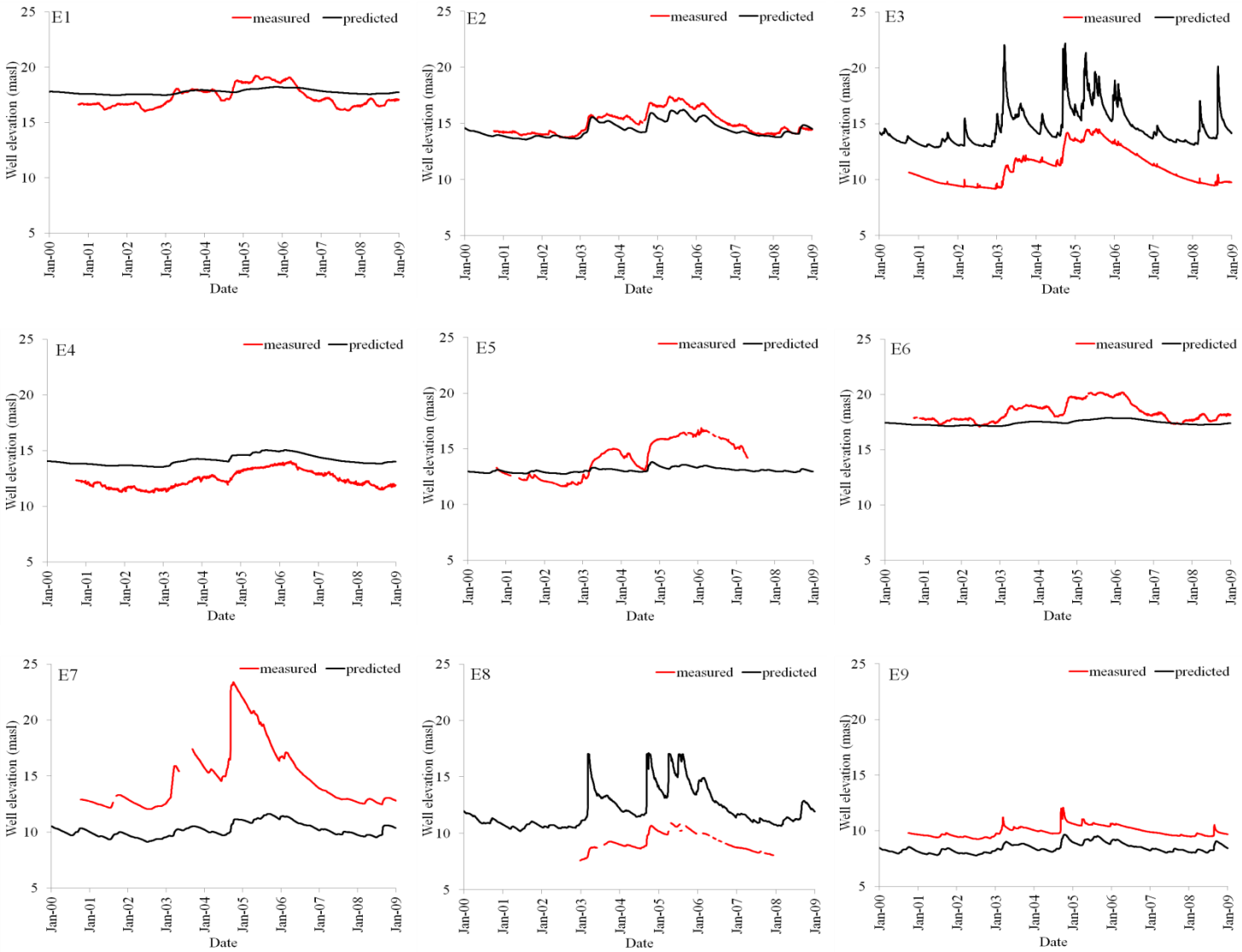

Figure 2-5. Comparison of observed and model simulated groundwater surface elevation at various locations across the domain. Wells 1 through 6 are in the Upper Confined Region (CR) and wells 7 through 9 are in the Lower Unconfined Region (UR).

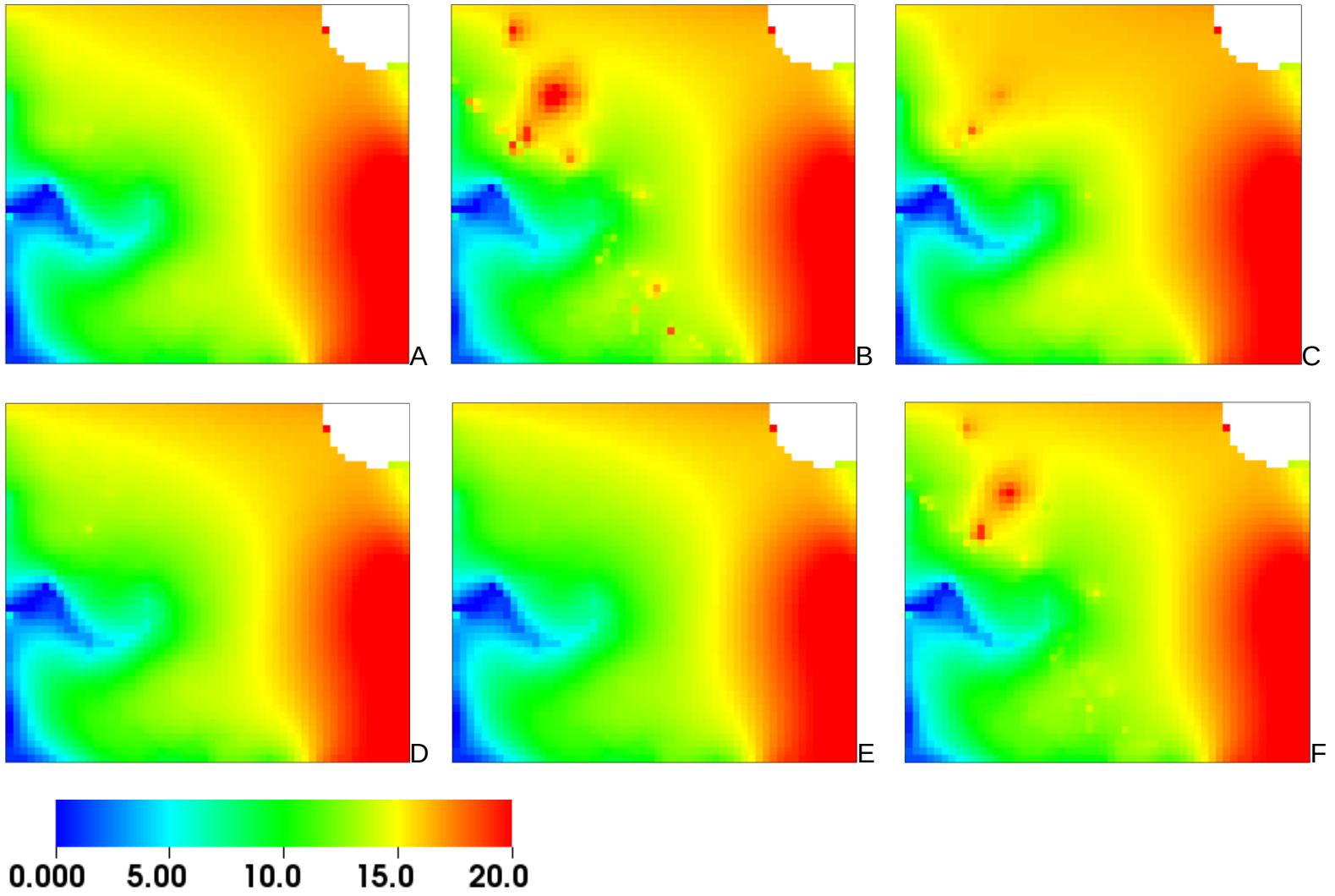

Figure 2-6. Potentiometric surface of UFAS with respect to mean sea level. A) pre- 2004 hurricane. B) peak during 2004 hurricanes. C) post- 2004 hurricanes. D) during dry period in 2006. E) during end of extended dry period of 2006-2007. F) peak during tropical storm Fay. Blank space on northeast corner of domain indicates that the UFAS is located at greater depth than the model domain.

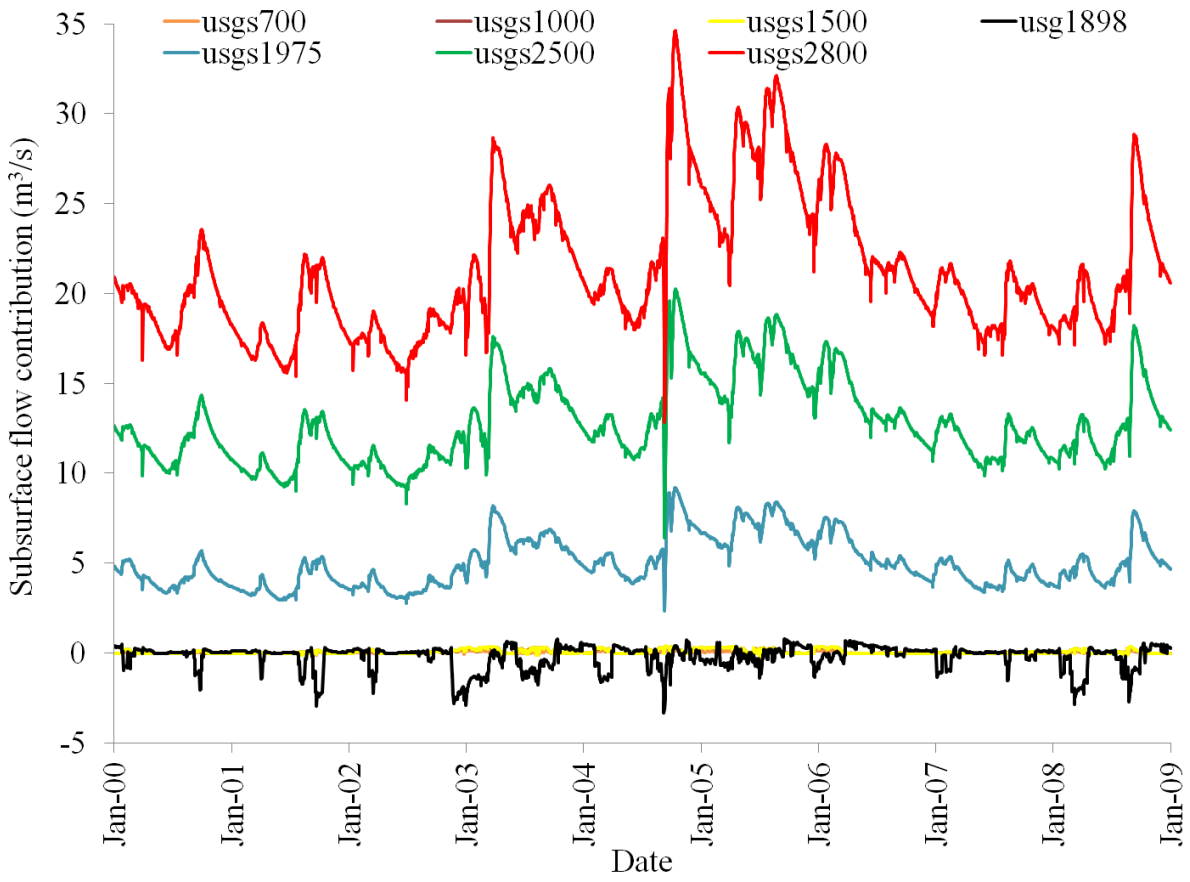

Figure 2-7. Time series of daily total subsurface flow contributions received by all the upstream river reaches from a given gage location. Note that time series for stations downstream to usgs1898 show only the daily subsurface flow contributions received downstream of usgs1898.

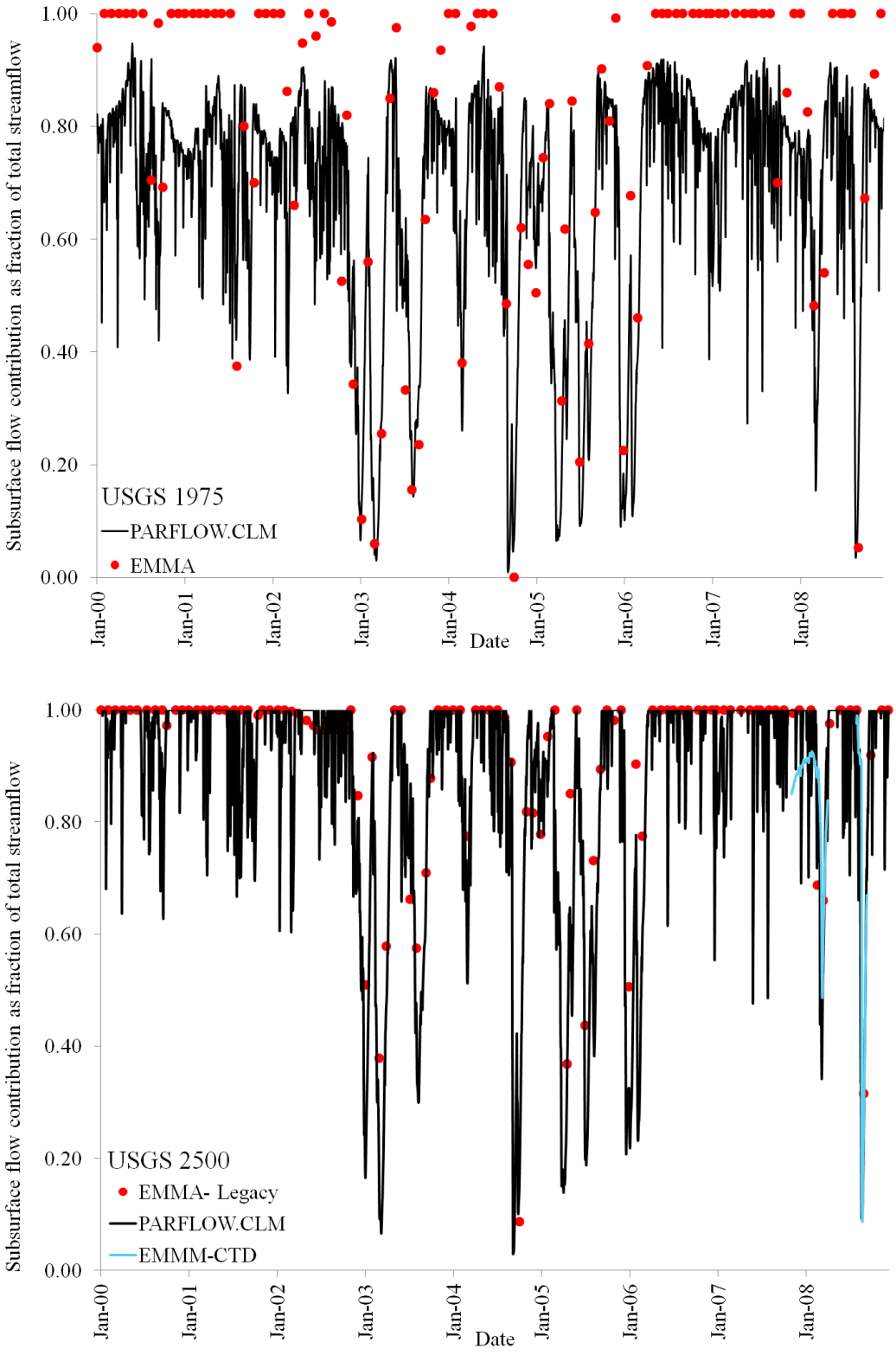

Figure 2-8. Comparison of EMMA based versus ParFlow.CLM simulated ratio of subsurface flow contributions to total streamflow at three UR river locations.

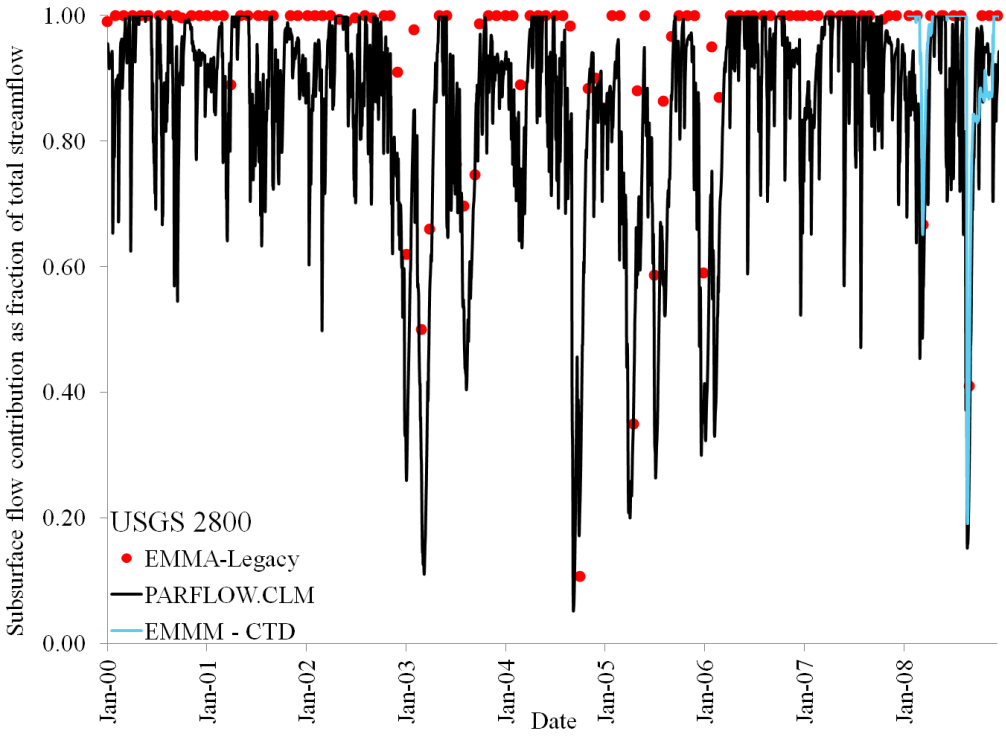

Figure 2-8. Continued.

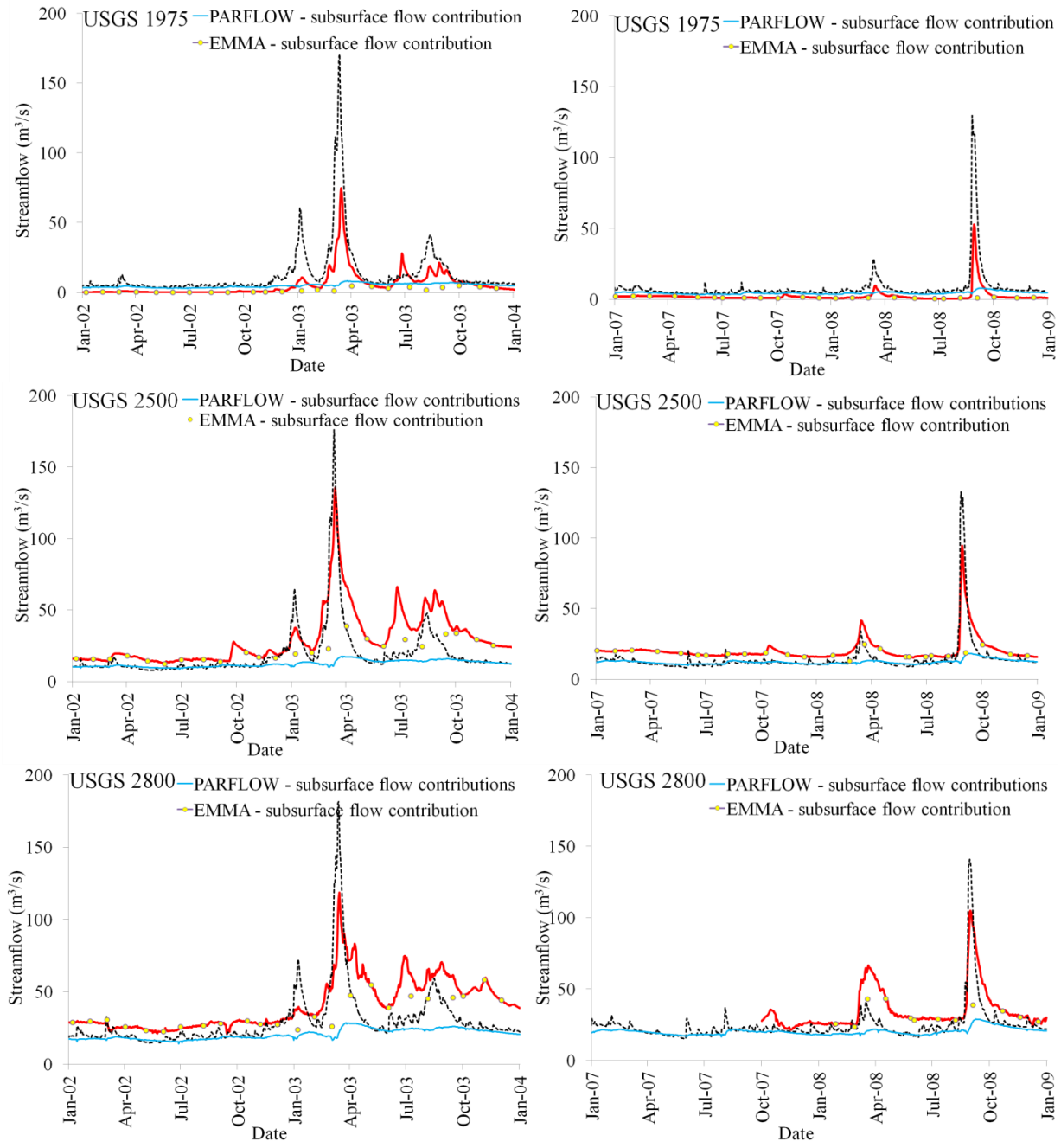

Figure 2-9. Comparison of measured and ParFlow.CLM predicted streamflow for calendar years 2002-2003 (left column) and 2007-2008 (right column). Also shown are EMMA estimated (yellow circles) and ParFlow.CLM predicted (light blue line) daily total subsurface flow contributions at three UR river locations.

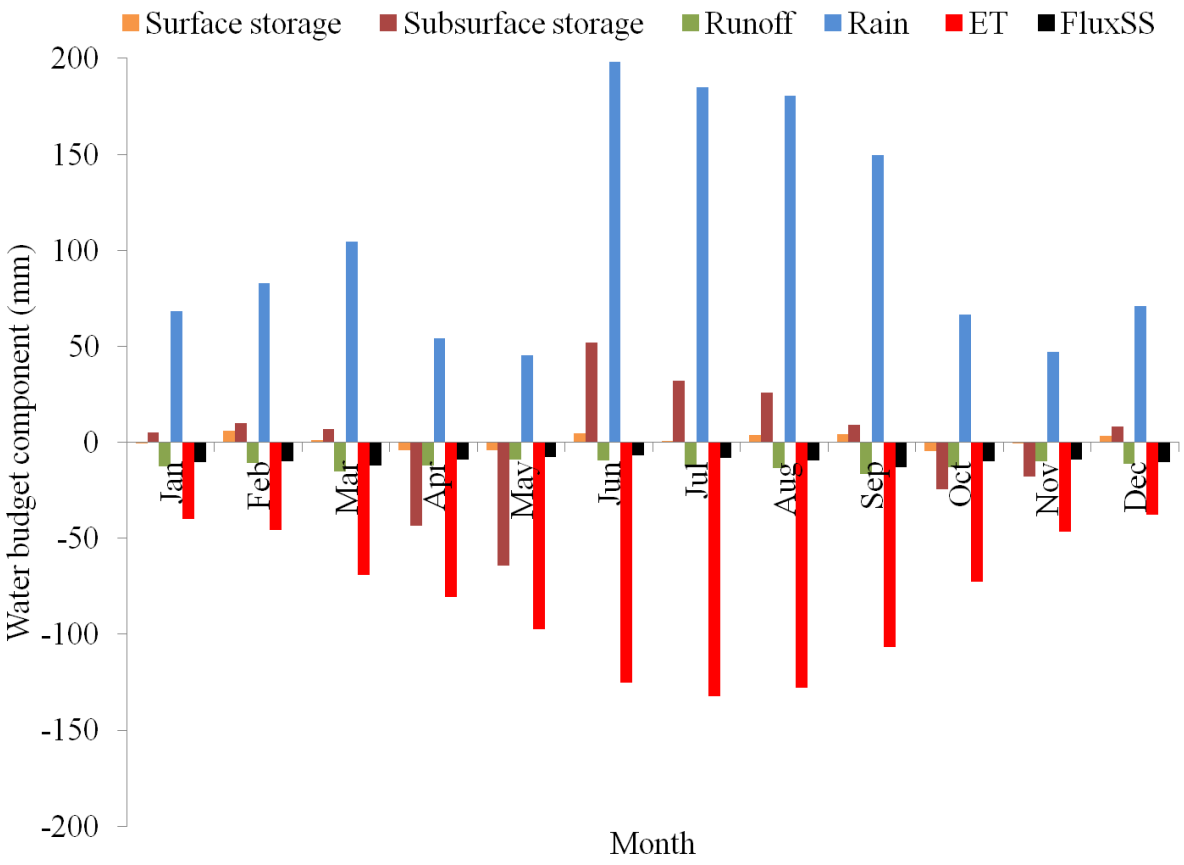

Figure 2-10. Monthly averaged water budget components for the study domain over entire simulation time period.

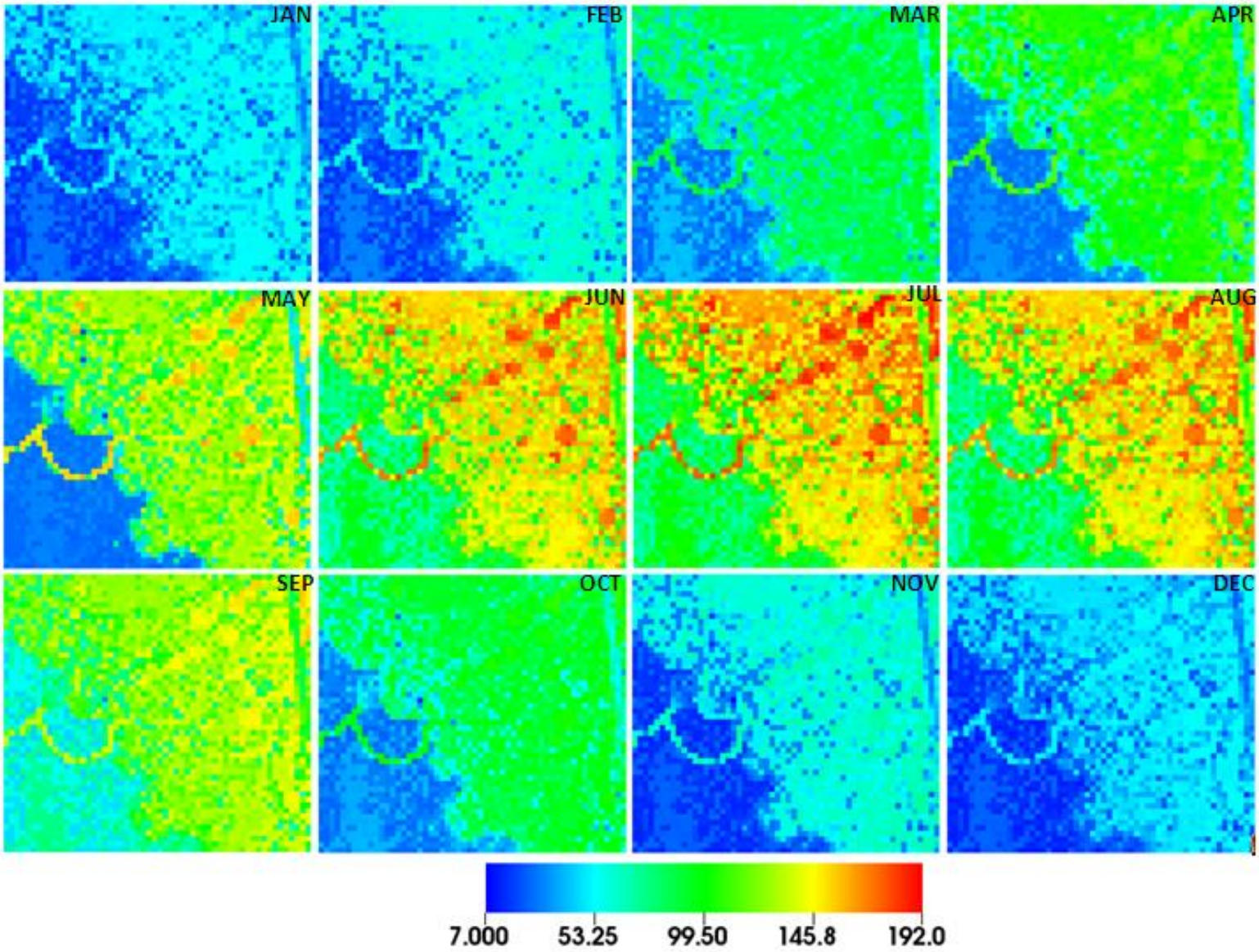

Figure 2-11. Spatial distribution of monthly averaged Evapotranspiration (ET; mm) across the study domain over entire simulation period.

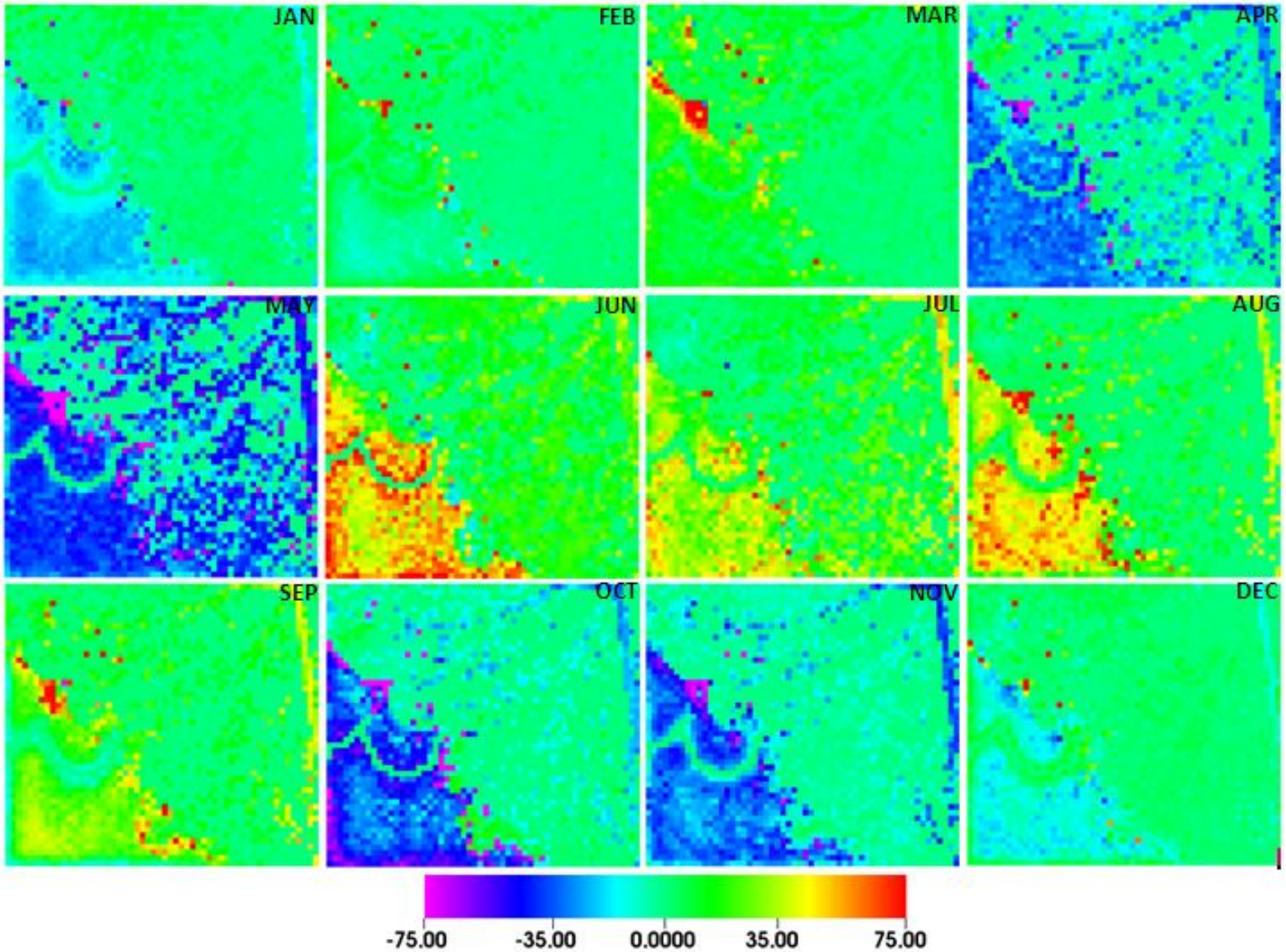

Figure 2-12. Spatial distribution of average monthly subsurface recharge (mm) across the study domain over the entire simulation period.

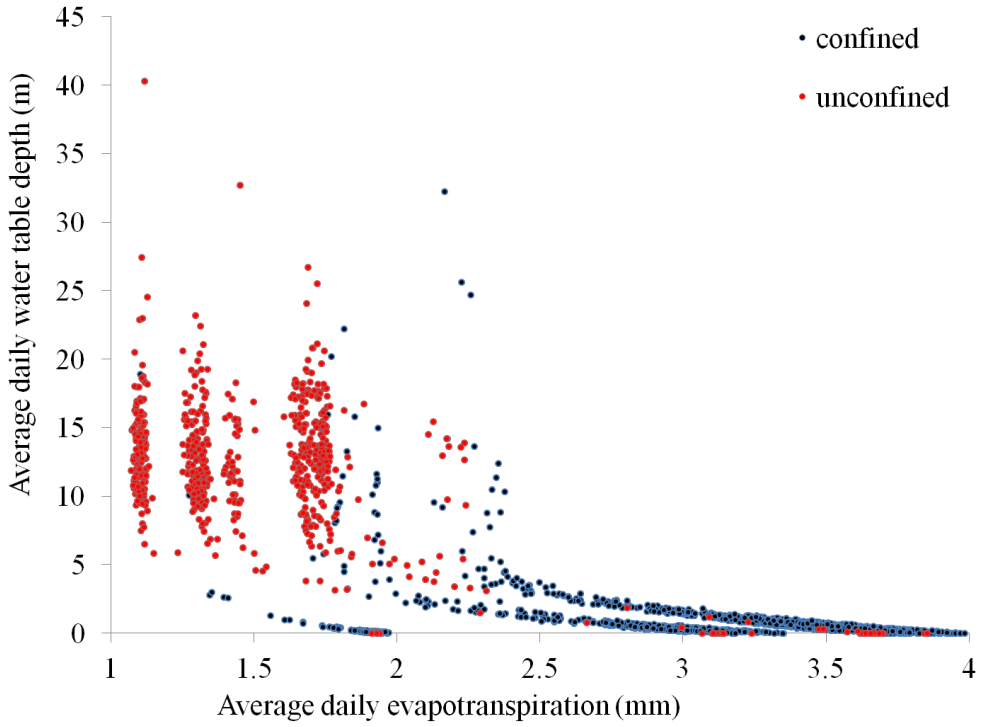

A

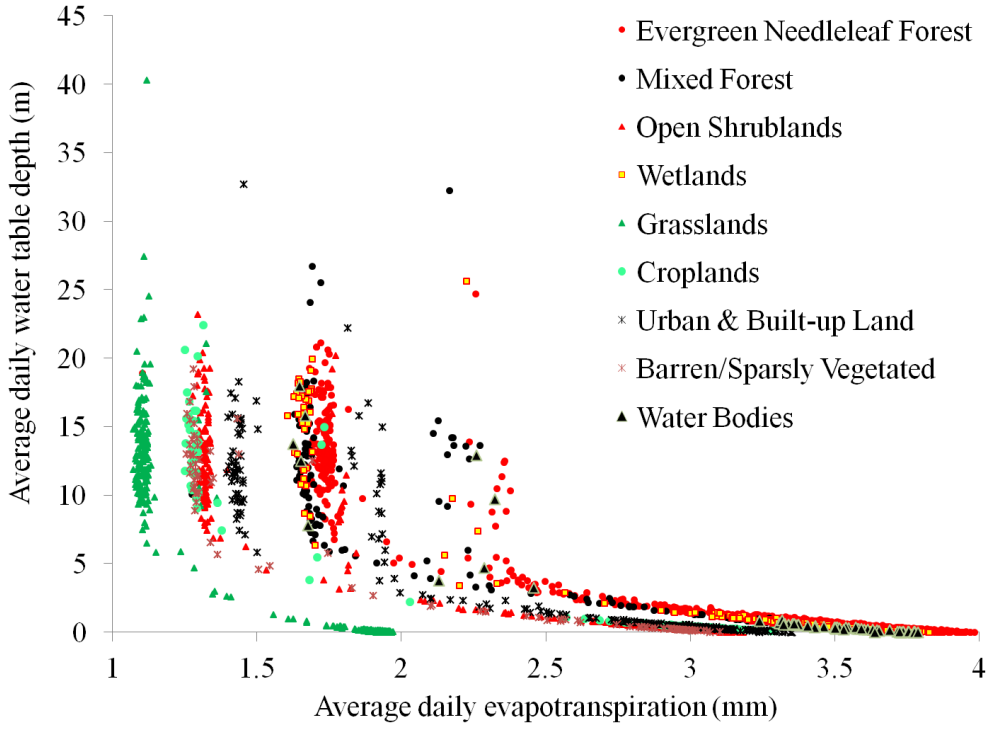

B

Figure 2-13. Controls on average daily ET (mm) and water table depth (m) dynamics in the SFRB. A) Geology. B) Landuse.

CHAPTER 3
GLOBAL SENSITIVITY ANALYSIS OF AN INTEGRATED HYDROLOGIC MODEL - INSIGHT ON GEOLOGIC AND VEGETATIVE CONTROLS OVER THE HYDROLOGIC FUNCTIONING OF A LARGE COMPLEX BASIN

3.1 Background

Increasing human impact on water resources has led to numerous studies on hydrologic functioning of large basins and more importantly on hydrologic system response to external stressors such as groundwater extraction, natural or synthetic contaminants, changes in climate and landuse conditions (Ferguson and Maxwell, 2010, Goderniaux et al., 2009, Bolger et al., 2011; Du et al., 2012). Establishing an accurate cause and effect relationship between any external stressor and corresponding hydrologic response in a basin requires an accurate accounting of dominant hydrologic processes as well as their spatiotemporal variations and interactions within the basin.

Hydrologic models are commonly used to test and improve our understating about dominant hydrologic processes within small to very large complex basins (Jones et al., 2008; Kollet and Maxwell, 2008a; VanderKwaak and Loague, 2001). Recent advances in hydrologic modeling have established significant feedback between surface water, groundwater and land surface processes (Ferguson and Maxwell, 2010; Goderniaux et al., 2009; Kollet and Maxwell, 2008a; Kollet and Maxwell, 2006) and thereby the need for integrated representation of various surface and subsurface flow processes that coexist within hydrologic systems. This integration is achieved by using highly complex and fully coupled hydrologic models (e.g. HydroGeoSphere, lnhm, ParFlow.CLM) which have high computational requirements. Moreover, the large number of inputs and complex mathematical algorithms within these fully integrated

models makes it difficult to identify parameters controlling dominant hydrologic processes simulated by the model and their interactions over space and time.

Sensitivity analysis (SA) is performed in hydrologic modeling studies to (1) gain insight on the working of complex models and identify dominant hydrologic processes within the study domain (e.g. Nossent and Bauwens, 2012); (2) identify parameters that have most influence over dominant hydrologic processes identified in step 1 (e.g. Francone et al., 2012); (3) help prioritize factors to be included (by process of factor fixing) in the parameter estimation or model optimization process so that computational resources are not exhausted on insensitive parameters (e.g. Linhoss et al., 2012); and (4) identify parameters that interact with other parameters in the coupled non-linear system (e.g. Linhoss et al., 2012). Studies introducing new SA techniques or applying existing techniques to range of hydrological problems are extensively documented (e.g. Linhoss et al., 2012; Muñoz-Carpena et al., 2007; Saltelli et al., 2004; Van Griensven et al., 2006). The need for cost effective SA and calibration of complex distributed models is also well documented (e.g. Foglia et al., 2009).

Despite the critical role that SA plays in the process of hydrologic model development and application, formal SA is often avoided in studies involving large-scale, fully integrated hydrological models primarily because of their extremely high computation cost. Instead, typically manual calibration and occasionally “one factor at a time” (OAT) SA are performed on these models. For example, Huntington and Niswonger (2012) manually calibrated the GSFLOW model for a 54 km^2 domain covering three snowmelt dominated watersheds in the Eastern Sierra Nevada. The model was then used to study the relationship between snowmelt timing and hydrologic

processes such as streamflow and groundwater recharge, and evapotranspiration losses. The modelers also evaluated the effect of variations in hydraulic conductivity on spatial distribution of groundwater head values. Jones et al. (2008) manually calibrated a steady state InHM model developed for the 75 km^2 Laurel Creek Watershed in Southern Ontario, Canada. Discrete groundwater heads at 50 observation wells were used to fit model simulated groundwater heads to field observations. However, no SA was performed on the model. Rihani et al. (2010) developed a ParFlow.CLM application for an idealized hillslope (5000 m x 100m x 80-310m). They executed 14 different model setups to study the effect of land cover, atmospheric conditions, and subsurface formation and terrain properties over major land surface and subsurface processes. Goderniaux et al. (2009) calibrated HydrogeoSphere model developed for 465 km^2 Geer basin, Belgium. No SA was performed on the model which was used to study the impact of climate change scenario on groundwater reserves.

SA methods can be classified into (1) local or OAT in which the value of one of the parameters is changed within the allowable parameter range (while keeping other parameters fixed) and the resulting change in model output is observed; (2) GSA methods (e.g. method of SOBOL (Sobol, 1993); extended Fourier Amplitude Sensitivity Test (FAST; Saltelli, 1999)) in which all the parameter values are changed simultaneously within the allowable parameter range and the resulting change in model output is observed. Both the methods have their merits and shortcomings. The OAT method is easy to implement however the sensitivity measure is for a single location within the entire parameter space and therefore does not account for parameter interactions which may lead to misleading results in highly nonlinear systems with

interacting parameters. The GSA methods randomly or systematically sample the entire parameter space and generate a large number of model input parameter combinations to overcome the abovementioned issues with OAT methods. However the large number of model runs needed in GSA methods can make them computationally prohibitive when evaluating fully integrated model for large basin.

Although providing qualitative results, global screening methods (e.g. Morris method, Morris, 1991 or Latin-Hypercube-One-factor-At-a-Time (LH-OAT) techniques, Van Griensven et al., 2006), are a more feasible option than quantitative GSA methods when dealing with computationally expensive models because of the considerably smaller number of model executions required to effectively identify the most sensitive parameters in the model (Yang, 2011). For example, Nossent and Bauwens (2012) conducted an extensive LH-OAT evaluation on a SWAT model developed for the 580 km^2 Klein Nete catchment. They used LH-OAT to better understand SWAT model parameters effecting flow and water quality processes. Francone et al. (2012) presented the first application of the Morris method on the land surface model-UTOPIA to investigate the influence of model input parameters such as leaf area index, maximum vegetation cover, and rooting depth on selected energy and hydrological budget components for a vineyard located in Cocconato, Northern Italy. Many studies have also demonstrated the use of global screening methods in a two step GSA and uncertainty analysis (UA) of hydrological and water quality models (Muñoz-Carpena et al., 2007; Yang et al., 2012; Linhoss et al., 2012). The two steps used in these studies involved (1) use of a screening technique such as Morris method (e.g. Muñoz-Carpena et al., 2007; Yang et al., 2012) to identify the most important parameters and reduce the

dimensionality of the parameter space by the process of factor fixing; and (2) further investigation of the shortlisted parameters using a quantitative and more exhaustive GSA approach such as a variance based technique (e.g. Muñoz-Carpena et al., 2007 used extended the FAST).

In this paper we apply the GSA screening technique developed by Morris (Morris, 1991) to the integrated hydrologic model ParFlow.CLM (Ashby and Falgout, 1996; Kollet and Maxwell, 2006; Maxwell and Miller, 2005), previously developed for the Santa Fe River Basin (SFRB) North-Central Florida USA (Srivastava et al., 2013a), to investigate the sensitivity of predictions to uncertainties in a wide range of parameters governing coupled surface, subsurface and land-atmosphere processes in the basin. The Morris method was selected over other GSA techniques because of the extremely high computation requirements of the ParFlow.CLM application built for the SFRB (discussed later in this paper).

The previously developed application of ParFlow.CLM for the SFRB (hereafter referred to as the baseline model) accurately reproduced regional and seasonal patterns of evapotranspiration, streamflow and groundwater elevation, as well as surface-groundwater mixing ratios in the UR of the basin. However, it consistently underpredicted streamflow-recession and baseflow at unconfined river locations. The specific objectives of this study were to (1) investigate the sensitivity of hydrologic processes throughout the basin to vegetation, land surface, soil and geologic parameter uncertainty during both flood and base flow conditions; (2) identify the most sensitive and interactive parameters governing surface and groundwater flow, particularly for streamflow recession and groundwater-surface water interactions in the UR of the

basin; (3) identify ranges of sensitive parameter values for the subset of models that performed satisfactorily throughout the basin over the study period; and (4) make recommendations for the design of more computationally-intensive spatially-distributed parameter estimation studies and field measurement campaigns to improve model predictions.

3.2 Methods

3.2.1 Hydro-Geologic Characteristics of the Santa Fe River Basin

The SFRB is a mixed-use basin with a drainage area of about 3700 km^2 covering nine counties in North-Central Florida. The basin spans three distinct yet linked hydrogeologic regions (Figure 3-1;Schneider et al., 2008) known as the confined region (CR), semi-confined region (SCR) and the unconfined region (UR). The three regions are named based on the degree of confinement of the Upper Floridan Aquifer System (UFAS), a regional aquifer system comprised mostly of limestone, that underlies the entire study area (see red region Figure 3-2A). The degree of confinement exerts important control over both the regional surface and groundwater system flow dynamics. Table 3-1 summarizes the physical attributes of the basin relevant to this study.

In the CR the UFAS is overlain with a thick clay-rich confining unit (the Intermediate Aquifer System, IAS, depicted as the green region in Figure 3-2A), and the Surficial Aquifer System (SAS) which consists of unconfined, saturated sands (Schneider et al., 2008; depicted as the blue region in Figure 3-2A). Poorly drained conditions in the CR result in shallow water table depths and well developed network of surface channels and wetlands. Annual average recharge from the SAS to the confined UFAS is estimated to be less than 0.3 m/year (Schneider et al., 2008).

In the UR, where the confining unit on top of the UFAS is completely eroded, limestone rocks are overlain with thin layer of sand which results in direct rapid recharge of the UFAS by infiltrating rainwater (Arthur, 2005). There are virtually no surface streams feeding the main river in this region, however the aquifer is known to have major conduits which create an internal subsurface drainage network connected to the river (Meyer et al., 2008; Upchurch, 2007). Unlike teleogenetic karst systems with low intergranular porosity, the eogentic karst features in Florida have retained high matrix porosity (Vacher and Mylroie, 2002; Florea and Vacher, 2007). As such, primary matrix porosity in the SFRB plays an important role in water storage, flow through the subsurface environment, and exchange with the river system.

The region that marks the transition from confined to unconfined conditions (known as the Cody Escarpment, CE) is characterized by the presence of numerous sinkholes, sinking streams, siphons, springs and other karst features which have the potential to rapidly recharge the UFAS (Upchurch, 2007). During baseflow conditions the upper Santa Fe River (SFR) is captured in its entirety by the SFR Sink in the CE region. The river emerges from the SFR Rise, located approximately 6 km downstream of the sink, as a first order magnitude spring. Hydrological behavior of the river in the transition zone is highly dynamic with no flow entering the sink during extreme drought conditions and with a portion of the river occasionally bypassing the sink as overland flow to the lower SFR during large flood events. Note that in some regions of the SFRB the UFAS is mapped as semi-confined (SCR) because of a leaky or discontinuous IAS (Schneider et al., 2008; see area enclosed by green lines in Figure 3-1). The recharge

to the UFAS is highly variable in these regions and is focused mainly around sinkholes and swallets.

3.2.2 Integrated 3D Model – ParFlow.CLM

In this study we used the fully-integrated surface water-groundwater-land surface process model ParFlow.CLM (Maxwell and Miller, 2005; Kollet and Maxwell, 2006; Ashby and Falgout, 1996; Jones and Woodward, 2001) to simulate hydrologic conditions within the SFRB. Here we present a brief summary of equations used by the model that are relevant to this study. Full details on model physics and how the surface and subsurface components are integrated can be found in the references cited above.

Variably saturated groundwater flow is simulated by ParFlow, which solves the 3D Richards equation using a cell-centered finite difference scheme in space and an implicit Euler scheme in time (Eq 3-1). Surface flow simulations and routing are performed by solving the 2D Kinematic wave equation (Eq 3-2) and Manning's equation (Eq 3-3). Surface and subsurface equations are integrated using a free surface overland flow boundary condition.

$$S_S S_w(\psi_p)\frac{\partial \psi_p}{\partial t} + \phi\frac{\partial S_w(\psi_p)}{\partial t} = \nabla.[k(x)\, k_r(\psi_p)\nabla(\psi_p - z)] + q_s \tag{3-1}$$

$$-k(x)\, k_r(\psi_o)\nabla(\psi_o - z) = \frac{\partial \|\psi_o, 0)\|}{\partial t} - \nabla\cdot\vec{\upsilon}\|\psi_o, 0\| - q_r(x) \tag{3-2}$$

$$\upsilon_x = \frac{\sqrt{S_{f,x}}}{n}\psi_o^{2/3} \qquad \upsilon_y = \frac{\sqrt{S_{f,y}}}{n}\psi_o^{2/3} \tag{3-3}$$

Where ψ_p is the subsurface pressure head [L]; $S_w(\psi_p)$ is the degree of saturation [-] represented as function of ψ_p as defined by van Genuchten model (Van Genuchten, 1980); S_s is the specific storage [L^{-1}]; ϕ is the porosity [-]; k(x) is saturated hydraulic

conductivity [LT^{-1}]; k_r is the relative permeability as a function of subsurface pressure head[-]; z is depth below the land surface [L]; q_s is a general source/sink term [T^{-1}]; q_r represents rainfall and evaporative fluxes [LT^{-1}]; ||A,B|| indicates the greater of A and B; $S_{f,x}$ and $S_{f,y}$ are the friction slopes in x and y direction [-]; n is the Manning's coefficient [$TL^{-1/3}$]; an **v** is the depth averaged velocity vector of surface runoff [LT^{-1}]; ψ_o in Eqs. (3-2) and (3-3) is the pressure head or water ponding depth at the land surface [L].

The coupled land surface energy and water balance is simulated by a modified version of the Common Land Model (CLM (Dai et al., 2003)) that is incorporated in ParFlow. CLM and it requires hourly atmospheric variables such as precipitation, air temperature, pressure, wind speed, specific humidity, and solar radiation, along with soil moisture estimates (which are provided by ParFlow) to simulate near land surface-atmospheric fluxes such as evapotranspiration loss (Kollet and Maxwell, 2008a). Details of equations used in CLM to simulate all the water and energy fluxes are provided elsewhere (Dai et al., 2003; Kollet et al., 2009; Maxwell and Miller, 2005). Equations relevant to work presented here are summarized in the following.

Energy balance equation for any given point in a basin is given by

$$R_n(\theta) = LE(\theta) + H(\theta) + G(\theta) \quad (3\text{-}4)$$

where R_n is net radiation at the land surface (W/m^2); LE is latent heat (W/m^2), H is sensible heat flux (W/m^2), and G is the ground heat flux (W/m^2). The water balance in the subsurface environment and the energy balance at the land surface are coupled together via the soil moisture content at or close to ground surface (θ; kg/kg). Each of the terms on the right hand side of Eq. (3-4) are independently calculated by CLM using

atmospheric forcing, soil, vegetation characteristics, and soil moisture provided by ParFlow. LE is calculated as:

$$LE = L_v E \tag{3-5}$$

$$E = E_c + E_g \tag{3-6}$$

where, L_v is latent heat of evaporation (J/kg) and E is the sum of evaporative fluxes from the foliage (E_c (kg/m^{2}s), if vegetation is present) and ground E_g (kg/m^{2}s). Evaporative fluxes from the ground are calculated as:

$$E_g = \rho_a \frac{(q_g - q_a)}{r_d} \tag{3-7}$$

Where ρ_a is the intrinsic density of air (kg/m^3); q_g is the air specific humidity at the ground surface (kg/kg); q_a is the air specific humidity at reference height z_q obtained from atmospheric forcing (kg/kg); r_d is the aerodynamics resistance at z_q (s/m). Evaporative fluxes from the foliage are estimated as the sum of evaporative flux from wet foliage E_w (kg/m^{2}s) and total transpiration flux E_{tr} (kg/m^{2}s) from the root zone cells:

$$E_c = E_w + E_{tr} * \sum f_{root,j*} \tag{3-8}$$

$$E_w = \sigma_f \, L_{SAI} \, [1 - \delta(E_f^{pot})(1 - \tilde{L}_w)] E_f^{pot} \tag{3-9}$$

$$E_{tr} = \sigma_f L_{SAI} \, \delta(E_f^{pot}) L_d \frac{r_b}{(r_b + r_s)} \tag{3-10}$$

Where $f_{root,j*}$ is effective root fraction in root zone layer j

$$f_{root,j*} = \frac{f_{root,j} \, w_{LT}[j]}{\sum f_{root,i} \, w_{LT}[i]} \tag{3-11}$$

$$w_{LT}[i] = \frac{\theta_i - \theta_{wp}}{\theta_{fc} - \theta_{wp}} \tag{3-12}$$

$$f_{root,j} = 1 - 0.5[\exp(-az) + \exp(-bz)] \quad (3\text{-}13)$$

Where σ_f is the vegetation fraction (-); L_{SAI} is the stem plus leaf area index (-); δ is the step function (one for positive and zero for zero and negative arguments); E_f^{pot} is the potential evaporation from wet foliage (kg/m^{2}s); $\tilde{L}_w$ is the wetted fraction of the canopy (-); L_d is the dry fraction of foliage surface (-); r_b is the conductance of heat and vapor flux from leaves (s/m); and r_s is the stomatal resistance (s/m). θ_i, θ_{fc}, and θ_{wp}, respectively, are soil moisture content in layer i, moisture content at field capacity, and permanent wilting point; $f_{root,j}$ is root fraction parameter which varies exponentially with the depth from land surface z (-) in root zone layer j; a and b are coefficients dependent upon vegetation type. In ParFlow.CLM the term q_s in subsurface mass balance equation (Eq. (1)) is expressed as

$$q_s = LE(\theta) + q_g(\theta) \quad (3\text{-}14)$$

Where q_g (s^{-1}) is the flux of water infiltrating at the land surface after accounting for precipitation, canopy throughfall, and/or surface runoff.

3.2.3 Baseline Model

The baseline scenario for the GSA was established using the ParFlow.CLM model for an area that covers and extends beyond the topographic boundaries of the SFRB to include major springsheds that are known to contribute subsurface flow to the river in the UR of the SFRB (Figure 3-1; Srivastava et al., 2013a). From here on any reference to SFRB implies the extended boundary study domain shown in Figure 3-1. The land surface elevation in the model domain ranges from about 4 m to 74 m above mean sea level, resulting in a maximum domain depth of 144m. The bottom of the domain was set at 70 m below mean sea level to include the top of the active

subsurface zone believed to contribute flow to the SFR. A lateral discretization ($\Delta x = \Delta y$) of 1500 m and vertical discretization (Δz) of 1 m was used to discretize the domain resulting in 56x50x144 cells, in x, y, and z dimensions, respectively. Thus the domain included a total of 403,200 rectilinear elements covering a total land surface area of 6300 km^2 (Figure 3-1). Table 3-2 summarizes the spatial input data used to develop ParFlow.CLM for the SFRB. Conduit locations were taken from Meyer et al. (2008) and were assumed to be 10m in height and to occur between depths of 5 m to 15 m below mean sea level based on previous field investigations (Langston et al., 2012). Since ParFlow does not contain algorithms for turbulent conduit flow, conduits were represented as high hydraulic conductivity zones in this study (Ando et al., 2003; Tsang et al., 1996). This assumption should be reasonable given the goal of the study is to assess the influence of these high hydraulic conductivity zones on seasonal hydrologic budgets and large-scale streamflow and groundwater interactions in the basin. The subsurface environment was assumed to be isotropic and homogeneous within each aquifer type (SAS, IAS, UFAS, conduits). The model was parameterized using literature values or values estimated based on previous groundwater flow modeling in the basin (see references in Tables 3-3 and 3-4). In the absence of study area specific information, default values of CLM related vegetation parameters were used in the model. Table 3-5 summarizes information related to the baseline model's initial and boundary conditions.

To minimize the influence of initial condition assumptions the baseline model was spun up by repeatedly simulating 9 years (years 2000 through 2008) of hydrological conditions within the basin. Spatially distributed hourly North American Land Data

Assimilation System (NLDAS) forcing data was used to drive the model until a quasi dynamic equilibrium was reached, i.e. until the difference between the beginning and ending subsurface water storage (over the 9 year period run) dropped to less than <0.05 % of average subsurface storage and the simulated streamflow and groundwater elevations time series at multiple locations across the domain showed minimal visual difference between two consecutive 9 year runs. These criteria were met by the end of the second 9 year simulation period, thus all the baseline model results presented in this paper are the model results obtained from round 3 of model spin-up.

3.2.4 Morris Screening Method

The Morris method is a so called "elementary effect method" introduced by Morris (Morris, 1991). In Morris method, the region of experimentation, Ω, is a k-dimensional p-level grid (Campolongo et al., 2007); k being the number of independent parameters included in the analysis (i.e. the model requires an input parameter vector $\boldsymbol{\theta}_i$ with i=1,2…..k) and p is the number of levels selected to span the specified value range for each parameter. Between consecutive model executions in the GSA only one parameter value is changed and the corresponding change in model output is observed. This individual change in model output (y) in response to a change in the i^{th} parameter value in $\boldsymbol{\theta}$ is known as the elementary effect (EE) of the i^{th} input on output y and is calculated as:

$$EE_i = \frac{\left[y(\theta_1, \theta_2 .....\theta_i + \Delta_i, ...\theta_k) - y(\theta_1, ...\theta_k)\right]}{\Delta} \tag{3-15}$$

Where Δ is a value in {1/(p-1),……..1-1/(p-1)}. For this study p = 8.

A finite sample of EE_i is obtained by randomly sampling different $\boldsymbol{\theta}$ from Ω. In the end, two Morris sensitivity indexes i.e. the mean (μ) and standard deviation (σ) of the of

EE_i samples are calculated. A large value of μ indicates an important influence of the corresponding input on model output and a large value σ indicates that the corresponding input exerts a non-linear effect on model output or is involved in interactions with other model parameters (Saltelli et al., 2004). Campolongo et al. (2007) proposed an improvement in the estimate of μ index of Morris by averaging the absolute values of the elementary effects (μ*) to eliminate the effect of opposite signs in non-monotonic models. Also, the new index μ* was shown to be an acceptable substitute for variance based total index (Campolongo et al., 2007). In this paper we have presented all the results using μ* which we refer to in the following as the Morris mean.

3.2.5 GSA Experiment Design

A total of 19 ParFlow and 14 CLM related parameters were considered in the GSA. The number of simulations required in Morris Analysis is given by:

$$N = r(k+1) \tag{3-16}$$

Where r is the sampling size for search trajectory and r = 10 used in this study is known to produce satisfactory results (Carpena et al., 2010) and k is the number of parameters (33 in this study). This resulted in a total of 340 model runs (see Tables 3-3 and 3-4). All ParFlow parameters for each geological region represented in the baseline model were included in the GSA. However due to the large computational requirement to execute a single ParFlow run (discussed in the end of this section), and the fact that CLM parameters varies with the 9 vegetation types occurring in the region, a reduced set of CLM vegetation parameters was obtained by (1) fixing the values of insensitive parameters (to their respective default values) based on results from a OAT SA performed on all CLM parameters for ParFlow.CLM simulations on a single

homogeneous soil column; and (2) limiting the analysis to only the vegetation parameters corresponding to major land cover types found in the basin (i.e. evergreen needleleaf forests (31%), grasslands (14%), open shrublands (13%), upland mixed forests (11%) , isolated wetland and floodplain mixed forests wetlands and water (13%)). All the CLM input parameters related to energy budget calculations were fixed to their default values.

The Morris method based sampling scheme in Simlab 2.2 software was used to generate 340 different combinations of parameter values using ranges summarized in Tables 3-3 and 3-4. The ranges of ParFlow parameter values used were based on the published literature or estimated from previous modeling studies in the SFRB. In absence of reliable basin specific information, CLM parameters were generated using a ±50% variation in their default values.

The pressure head distribution from the last time step of the baseline model was used to initialize each of the 340 models which were run for a four year simulation period, 1/1/2000 through 12/31/2003. To minimize the transient effect of change in parameter values from the baseline model values, we analyzed the model simulated outputs for only the last 15 months out of the total simulation period. This period includes a significant storm event during 2/1/2003-5/30/2003, well defined pre-storm low baseflow conditions during 10/1/2002 – 1/31/2003, and a variable post storm period (6/1/2003 – 12/31/2003). This period excludes the extreme hurricane, tropical storm, and drought events that occurred during years 2004 through 2008 in the baseline model to eliminate any possible bias in the analysis produced by unusual hydrologic conditions during these extreme events. The output variables assessed in the sensitivity analysis

are summarized in Table 3-6. Streamflow was assessed at 6 locations, and UFAS groundwater elevations were assessed at 10, where observations were available (Figure 3-1). Five out of the ten output variables (peak flow, flow ratios 1-3, and maximum streamflow loss to the subsurface) were studied for the storm event that occurred during 10/1/2002 – 5/31/2003 (Figure 3-3). Groundwater flow contributions to streamflow were assessed only at three unconfined river locations. ET estimates were assessed for the two major contrasting geological regions.

3.2.6 Measures of Goodness of Model Fit

In addition to calculating the elementary effect of each parameter for each selected model output, we calculated goodness of fit measures for streamflow and groundwater level predictions at each of the observation locations for each of the 340 model runs. We used the Nash Sutcliffe model efficiency coefficient (NSC, Eq 3-17; Nash and Sutcliffe, 1970) for streamflow and log-streamflow to evaluate goodness of fit for high streamflows and low streamflows, respectively. For groundwater elevations we used the coefficient of determination (R^2, Eq 3-18; Legates and McCabe, 1999) and percent bias (PBIAS, Eq. 3-19; Gupta et al., 1999) to evaluate goodness of fit.

$$NSC = 1 - \left[\frac{\sum_{i=1}^{n} \left(Y_i^{obs} - Y_i^{sim} \right)^2}{\sum_{i=1}^{n} \left(Y_i^{obs} - Y^{mean} \right)^2} \right] \tag{3-17}$$

$$R^2 = \left\{ \frac{\sum_{i=1}^{n} \left(Y_i^{obs} - Y_{obs}^{mean} \right) \left(Y_i^{sim} - Y_{sim}^{mean} \right)}{\left[\sum_{i=1}^{n} \left(Y_i^{obs} - Y_{obs}^{mean} \right)^2 \right]^{0.5} \left[\sum_{i=1}^{n} \left(Y_i^{sim} - Y_{sim}^{mean} \right)^2 \right]^{0.5}} \right\}^2 \tag{3-18}$$

$$PBIAS = \left[\frac{\sum_{i=1}^{n} \left(Y_i^{obs} - Y_i^{sim} \right) * 100}{\sum_{i=1}^{n} \left(Y_i^{obs} \right)} \right] \quad (3\text{-}19)$$

where Y_i^{obs}, Y_i^{sim}, Y_{obs}^{mean},and Y_{sim}^{mean},respectively, are the i^{th} observation, the i^{th} simulated value, mean of observed data, and the mean of simulated data; n is the number of observations. A threshold value of NSC >= 0.5 was used to screen out “non-behavioral” models (Beven and Binley, 1992; Beven and Freer, 2001) for both streamflow and log-streamflow. Threshold values of 0.7 for R^2 and 0.35 for PBIAS were used to screen out “non-behavioral models” based on groundwater predictions.

The model execution time depended on the difficultly level posed by combination of parameter values and for this study ranged from 63 hours to 201 hours for each model run (about 260 models finished within 100 hrs).

3.3 Results and Discussion

3.3.1 Baseline Model Performance

Detailed analyses of baseline model simulated streamflow, surface-groundwater interactions and groundwater elevation at multiple locations, along with analysis of major water budget components across the basin, were presented by Srivastava et al. (2013a). Here we briefly present comparison of field observations and model simulated streamflow at two locations (1500 and 2500), and groundwater elevations at four locations (E2, E3, E8, E9) to highlight the processes that are, and are not, well predicted by the baseline model. Understanding the sensitivity of these processes to uncertain parameter values is an important first step to improving the predictive capability of the model.

In general model performance at all the stations within a given hydro-geological region (i.e. CR and UR) was comparable. Stations 1000, 1500 and 1898 are located in the CR of the basin where streamflow is rainfall dominated, with zero or insignificant measured flow in the absence of rain (see mean and coefficient of variation (CV) values for CR streamflow stations in Table 3-1 and the time series of streamflow at 1500 in Figure 3-3). In contrast Stations 1975, 2500 and 2800 located in the UR of the basin, receive substantial streamflow contributions from groundwater throughout the year (see mean and CV values for UR streamflow stations in Table 3-1 and the time series of streamflow at 2500 in Figure 3-3). For brevity we focus our streamflow analyses on stations 1500 and 2500, as representative of behaviors in the CR and UR, respectively.

In general, model simulated streamflow at USGS 1500 in the CR showed good agreement with measured data during both low and high flow conditions (Figure 3-3). Timing and peaks of hydrographs were accurately simulated by the model during all storm events and insignificant groundwater contributions resulted in zero streamflow in absence of rain. At station 2500 in the UR the model simulated streamflow showed reasonable agreement with measured data during high flow conditions. The model adequately simulated the timing and peaks of storm events but consistently underpredicted flow during storm recession periods as well as during low flow conditions. These observations indicate that the baseline model is missing a near stream transient source of groundwater in the UR that is released after storm events, as well as underestimating the steady groundwater baseflow. Srivastava et al. (2013a) hypothesized that these problems may be attributed to inaccuracies in the extent and

thickness of the IAS, particularly in areas where the CR transitions to the UR, which could result in insufficient water infiltrating into the UFAS in the these regions.

Figure 3-4 compares model simulated and measured groundwater elevation at four UFAS locations; E1 and E3 in the UR, E8 in the SCR and E10 in the UR. These wells span the various behaviors observed by Srivastava et al. (2013a) throughout the SFRB. Wells E2 and E10 simulate both the mean groundwater level and the transient groundwater response accurately. Well E3 over estimates both the mean groundwater level and the magnitude of the transient response, and Well E8 underestimates both the mean groundwater level and the magnitude of the transient response. Srivastava et al. (2013a) attributed the differences between the model simulated and measured elevations at these location to uncertainty in the extent of and hydraulic conductivity of the IAS as well as uncertainty in conduit locations and properties in the vicinity of the affected wells. The goal of this GSA is test the Srivastava et al. (2013a) hypotheses and to provide insight on the relative influences of all ParFlow.CLM parameters on evapotranspiration, streamflow predictions, groundwater levels, and groundwater-surface water interactions throughout the basin.

3.3.2 Global Sensitivity Analysis

In the following sections Morris analyses are presented both in tabular and graphical formats. A table is provided for each output of interest which summarizes the ranking of all parameters based on their Morris mean, μ^*, and standard deviation, σ ,values. Parameters with the highest values (i.e. most sensitive or most interactive) are assigned a rank of one. Non influential parameters (i.e. parameters with zero values for μ^* and/or σ are represented by a blank cell). In addition scatter plots of the actual values

of μ* versus σ are presented to help assess the relative magnitudes of the sensitivities and interactions across rank.

3.3.2.1 Evapotranspiration

Evapotranspiration accounts for 75-80% of the water budget in the SFRB (Srivastava et al., 2013a; Schneider et al., 2008) and is thus an extremely important component of the water budget. Table 3-7 presents the parameter rankings based on μ* and σ for the area-weighted mean daily evapotranspiration occurring in the CR and UR of the basin over the study period. In the CR the hydraulic conductivity of the intermediate aquifer system (ias_k) was found to be the most sensitive and most interactive parameter influencing ET, through its control on the surficial water table depth in the CR. Vegetation properties of mixed wetland and floodplain forests (lai_mf) and evergreen needleleaf forests (lai_enf) were the next most sensitive parameters for ET, with lai_mf also showing a high interactive effect. The location of mixed wetland and floodplain forests in higher water table regions makes them more influential in determining average daily ET over the CR than the evergreen needleleaf forests, even though the evergreen needle forests occupy a greater land area (Table 3-1). These findings are consistent with previous results that show a strong dependency between ET losses and water table depth for shallow water table regions (Srivastava et al., 2013a; Kollet and Maxwell, 2008a). Table 3-7 indicates that surficial aquifer hydraulic conductivity (sas_k) is also sensitive and interactive, but Figure 3-7 shows that ias_k and lai_mf are by far the most important parameters affecting ET in the CR.

In contrast, Table 3-7 shows that wilting point (wp) is the most sensitive and interactive parameter affecting ET in the UR, followed by the hydraulic conductivity of the upper Floridan aquifer system (fas_k), and the van Genuchten n parameter (vg_n).

ET in the UR also shows some sensitivity to maximum LAI of mixed forest (lai_mf) and open shrubland (lai_os), but Figure 3-7 shows that wp is by far the most sensitive and interactive parameter. Thus in both the CR and the UR, ET is more sensitive to soil/geologic properties than vegetative properties. However in the energy-limited CR, where water tables are shallow, ET is most sensitivity to properties of the confining layer that control the height of the surficial water table. In the moisture-limited UR, where water tables are deep, ET is more sensitive to surficial soil/geologic parameters controlling unsaturated moisture retention.

3.3.2.2 Total streamflow

Tables 3-8 and 3-9 summarize the parameter rankings based on Morris mean and sigma for streamflow characteristics at each of the streamgage locations. Analyzing multiple characteristics of daily streamflow time series at multiple locations within the basin is useful to identify the spatial and temporal variability in dominant hydrological processes affecting streamflow across the basin.

In general total streamflow at all locations across the domain was significantly influenced by the same parameters affecting ET losses, with some differences in the order of importance (Table 3-8 and Figures 3-5A and 3-5B). This high influence of ET on total streamflow is expected in the basin where ET is the biggest water budget component besides rainfall (Table 3-1) and shows the importance of an integrated modeling approach which accounts for important bi-directional feedbacks between land surface – subsurface components of hydrologic cycle. ET exerts significant control over available surface and subsurface storage for rainfall, which in turn affects the amount of water contributing to streamflow via surface, shallow or deep subsurface flow paths.

In the CR total streamflow showed most sensitivity to lai_mf, followed by ias_k, with ias_k showing by far the most interactive effects (Figure 3-5A). Streamflow also showed some sensitivity to lai_enf, but significantly less than sensitivity to lai_mf. Again this is likely due to the proximity of the wetland and floodplain mixed forests to the river channels in the CR and is in agreement with previous studies in the basin which hypothesize that that streamflow in the CR is generated primarily from direct rain or surface runoff received from near stream locations (Upchurch, 2007).

In the UR total streamflow is most sensitive to fas_k followed by lai_mf and wp, indicating the primary control of the Floridan aquifer hydraulic conductivity properties on groundwater contributions to the stream and the secondary control of ET on total water available in the surface-subsurface system. In general the influence of land cover based ET parameters on total streamflow is more pronounced in the CR where land cover related parameters (such as lai_mf, lai_enf, z0_enf, and z0_mf) showed higher rankings relative to their UR rankings. In contrast in the UR the influence of soil based ET parameters (wp and vg_n) gained relative importance in comparison to rankings in the CR. Again this difference is attributed to the contrast in soil/geological characteristics which control the water available to plants for ET in the two regions.

3.3.2.3 Peak streamflow

Peak streamflow rates at all confined and unconfined locations showed highest sensitivity to Manning's coefficient in the CR (CR_mannings) followed by ias_k (Figure 3-5 C), with the exception of USGS2800 where the order of sensitivity of these parameters was reversed (Table 3-8). This indicates that streamflow peaks at unconfined locations generally originate from rainfall in the CR and are controlled by the rainfall-runoff response in that region. The strong influence of IAS aquifer is again due

to its influence on water table location in the CR, and confirms that saturation excess, rather than Hortonian streamflow generation processes dominate in this basin. ET related parameters (lai_mf, lai_en, wp, and z0_enf) showed influence over the peak flow rate at all the locations (Table 3-8) by virtue of their control over intra-event surface and subsurface storage.

3.3.2.4 Storm hydrograph recession

Flow ratios 1-3 (defined in Table 3-6) reflect the rate of peak flow recession for the February-May, 2003 storm event. In general, a slower decay rate implies a system with heterogeneous sources, travel paths and travel times for event water reaching the stream, often associated with a higher influence of subsurface contributions during recession of the storm hydrograph (Panagopoulos and Lambrakis, 2006) Investigating the sensitivity of flow ratios 1-3 to land surface, vegetative and geologic parameters provides insight into the surface and groundwater flow processes that play important roles over the duration of stormflow recession. In general, for all confined and unconfined locations, ratio 1 showed highest influence CR_mannings (with highest sensitivity and interactions) emphasizing the dominance of CR streamflow generation and transport processes during early hydrograph recession, even at unconfined locations (Table 3-9 and Figure 3-5 D). For stations in the UR, Manning's coefficient in the UR channel (UR_mannings) ranked second, closely followed by fas_k and and then ias_k. The sensitivity of ratio 1 to fas_k in the UR implies that even during the early period of hydrograph recession groundwater flow parameters are influential. For ratios 2 and 3 the relative ranking of the parameters changes, but the same four parameters retain the top four ranks. Hydraulic conductivity of the Floridan aquifer (fas_k) becomes

the most sensitive parameter for ratio 3, confirming an increased influence of Floridan groundwater flow on late hydrograph recession as baseflow conditions are approached.

In the CR, stations 1000 and 1500 showed large scatter in ranks from ratio1 to ratio 3 with CR_mannings maintaining the highest direct influence during entire hydrograph recession period. At station 1000 ET related parameter gained importance for ratio 3 (e.g. increased ranking of lai_mf, vg_n, sai_mf, lai_g, and wp) indicating higher influence of ET losses on streamflow during later parts of the recession period. Station 1500 showed increased influence of shallow subsurface flow contribution (in comparison to station 1000) with increased sensitivity to SAS properties (rank 2 based on sensitivity and rank 1 based on interactions for sas_k). Insignificant effect of upper Floridan aquifer system on streamflow throughout the region is evident from consistent low ranking of UFAS related parameters.

3.3.2.5 Mean and coefficient of variation of groundwater elevation

Table 3-10 and Figures 3-6A and 3-6B summarize the parameter rankings based on Morris mean and sigma for average daily potentiometric surface elevation at multiple Floridan well locations across the domain. Spatial patterns in potentiometric surface elevation across the upper Floridan aquifer control the direction of regional groundwater flow in the study domain and affect streamflow in the UR of the domain. In general, all CR wells (E1-E7) show high potentiometric head sensitivity to ias_k and fas_k, and some sensitivity to fas_ss. Wells E3 and E4, that are located in the vicinity of conduits also show high sensitivity to conduit hydraulic conductivity (c_k). The high influence of ias_k on all CR wells demonstrates the strong control the IAS exerts over recharge to the UFAS. Wells E9 and E10 in the UR showed dominant sensitivity to fas_k, with some sensitivity to wp which has a major influence on ET and thus recharge in the UR. Wells

close to the boundary of UR (wells E2-E6) also showed high rank for wp indicating the influence of UR recharge on the potentiometric surface in these locations. Well E8 in the SCR showed highest sensitivity to the hydraulic conductivity of the semi-confined region (SCR), followed by fas_k and wp.

Table 3-11 and Figures 3-6C and 3-6D summarize the parameter rankings based on Morris mean and sigma for the coefficient of variation (CV) of potentiometric surface at multiple well locations across the domain. In general, fas_ss, fas_k and ias_k were the most sensitive and interactive parameters for potentiometic surface CV at all wells, with fas_k being the most sensitive parameter in the UCR and fas_ss being the most sensitive in the CR. Wells E2 and E3 in the CR also showed some sensitivity to conduit specific storage (c_ss). Thus, “flashiness” of the potentiometric head is more sensitive to the storage properties of the aquifer resulting from compressibility of the water and porous matrix (specific storage) than the storage properties of the aquifer that result from raising the water table (porosity), even in the UR. At well E8 in the SCR geologic properties in that local region (sc_ss, sc_k, and sc_n) were the most influential.

3.3.2.6 Surface water- groundwater interactions

Exchange of water between river channels and the underlying UFAS was investigated to determine the most influential parameters controlling groundwater exchange with the unconfined river locations. It has been previously established that the CR stream locations does not receive any groundwater flow contribution from the UFAS and no significant groundwater contribution from the SAS (Upchurch, 2007). Table 3-12 and Figures 3-5E and 3-5F summarize the rank of parameters most influential to (1) total baseflow contributions for the 15 month study period, and (2) maximum surface water lost to groundwater during the peak of the February-May 2003 storm event. For

the purposes of the GSA the “baseflow” was calculated as the total daily groundwater contributions that all unconfined river cells upstream of a given location receive each day. For instance, total baseflow received by station 1975 was calculated as the total groundwater received by the river between stations 1898 and 1975 and total baseflow received by station 2500 was calculated as the total groundwater contributions received by all channel cells between 1898 and 2500.

Total baseflow contribution received by all UR locations was most significantly influenced by fas_k followed by c_k showing the importance of groundwater flow from the UFAS, including high hydraulic conductivity zones. The ET related parameter wp again shows high influence on the total groundwater contributions to streamflow at all three locations (rank 3 for stations 2500 and 2800 and rank 4 for station 1975). Maximum loss of surface water to the UFAS was significantly influenced by fas_ss, UR_mannings, and CR_mannings (Ranked 1-3) at all locations. Highest sensitivity to fas_ss shows the importance of subsurface storage in the near-river environment. Higher specific storage allows more water to be transferred to, and stored in, the aquifer without increasing the potentiometric head, and thus without reducing the head gradient between the river and the aquifer. Sensitivity to the two roughness coefficients shows the importance of peak river levels and thus again higher gradients between the river and aquifer.

3.3.3 Goodness of Fit of the GSA Model Runs

Hydrologic representation of large scale basins in integrated models is by necessity a simplification of reality in that homogeneous, isotropic conditions are commonly assumed within the major hydro-geologic units in the model domain, an assumption which is violated in all natural systems (McDonnell et al., 2007). Although

inconsequential during SA (because SA is only designed to identify the parameters that a specific output variable are most sensitive to) these simplifying assumptions often make it difficult to reproduce observed spatially variable hydrologic responses throughout a basin. In addition there is often a problem of “non-uniqueness” in which variety of different combinations of sensitive parameter values may achieve equally reliable model predictions (Beven and Binley, 1992). Furthermore combinations of parameters that reliably reproduce hydrologic response in one region of the basin may not produce reliable predictions elsewhere, particularly for large basins like the SFRB which span contrasting hydro-geologic conditions. In these cases allowing spatially variably parameter values within major hydro-geologic regions may be required to improve model performance. GSA is a useful screening tool to both determine the sensitive parameters that should be included in more comprehensive spatially variable parameter estimation techniques, and to help refine the range of parameters values that more reliably reproduce observed behavior in various regions of the basin.

In this study we examined the goodness of fit of the 340 GSA model runs at the 6 stream gage locations and 11 well locations where observations were available based on model performance criteria presented in section 2.6. “Behavioral models”, which met these performance criteria, were identified for each observation location. These behavioral models were then screened to identify those parameter sets that were behavioral at all observation locations within each subregion and then to identify the parameter sets that were behavioral at all locations in the SFRB (Figure 3-8)**.** These results show that 162 models were found to be behavioral at all confined streamflow locations, 56 were behavioral at all unconfined locations without accounting for model’s

behavioral at station 1975, and only 8 were behavioral at all groundwater locations. The short term, small scale interactions between conduit and aquifer matrix that are known to occur between stations 1898 and 1975 are not simulated by the model. In contrast to field observations where river water is lost to surrounding aquifer and recovered back at downstream locations, our model route the upstream contribution (with some interactions with surrounding aquifer) directly to the downstream river locations (i.e. 1975) via river channel. This results in model consistently simulating higher than observed streamflow during peaks of storm events and therefore making it difficult to obtain behavioral models at stations 1975 and downstream unconfined locations at the same time. As such when all streamflow stations are considered together there are no parameter sets that are behavioral at all six locations. However, if station 1975 is removed from the analysis then 28 out of 340 models were found to be behavioral for streamflow in remaining stations in the confined and unconfined regions of the basin, and of these 6 were also behavioral at the 10 well locations. The small number of models that were identified as behavioral throughout the basin underscores the need to use a parameter estimation technique that can account for spatial variability in the parameter values within hydro-geologic zones to improve the predictive performance of the model.

Figure 3-9 shows a comparison between measured and model simulated streamflow for the baseline model, the best fit model for the location, and the set of models found to be behavioral for the majority of the basin, for stations 1500 and 2500. At station 2500, total groundwater contributions received by channels upstream of station 2500 are also shown (dotted lines) for each of the selected models, along with

discrete estimates of total groundwater contributions (yellow circles) obtained in a previous study using EMMA with legacy specific conductivity data (Srivastava et al., 2013). For station 1500 both the best fit model and the set of 6 models that are behavioral throughout the domain reproduce streamflow quite well, although all models slightly underestimate the peak streamflow. At station 2500 the best fit model matches the pre-storm base flow conditions, the peak streamflow and the base flow recession quite well, however when compared with the EMMA results it underestimates the groundwater contribution to streamflow during the early storm recession. Thus, even with locally best-fit parameters, the model is unable to account for the near stream transient source of groundwater in the UR that is released after storm events. Model performance deteriorates slightly at station 2500 for the set of 6 models that are behavioral everywhere in the domain indicating that achieving good model results everywhere the domain, with parameters that are homogeneous in a limited number of hydrogeologic zones, is difficult. It is interesting to note that the 6 behavioral models show a more significant drop in groundwater contributions to streamflow during the storm event than the best fit model or the baseline model. Figure 3-10 shows a comparison between measured and model simulated groundwater elevation at wells E2, E3, E8, and E10, for the baseline and 6 behavioral model runs. These results indicate that the more behavioral models do not improve the mean groundwater levels significantly, but do improve the behavior of the groundwater coefficient of variation, particularly at E3. Additional insights can be gained by looking into the values of the most sensitive parameters for the behavioral models. For example at station 1500, 95% (199 out of 209) of models with ias_k values less then ~10^{-6} m/hr were found to be

behavioral where as only 44% (57 out of 131) of models with ias_k values greater than ~10^{-6} m/hr were found to be behavioral. Using a more strict criteria of NSC ≥ 0.65 showed that 77% (160 out of 209) of models with ias_k values less then ~10^{-6} m/hr were found to be behavioral whereas only 18% (23 out of 131) of the models with ias_k values greater ~10^{-6} m/hr were found to be behavioral. Thus a low hydraulic conductivity IAS is required to produce the shallow water table needed to produce sufficient streamflow in the CR. Further investigation reveals that for models with ias_k values less than ~10^{-6} m/hr all the models that were non behavioral are the models that have high lai_mf, lai_enf, z0_enf values indicating too much evaporation from the domain to produce sufficient streamflow. Similar analysis for station 2500 indicated that all models with extremely low values of ias_k (~10^{-9} m/hr) were non behaviora models (total of 141 models using NSC for flow and logflow ≥0.5 as goodness of fit cutoff criteria). A closer look at NSC values for flow and log flow values indicated that an ias_k value of ~10^{-9} m/hr produced reasonable NSC values for flow simulations but performed badly for NSC of logflow values indicating that ias_k values needs to be relaxed in order to improve baseflow predictions in the UR. Based on the results obtained in this study an ias_k value in between ~ 10^{-6} – 10^{-8} m/hr should give behavioral models for both the confined and unconfined locations.

3.4 Conclusions

The Morris method of screening was successfully applied and provided a reduced set of most sensitive and interactive parameters to be further investigated with more quantitative parameter estimation and uncertainty analysis techniques such as spatially distributed Ensemble Kalman Filtering (Graham and McLaughlin, 1989; Graham and McLaughlin, 1991). In general seven parameters (out of 33 parameters

included in the analysis), namely the hydraulic conductivity of the IAS, the hydraulic conductivity and specific storage of the UFAS, maximum LAI for mixed forests, wilting point, and the Manning's coefficient in the confined and unconfined regions were identified to be most sensitive towards ET, streamflow and groundwater level predictions. Of these seven parameters all but maximum LAI for mixed forests showed interactive effects, with the hydraulic conductivity of the IAS being the most interactive parameter. The sensitivity and interaction of the hydraulic conductivity of the IAS underscores the importance of better mapping of the lateral and vertical extent of IAS in confined, transition and Wacasassa Flat regions.

The significance of ET parameters such as lai_mf, and wp underscores the importance of ET and highlights the significance of feedback between land atmosphere, surface and subsurface processes throughout the basin. Vegetative properties of land covers, particularly those close to the river showed significant influence over several aspects of surface and groundwater flow. Vegetation properties were found to be more influential in the CR where ET is more energy limited than water limited due to the shallow surficial water table. In UR where water tables are and ET is water limited soil moisture retention properties such as wilting point and parameters of the van Genuchten equation were more influential.

Studying the range and median values of most sensitive parameters identified during Morris analysis (Figure 3-11), for base case, all the model runs in GSA, and the behavioral models for the entire basin, provided some useful information for future sensitivity and uncertainty analysis of the model. Behavioral models were found to have high parameter values ias_k, fas_k, CR_mannings, UR_mannings, fas_ss as compared

to the base case. In contrast wp and lai_mf were found to have lower values in the behavioral models (Figure 3-11). Further investigation on how the model's output variables responded to variations in most sensitive parameter values further enhanced our understanding about the most sensitive parameters and their effects on output variables (Figure 3-12).

Figure 3-12 illustrates the variations in some of the model simulated output variables in response to change in sensitive parameter's values during the Morris analysis. Evapotranspiration losses from the CR were found to decrease with an increase in ias_k values; this behavior might be attributed to the increase in water table depth with increased ias_k (Figures 3-12A). There was a dual trend in total and peak streamflow response at station 1500 and 2500 (Figure 3-12B), with both peak and total streamflow show an increase with increased ias_k values upto ~10^{-6} m/hr and thereafter there was an observed fall in peak and total streamflow values at both the stations. It was interesting to note that the water table was not significantly affected by an increase in ias_k values upto ~10^{-6} m/hr; after which it showed significant increase with an increase in ias_k values. In light of the above observations we can attribute an initial increase in flow characteristics at both the locations to more water reaching the channels from IAS cells that were closer to the channels. When the ias_k values were increased above ~10^{-6} m/hr more water might have recharged the underlying UFAS increasing the water table depths from the land surface; greater water table depths would mean that more rain water will be lost to the subsurface storage and less water will arrive at the stream.

Both the surface roughness coefficients were found to be sensitive towards peak flow and flow ratios in the UR. However, as clearly demonstrated in Figures 3-12 C and D, an increase in the value of these coefficients will improve the storm recessions at the cost of storm peaks. Therefore, caution must be taken to ensure that the storm recessions simulated by the model are not for the wrong reason (e.g. increasing surface roughness to hold water in the channels for longer time to get slow recession).

fas_k on the other hand showed an increase in total streamflow simulated at station 2500 along with an increase in flow ratio (i.e. slower storm recession; Figure 3-12E). An increase in fas_ss was found to significantly affect the total groundwater contributions received at station 2500 (Figure 3-12F). As such simultaneously varying both fas_k and fas_ss parameter values can provide a subsurface storage-release mechanism similar to that observed in between conduit-aquifer; where fas_ss can store water lost from the river channels during storm peaks and fas_k can facilitate quick return of the stored water once the storm has passed.

Parameters wp and lai_mf, respectively, showed a direct relationship with ET losses within the UR and CR of the basin. Increased value of wp meant that less water can be lost via vegetation whereas increase in lai_mf showed an increase in ET losses. To summarize above discussion, ias_k and lai_mf, respectively, are needed to be increased and decreased in order to achieve less ET losses and more recharge of UFAS in the CR of the basin. Whereas, fas_k and fas_ss should be varied simultaneously in order to obtain reliable storm recession simulations by the model.

Although qualitative, the result of the Morris GSA was successful in identifying spatial and temporal variability among the dominant hydrological processes and

sensitive parameters for this large complex basin. Moreover, the findings demonstrate important nonlinear interactions among geologic, soil and vegetation properties on land-atmosphere, surface and subsurface processes across large scales. The results presented in this paper helped in minimizing the number of parameters that require more accurate estimations. Moreover, based on our findings it can be concluded that any future sensitivity and uncertainty analysis on the model should account for spatial variability in the parameter values within the contrasting hydro-geologic regions of the basin.

Table 3-1. Physical characteristics of the Santa Fe River Basin.

Topography[a]	Mean elevation (m)	36.2
	Minimum elevation (m)	3.7
	Maximum elevation (m)	74.1
	Mean slope (%)	0.2
	Maximum slope (%)	1.0
Major land use[b]	Evergreen needleleaf (%)	31
	Open shrubland (%)	13
	Grassland (%)	14
	Mixed forest uplands (%)	11
	Mixed forest - isolated wetlands and floodplains (%)	13
Dominant soil type[c]	Confined region	sand to clayey sand
	Unconfined region	sandy soil
Hydrologic units[d]	Confined region	SAS,IAS,UFAS
	Unconfined region	UFAS
Water budget components	mean annual rainfall (mm)[e]	1252
	mean annual evapotranspiration (mm)[f]	1041
	Streamflow USGS 1000	(3.4,3.5)[g]
	Streamflow USGS 1500	(7.6,2.5)
	Streamflow USGS 1898	(8.3,2.7)
	Streamflow USGS 1975	(6.5,1.8)
	Streamflow USGS 2500	(30.1,0.8)
	Streamflow USGS 2800	(44.9,0.6)

[a] 1500 m resolution elevation dataset used in this study (USGS, 2010)

[b] FWCC land use data for year 2003

[c,d] Schneider et al., 2008

[e] NLDAS rain data 2000-2008

[f] Schneider et al., 2008

[g] (mean, coefficient of variation) daily USGS streamflow records for water years 2000-2008

SAS = Surficial Aquifer System

IAS = Intermediate Aquifer System

UFAS = Upper Floridan Aquifer System

Table 3-2. Input data used in ParFlow.CLM for the SFRB.

Data	Source	Original resolution	Final resolution	Resmapling method[a]
Digital Elevation Model (DEM)	USGS	10 m	1500 m	Bilinear interpolation
Land cover	FWCC	30 m	1500 m	Nearest neighbor
Aquifer extent	FGS	30-390 m[b]	1500 m	Bilinear interpolation
Channel location	NHD	-	-	-
Channel depth and roughness	SRWMD	-	-	-
Conduit spatial locations	Meyer and Kincaid (2008)	-	-	-
Climate data	NLDAS	1 hr, 12[c] km	1 hr, 1500 m	Bilinear interpolation

USGS = United states Geological Survey

FWCC = Fish and Wildlife Conservation Commission

FGS = Florida Geological Survey

NLDAS = North American Land Data Assimilation System

[a] all resampling were performed using Spatial Analyst Tool in ArcInfo except for the climate data

[b] value varied based on aquifer type and aquifer characteristic data

[c] first number gives the temporal resolution of the dataset and second number is the spatial resolution

Table 3-3. ParFlow parameters included in GSA by Morris method.

Parameter	Units	Region	Code used	Minimum	Maximum	Source	model
Porosity	-	SAS	sas_n	0.35	0.48	Rawls et al. (1982)	0.42
Hydraulic conductivity	m hr^{-1}	SAS	sas_k	0.001	1.79	Meyer et al. (2008)	0.83[a]
Specific storage	m^{-1}	SAS	sas_ss	1.00E-06	1.00E-02	Domenico and Mifflin (1965)	1.00E-04[b]
Porosity	-	IAS	ias_n	0.27	0.50	Rawls et al (1982)	0.39
Hydraulic conductivity	m hr^{-1}	IAS	ias_k	1.00E-09	2.00E-04	Meyer et al. (2008)	1.00E-09[c]
Specific storage	m^{-1}	IAS	ias_ss	1.00E-06	1.00E-02	Domenico and Mifflin (1965)	1.00E-04[d]
Porosity	-	UFAS	fas_n	0.20	0.42	Langston et al . (2012)	0.3
Hydraulic conductivity	m hr^{-1}	UFAS	fas_k	0.167	28.75	Meyer et al. (2008)	9[a]
Specific storage	m^{-1}	UFAS	fas_ss	1.00E-06	1.00E-02	Domenico and Mifflin (1965)	1.00E-04[b]
Porosity	-	SC	sc_n	0.20	0.42	Langston et al . (2012)	0.30[d]
Hydraulic conductivity	m hr^{-1}	SC	sc_k	9.00E-04	9.00E+00	Meyer et al. (2008)	9[e]
Specific storage	m^{-1}	SC	sc_ss	1.00E-06	1.00E-02	Domenico and Mifflin (1965)	1.00E-04[b]
Van Genuchten α	m^{-1}	Domain	vg_a	0.60	2.70	Meyer and Tiara (2001)	2.7
Van Genuchten n	-	Domain	vg_n	1.89	2.67	Meyer and Tiara (2001)	2
Porosity	-	Conduit	c_n	0.20	0.80	Langston et al . (2012)	0.30[f]
Hydraulic conductivity	m hr^{-1}	Conduit	c_k	28.75	290	Meyer et al. (2008)	270[g]
Specific storage	m^{-1}	Conduit	c_ss	1.E-06	1.E-02	Domenico and Mifflin (1965)	1.00E-04[b]
Manning's n	hr $m^{-1/3}$	CR channels	CR_mannings	6.14E-05	2.75E-04	WRA, 2007	6.14E-05
Manning's n	hr $m^{-1/3}$	UR channels	UR_mannings	2.15E-05	2.45E-04	WRA, 2007	2.15E-05

SAS = Surficial Aquifer System; IAS = Intermediate Aquifer System; UFAS = Upper Floridan Aquifer System

CR = Confined Region; SC = Semi Confined Region; UR = Unconfined Region

[a] used average of values reported for basecase and range of values for GSA

[b] clay and rock values were used as lower and upper limit in GSA, base values correspond to those of dense sand

[c] assumed five order of magnitude less than minimum value reported for basecase and lower limit for GSA

[d] assumed same as UFAS

[e] assumed minimum and maximum value of UFAS

[f] lower value same as UFAS and upper value equals two times the maximum value for UFAS porosity

[g] minimum value equals maximum UFAS value reported and maximum value equals an order of magnitude higher than lower value

Table 3-4. CLM parameters included in GSA by Morris method.

Parameter	Units	Region	Code used	Minimum	Maximum	Source	Baseline
Lower limit for plant water stress function (% of saturation)	-	Domain	wp	0.15	0.3	varied ± 50% of default value	0.2
Upper limit for plant water stress function (% of saturation)	-	Domain	fc	0.8	1	varied ± 50% of default value	1
Maximum LAI - evergreen needleaf forest	m^2m^{-2}	Domain	lai_enf	5	9	varied ± 50% of base value while maintaining laimax>laimin	6
Maximum LAI - mixed forest	m^2m^{-2}	Domain	lai_mf	3	9	varied ± 50% of default value	6
Maximum LAI - open shrubland	m^2m^{-2}	Domain	lai_os	3	9	varied ± 50% of default value	6
Maximum LAI - grassland	m^2m^{-2}	Domain	lai_g	1	3	varied ± 50% of default value	2
Maximum SAI- evergreen needleaf forest	m^2m^{-2}	Domain	sai_enf	1	3	varied ± 50% of default value	2
Maximum SAI- mixed forest	m^2m^{-2}	Domain	sai_mf	1	3	varied ± 50% of default value	2
Maximum SAI- open shrubland	m^2m^{-2}	Domain	sai_os	1	3	varied ± 50% of default value	2
Maximum SAI- grassland	m^2m^{-2}	Domain	sai_g	2	6	varied ± 50% of default value	4
Aerodynamic roughness length - evergreen needleleaf forest	m	Domain	z0_enf	0.5	1.5	varied ± 50% of default value	1
Aerodynamic roughness length - mixed forest	m	Domain	z0_mf	0.4	1.2	varied ± 50% of default value	0.8
Aerodynamic roughness length - open shrubland	m	Domain	z0_os	0.05	0.15	varied ± 50% of default value	0.1
Aerodynamic roughness length - grasslands	m	Domain	z0_g	0.015	0.045	varied ± 50% of default value	0.03

LAI = Leaf Area Index
SAI = Stem Area Index

Table 3-5. Summary of relevant information on intial and boundary condition used in baseline ParFlow.CLM.

	Aquifer	Condition applied	Source
Initial condition within major aquifers in domain	SAS	90% saturated everywhere	-
	IAS	Hydrostatic equilibrium with the UFAS	-
	UFAS	May 2002 Potentiometric surface map	SRWMD
Boundary condition over domain boundaries	East boundary	Constant pressure equal to the initial condition	-
	West boundary	Constant pressure equal to the initial condition	-
	North boundary	Constant pressure equal to the initial condition	-
	South boundary	Constant pressure equal to the initial condition	-
	Domain bottom	No flux	-
	Domain top	Overland flow	-

SRWMD = Suwannee River Water Management District

Table 3-6. ParFlow.CLM output variables assessed in the GSA.

Variable	Period of analysis	Measure	Units	Hydrologic region
Surface water flow	10/1/2002 - 12/31/2003	Cumulative	m^3	Confined, Unconfined
	2/1/2003 - 4/30/2003	Peak	m^3s^{-1}	
	2/1/2003 - 4/30/2003	Flow ratio 1 ($Flow_{15\ days\ post\ peakflow}$/Peak flow)	-	
	2/1/2003 - 4/30/2003	Flow ratio 2 ($Flow_{30\ days\ post\ peakflow}$/Peak flow)	-	
	2/1/2003 - 4/30/2003	Flow ratio 3 ($Flow_{45\ days\ post\ peakflow}$/Peak flow)	-	
Groundwater elevation	10/1/2002 - 12/31/2003	Mean	m	Confined, unconfined
	10/1/2002 - 12/31/2003	Coefficient of variation	-	Confined, Unconfined
Subsurface contribution to streamflow	10/1/2002 - 12/31/2003	Cumulative	m^3	Unconfined
Groundwater exchange	2/1/2003 - 4/30/2003	Groundwater exchange during peak of 2003 storm	m^3s^{-1}	Unconfined
Evapotranspiration	10/1/2002 - 12/31/2003	Area weighted average	m	Confined, Unconfined

Table 3-7. Morris mean and standard deviation based rank of individual parameters for mean daily ET Losses.

Parameter	Mean daily ET μ		Mean daily ET σ	
	Confined	Unconfined	Confined	Unconfined
c_k	28	17	28	10
c_n		23		23
c_ss	28	30	28	30
CR_mannings	23	30	22	31
fc	11	10	15	7
ias_k	1	11	1	5
ias_n	20	19	9	13
ias_ss	20	23	14	23
lai_enf	3	9	10	14
lai_g	11	13	23	15
lai_mf	2	5	2	6
lai_os	7	6	13	8
sai_enf	9	19	12	20
sai_g	15	12	19	16
sai_mf	10	23	17	23
sai_os	16	19	17	20
sas_k	4	13	3	11
sas_n	19		19	
sas_ss	20		19	
sc_k	18	19	23	20
sc_n	24	23	25	23
sc_ss	28	23	28	23
fas_k	16	2	5	2
fas_n		17		18
fas_ss	24	13	16	11
UR_mannings		13		19
vg_a	14	4	4	4
vg_n	11	3	7	3
wp	7	1	6	1
z0_enf	5	8	11	17
z0_g	24	23	25	23
z0_mf	6	7	8	9
z0_os	24	23	25	23

Table 3-8. Morris mean and sigma based rank of individual parameters for total and peak streamflow.

	Total Flow μ						Total Flow σ						Peak Flow μ						Peak Flow σ					
Parameter	1000	1500	1898	1975	2500	2800	1000	1500	1898	1975	2500	2800	1000	1500	1898	1975	2500	2800	1000	1500	1898	1975	2500	2800
c_k	25	25	21	17	11	8	25	23	20	17	14	13	26	25	24	25	25	26	25	23	23	24	24	26
c_n	33	29	30	30	30	31	31	28	28	28	29	29	25	31	29	28	28	28	33	27	31	30	30	28
c_ss	28	31	31	31	32	32	32	29	31	30	30	30	33	32	31	26	30	30	31	32	29	21	27	27
CR_mannings	21	21	20	22	24	24	19	20	18	21	23	24	1	1	1	1	1	2	2	2	2	2	2	2
fc	11	11	12	13	14	16	16	18	19	18	21	21	13	14	14	16	16	15	15	16	18	18	18	20
ias_k	2	2	3	5	9	11	1	1	1	3	3	3	4	2	2	2	2	1	1	1	1	1	1	1
ias_n	26	26	33	33	33	33	27	30	33	33	33	33	28	29	32	33	33	33	32	30	32	33	33	33
ias_ss	13	19	24	26	26	26	2	8	12	12	15	17	14	18	21	21	21	23	8	17	17	16	16	16
lai_enf	3	3	4	4	4	7	12	12	11	11	12	14	6	4	5	5	7	7	12	10	12	11	13	13
lai_g	16	14	13	14	16	17	20	19	25	26	27	25	22	21	22	22	23	22	22	21	22	23	23	21
lai_mf	1	1	1	1	2	3	3	2	3	4	4	5	2	3	3	3	3	4	3	7	8	8	9	7
lai_os	10	8	8	11	12	13	15	10	8	9	9	12	15	13	13	12	12	12	16	15	15	15	15	15
sai_enf	15	16	19	20	23	23	14	16	16	16	20	22	17	19	19	19	20	20	17	20	19	19	19	19
sai_g	18	17	16	16	18	18	21	22	23	23	24	23	23	17	20	20	21	24	21	18	20	20	20	22
sai_mf	17	15	18	19	21	21	18	17	21	22	25	26	16	15	18	18	18	19	18	19	21	22	22	23
sai_os	19	20	23	23	25	25	22	21	24	25	26	27	19	22	23	23	24	25	20	22	24	26	25	24
sas_k	5	5	5	6	6	9	4	4	5	6	7	9	8	10	10	11	13	13	5	11	11	13	11	10
sas_n	14	12	15	15	19	20	13	14	14	15	18	19	11	12	11	13	14	14	9	14	16	17	17	17
sas_ss	12	13	17	18	20	22	5	5	9	10	11	16	9	11	12	14	15	16	7	4	4	6	8	9
sc_k	31	32	22	21	15	6	29	31	22	20	19	11	29	27	28	29	26	21	28	29	28	28	26	25
sc_n	32	33	29	29	31	29	30	33	27	27	28	28	32	29	30	31	31	31	30	31	30	31	32	32
sc_ss	29	30	32	32	29	27	33	32	30	29	22	20	30	33	33	32	32	32	27	33	33	32	31	29
fas_k	20	18	14	2	1	1	6	3	2	1	1	1	18	16	17	17	17	17	14	5	9	14	14	12
fas_n	30	27	27	24	22	19	28	25	26	19	13	10	27	26	26	24	19	18	26	26	27	25	21	18
fas_ss	22	22	11	9	5	4	10	9	4	2	2	2	20	20	15	15	10	8	19	13	6	4	4	4
UR_mannings	27	28	25	25	17	14	26	27	17	24	16	6	30	28	16	7	4	3	29	28	10	3	3	3
vg_a	9	9	10	12	13	15	7	7	10	8	6	8	10	8	8	9	9	10	10	9	14	12	10	11
vg_n	8	10	9	10	6	5	9	13	13	13	8	7	7	7	7	8	8	9	11	8	7	9	12	14
wp	6	7	2	3	3	2	11	11	7	5	5	4	5	6	4	4	5	5	6	6	3	7	5	5
z0_enf	4	4	6	7	8	10	8	6	6	7	10	15	3	5	6	6	6	6	4	12	13	10	6	6
z0_g	23	23	26	27	27	28	23	24	32	32	32	32	24	24	27	30	29	29	24	25	26	29	29	31
z0_mf	7	6	7	8	10	11	17	15	15	14	17	18	12	9	9	10	11	11	13	3	5	5	7	8
z0_os	24	24	28	28	28	30	24	26	29	31	31	31	21	23	25	27	27	27	23	24	25	27	28	30

Table 3-9. Morris mean and sigma based rank of individual parameters for streamflow recession characteristics.

Parameter	Flow Ratio1 μ						Flow Ratio2 μ						Flow Ratio3 μ					
	1000	1500	1898	1975	2500	2800	1000	1500	1898	1975	2500	2800	1000	1500	1898	1975	2500	2800
c_k			24	16	14	18			24	15	9	15			17	10	8	17
c_n			29	30	24					26	25	30				27		28
c_ss		21	29	21	28	27		16	24	26	28	27				27	27	
CR_mannings	1	1	1	1	1	1	1	1	1	1	1	2	1	1	1	1	2	3
fc	16	18	13	14	16	20	16	16	23	18	18	19			17	16	17	19
ias_k	7	4	2	3	4	4	8	4	2	3	4	4	4	5	2	3	4	4
ias_n		27									28			11				
ias_ss	10	7	18	15	20	22	10	10	18	21	21	23	8		17	22	24	23
lai_enf	10	3	4	7	5	6	10	3	6	5	5	7	8	5	6	5	5	6
lai_g		21	23	25	21	25			18	24	23	23	4			22	24	23
lai_mf	9	9	13	8	7	9	10	6	15	9	8	8	2	11	15	10	7	7
lai_os	15	15	16	16	18	17	19	16	13	16	17	18	8	11	10	16	17	18
sai_enf	19	21	24	24	22	20	14	15	18	21	25	21	8			22	22	21
sai_g	14	13	20	21	22	23	13	10	16	24	25	23		5		22	24	25
sai_mf	16	15	19	18	19	19	19	21	16	18	19	21	4		10	19	20	21
sai_os	16	19	9	21	24	25	14	21	12	21	24	23	8		10	19	22	25
sas_k	12	2	8	12	15	14	4	2	8	12	11	17	8	2	8	13	13	12
sas_n	13	10	13	10	9	5	16	13	13	12	10	6	8	5	9	8	11	7
sas_ss	2	6	12	9	9	10	2	6	8	9	13	9	8	3	10	8	9	11
sc_k			24	27	28	7			24	20	20	10			17	19	21	12
sc_n			29	30	31	29	19					29			22	22		
sc_ss						31						30					27	25
fas_k	20	14	6	4	3	3	19	10	3	2	2	1		11	3	2	1	1
fas_n			24	25	24	23					22	20				27	19	19
fas_ss		19	20	18	11	16		16	24	17	15	13			22	16	16	10
UR_mannings		21	4	2	2	2		16	5	3	3	3			4	4	3	2
vg_a	3	10	9	12	11	12	2	8	10	8	11	13	8	5	10	10	13	12
vg_n	6	10	11	10	11	13	6	21	11	11	13	10	2	11	15	13	9	9
wp	8	5	3	5	8	11	8	4	4	5	7	12	4	3	5	7	12	15
z0_enf	4	8	7	6	6	7	4	8	7	5	6	5	8	5	7	6	5	5
z0_g	21	21	24	27	28	29						30			22			
z0_mf	5	17	17	18	16	14	6	13	18	14	16	15	8	11	17	15	13	15
z0_os	21	21	20	27	24	27	16		18	26	28	27		11		27		28

Table 3-9. Continued.

Parameter	Flow Ratio1 σ						Flow Ratio2 σ						Flow Ratio3 σ					
	1000	1500	1898	1975	2500	2800	1000	1500	1898	1975	2500	2800	1000	1500	1898	1975	2500	2800
c_k			24	22	22	28			24	20	20	24			17	21	19	18
c_n			29	30	25					26	26	30				27		28
c_ss		21	29	18	28	28		13	24	26	28	27				27	27	
CR_mannings	1	2	1	2	3	4	1	2	2	3	4	9	1	2	4	3	7	7
fc	18	16	14	14	16	20	17	19	17	14	16	18			17	15	18	17
ias_k	6	7	5	1	1	3	5	4	3	1	1	1	4	5	1	1	1	2
ias_n		27									28			10				
ias_ss	7	4	9	10	7	19	10	6	19	19	19	19	8		17	21	24	21
lai_enf	11	3	4	5	8	13	14	3	6	6	5	7	8	5	5	6	8	8
lai_g		23	23	24	18	21			19	24	24	25	4			21	24	24
lai_mf	9	8	11	8	13	10	12	12	15	9	10	8	2	10	13	9	13	9
lai_os	16	13	17	26	21	18	19	13	8	16	14	21	8	10	7	11	16	20
sai_enf	19	23	24	23	24	26	15	18	19	22	26	19	8			21	22	22
sai_g	12	6	20	18	23	22	9	6	18	24	23	22		5		21	24	25
sai_mf	17	15	15	17	15	17	19	21	12	14	18	22	4		11	15	17	22
sai_os	15	19	3	21	25	27	15	21	5	22	22	25	8		6	15	22	25
sas_k	13	1	6	9	12	14	11	1	7	10	12	14	8	1	8	14	14	12
sas_n	14	9	11	11	9	2	13	11	14	10	11	2	8	5	14	12	11	5
sas_ss	2	10	13	12	10	11	3	10	10	8	7	11	8	3	15	8	6	9
sc_k			24	27	28	1			24	21	25	4			17	20	20	6
sc_n			29	30	31	25	19					29			22	21		
sc_ss						31						30					27	25
fas_k	20	10	7	6	2	5	19	5	4	2	2	3		10	2	2	2	3
fas_n			24	24	20	22					21	17				27	20	19
fas_ss		16	18	16	11	9		19	24	12	8	6			22	12	4	4
UR_mannings		21	16	7	6	6		13	13	5	3	5			9	4	3	1
vg_a	5	14	10	13	19	15	4	16	10	13	14	15	8	10	11	9	10	15
vg_n	7	18	22	15	14	16	8	21	23	17	13	16	2	10	16	18	15	16
wp	10	5	2	3	4	7	5	8	1	4	9	9	4	3	3	5	5	14
z0_enf	4	12	7	4	5	8	7	9	9	7	6	12	8	5	10	7	9	11
z0_g	21	23	24	27	28	30						30			22			
z0_mf	3	20	19	20	17	12	2	16	19	18	17	13	8	10	17	19	12	13
z0_os	21	23	20	27	25	22	17		16	26	28	27		10		27		28

Table 3-10. Morris mean and standard deviation based rank of individual parameters for mean daily groundwater elevation.

Parameter	Mean Grounwater Elevation μ										Mean Grounwater Elevation σ									
	E1	E2	E3	E4	E5	E6	E7	E8	E9	E10	E1	E2	E3	E4	E5	E6	E7	E8	E9	E10
c_k	6	5	3	3	5	9	6	6	8	4	9	6	6	6	7	11	9	6	7	6
c_n	21	21	25	14	10	17	17	28	27	20	15	19	26	8	8	14	12	29	24	12
c_ss	30	22	19	21	22	22	25	14	19	21	30	22	13	19	22	27	25	12	14	21
CR_mannings	20	24	30	29	28	30	22	29	32	31	18	24	31	29	28	31	22	31	31	31
fc	19	19	15	17	16	13	19	15	15	18	20	19	20	18	15	12	17	18	17	17
ias_k	1	1	2	2	1	1	1	17	6	6	1	1	2	2	1	1	1	14	4	2
ias_n	32	33	32	32	29	25	33	32	33	32	31	32	33	32	26	19	28	31	32	33
ias_ss	4	9	21	23	9	14	4	29	30	27	3	5	15	14	6	9	4	28	25	19
lai_enf	12	14	17	20	18	15	12	10	16	15	11	13	19	23	19	18	13	10	15	20
lai_g	18	17	13	10	14	21	18	16	21	14	19	17	14	11	13	26	18	15	19	14
lai_mf	10	11	9	8	8	7	8	19	13	9	10	11	12	12	10	8	10	20	13	15
lai_os	16	12	11	13	15	11	16	11	12	10	17	14	11	16	17	13	20	11	11	10
sai_enf	27	31	31	30	30	27	27	23	26	30	25	30	32	29	32	30	27	22	27	30
sai_g	22	20	16	15	21	23	21	20	20	19	22	23	18	20	23	25	21	19	22	24
sai_mf	25	29	24	26	27	25	26	27	29	29	26	28	27	27	29	23	28	27	30	28
sai_os	29	30	27	31	30	26	29	25	28	30	29	29	28	30	27	24	28	26	29	27
sas_k	9	6	8	11	7	6	9	26	11	11	7	4	4	10	9	7	8	25	10	11
sas_n	24	23	22	22	20	16	23	30	23	22	23	25	25	22	20	15	24	30	21	26
sas_ss	23	26	28	24	24	19	24	31	31	25	21	21	24	24	21	17	23	32	28	25
sc_k	14	8	6	18	23	24	20	1	3	12	13	8	7	15	16	21	19	1	5	16
sc_n	26	13	12	27	31	31	31	5	10	24	24	12	9	26	31	33	29	4	9	23
sc_ss	30	28	26	26	26	29	30	4	22	23	27	26	21	21	25	29	26	2	16	13
fas_k	2	2	1	1	2	2	2	2	1	1	2	2	1	1	2	2	2	5	1	1
fas_n	11	25	23	6	6	5	7	18	17	7	5	18	23	4	4	4	5	17	17	4
fas_ss	3	3	5	5	3	3	3	12	4	5	4	3	3	3	3	3	3	9	2	5
UR_mannings	17	15	18	7	17	20	15	9	9	3	16	15	17	9	18	20	16	13	12	7
vg_a	7	10	10	16	11	10	10	7	7	17	6	9	10	13	11	10	6	7	8	9
vg_n	8	7	7	9	12	8	11	8	5	8	12	10	8	7	12	6	11	8	6	8
wp	5	4	4	4	4	4	5	3	2	2	8	7	5	5	5	5	7	3	3	3
z0_enf	13	18	19	19	19	18	14	13	18	16	14	20	22	25	24	22	14	16	18	22
z0_g	28	27	20	25	25	29	28	22	24	26	28	27	29	28	30	32	30	23	23	32
z0_mf	15	16	14	12	13	12	13	21	14	13	17	16	16	17	14	16	15	21	20	18
z0_os	31	32	29	28	30	28	32	24	25	28	32	31	30	31	33	28	31	24	26	29

Table 3-11. Morris mean and standard deviation based rank of individual parameters for coefficient of variation daily groundwater elevation.

Parameter	Coefficient of Variance of Groundwater Elevation μ										Coefficient of Variance of Groundwater Elevation σ									
	E1	E2	E3	E4	E5	E6	E7	E8	E9	E10	E1	E2	E3	E4	E5	E6	E7	E8	E9	E10
c_k	14	15	10	4	10	15	9	6	14	8	14	14	6	5	14	14	16	5	15	6
c_n	10	8	10	19	12	18	14	32	23	23	8	6	12	14	7	16	7	32	21	26
c_ss	12	4	4	16	23	31	20	8	11	22	7	4	4	14	21	31	12	6	13	20
CR_mannings	7	16	28	25	25		10	29	27	25	10	13	29	26	25		9	29	28	23
fc	19	24	17	20	14	12	16	14	21	18	21	23	25	21	9	12	15	12	22	22
ias_k	3	2	2	2	2	2	3	20	6	2	4	3	1	1	2	2	3	21	7	2
ias_n				32	32	25	32	33		33				32	30	25	32	33		33
ias_ss	4	22	26	24	21	23	6	28	27	27	3	19	16	7	19	23	5	27	27	18
lai_enf	19	18	19	15	17	13	16	11	13	10	21	17	21	22	9	13	20	11	11	13
lai_g	25	26	22	12	14	19	19	10	18	16	23	29	22	10	13	19	18	7	16	15
lai_mf	9	10	5	6	6	5	12	17	16	6	11	16	12	7	6	7	13	17	18	8
lai_os	19	13	14	14	8	10	16	18	14	14	18	21	16	14	8	10	11	19	14	16
sai_enf	30	28	30	31	28	20	26	26	26	29	27	27	27	31	28	22	26	26	25	29
sai_g	22	27	24	16	22	21	25	20	24	18	15	28	26	13	22	20	21	20	26	21
sai_mf	27	29	25	23	24	27	29	29	29	21	29	26	24	23	24	27	29	29	29	25
sai_os	30	30	29	26	25	21	29	23	29	30	31	30	28	30	26	20	29	22	29	30
sas_k	16	16	9	9	12	8	13	24	9	11	16	18	10	9	14	4	19	25	4	7
sas_n	22	19	16	16	16	11	20	29	19	15	20	20	23	19	12	11	23	29	19	19
sas_ss	26	25	21	22	19	16	24	27	25	18	28	25	20	19	17	18	23	28	24	12
sc_k	16	5	6	27	27	27	27	2	7	23	16	7	7	24	29	27	27	2	6	27
sc_n	14	6	7	29	30		23	3	5	26	8	5	5	29	27		17	3	5	28
sc_ss	27	20	17	30	30	27	27	1	12	28	25	11	11	28	31	27	27	1	10	24
fas_k	2	3	3	1	1	1	1	5	1	1	1	1	2	2	1	1	1	9	1	1
fas_n	5	10	20	4	4	6	4	13	3	5	5	9	15	4	4	8	4	15	9	5
fas_ss	1	1	1	3	3	3	2	9	2	3	2	2	3	3	3	3	2	8	2	3
UR_mannings	18	23	27	7	20	27	15	15	17	4	24	24	30	6	23	27	21	14	20	4
vg_a	6	9	12	8	10	9	7	4	10	7	6	10	9	11	14	9	8	4	8	9
vg_n	10	12	13	13	7	6	8	12	4	9	13	15	14	14	18	4	14	13	3	13
wp	7	7	8	10	5	4	5	7	8	13	12	8	8	18	5	4	6	10	12	10
z0_enf	24	14	23	20	18	16	22	16	22	17	26	12	19	25	20	17	25	16	23	17
z0_g	29	31	31	27	29	25	29	24	31	31	30	31	31	27	32	25	29	24	31	31
z0_mf	13	21	14	10	9	14	10	19	20	11	19	22	18	12	9	15	10	23	17	10
z0_os		32	32	32	33	23	32	22	31	32		32	32	32	33	23	32	17	31	32

Table 3-12. Morris mean and standard deviation based rank of individual parameters for total baseflow contribution received by three unconfined river locations.

Parameter	Total Baseflow			Total Baseflow			Groundwater exchange			Groundwater exchange		
	μ			σ			μ			σ		
	1975	2500	2800	1975	2500	2800	1975	2500	2800	1975	2500	2800
c_k	2	2	2	6	7	8	17	19	17	21	19	20
c_n	17	23	24	17	23	26	22	27	26	26	29	29
c_ss	24	20	23	25	20	24	18	13	16	15	12	12
CR_mannings	25	31	31	24	28	29	3	3	3	2	2	2
fc	18	19	18	19	16	14	14	18	21	13	15	17
ias_k	3	5	7	2	3	4	4	4	5	4	3	3
ias_n	33	33	33	33	33	33	33	33	33	33	33	33
ias_ss	22	28	30	12	14	18	27	24	24	24	22	22
lai_en	19	22	21	26	24	25	7	6	7	8	7	8
lai_g	13	14	19	16	17	19	26	25	27	23	24	28
lai_mf	9	10	10	9	12	12	8	8	6	6	5	4
lai_os	15	11	12	15	13	13	20	21	20	16	20	18
sai_en	26	24	22	29	29	28	24	22	23	22	23	25
sai_g	16	18	20	18	21	23	23	28	29	27	28	30
sai_mf	28	26	25	28	27	27	21	23	22	17	21	23
sai_os	31	29	27	31	31	30	28	26	25	29	25	26
sas_k	12	15	17	13	19	15	9	12	18	12	14	19
sas_n	23	25	26	27	26	21	10	10	15	10	9	10
sas_ss	29	30	29	22	25	20	12	16	19	7	10	14
sc_k	10	7	5	11	10	6	25	20	14	25	26	21
sc_n	20	21	16	20	18	17	30	31	31	31	31	31
sc_ss	30	16	13	23	11	11	32	29	28	32	27	24
fas_k	1	1	1	1	1	1	6	5	4	9	11	5
fas_n	8	9	9	8	8	10	16	11	8	20	16	11
fas_ss	5	4	6	3	2	3	1	1	1	1	1	1
UR_mannings	6	6	4	5	5	2	2	2	2	3	4	6
vg_a	11	12	11	10	9	9	13	15	10	18	18	16
vg_n	7	8	8	7	6	7	11	9	11	11	6	7
wp	4	3	3	4	4	5	19	17	12	19	17	15
z0_en	21	17	15	21	22	16	5	7	9	5	8	9
z0_g	27	27	28	30	30	31	31	32	32	30	32	32
z0_mf	14	13	14	14	15	22	15	14	13	14	13	13
z0_os	32	32	32	32	32	32	29	30	30	28	30	27

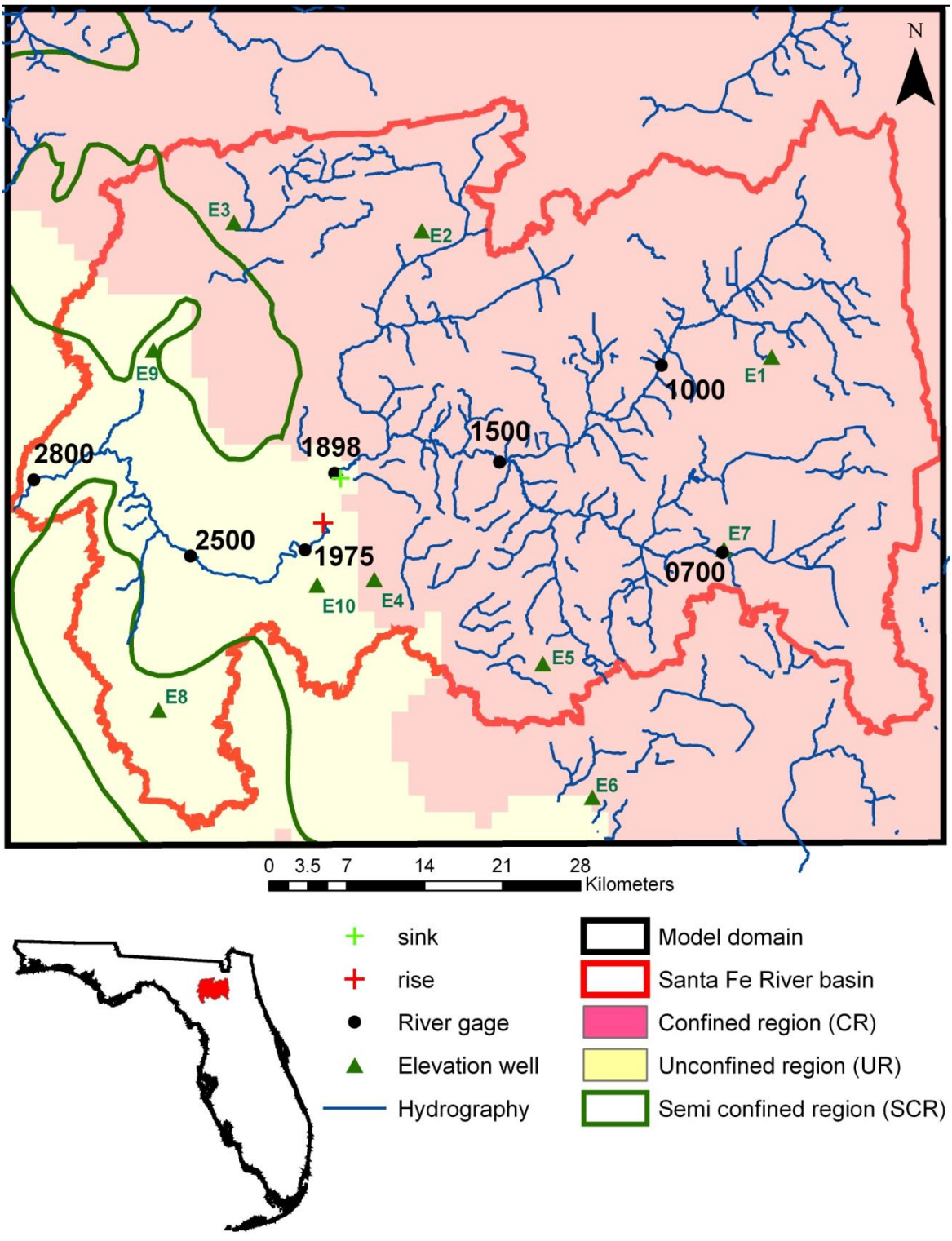

Figure 3-1. Map of the model domain. Also shown are the extents of the Santa Fe River Basin, locations of the river channels, monitoring wells, USGS stream gages and major hydrogeological regions in basin.

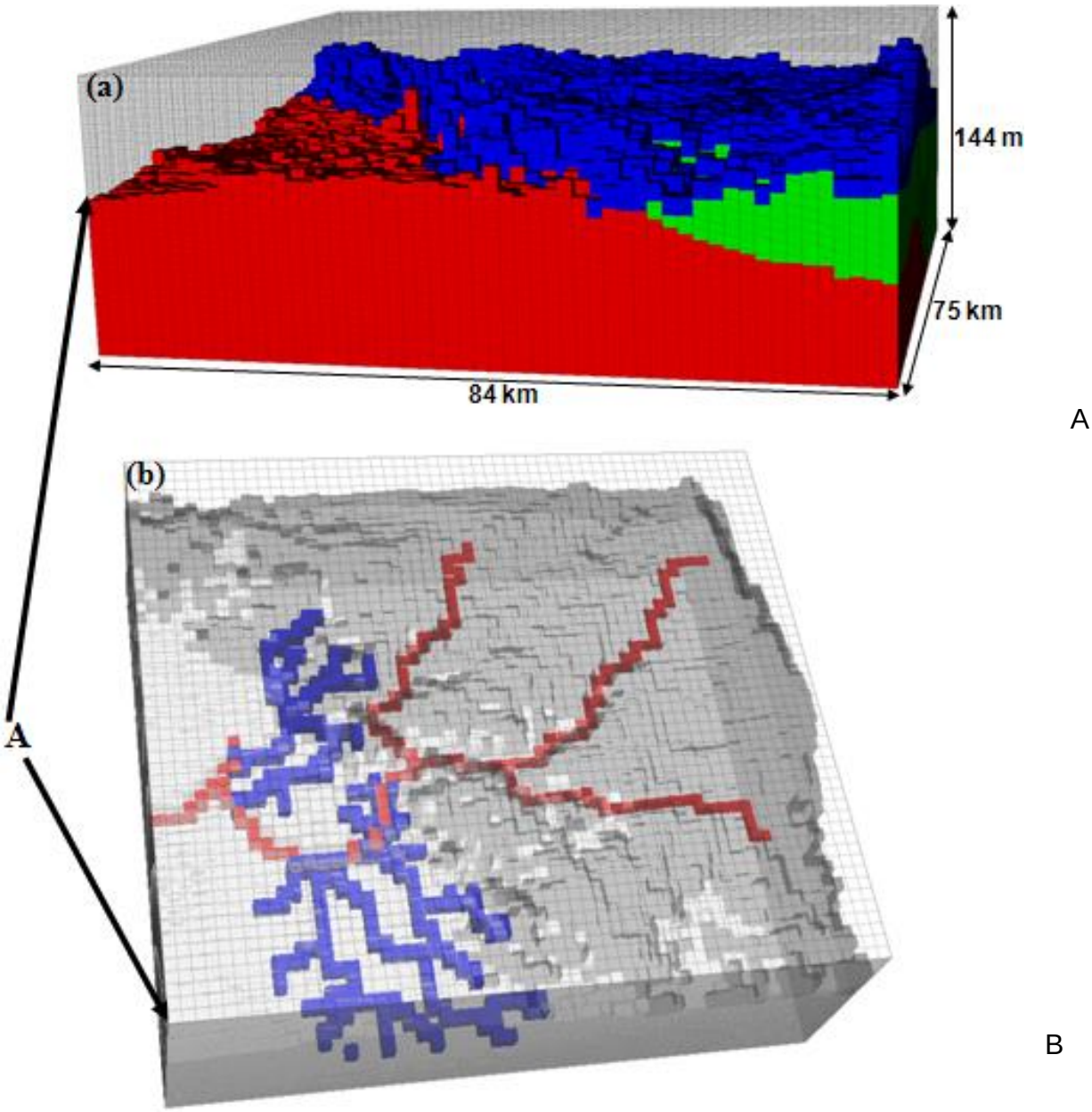

Figure 3-2. 3D mesh used to define the domain. A) the extent of the three major hydrogeological regions based on Floridan Aquifer Vulnerability Assessment (FAVA) dataset within the mesh along with their indicator variables, Surficial Aquifer System – blue region, Intermediate Aquifer System – green region, and Upper Floridan Aquifer System – red region. B) Locations of high hydraulic conductivity zones (blue cells) and main channels (red cells).

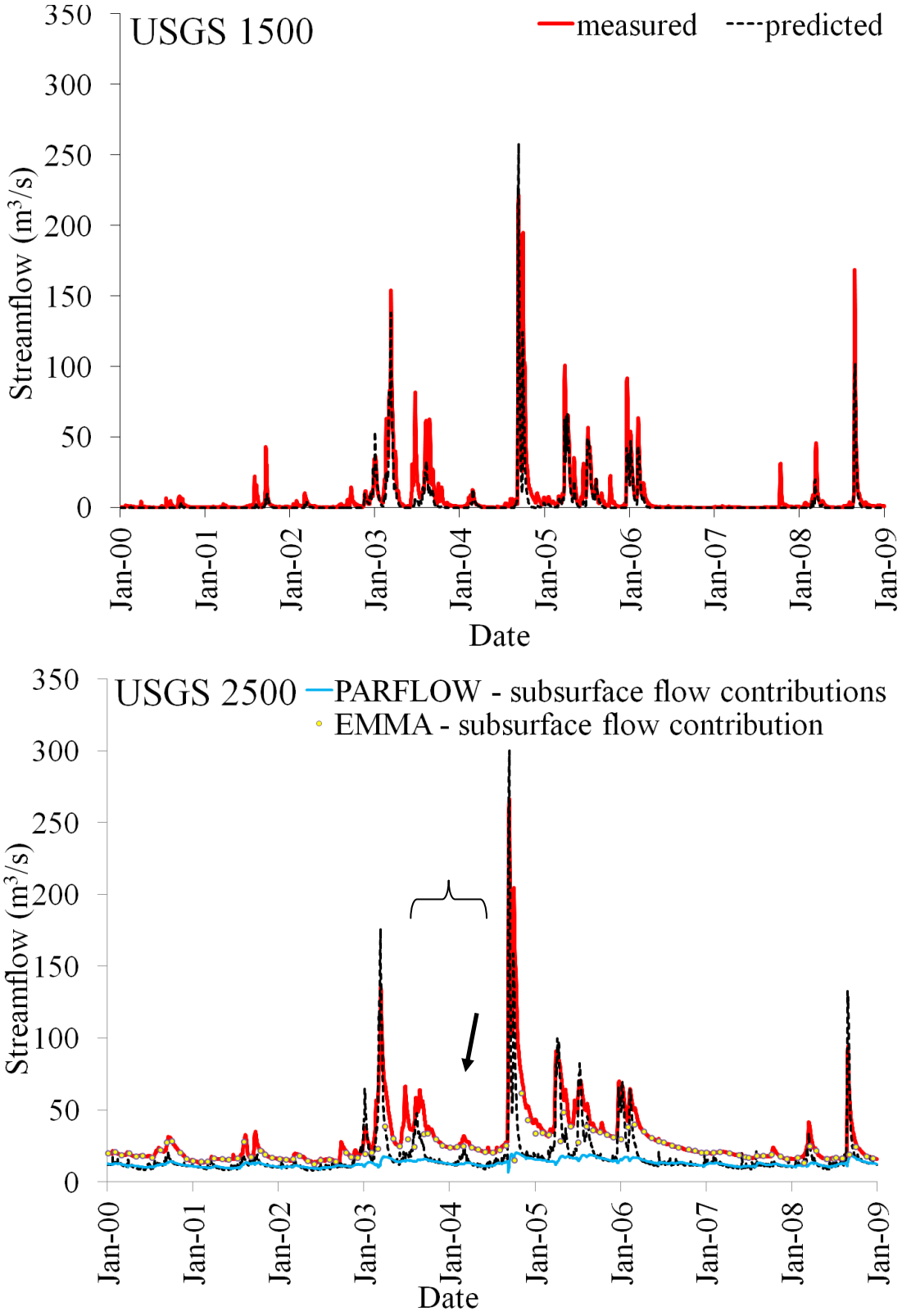

Figure 3-3. Comparison of observed and model predicted daily streamflow measurements at various streamgage locations across the domain.

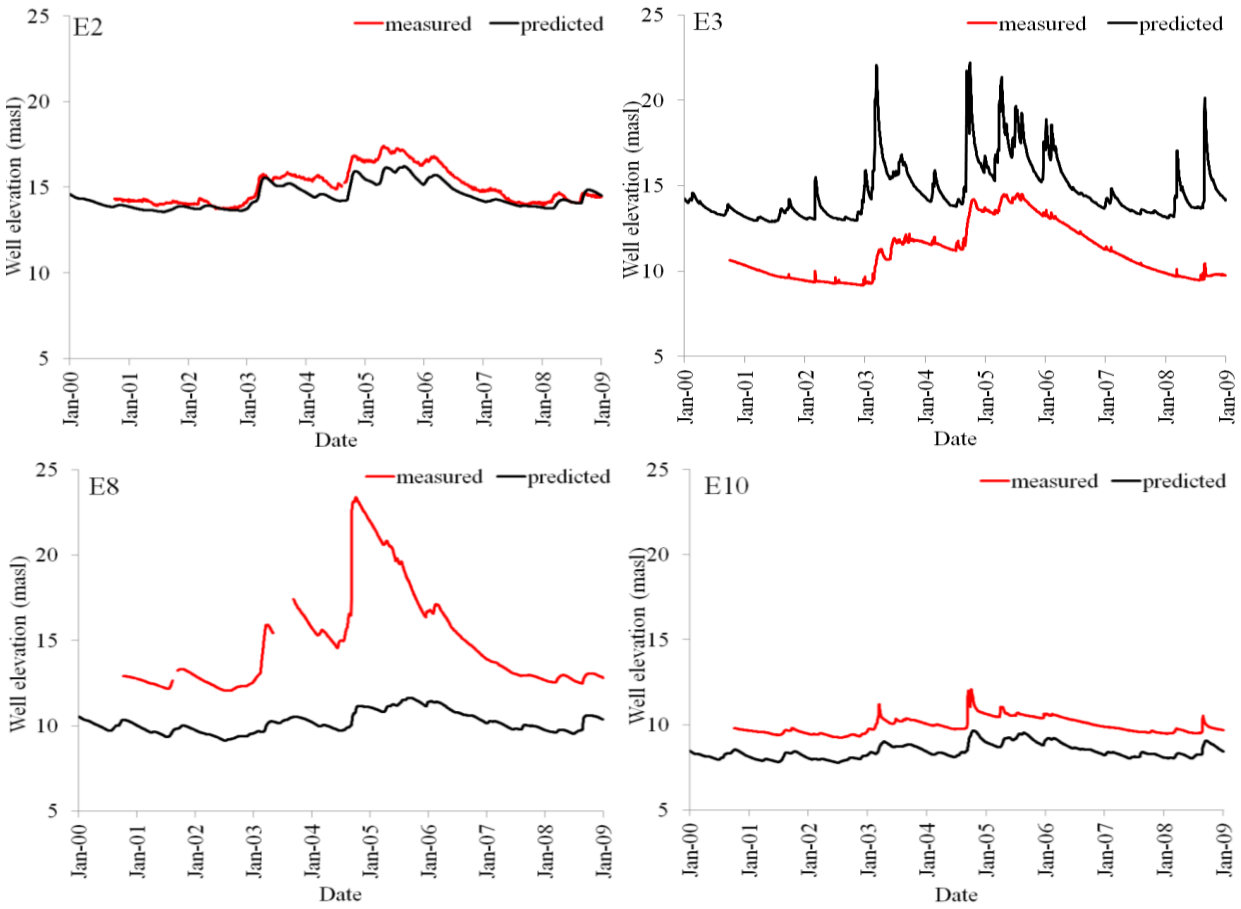

Figure 3-4. Comparison of observed and model simulated groundwater elevation at various locations across the domain. Wells E2 and E3 are in the Upper Confined Region (CR) and wells E8 and E10 are in the Semi Confined Region (SCR) and the Lower Unconfined Region (UR).

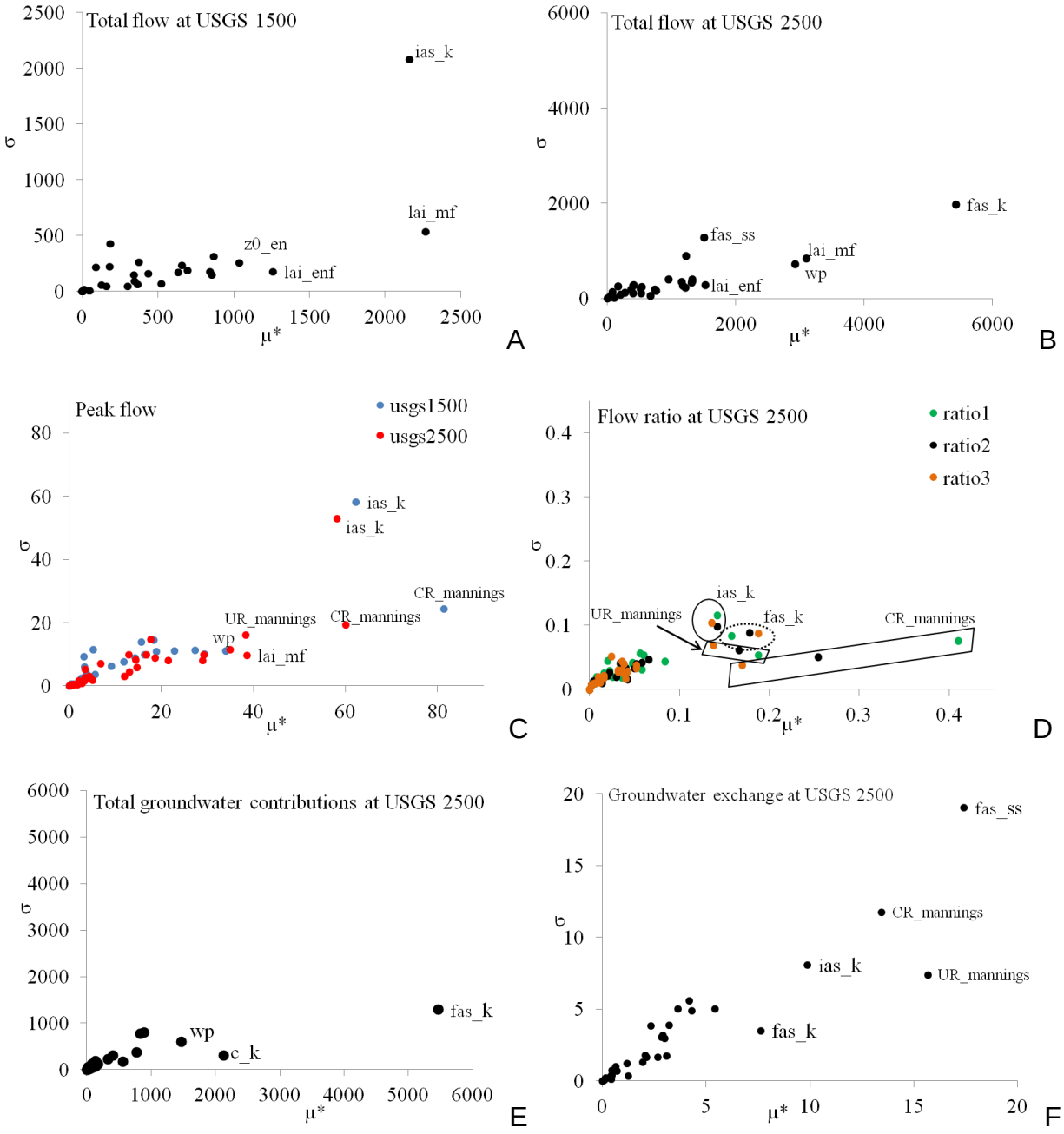

Figure 3-5. Scatter plots of μ* versus σ of the distribution function of the elementary effects of each parameter. Results are presented for the simulation of A) Total flow at USGS 1500. B) Total flow at USGS 2500. C) Peak flow at USGS 1500 and USGS 2500. D) Flow ratio 1-3 for USGS 2500. E) Total groundwater contribution received by USGS 2500. F) Exchange of groundwater during peak of 2003 storm at USGS 2500. Labels are provided for the most significant parameters.

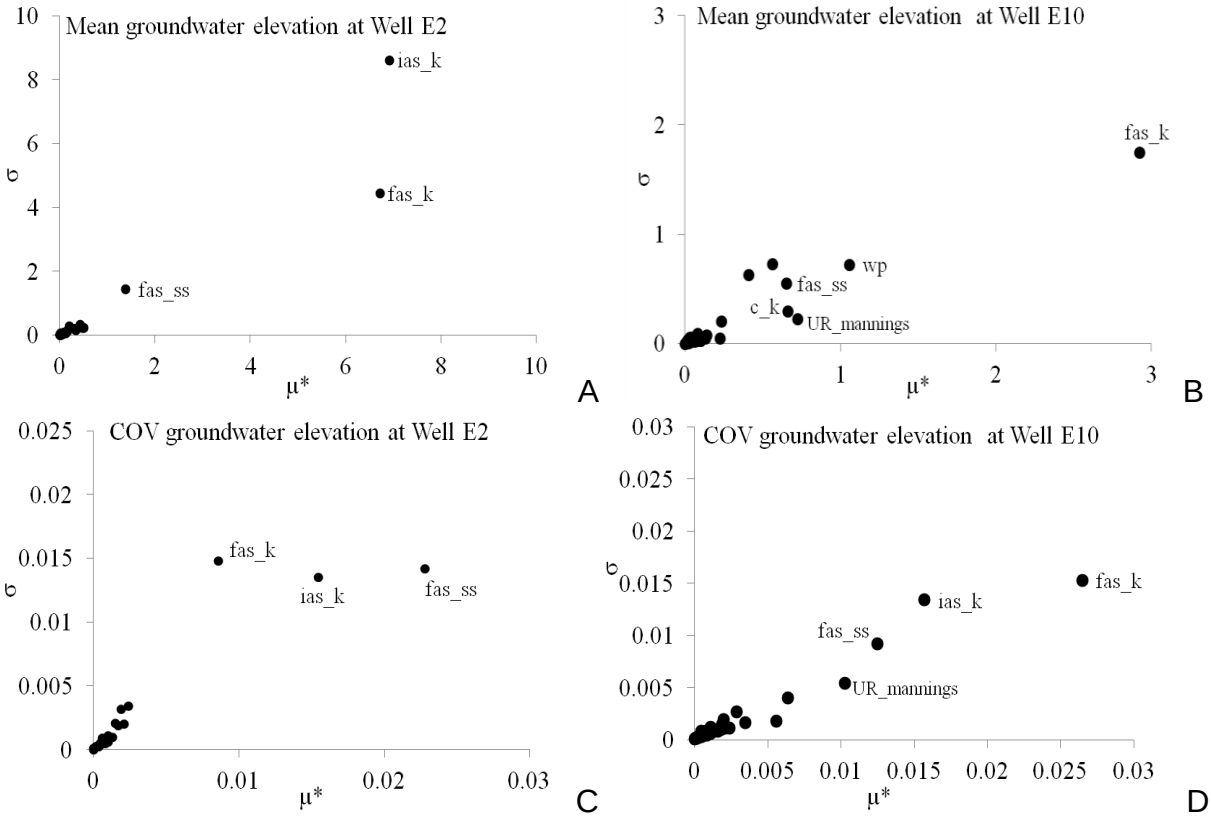

Figure 3-6. Scatter plots of μ* versus σ of the distribution function of the elementary effects of each parameter. Results are presented for the simulation of A) Mean groundwater elevation at well E2. B) Mean groundwater elevation at well E10. C) Coefficient of variation (COV) at well E2. D) COV at well E10. Labels are provided for the most significant parameters.

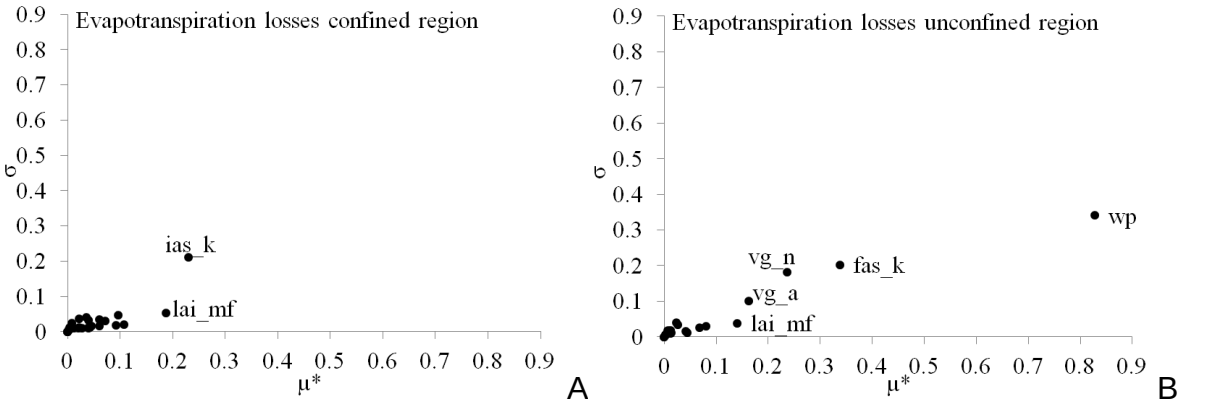

Figure 3-7. Scatter plots of μ* versus σ of the distribution function of the elementary effects of each parameter. Results are presented for the simulation of evapotranspiration losses from the A) Confined region. B) Unconfined region of the basin. Labels are provided for the most significant parameters.

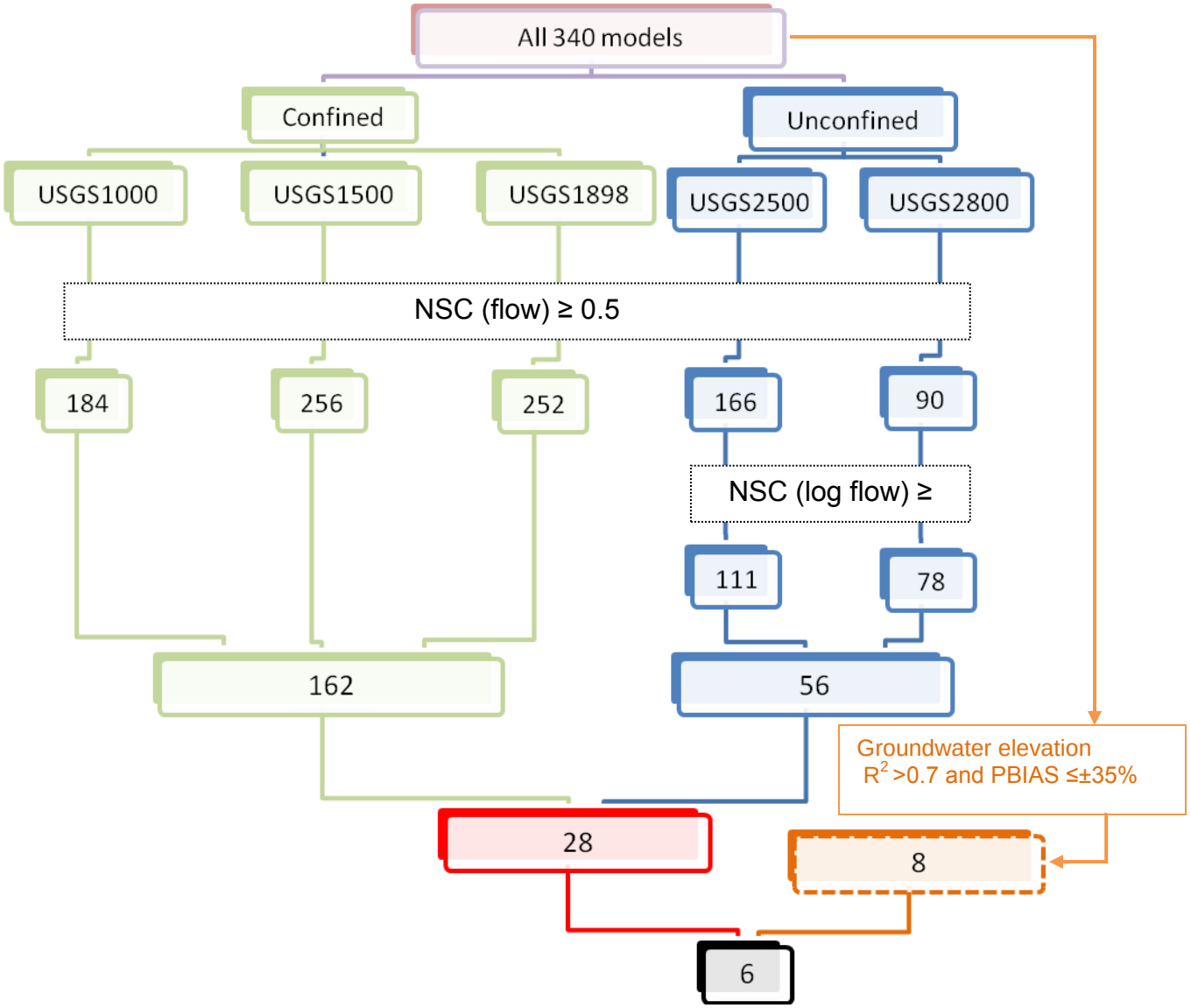

Figure 3-8. Flow chart of separation of behavioral models from non behavioral models based on streamflow simulation by 340 GSA model runs. Also shown is the number of behavioral models (dotted brown box) for groundwater elevation at all the ten well locations.

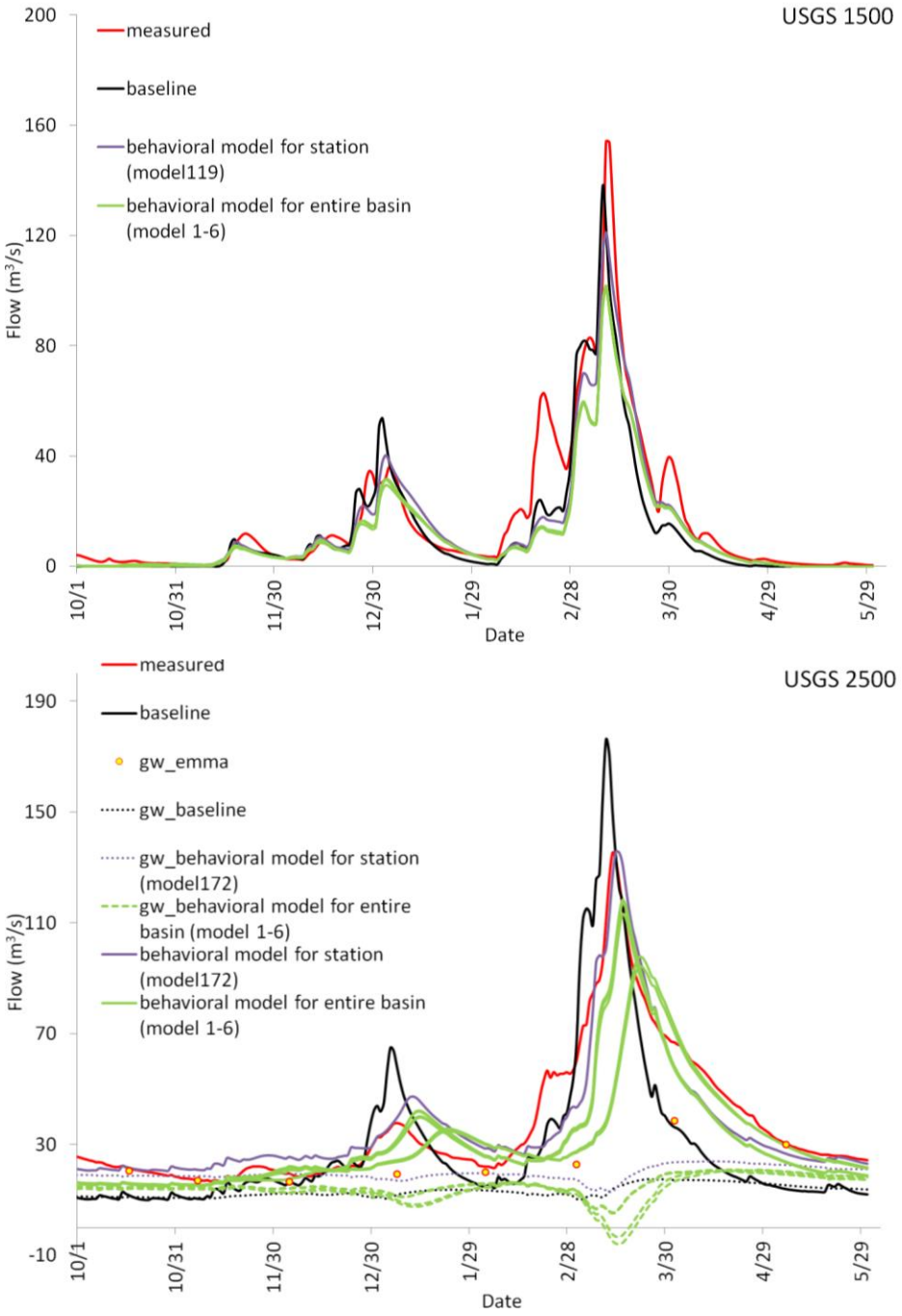

Figure 3-9. Comparison of observed and model simulated total streamflow at USGS 1500 (top) and USGS 2500 (bottom). Model simulated flow are shown for best behavioral models considering flow and groundwater elevation predictions at all confined and unconfined locations (green line) and baseline model (black line). Also shown are model simulated total groundwater contributions (dotted lines) and measured flow hydrograph separation results using specific conductivity measurements and end member mixing modeling for USGS 2500.

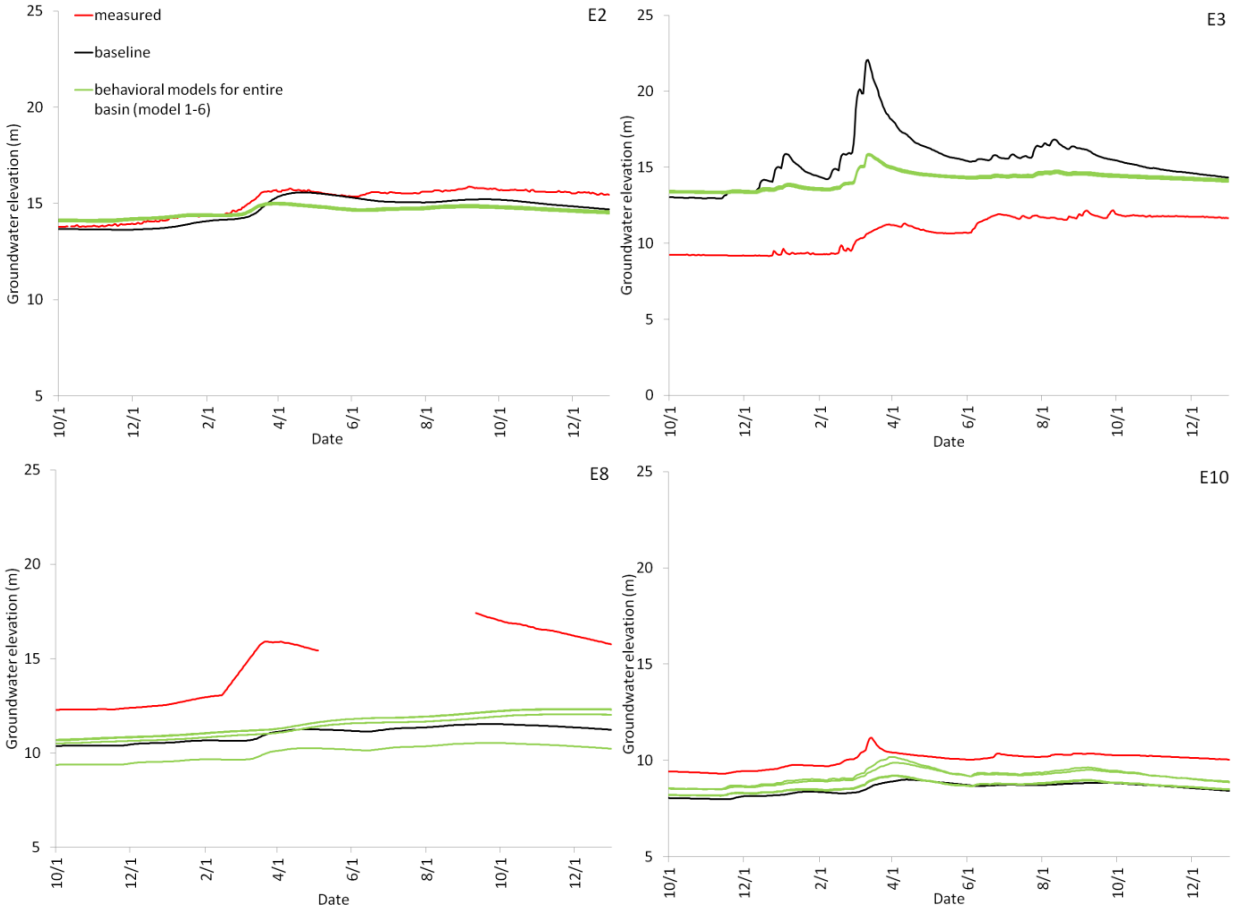

Figure 3-10. Comparison of observed and model simulated total streamflow at wells E2, E3, E8, and E10. Also shown are groundwater elevation simulated by six models found behavioral towards streamflow and groundwater elevation for everywhere in the basin (green line) and results for baseline model (black line).

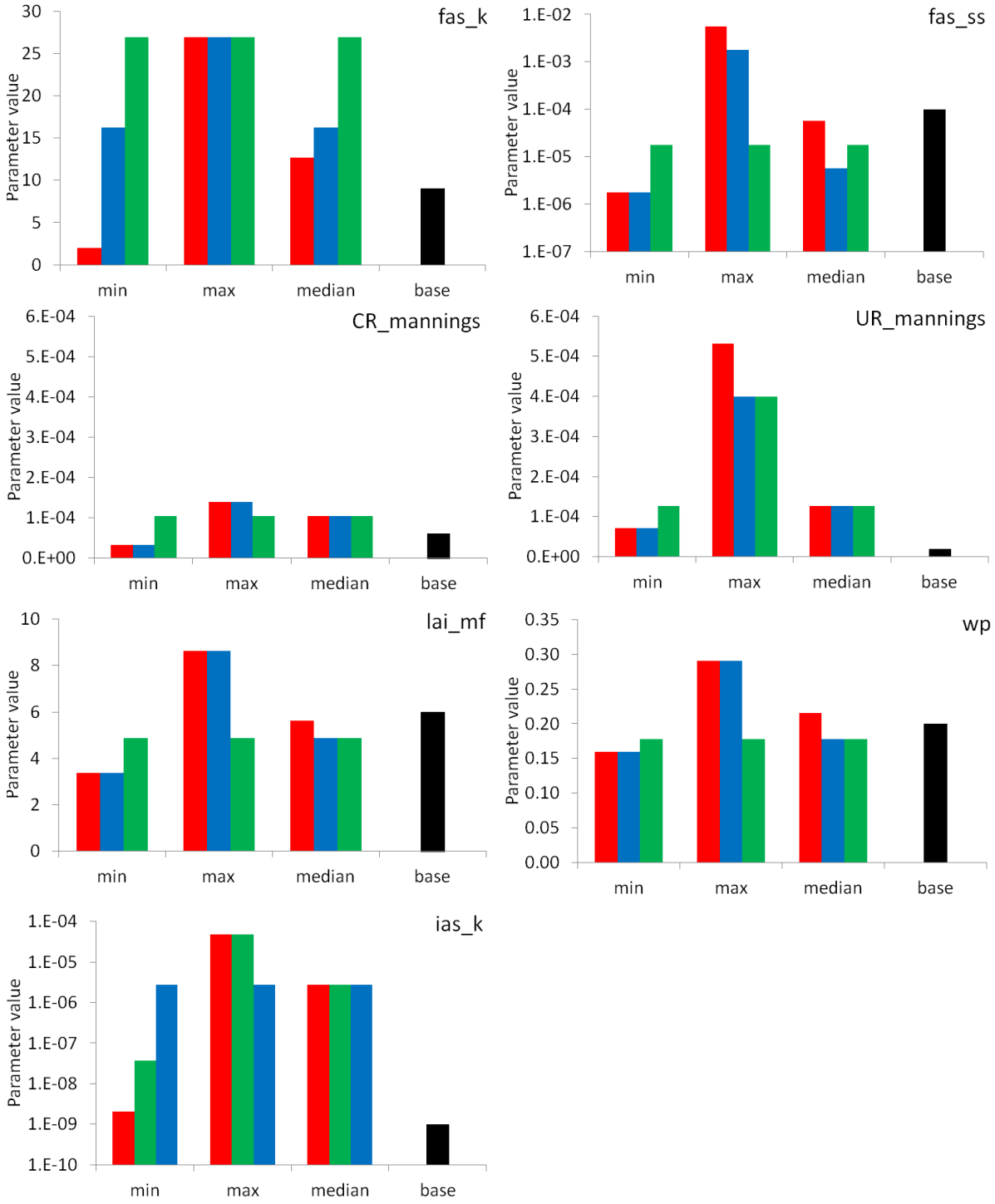

Figure 3-11. Range and median values for most sensitive parameter identified during the Morris Analysis. Red, blue and green bars, respectively, represent values for entire sample generate for Morris Analysis (all 340 models), models behavioral for flow everywhere in the basin (28 models), and models behavioral for both flow and groundwater elevation everywhere in the basin (6 models). Also shown is the value of parameter used in baseline model (black bar).

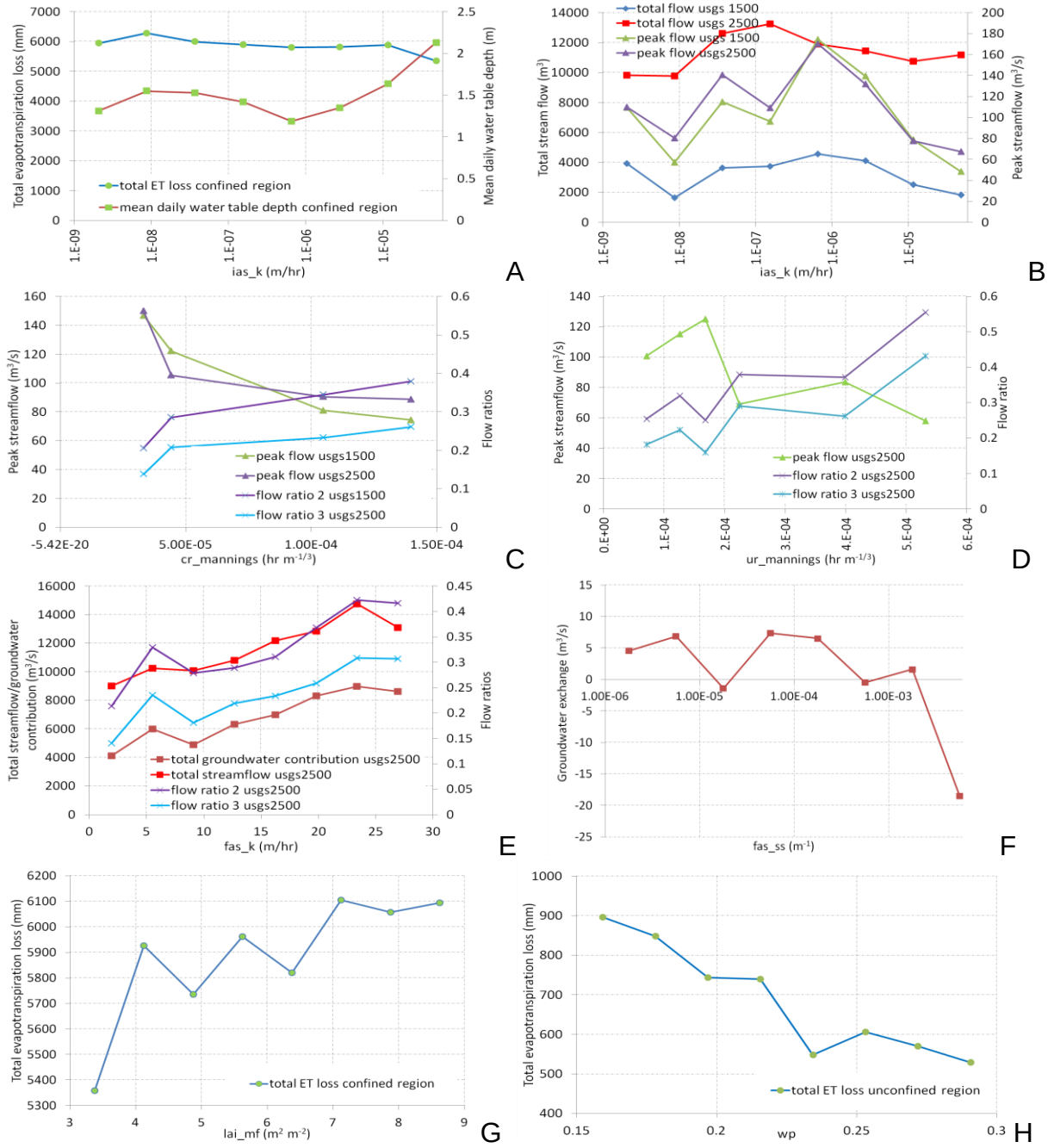

Figure 3-12. Influence of most sensitive parameters identified during Morris global sensitivity analysis on median values of output variables of interest. Influence of A) ias_k on total ET losses and mean water table depth in the confined region. B) ias_k on total and peak streamflow at stations 1500 and 2500. C) CR_manning's on peak flow at station 1500 and 2500 and flow ratios at station 2500. D) UR_mannings on peak flow and flow ratios at station 2500. E) fas_k on total streamflow, groundwater flow contributions and flow ratios at station 2500. F) fas_ss on total groundwater exchange at station 2500 during 2003 storm. G) lai_mf on total ET losses from confined region. H) wp on ET losses from unconfined region.

CHAPTER 4
TOPOGRAPHIC, GEOLOGIC AND CLIMATIC CONTROLS OVER RIVER WATER SOURCES, MIXING DYNAMICS AND TRAVEL TIME DISTRIBUTIONS IN A LARGE COMPLEX BASIN

4.1 Background

Growing concern over degrading water quality in springs, rivers and aquifers has led to many studies focused on determining sources, travel paths, and travel times of pollutants to these water bodies (Darracq et al., 2010; Botter et al., 2008; Van der Velde et al., 2010). Strong linkages between water pollutants and specific anthropogenic activities have been established (Katz, 2004; Katz et al., 2001; Katz and Griffin, 2008; Mueller-Warrant et al., 2012) and various water quality management measures have been proposed and implemented to protect and restore natural water bodies throughout the world over the past few decades (Duriancik et al., 2008; Maresch et al., 2008; Osmond et al., 2012). A recent review of U. S. Nonpoint Source (NPS) watershed projects in last four decades indicated that little or no water quality improvement has been achieved in most of the watershed scale NPS studies across the country (Meals et al., 2010). Uncertainty in groundwater travel paths and travel time distributions was found to be one of the important underlying causes of failure in many case studies discussed in the paper. The review highlighted the need for better characterization of hydraulic residence time, transport rate and flowpaths and more specifically groundwater travel time, amongst several other design and management factors involved in watershed scale NPS projects.

The mean transit time of water in a basin is a single integrated measure that has been frequently used as a hydrological descriptor for various storage and flow characteristics of a basin (Basu et al., 2012; McGuire and McDonnell, 2006). Moreover,

the transit time distribution (TTD) has been used to provide a robust stochastic description of hydrologic functioning of basins in a single curve (Botter et al., 2010). Previous efforts to identify first order controls on transit times in contrasting geographical regions indicated that TTD of water within a basin is influenced by varying climatic and landscape characteristics. For example, McGuire et al. (2005) found a link between various topographic indices and transit time in steep landscapes of Western Cascades, USA. Soulsby et al. (2006) found that soil hydrologic characteristics exert significant control on mean transit time (MTT) in a glaciated catchment in Scotland.

Although insightful, most of these studies on transit times focused on small experimental catchments (<10 km^2; e.g. Dunn et al., 2010; Roa-García and Weiler, 2010; Birkel et al., 2012) with fewer studies focusing on meso-scale (>100 km^2) and macro-scale (>1000 km^2) basins (Darracq et al., 2010; Speed et al., 2010; Tetzlaff et al., 2011). Small scale experimental catchments (e.g. Kirchner et al., 2000) have an important place in conceptual and numerical hydrologic model development as they provide testbeds for emerging theories and improve our understanding about hydrologic functioning of natural systems. However, most of the water resources management decisions are made in large scale basins where we posses limited predictive understanding (Dunn et al., 2008).

A few studies have investigated how tracer dynamics and subsequently MTT evolve in large scale basins that span contrasting geologic regions (Ogrinc et al., 2008; Tetzlaff et al., 2011; Koeniger et al., 2009). These studies focused on the dynamics of landscape controls and increased influence of groundwater inputs on MTT in the downstream direction where the lowland landscape feature become more important

than upland landscape features. For example, Tetzlaff et al. (2011) found an overall increase in MTT estimates as more groundwater mixed with water from catchment headwaters. Koeniger et al. (2009) found that water ages in lowlands of 46,000 km^2 Weser catchment in Germany ranged from 14-50 years and increased in the downstream direction as the groundwater inputs gained importance over headwater contributions.

One of the most discussed and critical assumptions in TTD modeling studies has been the time invariant characteristic of the functions used to represent TTD (Botter et al., 2010; Botter, 2012; Małoszewski and Zuber, 1982; Van der Velde et al., 2010; McMillan et al., 2012; Hrachowitz et al., 2010b; Rinaldo et al., 2011). Kirchner et al. (2000) used spectral analysis to show that a time invariant Gamma distribution with shape factor $\alpha = 0.5$ fit both short (sub daily) to long (>1 year) term tracer travel times in 1 – 3.5 km^2 headwater catchments at Plynlimon Wales. Several other catchment studies reported satisfactory results while applying different time invariant functions (e.g. exponential, piston flow amongst others) for TTD (see benchmark review by McGuire and McDonnell, 2006 for a comprehensive list). Beven (2010) suggested the use of a hypothesis testing framework while modeling TTD, instead of using a pre-assumed form of TTD.

Recent work by (Botter, 2012; Botter et al., 2010; Van der Velde et al., 2010; Hrachowitz et al., 2010b; Hrachowitz et al., 2010a) presented an argument that TTD are in general time-variant and reflect variability in climate and hydrogeologic conditions within basins. Hrachowitz et al. (2010a) used long term hydrometeorological and tracer data available for contrasting catchments in the Scottish Highlands (6.8 – 9.6 km^2 in

area) to study inter-annual and intra-annual variations in α and β parameters of the Gamma distribution commonly used in TTD studies. Results showed a link between β and rainfall intensity above catchment specific thresholds; whereas, α showed a relationship with hydrologic characteristic of the catchments. It was further suggested that time-variant TTDs could help in more realistic representation of contaminant transport through catchments. Botter (2012) showed that water residence time pdfs (defined as pdfs of ages of the water particles stored in a catchment at a given time) reflect rainfall variability with mean resident time dynamics dependent on rain event frequency, whereas travel time pdfs (defined as pdfs of time water particles spent in a basin) are streamflow dependent. A numerical particle simulation study on a 6.6 km^2 lowland catchment in the Netherlands indicated high variability in TTDs mostly due to the influence of rainfall and evapotranspiration dynamics (Van der Velde et al., 2010). This study showed that the numerical TTDs were highly dynamic and irregular with spikes reflecting rainfall and evapotranspiration variability.

With few exceptions both small and large scale TTD modeling studies have used predetermined time invariant functions to represent TTD; the exceptions being studies which relied on generalized analytical models (Botter, 2012; Botter et al., 2010; Rinaldo et al., 2011) or have applied time variant TTD in very small basins (<10 km^2; e.g., McGuire et al., 2007; McMillan et al., 2012; Hrachowitz et al., 2010a; Van der Velde et al., 2010). Moreover, previous applications of time variant TTD in modeling have mostly used simplistic lumped parameter models (e.g. McGuire et al., 2007; McMillan et al., 2012). While numerous studies have provided useful insights on time variant TTDs and their effect on solute (or simply water) transport, relatively little advancement has been

made in studying hydrologic controls over time variant TTD in large scale basins (> 10^3 km^2) spanning contrasting hydrogeologic regimes. Therefore modeling efforts that examine time variance in TTD on mixing dynamics of major water sources within large scale basins under varying hydrologic conditions are needed. Understanding and predicting TTD of water in large basins is important for water quality management because TTDs provide insights on how water is stored, released and travels through a basin (McGuire and McDonnell, 2006) which in turn directly controls contaminant transport and delivery to receiving water bodies. For instance, a high proportion of long travel times indicates longer time for biogeochemical reactions in the subsurface environment (McGuire and McDonnell, 2006) and implies prolonged release of more persistent pollutants via diffuse groundwater contributions to streams (Butscher and Huggenberger, 2009). In contrast, systems with a high proportion of short travel times are more vulnerable to highly reactive contaminants because the faster travel times in these systems do not allow sufficient time for pollution mitigating processes such as adsorption, degradation and decay (Butscher and Huggenberger, 2009). Studies of large basins have reported dominance of fast surface processes in uplands regions and increased dominance of slow groundwater processes in lowland regions (e.g. Tetzlaff et al., 2011; Ogrinc et al., 2008; Koeniger et al., 2009). These large basins are prone to dual vulnerability as they may receive both rapidly transported reactive contaminant from the upland regions and persistent contaminants from regional groundwater sources.

Numerical particle tracking schemes used in conjunction with integrated physical hydrologic models offer a relatively inexpensive alternative to extensive field sampling

based studies to understand factors controlling TTDs in catchments. Particle tracking experiments typically introduce solute particles (or water particles) into flow fields produced by a groundwater model and subsequently record the particles' movement with time. Results obtained include the particles' flow paths and transit times through the hydrologic system. If introduced in sufficiently large number, particles TTDs can be obtained without defining the functional form of the TTD a priori (e.g. Kollet and Maxwell, 2008b; de Rooij et al., 2012). Recent advancements in particle tracking schemes have made it possible to track particles flow paths through fully integrated surface water-groundwater-atmosphere (de Rooij et al., 2012). As such all the relevant physical processes such as three-dimensional saturated or unsaturated flow, two-dimensional overland flow, evapotranspirative fluxes from the land surface and shallow subsurface environment and infiltration into the subsurface can be accounted for while evaluating hydrologic and geologic factors controlling TTDs in a basin. This information may then be useful for predicting response of water bodies to changes in land and water management practices.

In this paper we present results obtained by applying Slim-Fast, a novel particle tracking scheme (de Rooij et al., 2012) which tracks solute or water particles through a fully integrated surface water – groundwater – land surface atmosphere system, to a large complex basin in North Central Florida. Slim-Fast works in conjunction with ParFlow.CLM, a fully integrated three dimensional variably saturated groundwater- two-dimensional surface water-one-dimensional land surface model that may be driven by spatiotemporally variable atmospheric forcing data. Particle tracking in transient flow fields was used to estimate time varying TTDs for water particles arriving at multiple

river locations within the Santa Fe River Basin (SFRB) during wet and dry hydrologic conditions in order to provide insights on factors controlling sources, travel paths, and travel time distributions for streamflow throughout the basin. In particular particle tracking experiments were designed to investigate (1) how river water sources evolve, interact and integrate in large basins spanning contrasting hydro-geological regimes; (2) how the spatiotemporal dynamics of dominant water sources, travel paths and TTD change under wet and dry hydrologic conditions; and (3) what topographic, geologic and climatic characteristics act as first order controls on TTDs and how these controlling factors vary with space and time in large basins.

4.2 Santa Fe River Basin

The SFRB is a mixed-use basin spanning an area of about 3700 km^2 in North-Central Florida. A complete description of the basin and its hydrogeologic characteristics are presented elsewhere (Srivastava et al., 2013a). Briefly, the SFRB consists of three distinct yet interconnected hydrogeological units (Figure 4-1; Schneider et al., 2008); (1) a confined region (CR) where the regional karst aquifer (Upper Floridan Aquifer System (UFAS)) is confined by the clay-dominated Intermediate Aquifer System (IAS) which is overlain by an unconfined sand-dominated surficial aquifer system (SAS); (2) an unconfined region (UR) where due to erosion the IAS confining unit is completely missing and the UFAS is overlain by a thin sand layer ; and (3) the semi-confined region (SCR) located where the CR transitions to the UR and the UFAS is variably confined by leaky or discontinuous clay-rich beds.

The CR is characterized by flat topography and poorly drained soil resulting in shallow water table conditions and a well developed stream network. In contrast, the UR has well drained soil which along with a major conduit network within the UFAS creates

internal subsurface drainage toward the main river. Eogenetic karst features found in Florida have retained their high matrix porosity in comparison to the more commonly known teleogenetic karst systems with low intergranular porosity (Vacher and Mylroie, 2002; Florea and Vacher, 2007). Therefore, in addition to the conduit network, primary matrix porosity in the UFAS plays an important role in groundwater storage and flow towards the river.

4.3 Methods

In this study, the TTDs for water particles were estimated following a two step experiment which included; (1) development and testing of a 3D integrated surface-subsurface-land process model ParFlow.CLM for the SFRB (Srivastava et al., 2013a); (2) use of three dimensional subsurface pressure fields and two dimensional surface pressure fields obtained from the integrated model in Slim-Fast to simulate the flow path and transit times of tagged water particles in the SFRB. Details regarding the methodology for developing the integrated model and its simulation results (step 1) are described in Srivastava et al., (2013a). Details on the numerical technique used to develop Slim-Fast are summarized in (de Rooij et al., 2012). For brevity here we provide details pertinent only to the work presented here.

4.3.1 Integrated Hydrologic Modeling

An integrated three dimensional surface water-groundwater-land surface model was previously developed for the SFRB (Srivastava et al., 2013a). The numerical platform used to develop the integrated model included: (1) ParFlow (Ashby and Falgout, 1996; Kollet and Maxwell, 2006; Kollet and Maxwell, 2008a; Maxwell and Miller, 2005) which simulates three dimensional variably saturated subsurface flow using Richards equation along with two dimensional overland flow using the Kinematic

wave equation along with Manning's equation; and (2) a modified version of Common Land Model (CLM; Dai et al., 2003; Maxwell and Miller, 2005; Kollet et al., 2009) which calculates near land surface-atmospheric fluxes, such as evapotranspiration losses, snow accumulation and melt processes, latent, sensible and ground heat fluxes, as a function of atmospheric variables such as precipitation, air temperature, pressure, wind speed, specific humidity, solar radiation and soil moisture in shallow subsurface and land surface.

ParFlow simulates the moisture content in the shallow subsurface environment and passes it to CLM which uses it, along with various atmospheric variables (listed above), to calculate energy and water balance in near land surface environment. CLM then returns net infiltration (or exfiltration in absence of rain) to ParFlow for use in calculating various surface and subsurface water balances and fluxes. This process is continued iteratively until the end of the simulation.

As described above, and in Srivastava et al. (2013a), SFRB is a complex and large eogenetic karst basin spanning three distinct yet interconnected hydrogeological regions with varying hydrologic behavior in terms of surface-groundwater interactions. The ParFlow.CLM application for the basin was developed and tested for the period January 1, 2000 through December 31, 2008 which included diverse climatological conditions including several extreme events. For instance year 2004 was an extremely wet period during which four major hurricanes and a major tropical storm crossed the state of Florida causing flooding over much of the study area. Conversely, years 2006 - 2007 were one of the driest periods ever recorded for the basin and were followed by

relatively wet conditions as a result of a tropical storm which occurred in September 2008.

The reliability of model predictions was established by validation of model predictions against long term field observations at multiple locations. In addition to commonly used criteria of streamflow and groundwater elevation predictions, high resolution (daily) as well as discrete (monthly) specific conductivity measurements based hydrograph separation results were used to evaluate surface and groundwater flow dynamics at multiple locations within the basin. Overall, the model predictions were found to provide a reasonable representation of regional hydrologic conditions over the study period.

To study the effect of variability in subsurface properties on source water locations, travel , and TTDs characteristics, the baseline model (described above) was rerun to obtain following three additional models; (1) baseline model with no high hydraulic conductivity 'conduit' regions; (2) baseline model with higher hydraulic conductivity 'conduit' zone (conduit k increased to 600 m/hr from baseline value of 270 m/hr); and (3) four order of magnitude higher hydraulic conductivity in IAS (10^{-5} m/hr as compared to baseline model value10^{-9} m/hr). Pressure fields from the first two models were used to study subsurface characteristics control over TTD in the UR whereas the last model were used to study the same for the CR.

4.3.2 Surface-Subsurface Particle Tracking

Particle tracking schemes accept pressure fields from flow models to reconstruct flux and flow velocity fields within the domain which can be used to trace flow paths of small imaginary particles introduced in the flow field (Anderson and Woessner, 1992). A modified version of the Lagrangian particle tracking scheme Slim-Fast (Maxwell et al.,

2003; Maxwell and Kastenberg, 1999) was used in this study to simulate TTDs of water particles in the SFRB. Previous versions of Slim-Fast used the classical advective particle tracking method of Pollock (Pollock, 1988) and allowed tracking of particles only within three dimensional variably saturated subsurface flow fields. The modified particle tracking scheme used here allows the movement of particles through a fully coupled surface and subsurface flow system using flow fields generated by ParFlow (de Rooij et al., 2012). Pathlines in both the subsurface and overland domains are obtained using Pollock's method (Pollock, 1988) which is a simple linear interpolation scheme that computes velocity components at a given particle location and subsequently moves the particle (within a given cell) to a new location (by multiplying the velocity components by a finite time step. Transfer of particles from the subsurface to the surface flow system or the atmosphere occurs if their trajectory intersects the land surface. Transfer of particles from the overland to subsurface domain or the atmosphere is achieved by using pathline specific transfer probabilities determined based on the mass balance of water within a narrow streamtube around particle's pathline (de Rooij et al., 2012). The purely advective particle tracking scheme used in this study does not account for local dispersion or molecular diffusion.

4.3.3 River Water Source Mixing Dynamics and Travel Time Distribution

Particle tracking schemes, when used in conjunction with integrated hydrologic models, provide maps of the spatial extent of varying water sources, travel paths and travel times under transient hydrologic conditions. For the experiments conducted in this study, 100,000 particles were placed in the river cells for stations 1500 and 2500 in the CR and UR of the SFRB, respectively (Figure 4-1). ParFlow.CLM generated pressure fields from the baseline ParFlow.CLM model (Srivastava et al., 2013a) and its three

variants (presented in section 3.1) were used to calculate daily cell velocities. The cell velocities were reversed in time to run the model in “backward mode” to transport the water particles back to their source location. The nine-year daily cell velocity sequence was repeated as necessary allow backtracking for 1000 years. This approach is similar to that adopted by (Kollet and Maxwell, 2008b) who repeatedly used one year of pressure field from a previous ParFlow simulation to obtain the age distribution of groundwater particles in Little Washita Basin.

Slim-Fast keeps track of and writes output files with information on particle locations as they move through the model domain with passage of time. When executed in backtrack mode the particles start from the end point (i.e. at river stations 1500 or 2500 in this study) and move backward in time towards their location of origin, either one of the domain boundaries or the atmosphere (which implies that the particle arrived as rain water within the domain). The location where a particle stops moving through the flow field indicates its entry point into the domain, and the time it takes to reach this entry point (from the starting river location) is its transit time in the domain. If large number of particles are introduced in the domain, transit times for all the particles can be used to construct the TTD of water arriving at a given river location at a given time. Releasing large numbers of particles at various locations and at multiple times allows investigation of the spatial variability as well as the effect of varying hydrologic conditions on the shape of TTDs. To study the effect of antecedent hydrologic conditions and storm magnitude on source water location and TTDs for stations 1500 and 2500 we conducted particle tracking experiments at multiple points along the streamflow hydrographs from three storms with varying antecedent hydrologic

conditions and an extended drought period (storms a, b, and e; droughts d1 through d3 in Figures 4-3 - 4-5). Results obtained for stations 1500 and 2500 were used to deduce and represent hydrologic behavior in the confined and unconfined hydrogeologic regions within the SFRB, respectively.

4.4 Results and Discussion

4.4.1 Streamflow Age Distribution Under Time Varying Hydrologic Conditions

In the CR of the watershed streamflow is episodic with virtually no inter-event subsurface baseflow. Thus there was no streamflow during the drought period d1-d3 at station 1500 (Figure 4-3) so CR particle tracking experiments were only performed for storms ‘a’, ‘b’, and ‘e’. Storm ‘a’ and ‘e’ occur after drier conditions when subsurface storage was relatively low, whereas storm ‘b’ occurred in a wetter period when the subsurface storage was relatively high (Figure 4-3). Storm ‘a’ is characterized by a series of moderate intensity rain events that were distributed fairly uniformly over a period of 2 months (i.e. approximately from Feb 15 2003 (a1) through April 5 2003 (a7) in Figure 4-4). In contrast storms ‘b’ and ‘e’ received rain via a few high intensity events and were of shorter duration (Figure 4-4). Hydrologic conditions during the period when these storms occurred are summarized in Table 4-1.

Cumulative distribution functions (CDFs) for water travel times to station 1500 for the three selected storms are shown in Figure 4-6. The median age of water arriving at station 1500 was less than 7 days throughout the rising and falling limbs of the hydrographs for each of the storms, and 95% of the water arriving at station 1500 was less than 15 days old. The short median travel times for all TTDs at station 1500 indicates the dominance of rapid surface flow paths in this region. The variation among the TTDs over the hydrograph and by storm indicates the influence of rainfall spatial

pattern, rainfall intensity and antecedent conditions on TTDs for streamflow in the CR of the basin. Slightly longer travel times predominate at the beginning and end of each storm event, and there is more variability in the shapes of these TTDs across storms than those corresponding to peak streamflows. These results indicate that antecedent conditions do not have a strong control on TTDs for these large storms, however they do influence the total streamflow generated by the storms. For example despite approximately similar total rainfall, similar TTDs shapes, and roughly equivalent median water age (<7 days), less total streamflow and a lower streamflow to rainfall volume ratio was observed for storm 'e' in comparison to storms "a' and 'b' (see Table 4-1). These observations indicate that streamflow in the CR is triggered only when sufficient rainfall occurs to raise the water table above a particular threshold that creates direct floodplain-channel connectivity. The pattern of flood-plain connectivity controls the TTD which is relatively time invariant, particularly at peak flow; however the volume of rainfall above the trigger threshold varies with storm magnitude and antecedent conditions and controls the total streamflow volume.

At station 2500 in the UR TTDs showed a dramatically different shape from those for station 1500 (Figure 4-7). TTDs for the three storm events showed similar structure at 2500 with the percentage of "new" water (i.e. event water less than ~15days, or ~0.04 years old) increasing rapidly with the rising limb, reaching its peak value during peak of the storm hydrographs, and dropping more slowly with the recession limb. The fraction of new water ranges from about 12% of total flow during baseflow and drought conditions, up to about 90% of total flow during the largest storm peak (storm b). A break in the slope of the TTDs for all storms occurred at ~ 15 days, and indicated a

relatively small fraction of moderately old (i.e. >15 days to 20 years) near- stream subsurface contributions for all storm events (~ 6% during storm b to ~20% during storm e) to and the drought conditions (~44% during drought d1-d3). A second break the slope of the TTDs occurs at about 20 years reflecting a variable fraction very old subsurface contribution to streamflow, ranging from ~ 4% at the peak of the largest storm 'b' to ~44% for base flow and drought conditions. This slow moving "very old" water produces long tails in the TTDs at station 2500 indicative of fractal behavior similar to that observed in experimental catchments using environmental isotopes and geochemical tracers (e.g. Kirchner et al., 2000). TTDs during drought periods and in the "old" water region for storm events showed remarkable resemblance to each other (Figure 4-7); with drought periods showing an overall dominance of "moderately old" and "very old" water, with a small fraction of "new" water due to small rain events occurring directly on the stream channel.

The median age of water age of stream water at station 2500 varies with position on the streamflow hydrograph for each storm (Figure 4-8). During baseflow conditions (before and after the storm event) the median age of water arriving at station 2500 was similar to that during droughts d1-d3 (~ 16 years; Figure 4-8). Over the storm event the median age drops to <15 days at peak flows, with a more rapid drop and faster rebound in median age occurring for the wetter antecedent conditions (i.e. storms a and b). Storm e, with a drier antecedent condition and smaller streamflow to rainfall ratio, showed a slower drop in median age over the rising limb of the hydrograph, and a more rapid increase in median age over the receding limb of the hydrograph indicating a greater contribution of subsurface flow for this event. This

pattern of shift towards younger streamflow with increased antecedent moisture and therefore increased connectivity in the basin is consistent with findings in previous studies (e.g. McGuire et al., 2007).

4.4.2 Streamflow Origin and Flowpaths Over Contrasting Hydrogeologic Regions Under Different Hydrologic Conditions

Although insightful, TTDs alone do not provide information regarding the spatial origins of various sources of water within a basin. Particle tracking schemes have an advantage over methods which rely on only experimental tracer data to estimate TTDs in that they not only provide information on particles travel times but also provide information on source locations and flowpaths. The temporal variations in spatial extent of water sources help to identify dominant topographic, geologic, climatic and hydrologic processes that control observed hydrologic behavior at any given time and location in the basin.

Figures 4-9 and 4-10 illustrate the spatial extent of the contributing source area for streamflow at station 1500, as well as the time taken to travel from the point of origin (as rainfall) to the streamflow station during different times within storm hydrographs ‘b’ and ‘e’, respectively (Figure 4-3). As discussed previously these storms vary in terms of antecedent hydrologic conditions (Table 4-1; Figure 4-3). For the storm b, with higher rainfall volume and wetter antecedent conditions, a more rapid increase in contributing area occurs during the rising limb of the hydrograph. In contrast during storm e rainfall must initially fill the soil moisture deficit and raise the water table before generating significant runoff. However at peak flows, and at the end of the receding limb of the hydrographs, the contributing areas for the two storms look quite similar in spatial extent. In both cases, rainfall ultimately raises the water table to the land surface in the

vicinity of the stream, resulting in increased overland connectivity of river with the immediate floodplain resulting in high flow conditions. At the last point on the streamflow recession curve the contributing area is reduced from the peak, but is still substantially larger than the contributing area for the equivalent flow on the rising limb of the hydrograph, especially for storm e with the drier antecedent conditions. At this end of the storm, flow at station 1500 is sourced mainly by channel water collected during early part of storm events and surface contributions from low lying topographic depressions temporarily connected to the channel in the headwaters of the basin (e.g. Lake Santa Fe and the Santa Fe Swamp which constitute the headwaters of the Lower Santa Fe River). Based on the spatial extent, age distribution and the original source of particles identified by particle tracking (Figure 4-9G and 4-10H) recent rainfall falling directly on the floodplain was confirmed to be the source of streamflow for station 1500.

In contrast to station 1500 in the upper CR of the SFRB, streamflow at station 2500 in the UR was found to be a mixture of water of widely varying ages and sources. Based on shape and characteristics of TTDs water arriving at 2500 was classified as “new” (<15 days) , “moderately old” (16 days-20 years), and “very old” (20 years-1000 years). Figures 4-11 – 4-13, respectively, illustrate the spatial extent from which “new”, “moderately old”, and “very old” water traveled to station 2500 at different points along the storm ‘b’ hydrograph. Figures 4-14 – 4-16 illustrate the same for storm event ‘e’. Also shown in the plots is the age distribution within the water particles belonging to the three age categories. Comparison of spatial extent and location of water particles within different age categories confirms that the “new” water originates as rainfall in the upper CR of the basin that travels to the stream following fast surface flow paths, or as rain

falling directly on the unconfined stream channel, and that its spatial evolution with time follows that of station 1500 (Figure 4-9 and 4-10). In the early part of the storm hydrographs (Figure 4-11 A,B and 4-14 A,B,C) the unconfined river is disconnected from the lower UR of the watershed, thus rain directly over the channels is the only source of “new” water originating in the UR.

These figures also reveal that the “moderately old” water is primarily rain that fell on UR of the basin then infiltrated through the vadose zone to recharge the UFAS, with very small portion arriving from the CR via stream channels (Figures 4-12, 4-15). Within the UFAS this water either moved directly to the nearby stream channel or to nearby high hydraulic conductivity zones which then rapidly delivered it to the stream. The geometry of the high hydraulic conductivity regions and the contrast in hydraulic conductivity between the slow porous matrix and the high hydraulic conductivity regions explain the wide range of age of the moderately old water (~15 days to 7300 days (20 years)), with water age increasing dramatically with distance from the high hydraulic conductivity zones (see Figure 4-2 for high hydraulic conductivity zone locations for comparison with “moderately old” water flowpaths). It should be noted that according to the color scale in Figures 4-12 and 4-15 the red particles are older than 20 years. Thus these particles are still moving backward in the domain toward their point of entry 20 years prior to the storm event. Blue to orange particles exited the domain at the location indicated by their position and the time (less than 20 years) indicated by their color.

The “very old” water at 2500 arrives mostly from rainfall on the UR of the domain (Figures 4-13 and 4-16). This rainfall moved through the vadose zone to recharge the

UFAS in regions farther from the high hydraulic conductivity zones, leading to longer travel paths and longer travel times to the high hydraulic conductivity zones and to the river. It should be noted again that in Figures 4-13 and 4-16 blue to orange colors indicate that the particles have arrived at their entry point into the domain (i.e. they are no longer moving). A very small fraction of the particles (red) are located with the confined UFAS, still traveling toward the domain boundaries 1000 years prior to the study period.

4.4.3 Geologic Controls Over Water Travel Time and Flow Paths in an Unconfined Aquifer

To investigate the control of hydraulic conductivity contrasts between the porous matrix and high hydraulic conductivity regions on source water locations, travel paths and TTDs, ParFlow- Slim-Fast simulations were run for two basecase variants: a “no conduit” case where high hydraulic conductivity regions were assigned the same hydraulic conductivity as the porous matrix (9 m/hr) and a “high hydraulic conductivity conduit” case where high hydraulic conductivity regions were assigned a hydraulic conductivity of 600 m/hr (versus 270 m/hour for the base case). Significant variations in the shape of TTDs and spatial pattern of particle source locations were observed at station 2500 between these cases for storm events as well as during droughts (Figures 4-7, 4-17 and 4-18). Similar behavior was observed for all storm events, so for brevity only storm e and the drought d results will be discussed here. Analogous plots for storm b can be found in the Appendix Figure A-3.

Comparison of TTDs at 2500 for the three cases shows that the fractions of new water, moderately old water and very old water vary differently throughout the storm hydrograph based on the hydraulic conductivity contrast between the high hydraulic

conductivity zones and the porous matrix (Figures 4-17 and 4-19). At baseflow conditions (point e1 before and point e7 after the storm) the no conduit case shows the lowest fraction of new water and moderately old water, and the highest fraction of very old water compared to the other cases (Figure 4-19). In contrast during high flows (points e3 through e5) the no conduit case shows the highest fraction of new water, the lowest fraction of moderately old water, and about the same fraction of very old water as the other cases (Figure 4-19). The inflection points of the hydrograph (points e2 and e6) show transitional behavior between these two regimes.

Figure 4-20 shows that the influence of hydraulic conductivity contrast on median age of the streamflow is most pronounced on the falling limb of the hydrograph (i.e. point e6). Points at the beginning and end of the streamflow hydrograph (e1, e7) have a median age of 16 and 12 years (base case and conduit cases) to 26 years for the no conduit case. At high streamflows (points e3-e5) the median water age is <15 days for all cases. However at the inflection point of the falling limb (point e6) the median age ranges from <15 days for the no conduit case, to < 60 days for the base case, to >1 year for the high hydraulic conductivity case. The increase in conduit hydraulic conductivity also increases the spatial extent of the influence of high hydraulic conductivity zones by draining more of the surrounding matrix and thus facilitating more transport of “moderately old” water towards the river during low flows (Figure 4-21). This is reflected by the fact that the “moderately old” water fraction is consistently higher for the “high hydraulic conductivity conduit” case (Figure 4-19) and by the increased spatial distribution of moderately old water blue particles in the UR for storm e (Figure 4-21), storm b (Appendix) and the drought condition (Appendix).

Comparison of “new” and “old” fractions of water contributed to streamflow during storm event e reveals useful insights on the influence of conduit hydraulic conductivity on surface-groundwater interactions within the UR of the basin (Figure 4-22). Srivastava et al., (2013a) compared ParFlow-predicted versus EMMA-estimated subsurface contributions to streamflow during storm events for the base case model and concluded that the model was missing an important transient source of subsurface water during the storm recession period. Figure 4-22 compares EMMA versus ParFlow predictions of subsurface contributions to stream flow for the three conduit hydraulic conductivity cases during 2008 which includes storm e. This figure shows that increasing the hydraulic conductivity of the conduits increases the subsurface contribution to stream flow during the recession of the streamflow curve and thus improves the fit of model predictions of groundwater contributions to EMMA results. This indicates that transient source of old water missing from the base case streamflow recession curves may be released by high hydraulic conductivity conduits that are not well-represented in the base case.

Comparison of TTDs during storm e at 1500 and 2500 for the high IAS hydraulic conductivity test case showed that the TTDs for the base case and its high hydraulic conductivity variant are similar. However, the TTDs at 2500 showed that an increase in IAS hydraulic conductivity decreased the fraction of new water originating in the CR and increase in moderately old and very old water fractions at 2500 (Figures 4-23).

4.4.4 On Time Invariant Assumptions in TTD Modeling

Most of the studies of TTDs rely on inverse modeling techniques where rainfall and tracer time series are used to estimate the TTD of water (or some solute of interest) through an experimental or modeled catchment (Kirchner et al., 2001, McGuire and

McDonnell, 2006). These methods require a pre-defined functional form of the TTD which is often assumed to be invariant in time, an assumption which has been debated in the literature (Botter et al., 2010; Botter, 2012; Van der Velde et al., 2010). Recent work by (Van der Velde et al., 2010; Rinaldo et al., 2011; Botter et al., 2010b; Botter, 2012) showed that the TTD are not smooth and may vary with precipitation patters and antecedent conditions. Hrachowitz et al. (2010a) showed that the beta parameter of the gamma function fit to TTDs could be related to precipitation intensity and that the TTDs can vary inter-annually. McMillan et al. (2012) found that in the 0.9 km^2 Loch Ard Burn catchment a time invariant TTD was not able to reproduce the expected tracer response at shorter time scales. Longer time scale responses, on the other hand, were found to be reasonably well-represented by a steady state TTD. All these studies focused on small catchments (<10 km^2) and have not been tested at large scale.

Figure 4-24 shows the TTD observed during various times within storm 'b' and 'e' for station 1500 along with the best-fit log-normal TTD for each curve. As evident from Figure 4-24 the lognormal function was able to capture general shape and characteristics of the TTDs as long its parameters were allowed to vary over the storm. Furthermore this figure and Table 4-2 shows that the lognormal TTDs fit to the high flow portions of the hydrograph, when the maximum contributing area of the flood plain is connected to the river, have quite similar parameters.

TTDs for stations 2500 were separated into their "new" and "old" (comprised of both moderately and very old water) component's by (1) splitting the overall CDF into two time periods, the first consisting of particles less than 15 days old and the second consisting of particles older than 15 days; then (2) rescaling each CDF by the total

number of particles that arrived each time period. Similar to station 1500, a lognormal distribution fit the "new" water CDF for each storm quite well as long as the parameters were allowed to change throughout the hydrographs (Figure 4-25). The "old" CDFs for all storms and drought periods were well approximated by the gamma function with α parameters that indicate fractal behavior and are fairly constant over time (Figure 4-25 and Table 4-2). The small differences in shape and characteristics of "old" TTDs for wet and dry conditions is in agreement with previous findings from small scale studies (e.g. McMillan et al., 2012).

4.5 Summary and Conclusions

Slim-Fast, a fully coupled surface-subsurface particle tracking scheme, was used in conjunction with ParFlow.CLM, an integrated 3D surface water-groundwater-land surface hydrologic model, to study water source areas, travel paths and transit times within the Santa Fe River Basin. In addition to improving our understanding of the hydrologic functioning of this large complex basin, TTDs and spatiotemporal dynamics of major flow components estimated using Slim-Fast provided a valuable additional diagnostic tool for model evaluation and improvement.

Results indicate that in the CR of the SFRB channel-floodplain connectivity, which depends on topography and properties of the confining layer, exerts strong and largely time-invariant control on the shape of the TTD. However antecedent storm conditions and storm volume exert a transient and non-linear (threshold) control on total volume of streamflow generated in this region. In the UR of the SFRB the total streamflow TTDs were found to be composed of two components: a rapid "new water" contribution that originates as rainfall and travels overland in the CR, and a slow "old

water" contribution that originates as rainfall in the UR that recharges groundwater then moves to the stream via both localized high hydraulic conductivity flow paths (conduits) and the porous limestone matrix. The shape of "new water" TTD is controlled by the same factors which control total streamflow TTDs in the CR, whereas the shape of the "old water" TTD is controlled by the regional groundwater flow system and the contrast in hydraulic conductivity between high hydraulic conductivity regions and the porous matrix. The relative weights of the "new water" TTD and "old water" TTD to the total streamflow TTD in the UR are a function of antecedent conditions and storm magnitude via their control on streamflow volumes generated in the CR. These findings underscore the dual vulnerability of the Santa Fe River to the rapid transport of reactive contaminants (e.g. pesticides) generated in the CR during storm events as well as long term persistent transport of more stable contaminants (i.e. nitrates) that have been leached into the unconfined Floridan aquifer system groundwater system.

The median age of streamflow in the CR of the basin ranged from approximately 1 day at the peak of storm hydrographs to approximately 7 days at the end of stormflow recession, with travel time distributions that varied over the hydrograph and between storms, but were generally well-fit by log-normal distributions with time-varying parameters. These results are similar to previous theoretical studies (e.g. Van der Velde et al. 2010) that at short time scales TTDs are transient in nature and not well-represented by a single function. The median age of subsurface contributions to streamflow in the lower portion of the basin was approximately 17 years, in close agreement to mean water ages estimated in springs that feed the river in this region using both chlorofluorocarbons (CCl_3F, CCl_2F_2 and $C_2Cl_3F_3$) and environmental isotopes

($^{18}O/^{16}O$, D/H, $^{13}C/^{12}C$, $^{15}N/^{14}N$) (Katz, 2004; Katz et al., 2001; Katz and Griffin, 2008). The travel time distribution of old subsurface contributions to streamflow in the unconfined area was well-fit by a gamma distribution showing fractal properties that did not significantly vary over time.

The coupled ParFlow.CLM- Slim-Fast modeling system was used to explore the effect of geologic heterogeneity on surface water-groundwater interactions in the SFRB. These experiments showed that increasing the hydraulic conductivity of the confining layer decreased total streamflow in both the CR and unconfined regions of the basin by lowering water tables in the CR. However changes in the hydraulic conductivity of the confining layer did not significantly affect the shape of the TTDs or the median age of streamflow in the CR for rainfall events large enough to induce direct flood-plain stream connectivity. These experiments also showed that while increasing conduit hydraulic conductivity had a relatively minor effect on total streamflow in the UR (Srivastava et al., 2013b) increasing conduit hydraulic conductivity significantly affected the spatial pattern of the sources of subsurface contributions to streamflow. Furthermore increasing conduit hydraulic conductivity increased groundwater contributions to the recession limb of the streamflow hydrograph, producing behavior more similar to that observed from EMMA (Srivastava et al., 2013a). These results indicate that more accurate representation of conduit-matrix interactions via finer discretization and/or explicit representation of discrete conduits will likely improve model representation of streamflow and subsurface flow dynamics in the UR of the basin.

Table 4-1. Summary of hydrologic conditions during storm events ‘b’ and ‘e’ at station 1500.

	Subsurface storage at beginning of storm event (mm)	Storm cummulative rain (mm)	Storm cummulative flow (m^3/s)	Flow:rain
storm 'a'	35033	357	2163	0.04
storm 'b'	35075	401	2049	0.03
storm 'e'	35040	297	1041	0.02

Table 4-2. Parameter values for best fit function for overall CDFs at station 1500 and “new” and “old” water CDFs at station 2500

	USGS 1500 lognormal		USGS 2500 "new water" lognormal		USGS 2500 "old water" gamma	
Storm point	mean	standard deviation	mean	standard deviation	α	β
a1	1.51	0.76	1.14	0.45	0.66	58.79
a2	0.60	1.50	1.66	0.87		
a3	0.85	0.70	1.90	0.35		
a4	0.50	0.80	1.89	0.48		
a5	0.86	0.86	2.02	0.27		
a6	1.02	0.88	2.17	0.30		
a7	1.71	0.70	1.19	0.65		
b1	0.70	1.40	0.77	0.46	0.65	59.15
b2	0.10	0.64	0.1	0.91		
b3	0.55	0.63	1.54	0.29		
b4	0.70	0.83	1.76	0.28		
b5	0.64	0.83	1.93	0.28		
b6	1.10	0.81	2.17	0.27		
d1	-	-	-	-	0.68	57.21
d2	-	-	-	-		
d3	-	-	-	-		
e1	0.09	0.94	1.14	0.45	0.71	52.92
e2	0.01	0.10	1.06	0.31		
e3	0.01	0.50	0.82	0.64		
e4	0.71	0.63	2.06	0.28		
e5	0.76	0.84	2.13	0.28		
e6	0.92	0.82	2.22	0.33		
e7	1.77	0.77	1.27	0.64		

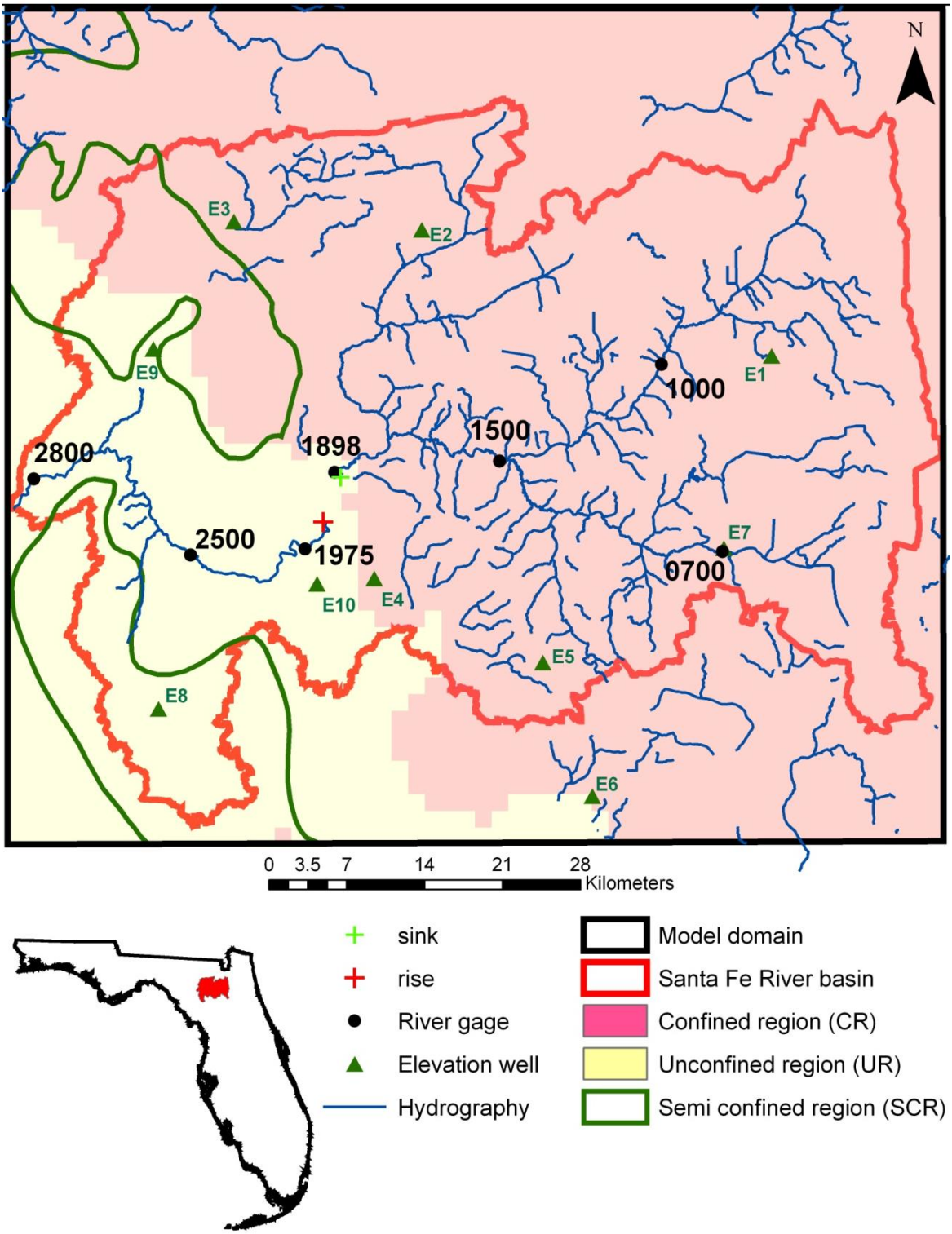

Figure 4-1. Map of the model domain. Also shown are the extents of the Santa Fe River Basin, locations of the river channels, monitoring wells, USGS stream gages and major hydrogeological regions in basin.

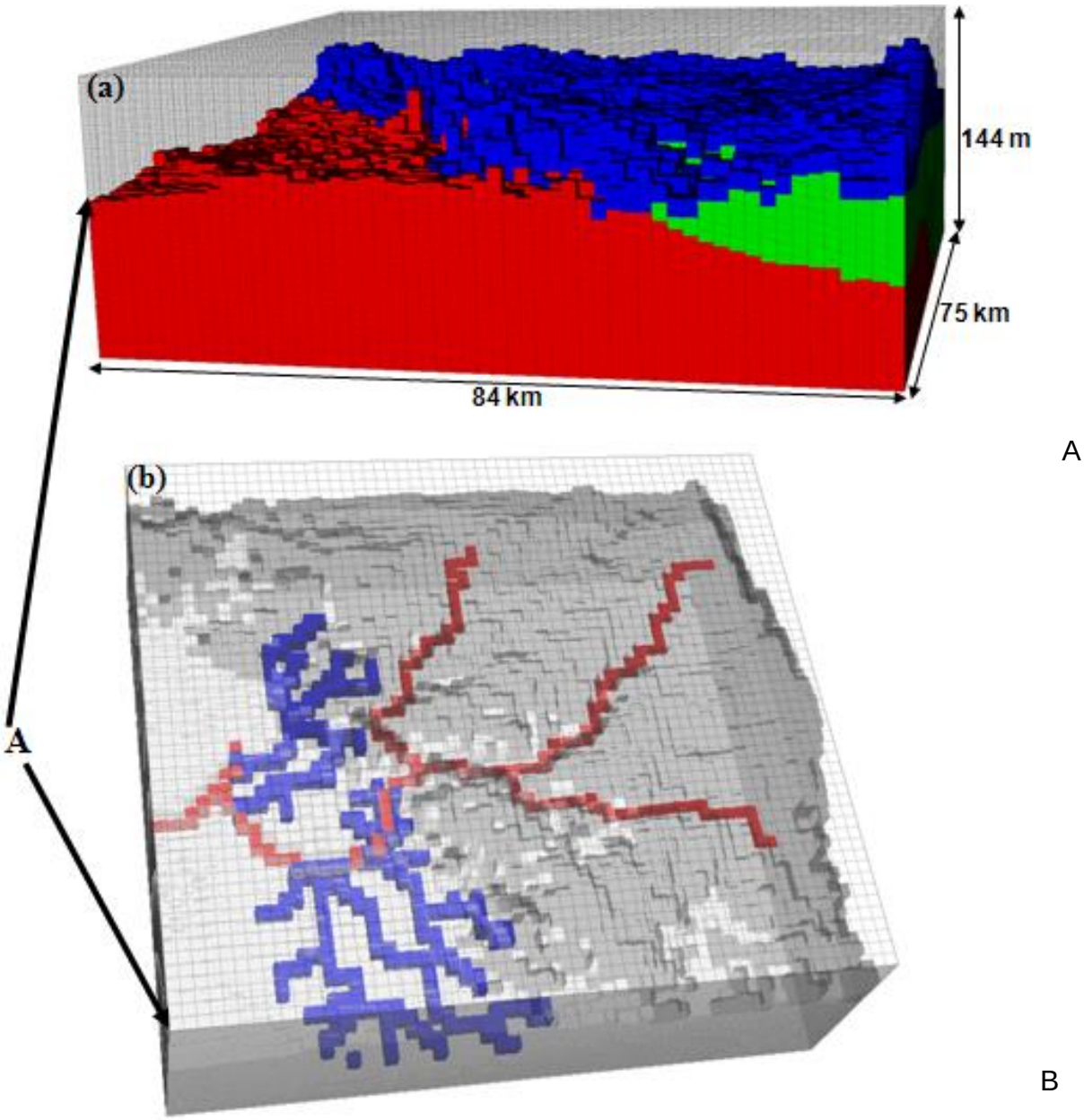

Figure 4-2. 3D mesh used to define the domain. A) the extent of the three major hydrogeological regions based on Floridan Aquifer Vulnerability Assessment (FAVA) dataset within the mesh along with their indicator variables, Surficial Aquifer System – blue region, Intermediate Aquifer System – green region, and Upper Floridan Aquifer System – red region. B) Locations of high hydraulic conductivity zones (blue cells) and main channels (red cells).

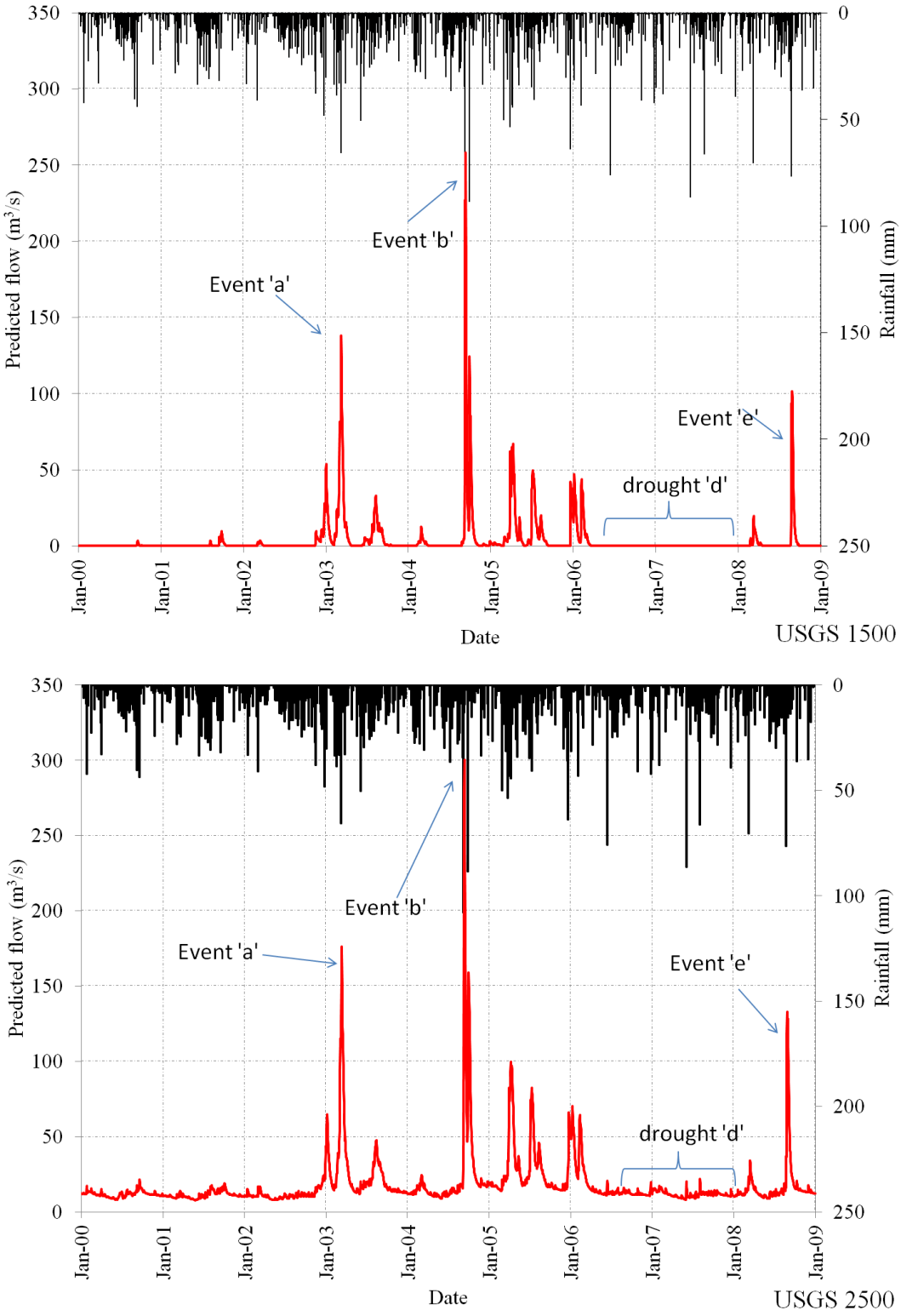

Figure 4-3. Time series of ParFlow.CLM simulated daily flow at station 1500 and station 2500. Storm events a, b, and e are marked along with drought d. Also shown is mean daily rainfall received by the domain (inverted bars in top plot).

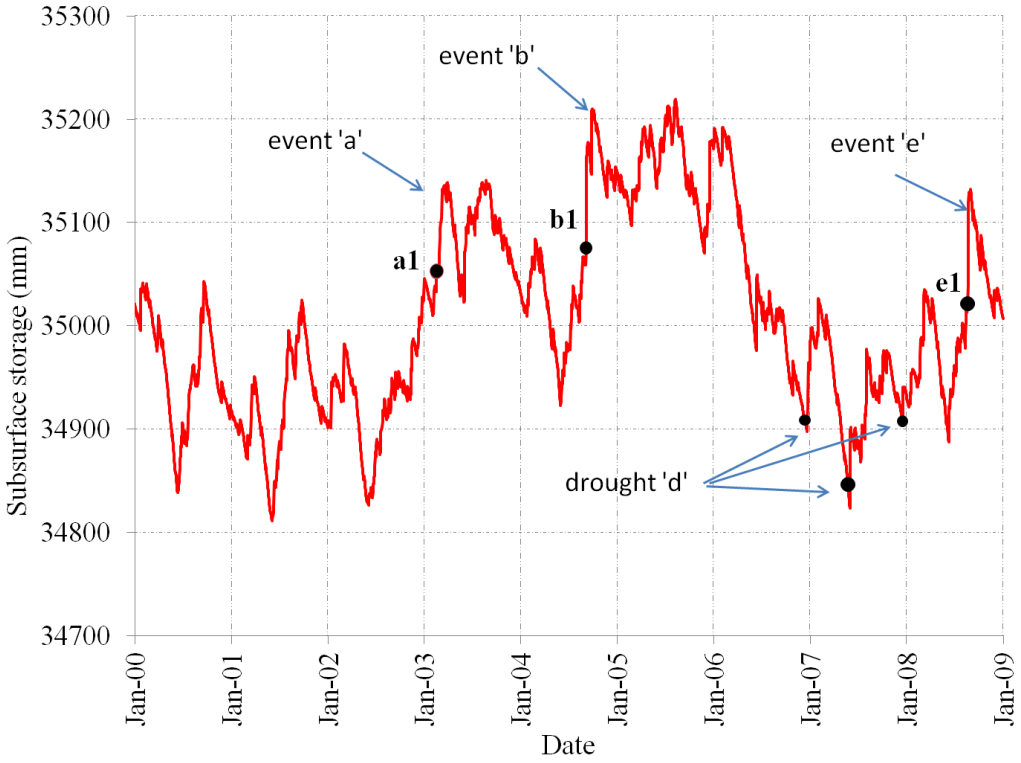

Figure 4-3.Continued.

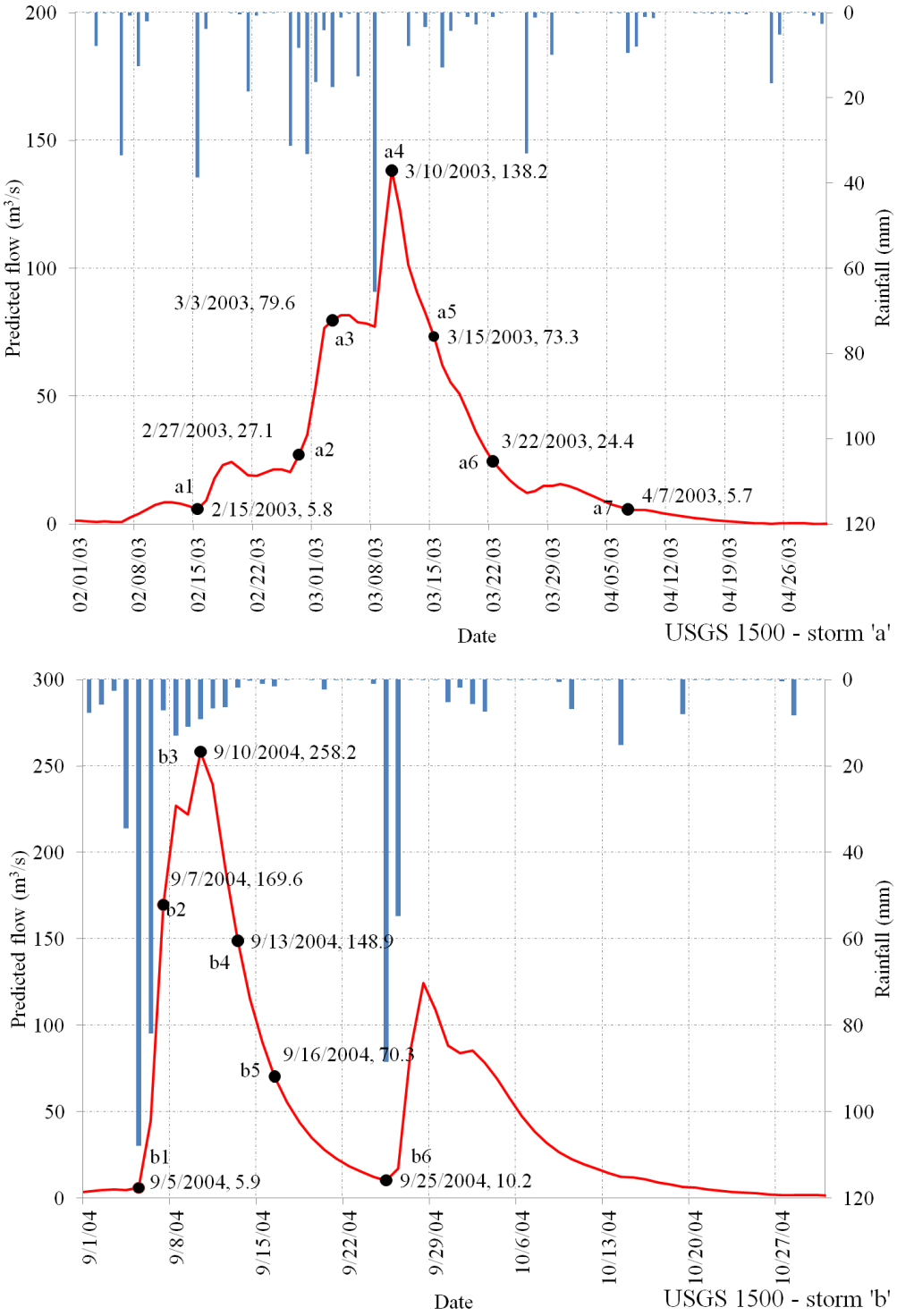

Figure 4-4. Hydrograph points where particle tracking experiments were conducted during year 2003 and year 2004 storm events at station 1500. These storms are referred to as ‘a’ and ‘b’ in figure 4-3. Numbers next to each point show date and flow value corresponding to each point. Also shown is mean daily rainfall received by the domain (inverted bars).

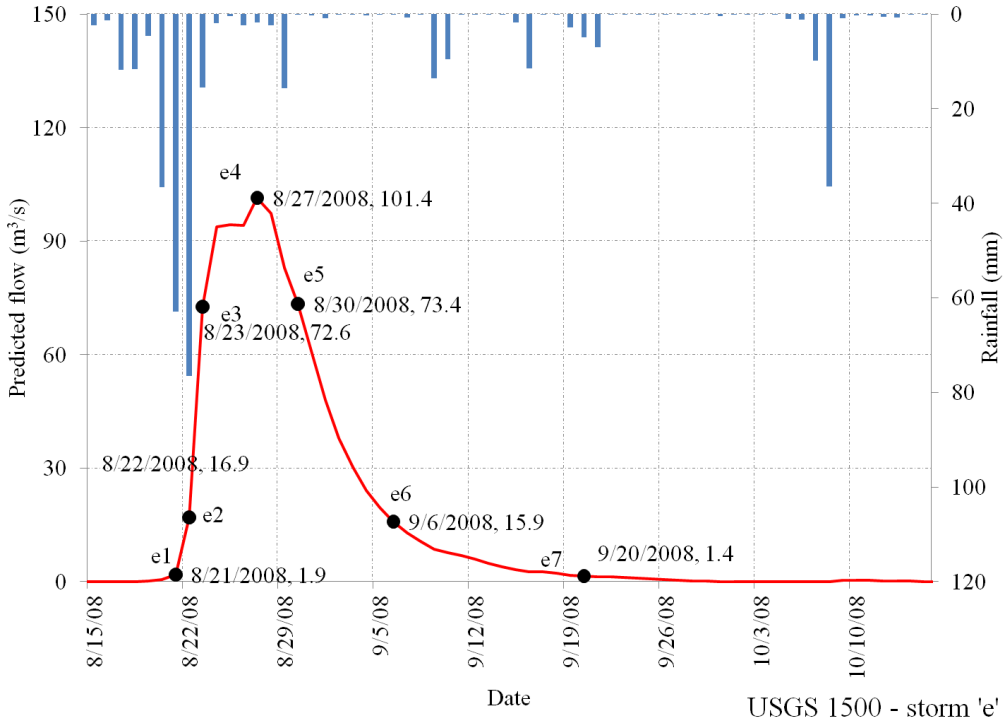

Figure 4-4. Continued.

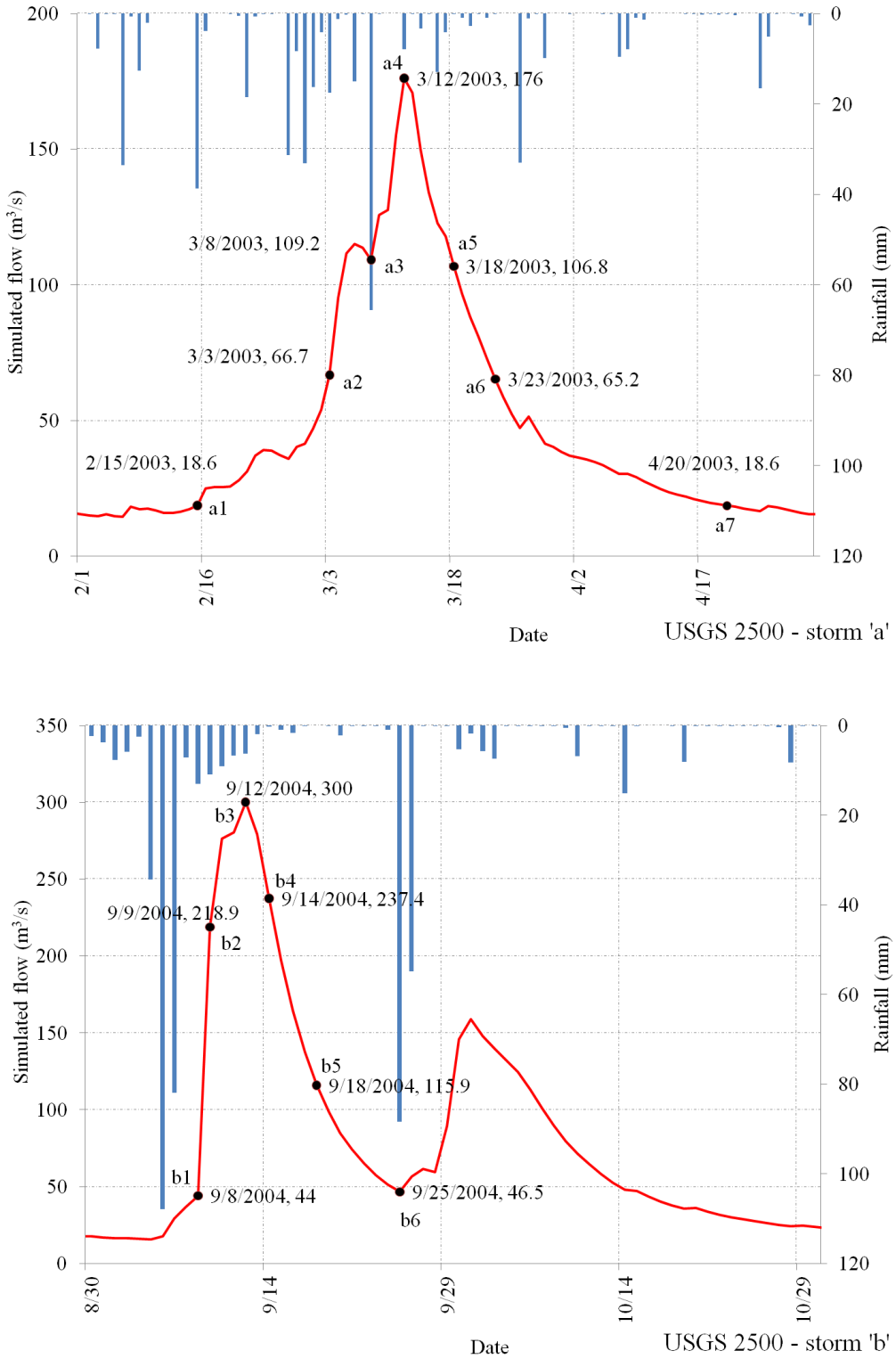

Figure 4-5. Hydrograph points where particle tracking experiments were conducted during year 2003 and year 2004 storm events. These storms are referred to as ‘a’ and ‘b’ in figure 4-3. Numbers next to each point show date and flow value corresponding to each point. Also shown is mean daily rainfall received by the domain (inverted bars).

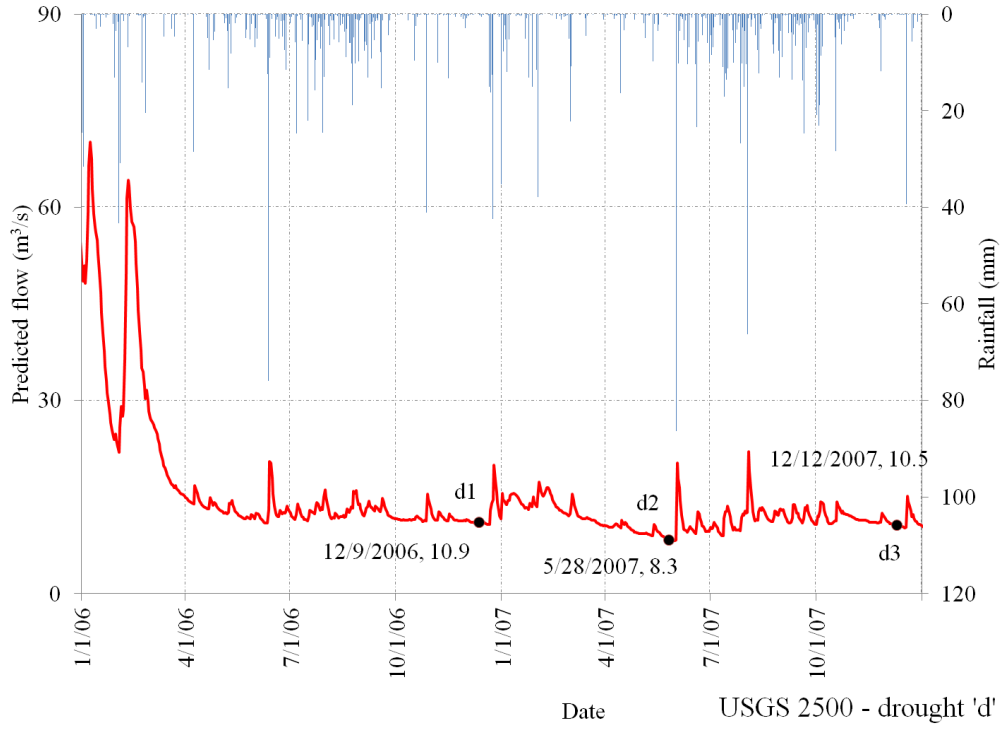

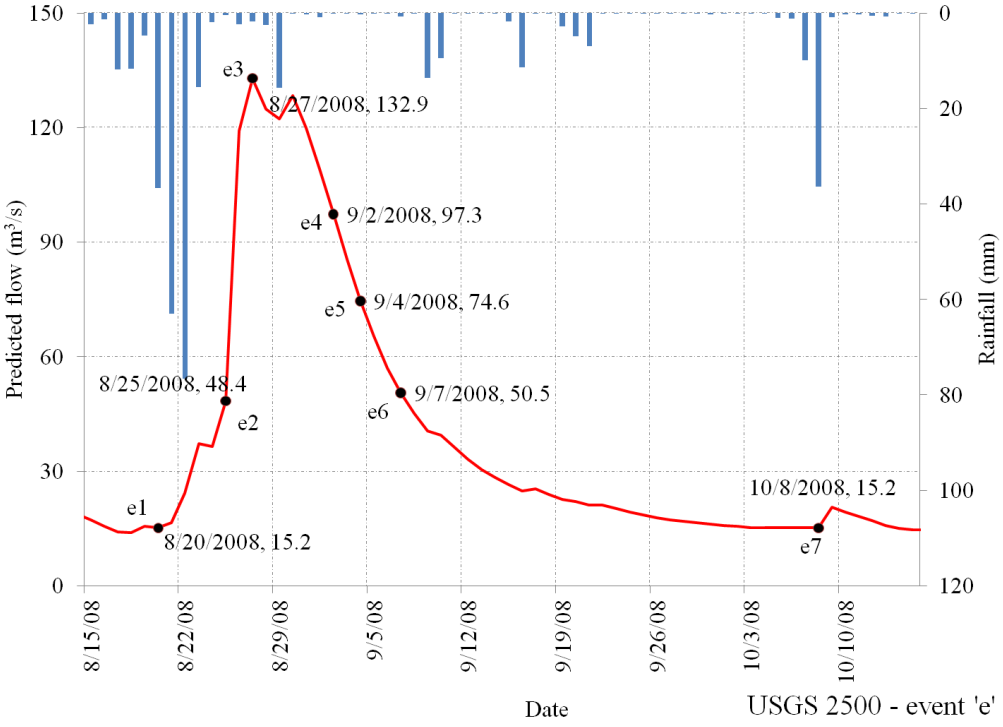

Figure 4-5. Continued.

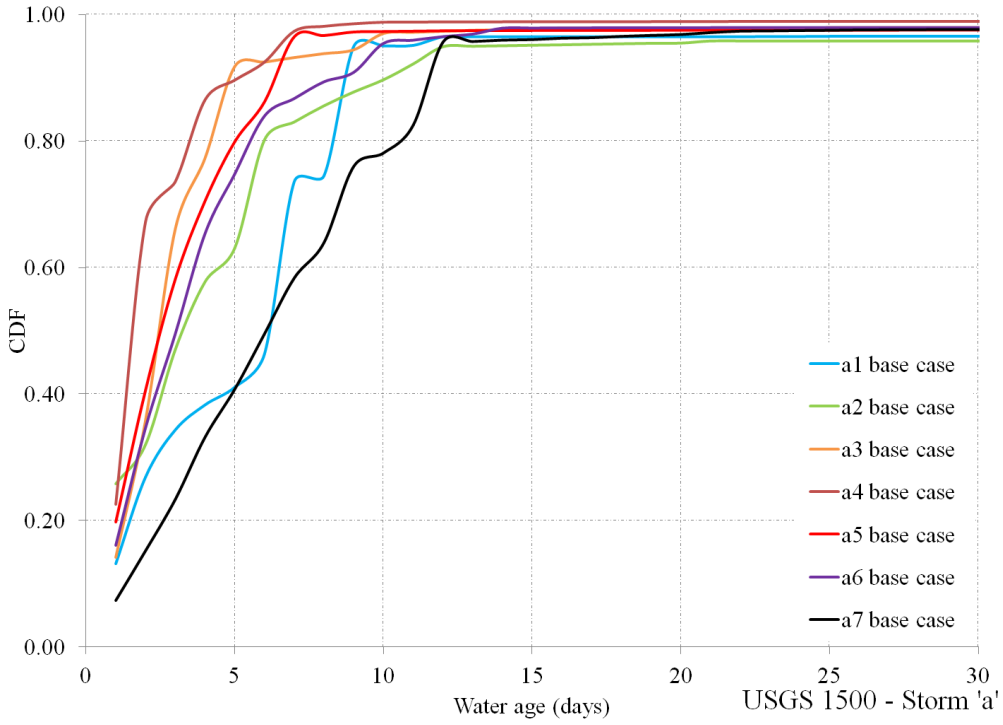

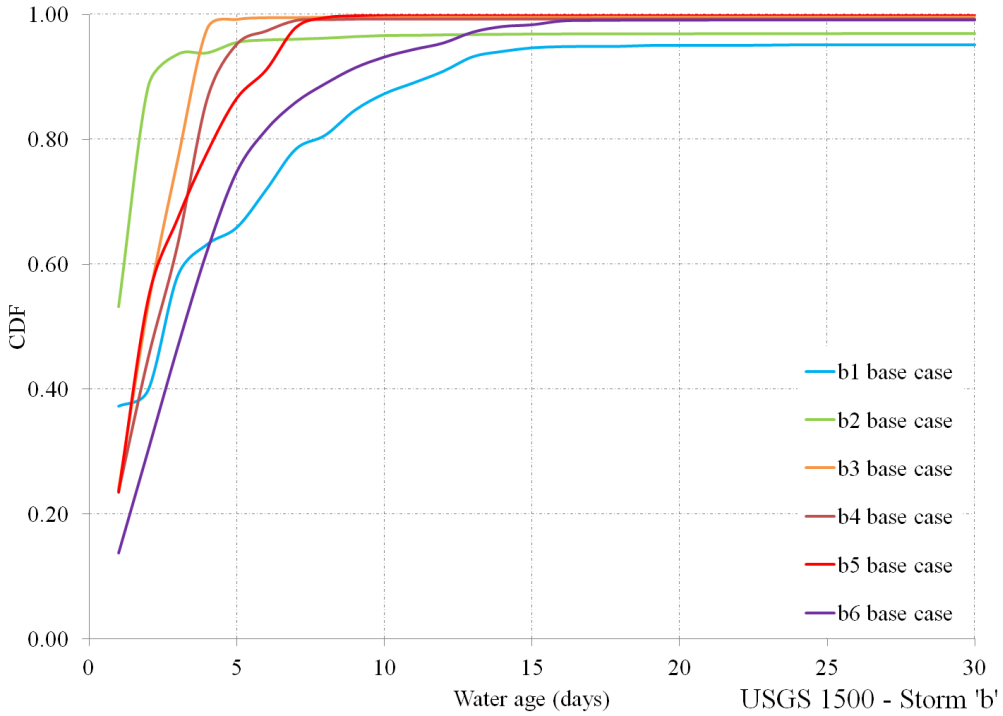

Figure 4-6. Water particle age distribution at station 1500 for various points on storm events ‘a’ and ‘b’. Note that the water age is reported in days at station 1500.

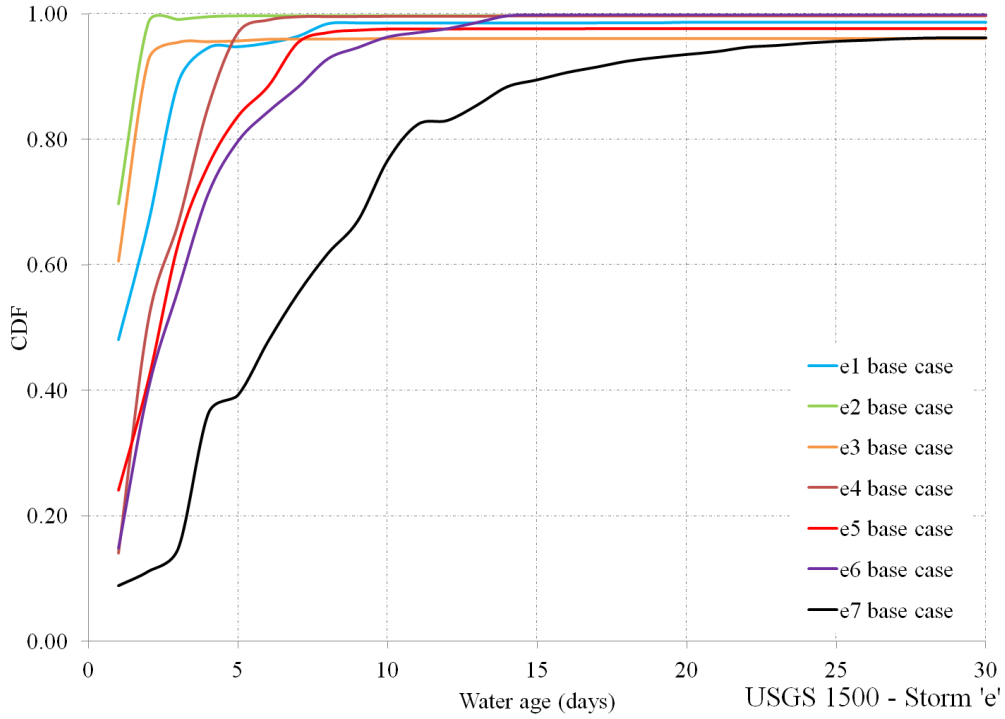

Figure 4-6. Continued.

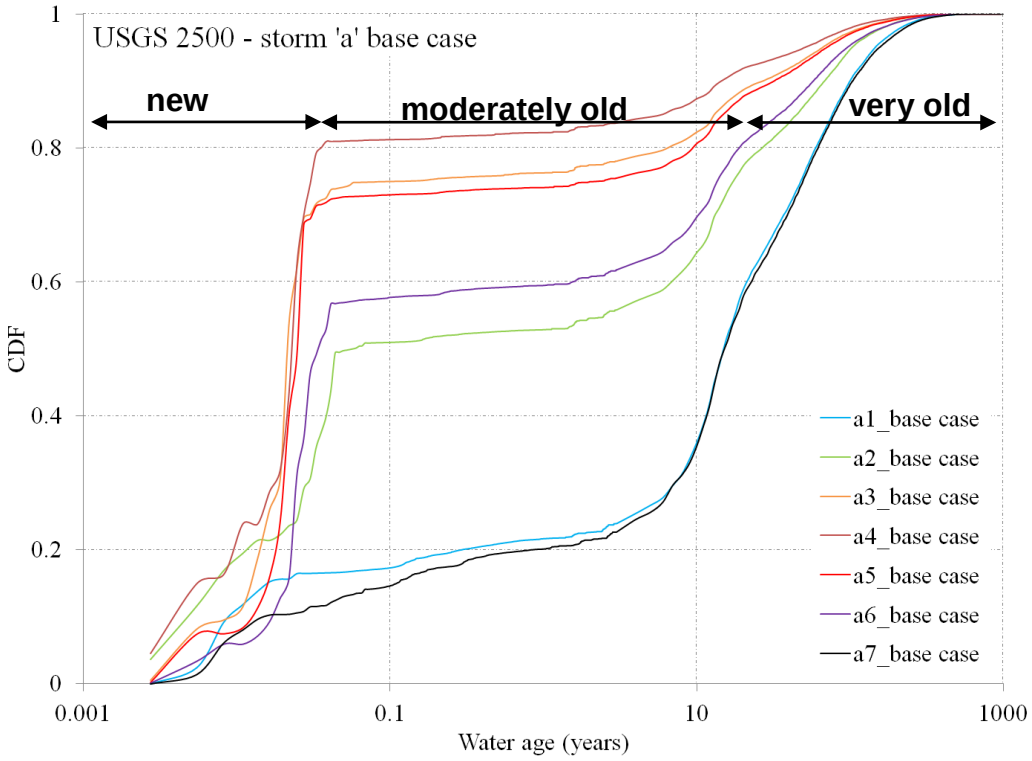

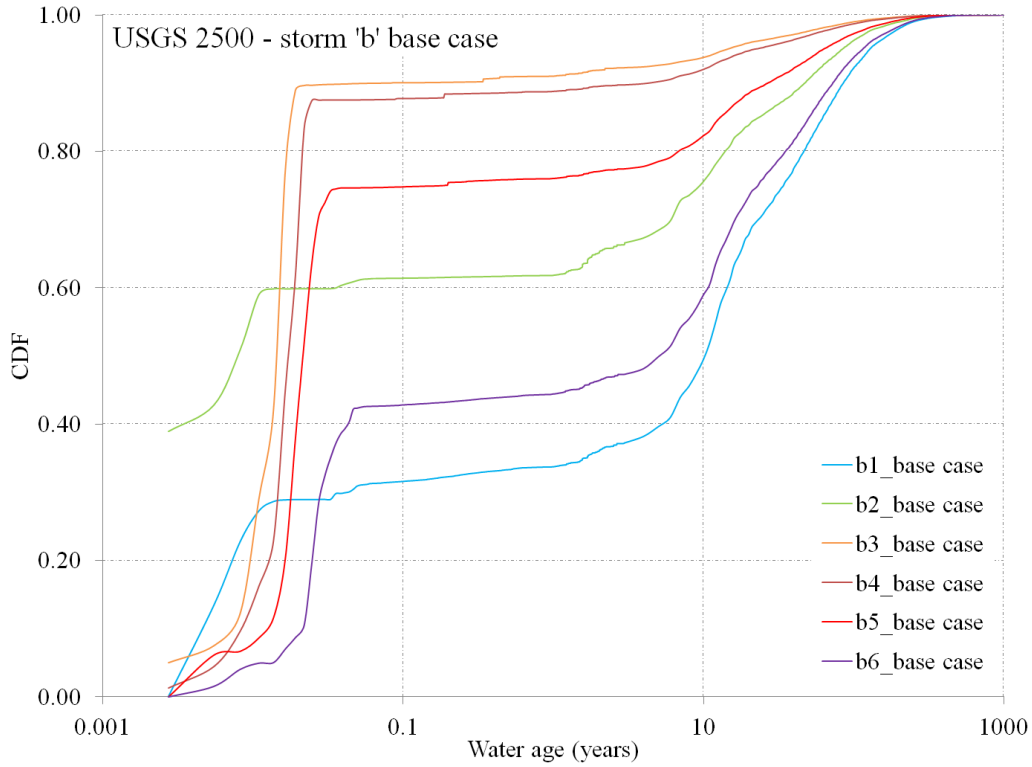

Figure 4-7. Water particle age distribution at station 2500 for various points on storm event ‘a’ and ‘b’ for base case model.

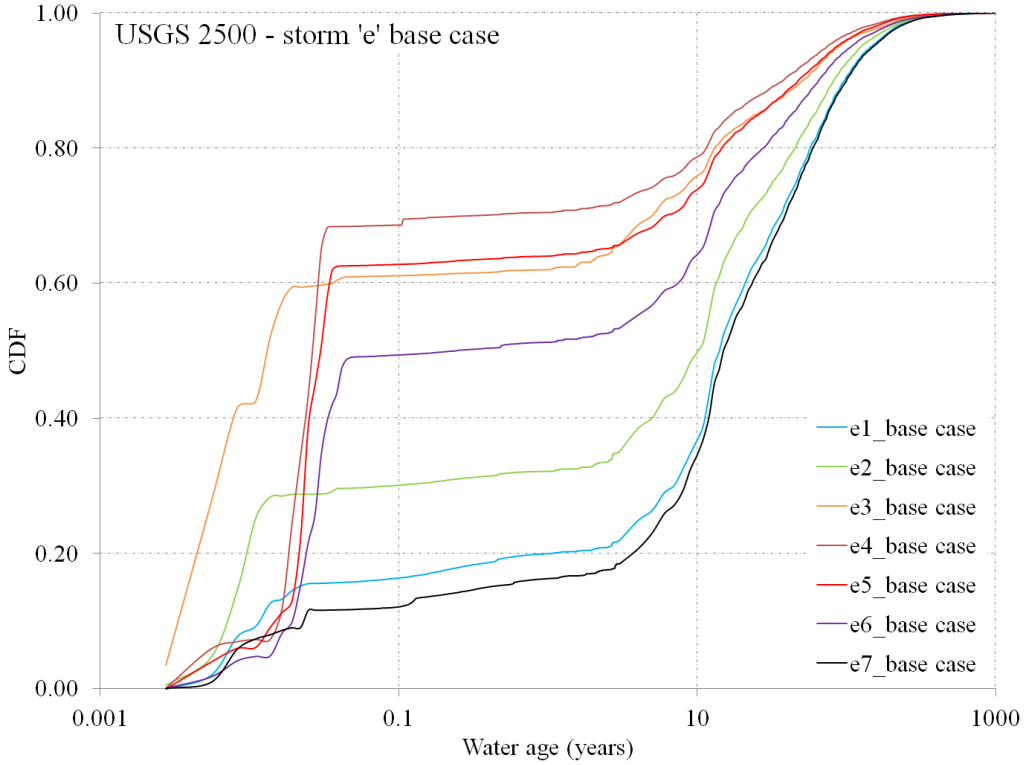

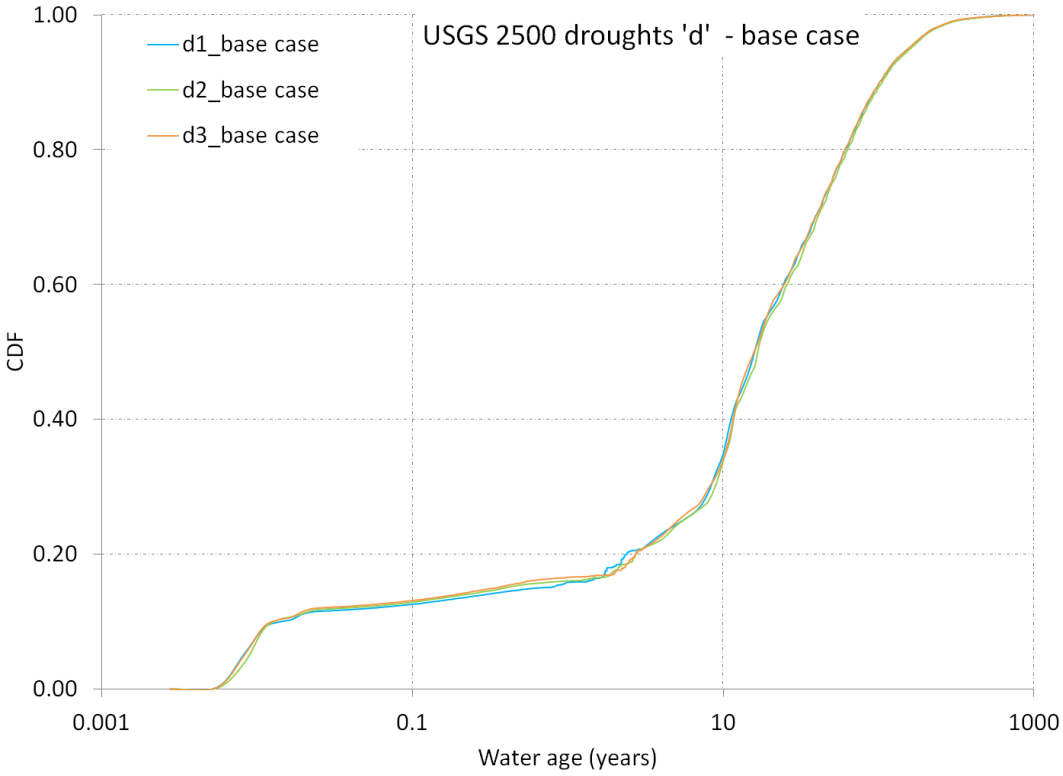

Figure 4-7. Continued.

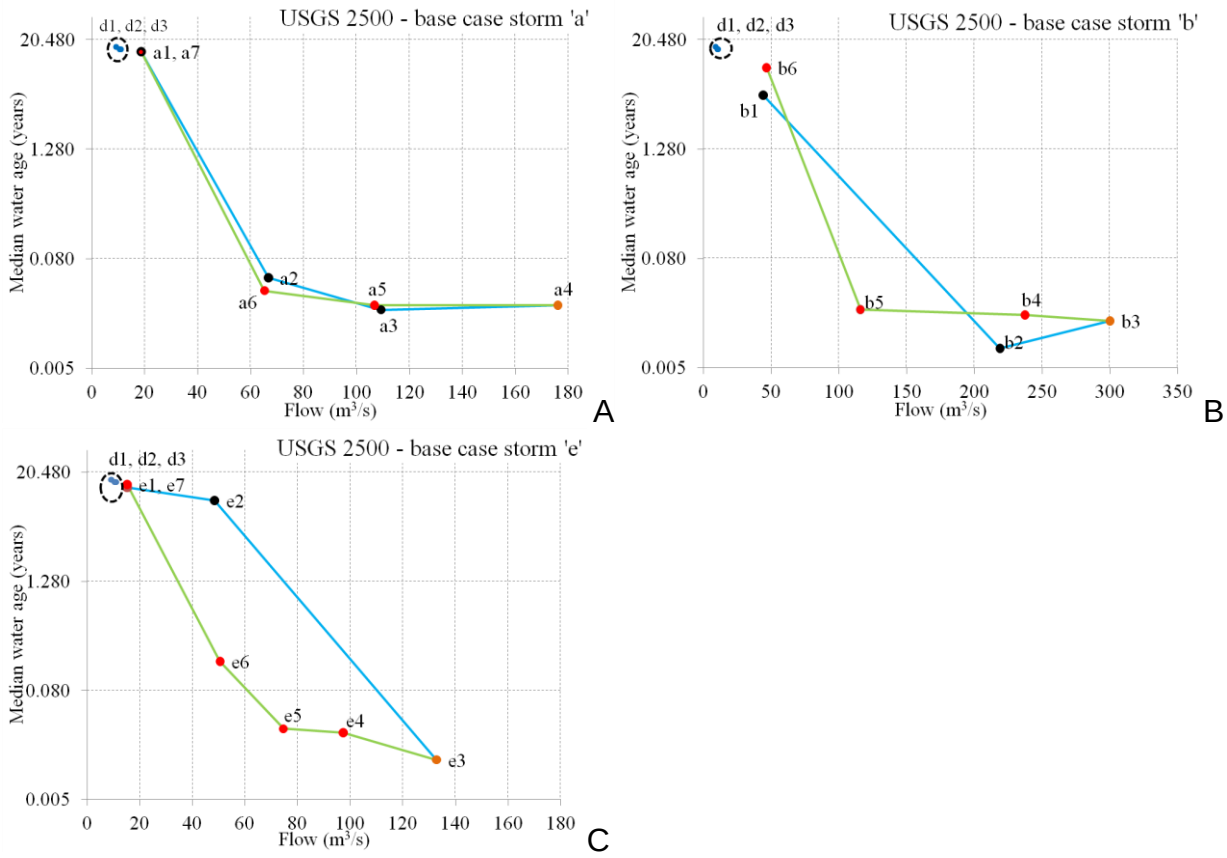

Figure 4-8. Water particle median age versus flow for base case model at various times during storm hydrographs for A) Storm ‘a’. B) Storm ‘b’. C) Storm ‘e’. Blue line with black circles present data for the rising limb and green lines with red circles present data for the recession period; value corresponding to storm peak is represented by orange circle. Also shown are the median water ages for the three drought periods (dotted circle on upper left corner of each plot).

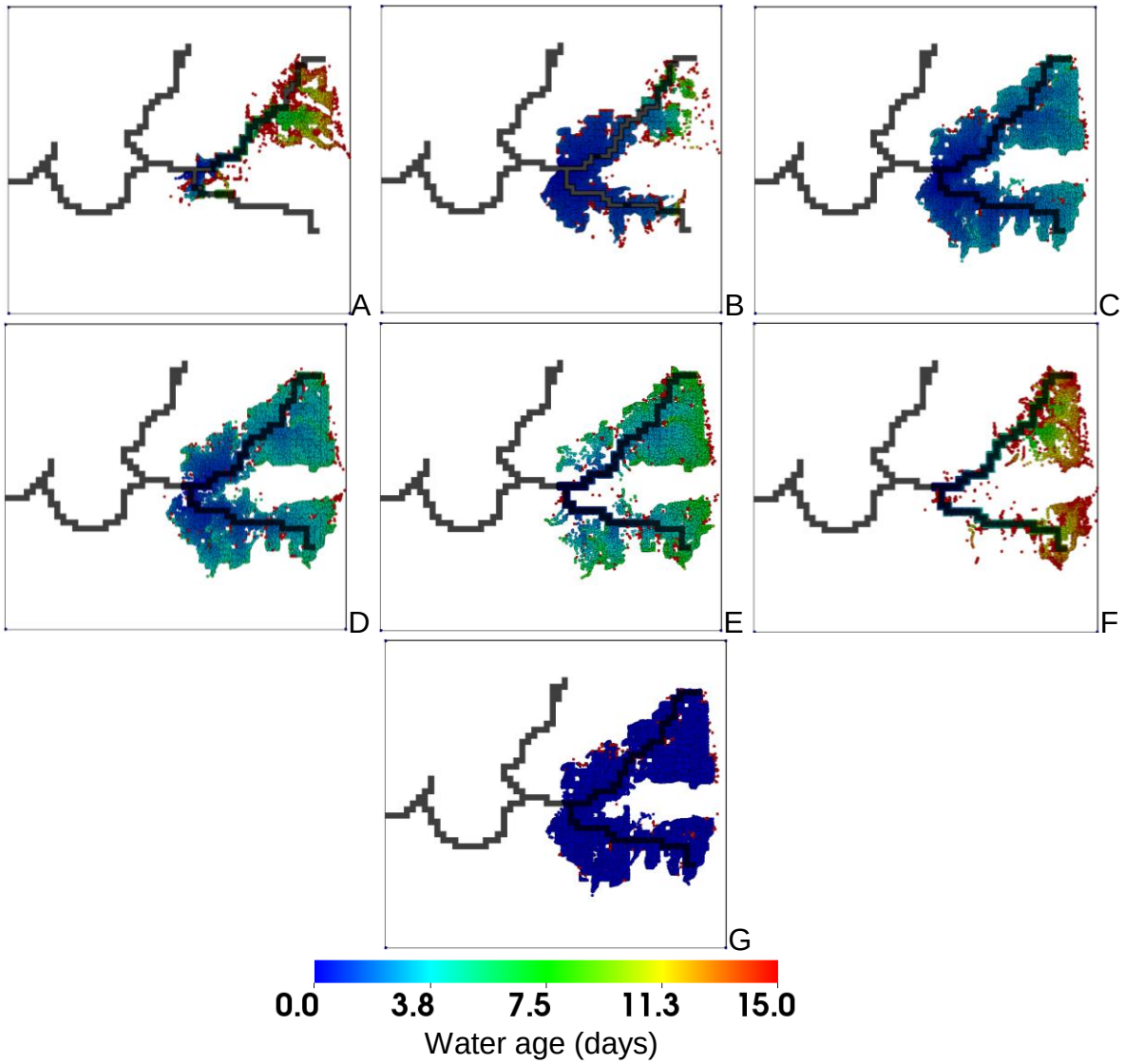

Figure 4-9. Spatial extent from which water particles arrived at station 1500 during storm event ‘b’. A - F corresponds to points b1-b6 in figure 4-4. The color scheme shows the age (days) of all the particles arriving at station 1500 during storm ‘b’. (G) Source of water arriving at station 1500 during peak of storm ‘b’ (point b3 in figure 4-4) with blue and red dots representing rainfall or surficial aquifer system.

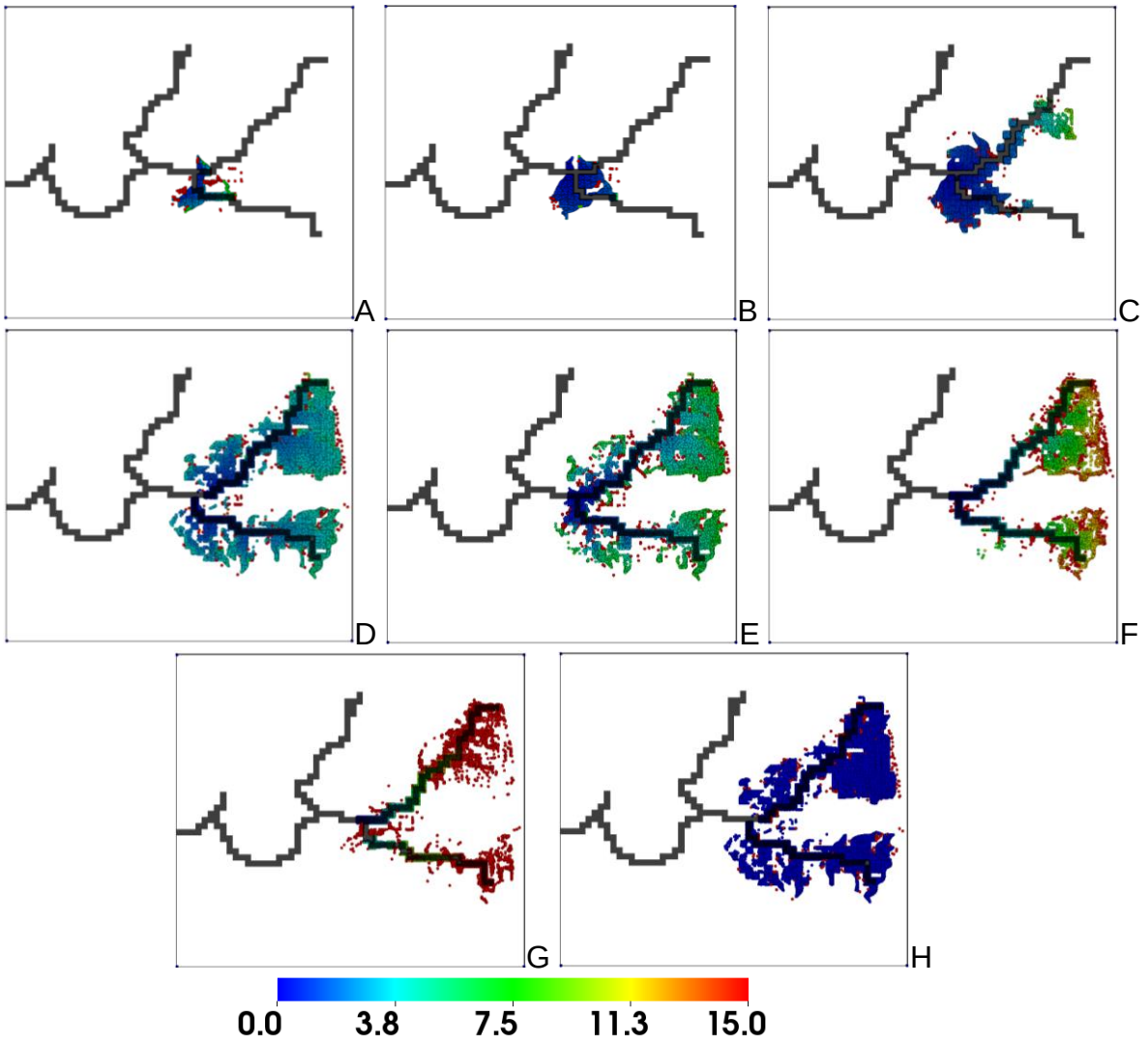

Figure 4-10. Spatial extent from which water particles arrived at station 1500 during storm event ‘e’. A - G corresponds to points e1-e7 in figure 4-4. The color scheme shows the age (days) of all the particles arriving at station 1500 during storm ‘e’. (H) Source of water arriving at station 1500 during peak of storm ‘e’ (point e4 in figure 4-4) with blue and red dots representing rainfall or surficial aquifer system.

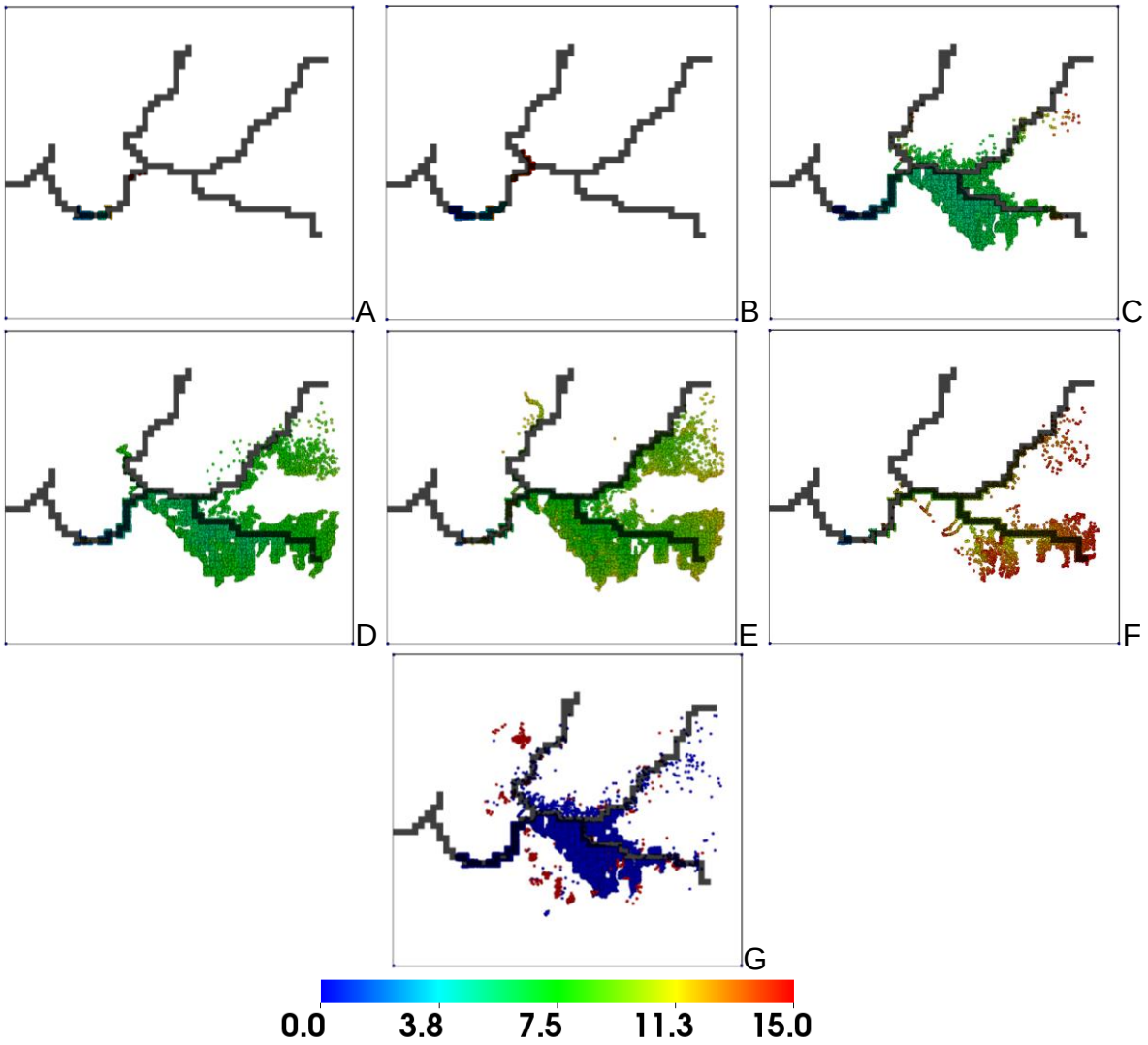

Figure 4-11. Spatial extent from which “new” water particles arrived at station 2500 during storm event ‘b’. A - F corresponds to points b1- b6 in figure 4-5. The color scheme shows the age (days) of all the particles arriving at station 2500 during storm ‘b’. (G) Source of water arriving at station 2500 during peak of storm ‘b’ (point b3 in figure 4-5) with blue and red dots representing rainfall or surficial aquifer system.

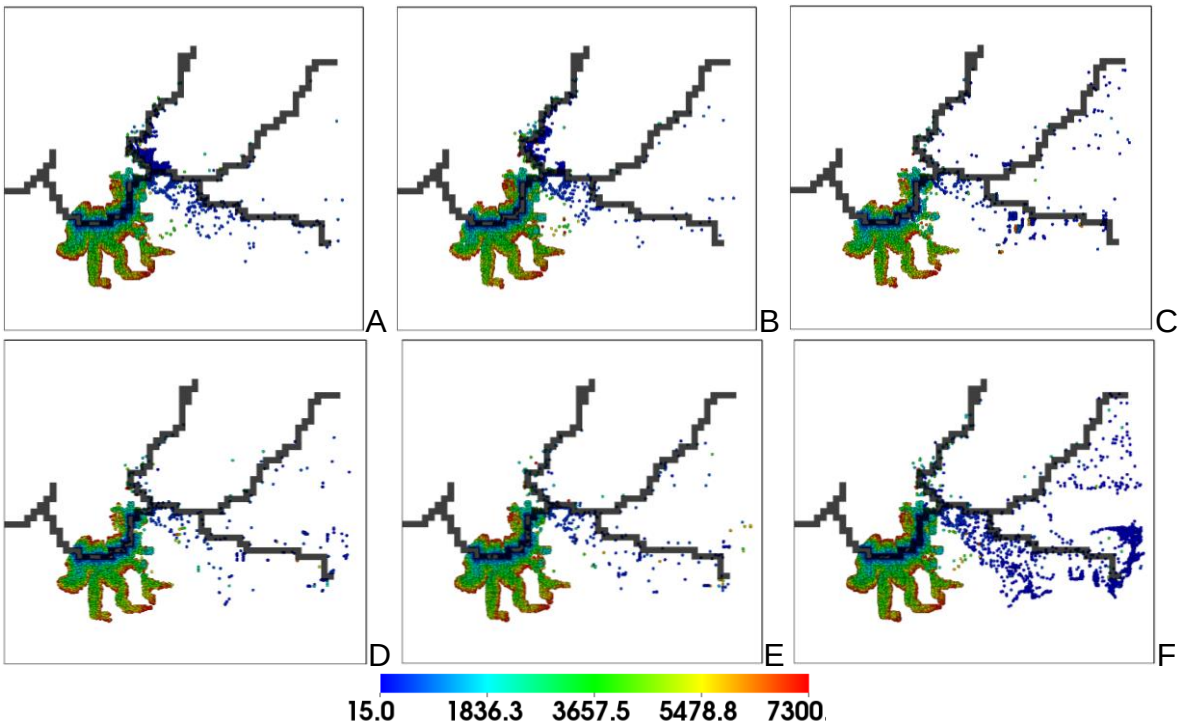

Figure 4-12. Spatial extent from which “moderately old” water particles arrived at station 2500 during storm event ‘b’. A - F corresponds to points b1- b6 in figure 4-5. The color scheme shows the age (days) of all the particles arriving at station 2500 during storm ‘b’.

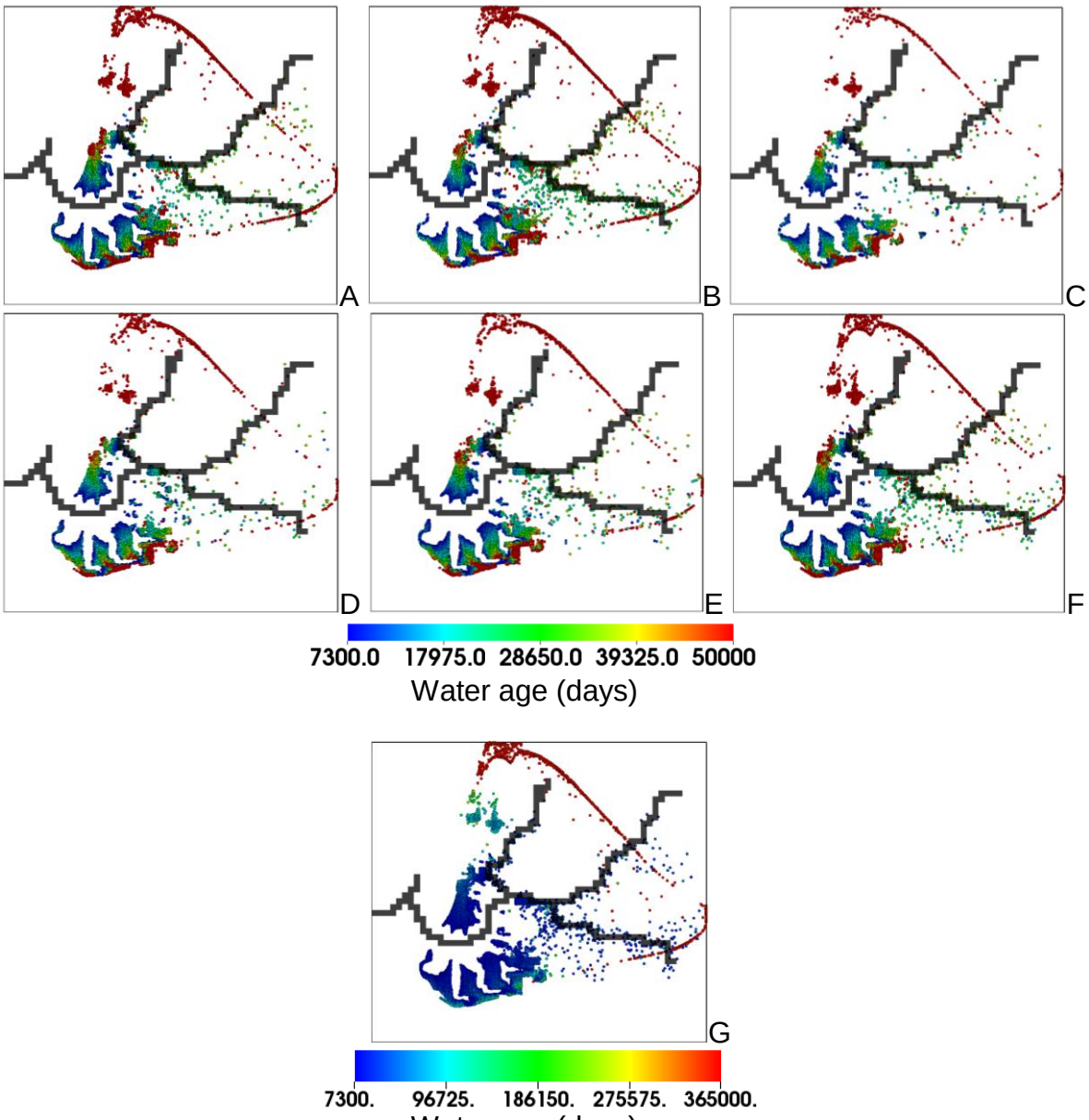

Figure 4-13. Spatial extent from which “very old” water particles arrived at station 2500 during storm event ‘b’. A - F corresponds to points b1- b6 in figure 4-5. The color scheme shows the age (days) of all the particles arriving at station 2500 during storm ‘b’. (G) Point b6 result (F above) with new scale shown below the figure which shows full range of age distribution of particles at the end of 1000 years.

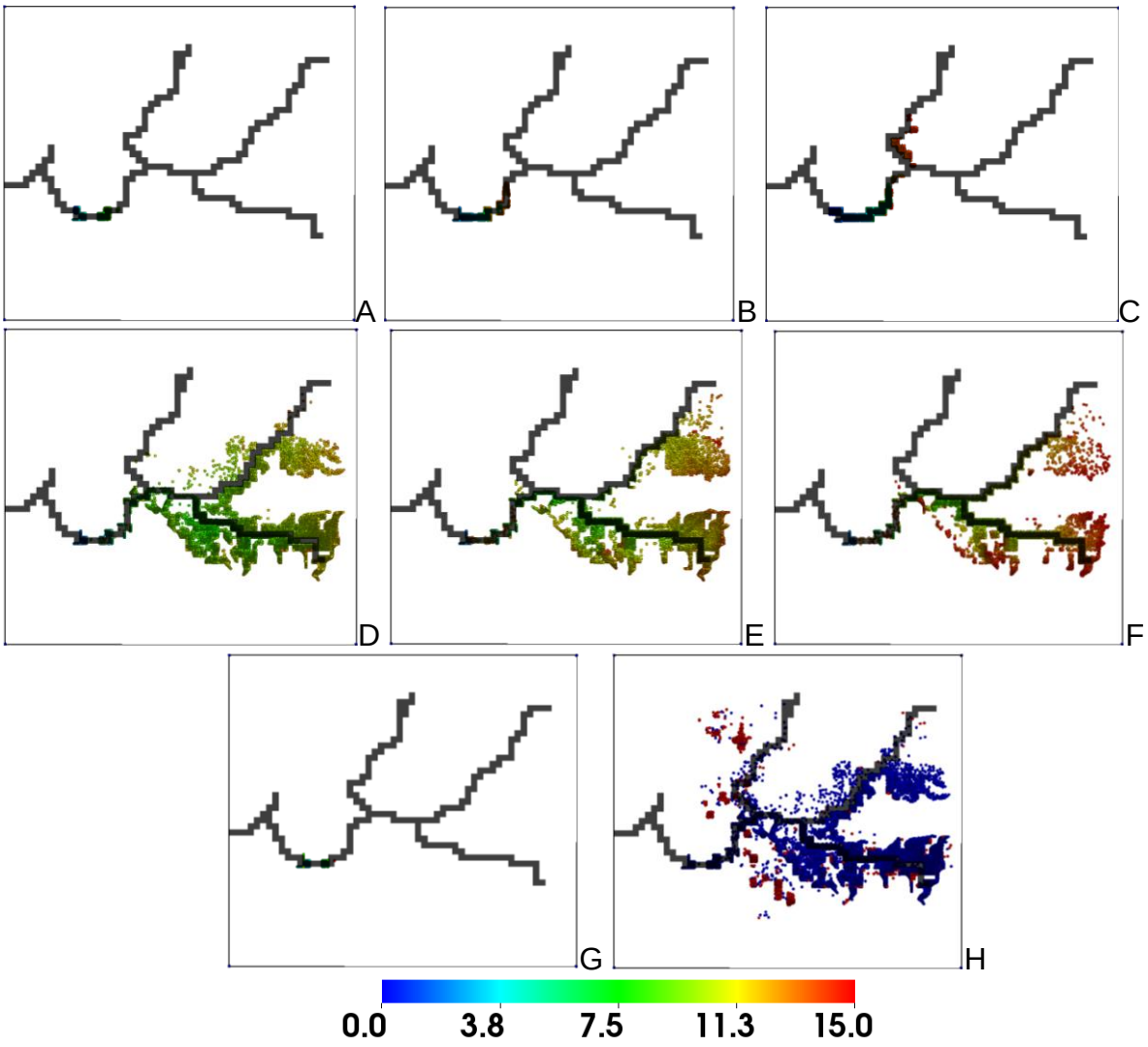

Figure 4-14. Spatial extent from which “new” water particles arrived at station 2500 during storm event ‘e’. A - G corresponds to points e1- e7 in figure 4-5. The color scheme shows the age (days) of all the particles arriving at station 2500 during storm ‘e’. (H) Source of water arriving at station 2500 during point e4 in figure 4-5 with blue and red dots representing rainfall or surficial aquifer system.

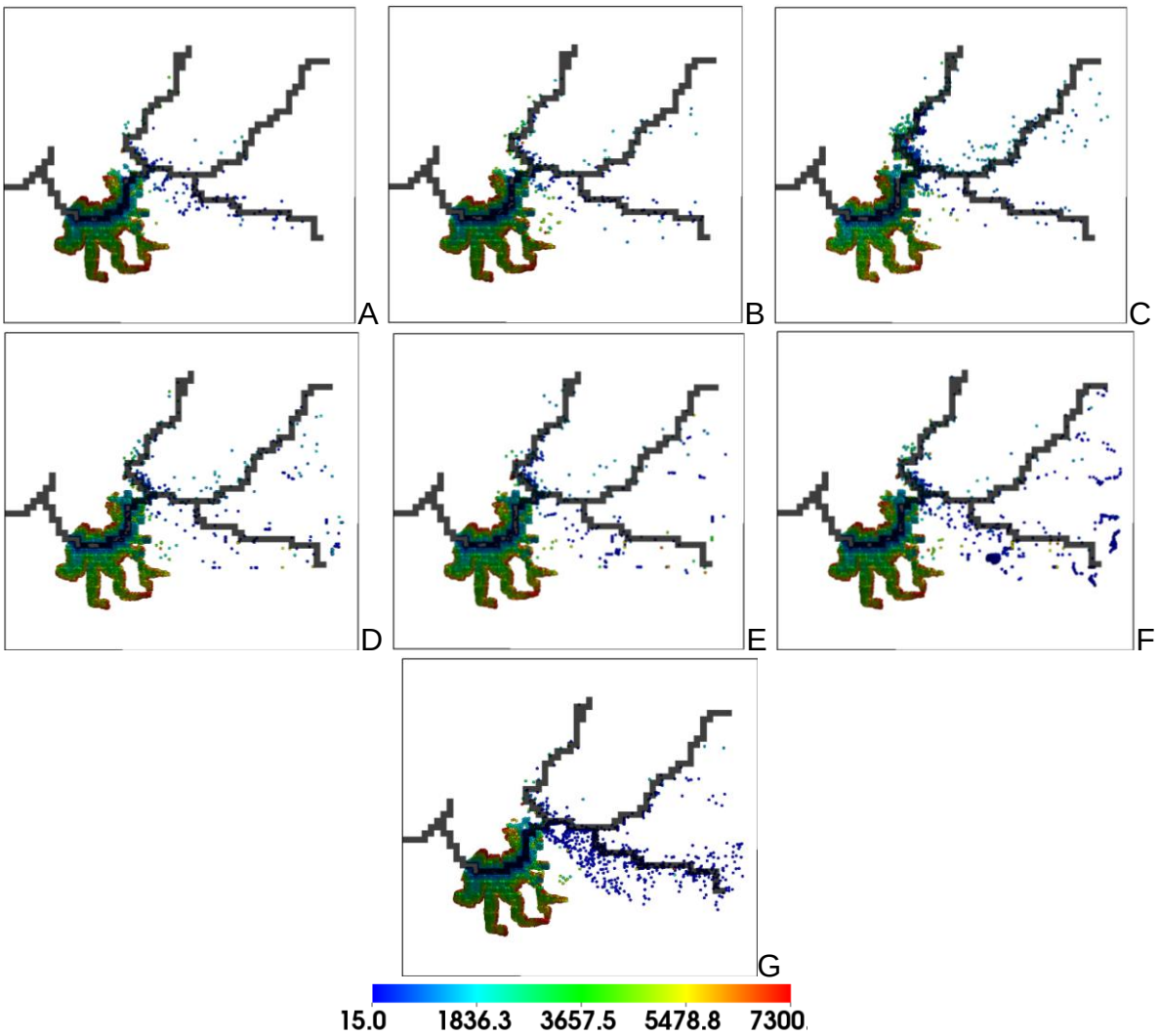

Figure 4-15. Spatial extent from which “moderately old” water particles arrived at station 2500 during storm event ‘e’. A - G corresponds to points e1- e7 in figure 4-5. The color scheme shows the age (days) of all the particles arriving at station 2500 during storm ‘e’.

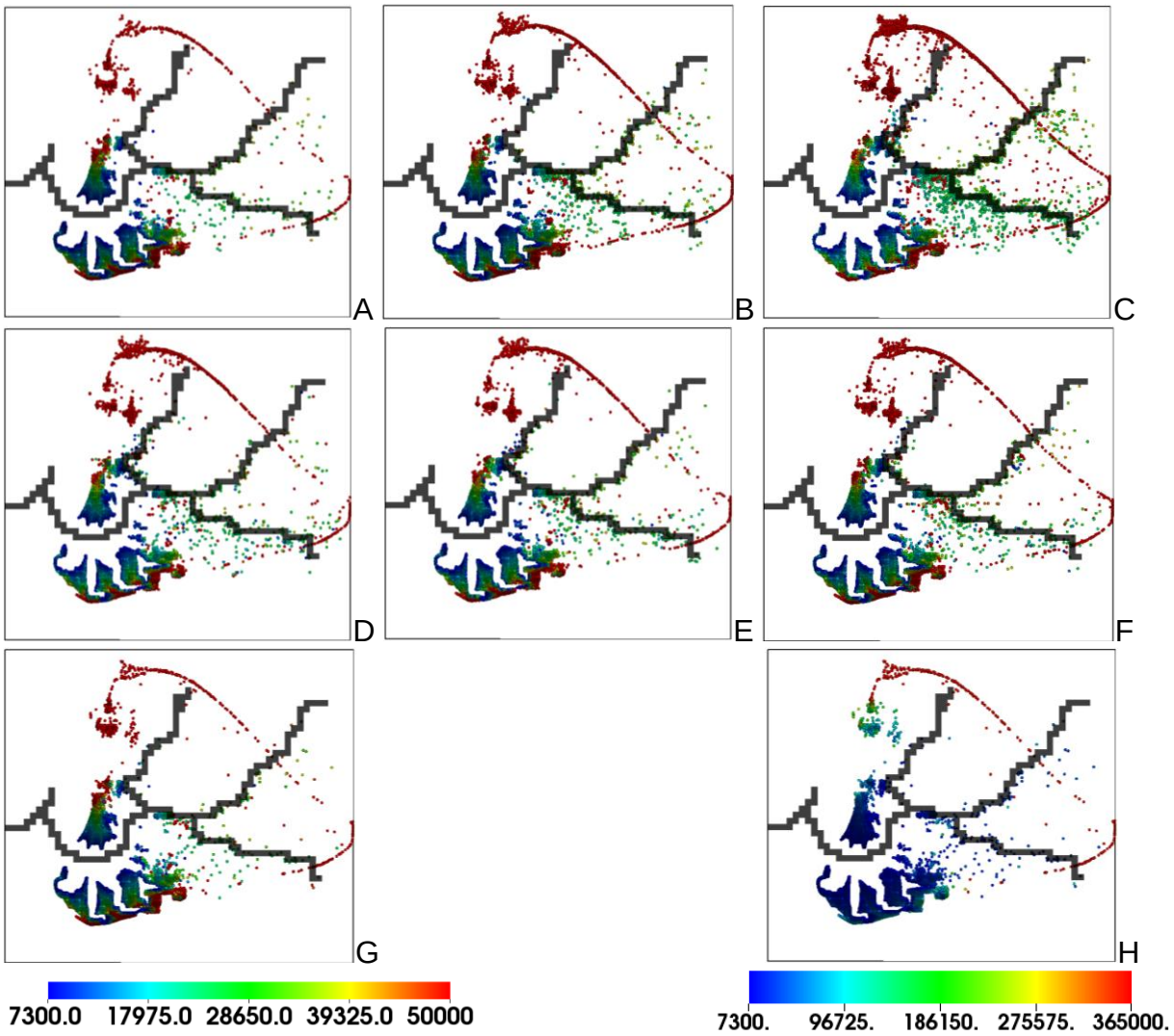

Figure 4-16. Spatial extent from which “very old” water particles arrived at station 2500 during storm event ‘e’. A - G corresponds to points e1- e7 in figure 4-5. The color scheme shows the age (days) of all the particles arriving at station 2500 during storm ‘e’. (H) Point e4 result (G above) with new scale shown below the figure which shows full range of age distribution of particles at the end of 1000 years.

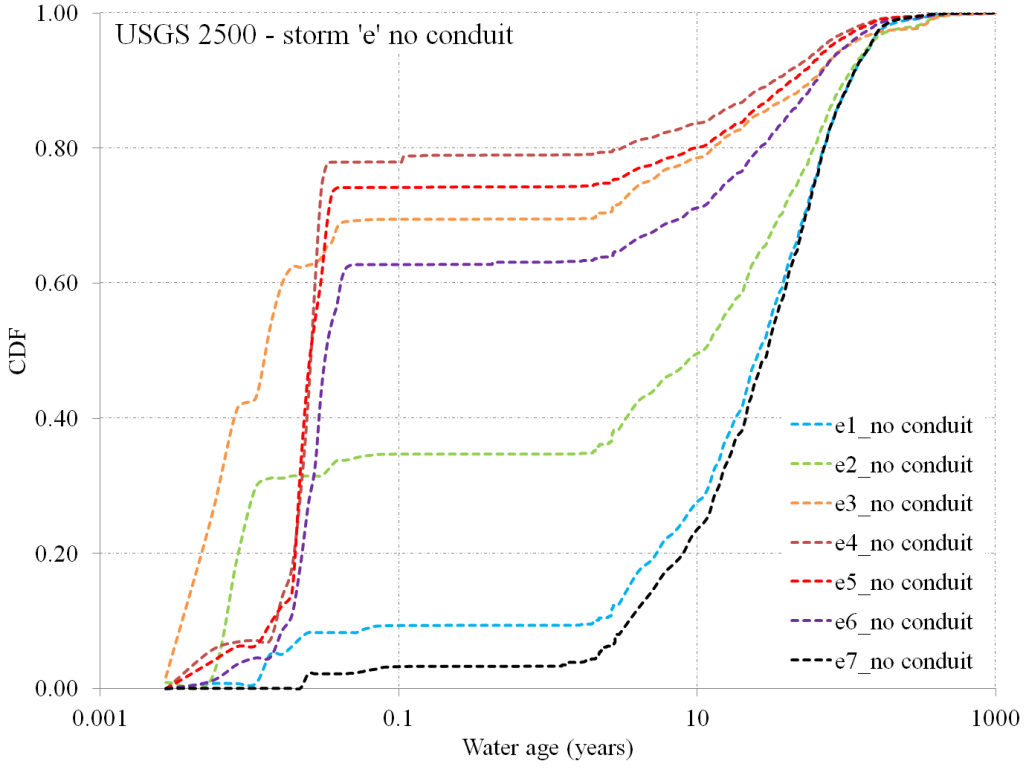

A

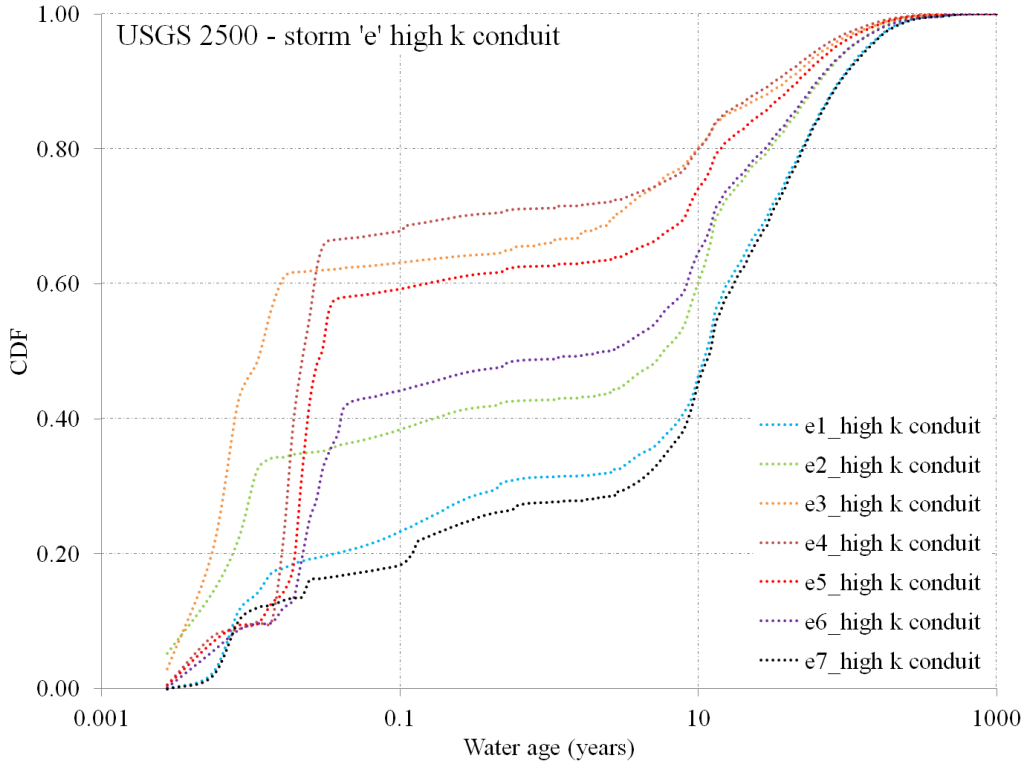

B

Figure 4-17. Water particle age distribution at station 2500 at various points on storm event ‘e’ for base case variants. A) No conduit. B) Higher hydraulic conductivity conduit.

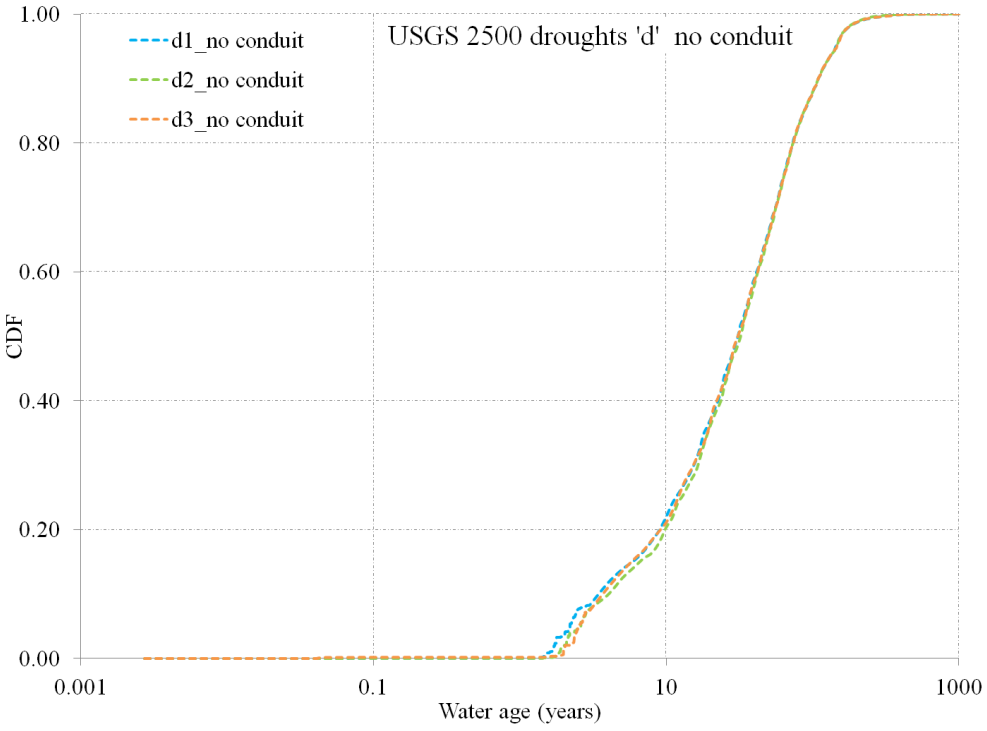

A

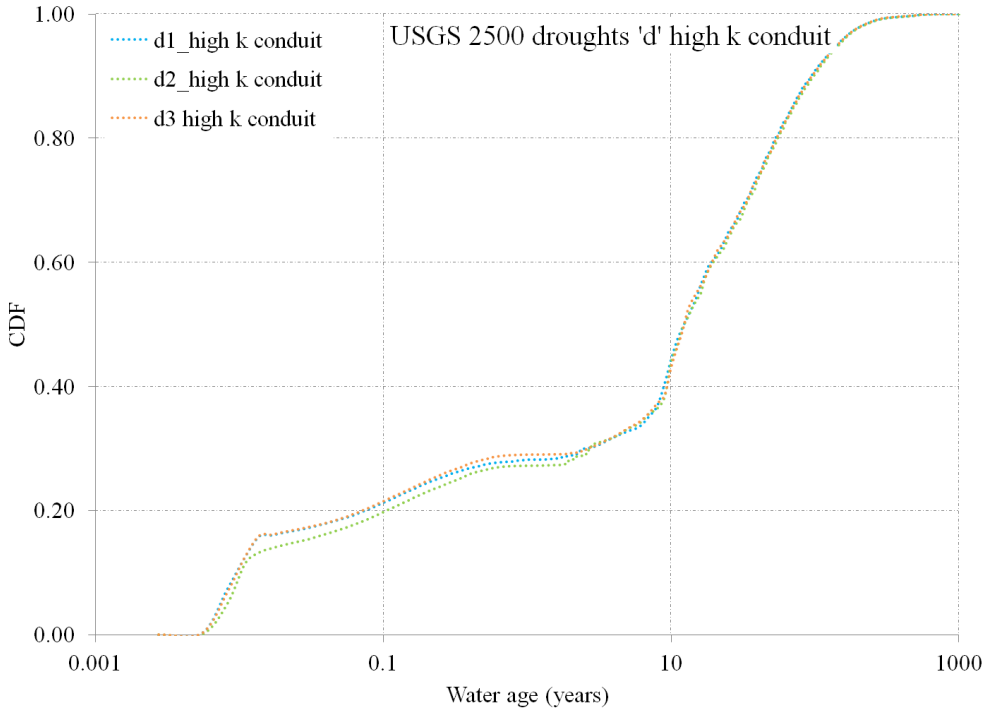

B

Figure 4-18. Water particle age distribution at station 2500 at various points during droughts ‘d’ for base case variants. A) No conduit. B) Higher hydraulic conductivity conduit.

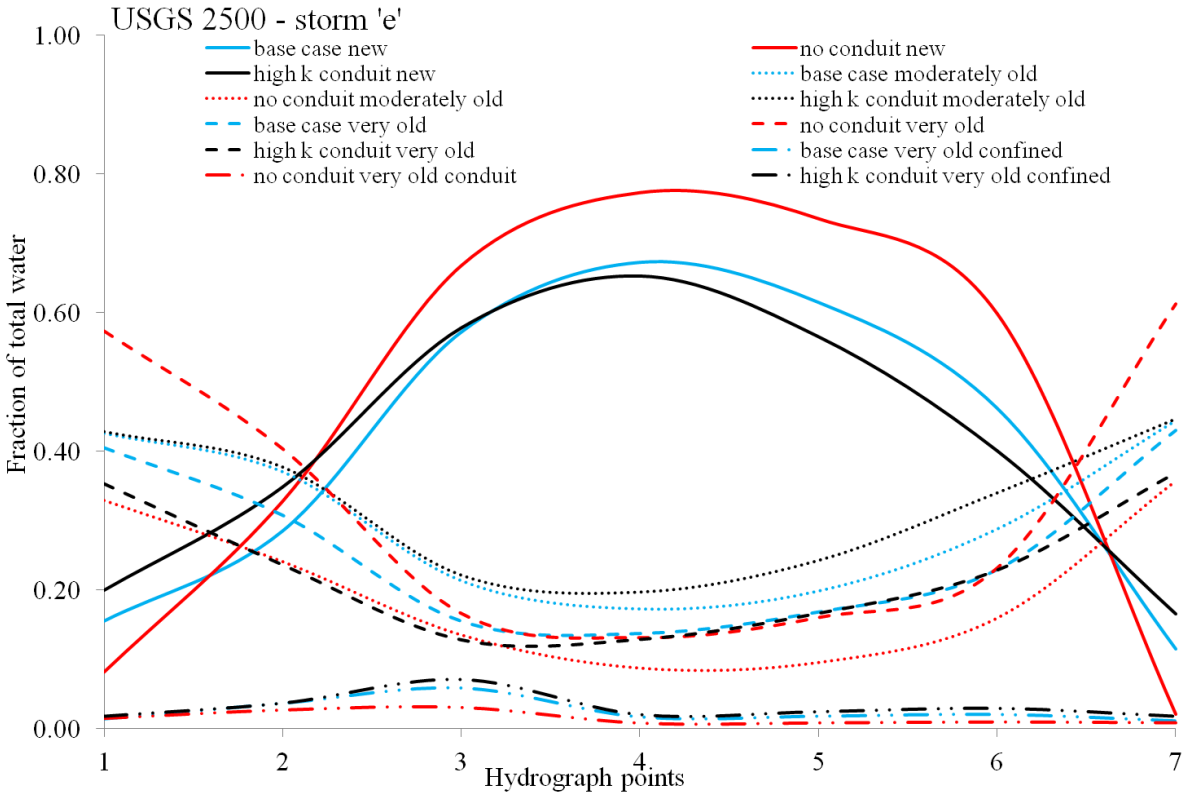

Figure 4-19. Temporal dynamics of various sources of water at 2500 during various time within a storm hydrograph for base case and its variants. Variants are “no conduit” (red lines) and “high hydraulic conductivity conduit” (black lines) during storm ‘e’.

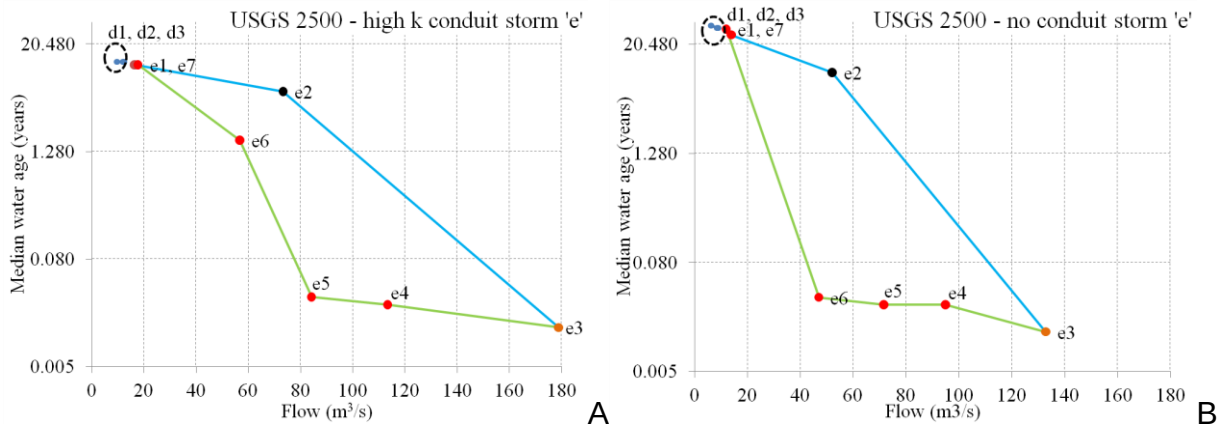

Figure 4-20. Water particle median age versus flow for base case model variant at various time during storm hydrograph ‘e’. A) Higher hydraulic conductivity conduit. B) No high hydraulic conductivity conduit. Blue line with black circles present data for the rising limb and green lines with red circles present data for the recession period; value corresponding to storm peak is represented by orange circle. Also shown are the median water ages for the three drought periods (dotted circle on upper left corner of each plot).

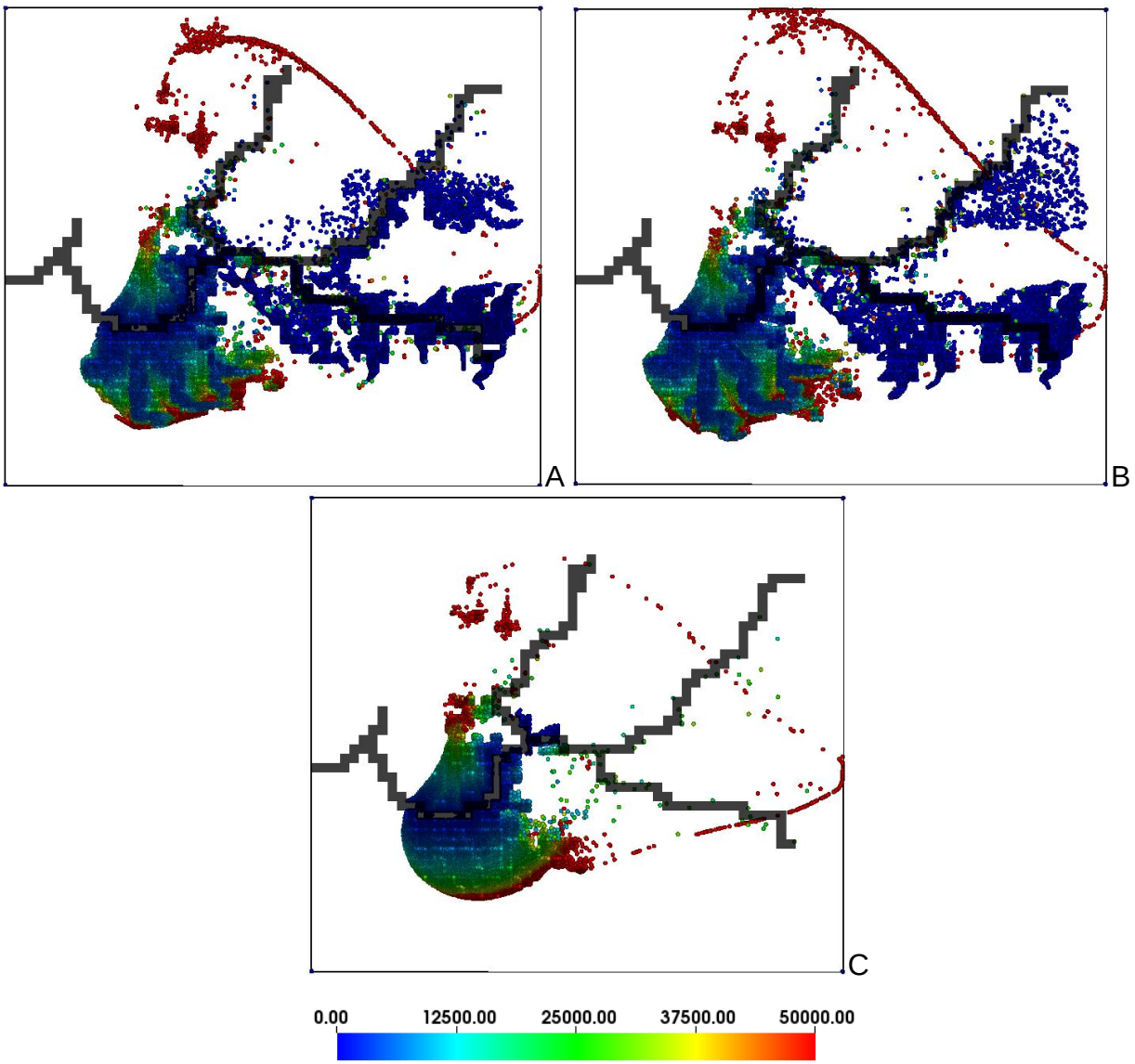

Figure 4-21. Spatial extent of water particle source location during point e4 of storm event ‘e’. A) Basecase. B) Base case with higher hydraulic conductivity conduits. C) Base case with no conduit. The color scheme shows the age (days) of all the particles arriving at station 2500 during storm ‘e’.

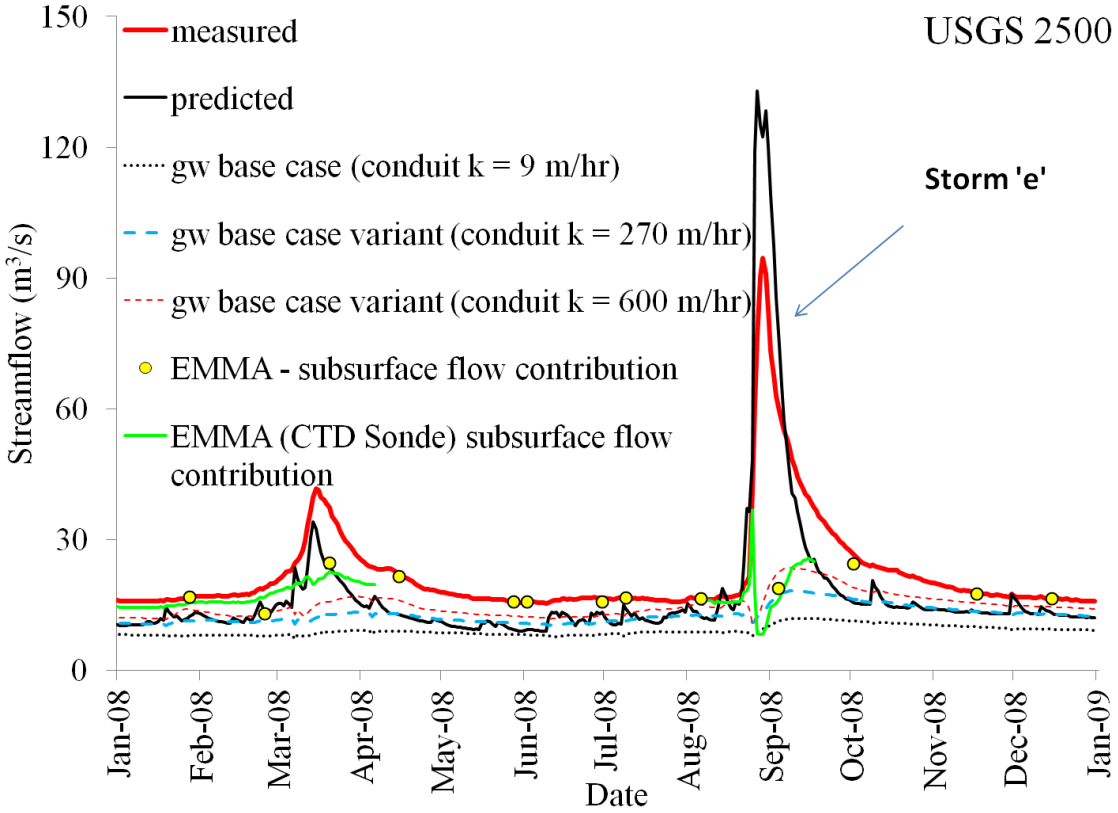

Figure 4-22. Comparison of measured and ParFlow.CLM simulated total streamflow and subsurface contributions. Also shown are end member mixing analysis based subsurface flow contribution at station 2500 during storm ‘e’.

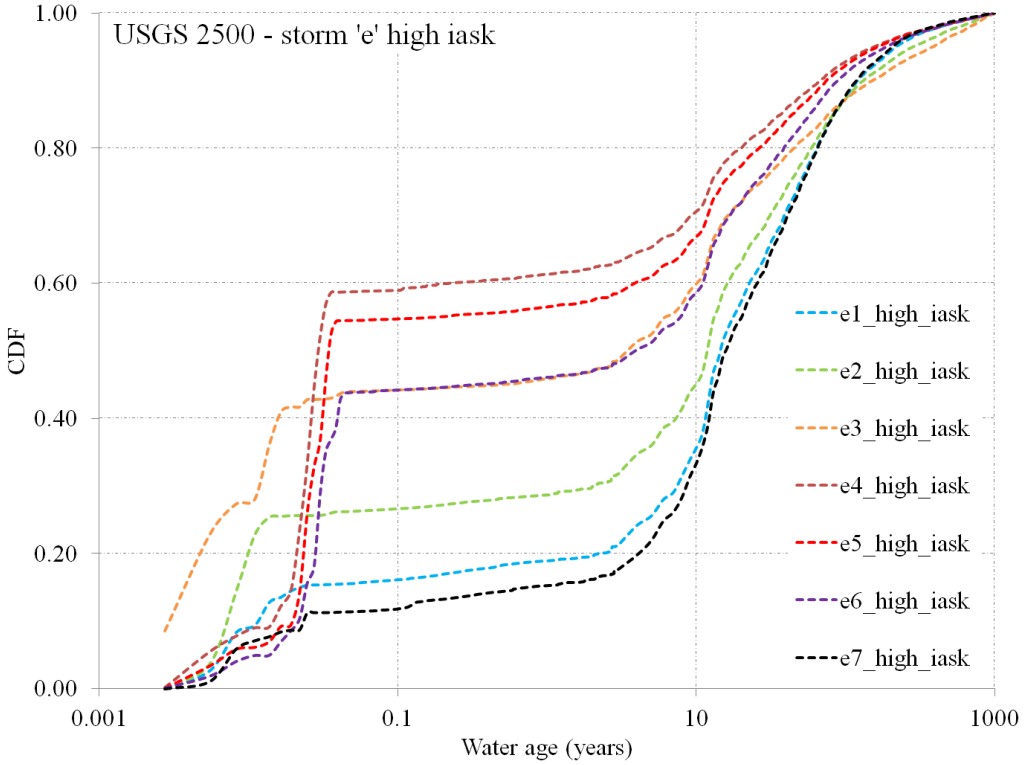

Figure 4-23. Water particle age distribution at station 2500. Results shown for various points on storm event ‘e’ for high intermediate aquifer hydraulic conductivity variant of base case.

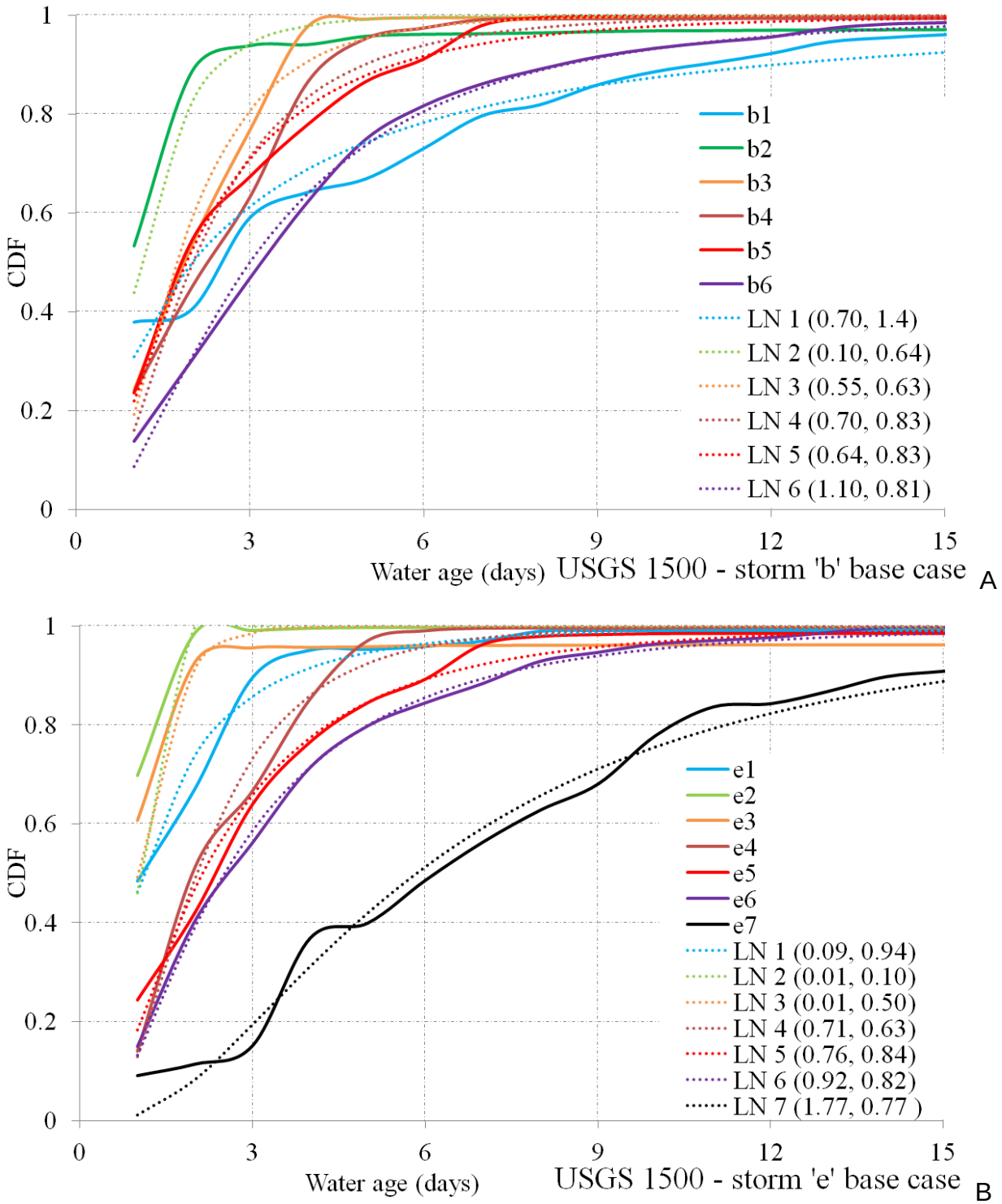

Figure 4-24. Water particle age distribution at station 1500. A) During storm event 'b'. B) During storm event 'e'. Also shown are the best fit lognormal distribution (broken line of various colors). Numbers in bracket are best fit parameter values for each distribution.

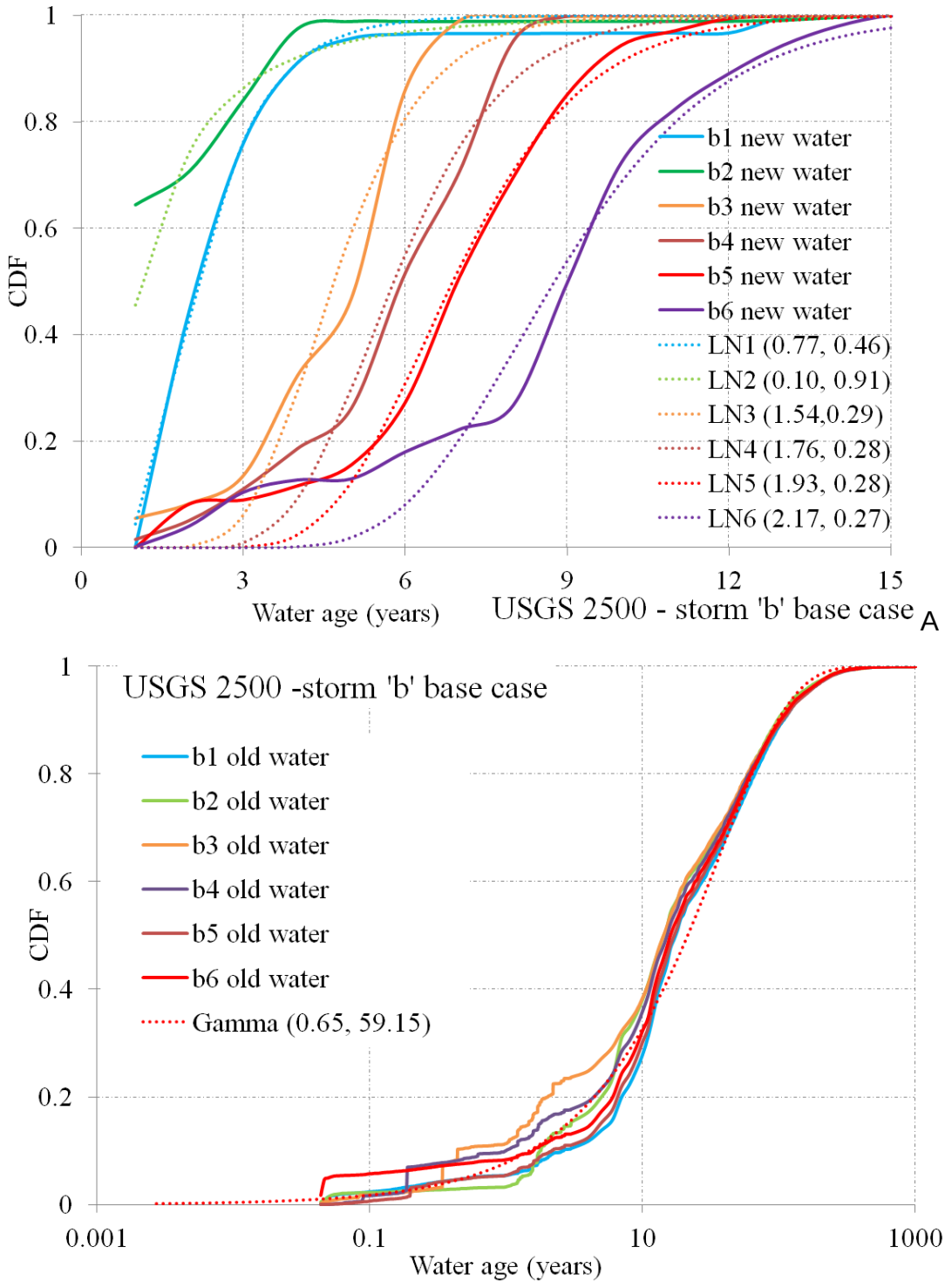

Figure 4-25. Water particle age distribution at station 2500 during various time in storm event 'b' for base case model. A) New water. B) Old water. Also shown are best fit lognormal distribution (variable colors dotted lines on top plot) and Gamma distribution (broken red line in bottom plot). Numbers in bracket are parameter of various distribution fitted to CDFs.

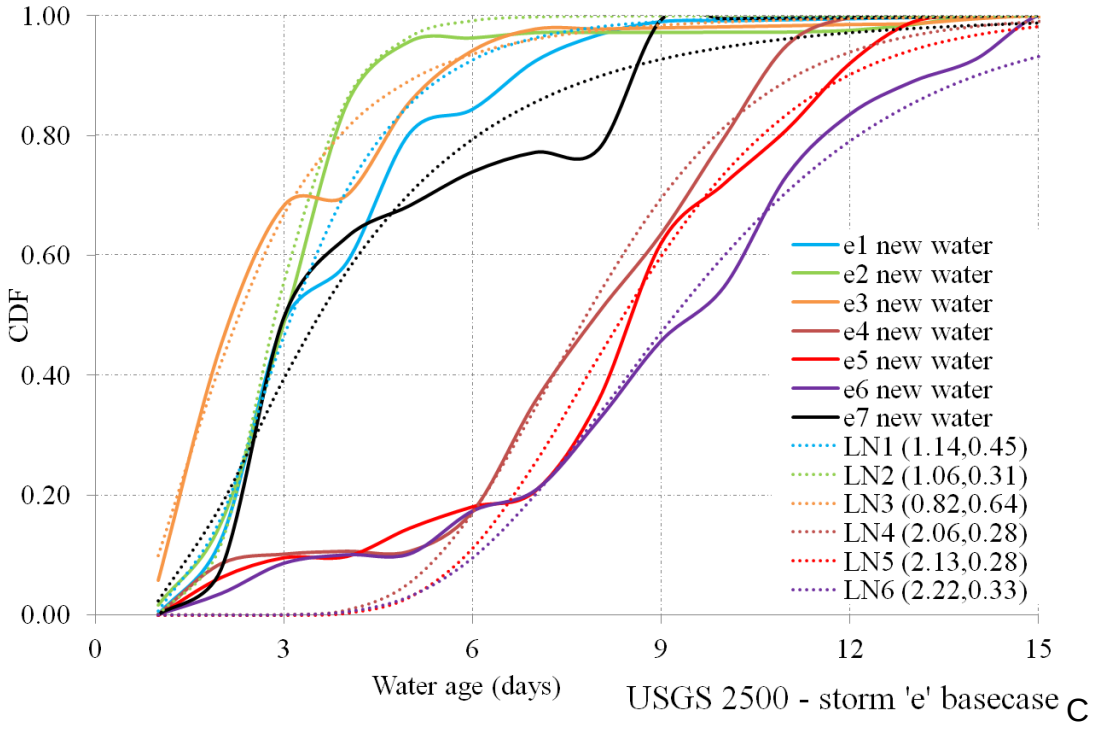

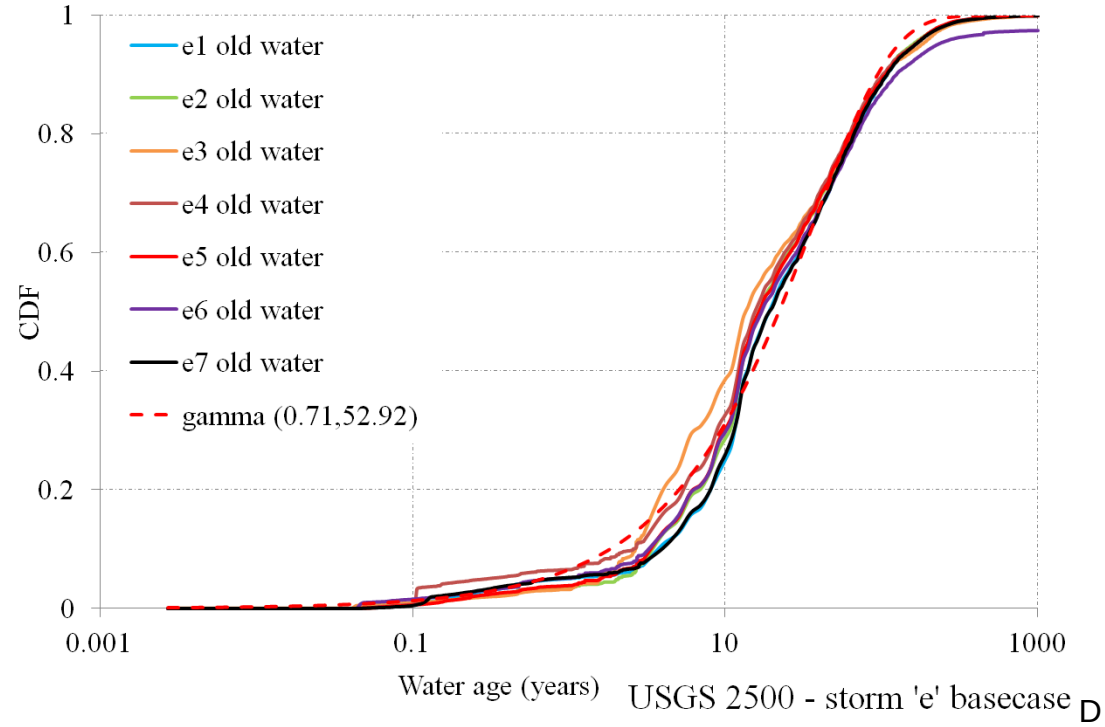

Figure 4-25. Continued.

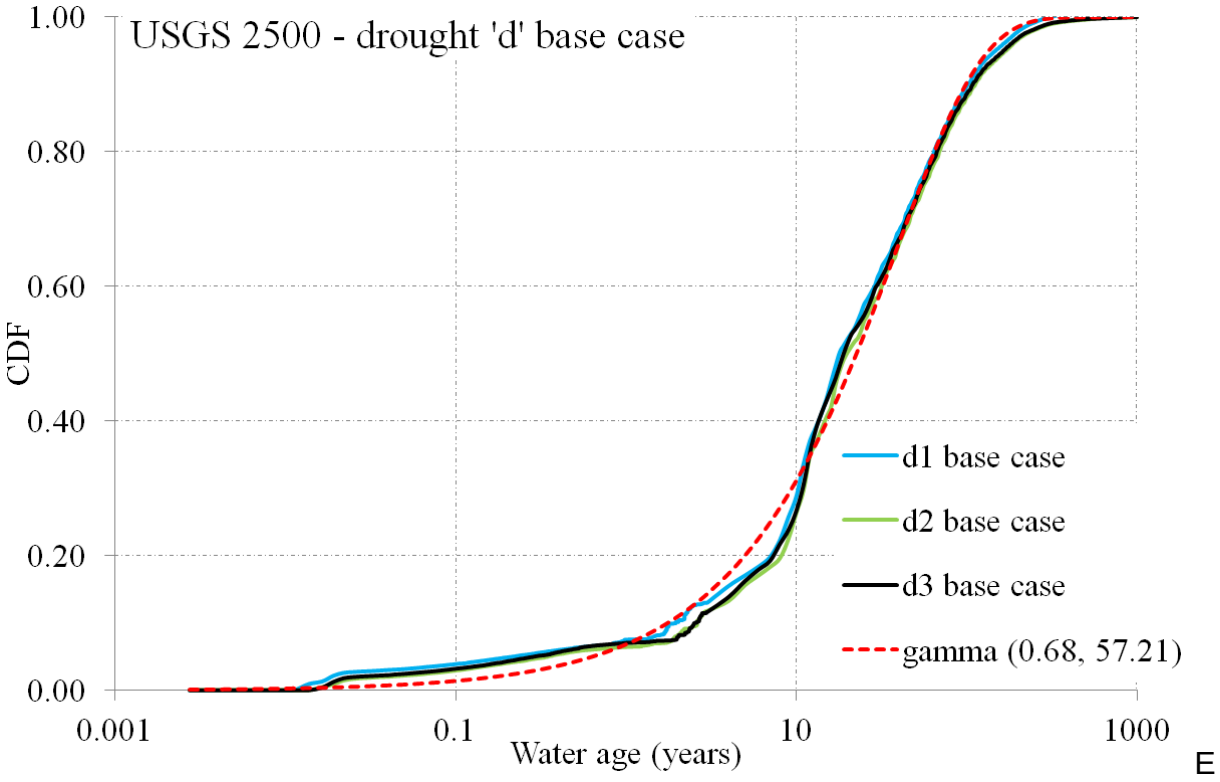

E

Figure 4-25. Continued.

CHAPTER 5
CONCLUSIONS, CONTRIBUTIONS AND RECOMMENDATIONS FOR FUTURE REASEARCH

Understanding the hydrologic functioning of a river basin at any scale is a complex problem. Hydrologic models are commonly used to gain insights on the hydrologic functioning of river basins, to make water management decisions, and to design future field experiments to improve conceptual models and parameter estimation to enhance future modeling of the system. This study demonstrated the potential of a fully integrated modeling platform to simulate and understand complex surface water - ground water – near land surface hydrologic processes and their interactions in a large river basin. The modeling platform provided a robust tool to better understand how various surface and subsurface water sources coexist and interact in space and time within the study area.

McDonnell et al., (2010), Kirchner (2006) and many others in the hydrologic modeling community have argued that there is a need to not only validate the model simulated outputs but also to validate that those outputs are produced for the right reasons. This requires for example, validating that the model is not only simulating the total streamflow correctly but it is simulating the proportion of surface and groundwater water, and the age of water forming the streamflow correctly. It has been long recognized that the traditional model evaluation criteria (i.e. comparison of streamflow and groundwater elevation) do not contain enough information to fully validate whether the model simulated outputs are occurring for the right reasons. Tracer information and additional water chemistry measurements can provide extra insights to validate models; however, field experiments and data collection can be expensive which limits their use. As such there is a need for modeling studies introducing and demonstrating the

application of additional criteria that are inexpensive and facilitate comprehensive testing of hydrologic models and their underlying conceptual models.

A significant contribution of this study is that it demonstrated the potential use of groundwater flow fractions estimations obtained using high resolution river water specific conductivity measurements as an additional model validation criterion. Recent developments in sensor technology allowed relatively inexpensive and high frequency measurement of specific conductivity of water at multiple river locations within the SFRB. This new validation criteria helped testing the adequacy of surface and groundwater flow interactions as simulated by fully integrated model over a large river basin.

Based on the broader objectives defined in the beginning of this dissertation, the research and its findings can be partitioned into three major research components (RCs). Major findings and conclusions on each of these major RCs are summarized below.

RC1: What are the major water budget components in the basin and how do they vary in space and time? How do surface and subsurface water contributions to streamflow vary along the river?

- ET is the most important water balance component in the basin comprising 77% of rainfall. The remaining water balance components namely, runoff, surface storage, and subsurface storage are governed by seasonal and interannual differences between rainfall and ET patterns over the basin. In general recharge to groundwater occurs primarily in June through September when rainfall significantly exceeds ET. Peaks in average streamflow occur both in March, when winter frontal rainfall is relatively high and ET losses are low, and in September at the end of the summer rainy season.

- ET varies spatially throughout the basin with water table depth and land cover. On average 85% of the ET occurs in the confined region where water tables are shallow (averaging 0.84 m below land surface) and thus ET is primarily energy-limited. In the unconfined region water tables are deeper (averaging 12.1 m below land surface) and thus generally moisture-limited. In both the confined and

the unconfined regions grass lands show the lowest ET losses and forests and wetlands show the highest ET losses.

- Streamflow in the confined region of the basin is episodic, with more than 95% generated by recent near-stream rainfall that temporarily raises the water table above the land surface near stream channels. Virtually no inter-event subsurface baseflow from the surficial aquifer occurs in the confined region.

- In the unconfined region of the basin there is little surface connectivity between the watershed and stream resulting in 52% of the streamflow in the upper portion of the unconfined region to 77 % of the streamflow at basin's outlet being generated by subsurface contributions from Floridan aquifer that originated as diffuse infiltration through the epikarst. Surface contributions to streamflow are episodic and originate in the upper confined region of the basin.

- Geologic conditions were found to exert primary control on the spatial variability of streamflow generation processes in this basin through their influence on the balance between rainfall, evapotranspiration, runoff and infiltration processes.

- Climatic variability was found to provide primary control on the temporal variability of streamflow generation processes, resulting in significant seasonal and interannual variability in both the timing and sources of streamflow.

RC2: What Parflow.CLM processes and parameters are ET, groundwater level, streamflow, and subsurface contributions to streamflow most sensitive to? How does parametric sensitivity, and interaction among sensitive parameters, vary across the basin?

- The global sensitivity analysis of ParFlow.CLM identified seven parameters (out of 33 parameters included in the analysis) to be most sensitive towards ET, groundwater level, streamflow, and subsurface contributions to streamflow. These parameters include the hydraulic conductivity of the IAS, the hydraulic conductivity and specific storage of the UFAS, maximum LAI for mixed forests, wilting point, and the manning's coefficient in the confined and unconfined regions.

- Of the seven sensitive parameters identified during GSA, all but maximum LAI for mixed forests showed high interactive effects, with the hydraulic conductivity of the IAS being the most interactive parameter. The sensitivity and interaction of the hydraulic conductivity of the IAS underscores the importance of better mapping of the lateral and vertical extent of IAS in confined, transition and Wacasassa Flat regions.

- The hydrologic response of the confined region of the basin showed highest sensitivity to the hydraulic conductivity of the Intermediate Aquifer System confining unit (IAS). Changes in hydraulic conductivity of the IAS changed the

surficial aquifer water table depth in the confined region which in turn influenced average ET, total streamflow and peak streamflow in this region.

- After the hydraulic conductivity of the IAS, the maximum LAI of mixed forests in the confined region was the second most influential parameter controlling both average ET and total streamflow in the confined region. This illustrates the importance of vegetation properties in determining average hydrologic behavior in this region. Mannings coefficient in the confined region was the second most influential parameter controlling peak streamflow in this region.

- Total streamflow and subsurface contributions to streamflow in the unconfined region were most sensitive to the hydraulic conductivity of the Upper Floridan Aquifer System (UFAS). Total streamflow also showed significant sensitivity to maximum LAI of mixed forest and wilting point in the unconfined region. For subsurface contributions to streamflow in the unconfined region hydraulic conductivity of the conduit system was the second most sensitive parameter after hydraulic conductivity of the UFAS.

- Peak streamflow in the unconfined region was most sensitive to the hydraulic conductivity of the IAS and the mannings coefficient of the confined region, underscoring the dominance of the confined region characteristics in determining streamflow response to major rainfall events throughout the entire basin.

- In the unconfined region ET was most sensitive to wilting point, followed by the UFAS hydraulic conductivity and parameters of the van Genuchten function, indicating that due to the generally lower water tables ET is moisture limited in this region.

- Mean groundwater levels and the magnitude of groundwater level fluctuation in the UFAS were generally most sensitive to UFAS hydraulic conductivity, UFAS specific storage and IAS hydraulic conductivity throughout the basin.

- The significance of ET parameters in controlling hydrologic behavior throughout the watershed underscores the importance of ET and highlights the significance of feedback between land atmosphere, surface and subsurface processes throughout the basin. This finding also highlights the significance of adequate representation of ET processes within the modeling framework; something which was consistently missing in previous regional groundwater models for the region.

- Analysis of hydrologic response (e.g. streamflow, groundwater elevation) of the model over 340 GSA model runs indicated that parameter values that produce reliable hydrologic response in one of region of the basin may not reproduce reliable predictions elsewhere. As such future sensitivity/uncertainty analysis studies should incorporate spatial variability in parameter values within major hydro-geologic regions of the basin.

RC3: How do streamflow sources, flow paths and travel times vary along the river and between base flow and storm events? What processes and parameters exert primary control on travel time distributions?

- Streamflow in the confined region is episodic and travel time distributions are temporally variable. However Parflow-Slim simulations indicate that all streamflow in this region is "new water", generally having entered the domain as rainfall within the previous 30 days and having a median age of less than 7 days.

- Channel-floodplain connectivity in the confined region, which depends on rainfall spatial patterns, antecedent hydrologic conditions and topography, controls the source area for streamflow, total volume of streamflow, and the shape of the travel time distributions. In general simulations indicate that even during the extreme 2004 hurricane season most confined region streamflow originates as rainfall within 1500 m of the river.

- Travel time distributions in the unconfined region show a wide distribution of ages with two distinct components: a "new" surface water contribution originating as recent rainfall in the confined region of the basin, and an "old" Upper Floridan Aquifer System contribution originating primarily from rainfall falling in the unconfined region, infiltrating through the epikarst, and making its way through the porous matrix of the UFAS and higher permeability conduits to the river.

- The "new" water travel time distribution in the unconfined region is governed by the shape of the confined region travel time distribution and is well fit by a log-normal travel time function with parameters that vary slightly between storms and with hydrograph position.

- The "old" water travel time in the unconfined region is approximately time invariant and well fit by a gamma function with parameters that indicate fractal behavior. The shape of the travel time distribution is sensitive to conduit geometry, the contrast between conduit and UFAS hydraulic conductivity, and the geometry of the model-predicted extent of the unconfined contributing area.

- The relative weight of the "new" and "old" water travel time distributions in the unconfined region varies with hydrologic condition, ranging from 100% old water during baseflow conditions to 10-30% old water at the peak flow major storm hydrographs. The relative weight of new and old water travel time distributions is sensitive to IAS hydraulic conductivity which governs the total streamflow generated in the confined region.

- During baseflow conditions the median age of streamflow in the unconfined region is predicted to be approximately 15-17 years, in close agreement to age previously determined by Chlorofluorocarbon and isotopic measurements taken at springs within the basin. During high streamflow events the median streamflow age drops rapidly to approximately 15-17 days at the peak of the hydrograph.

The fully integrated ParFlow.CLM model developed during this study represents a baseline scenario that provides a strong basis to quantitatively predict the impacts of major changes in landuse (e.g. wetlands and forests cleared for agricultural or urban development), groundwater extraction and climate on stores, fluxes, flowpaths and travel times of water in the SFRB. These predictions are essential to inform holistic land and water resource planning in the region in order to provide reliable water supply for human uses as well as environmental flows that are protective of aquatic ecosystems. Furthermore accurate predictions of surface versus groundwater contributions to streamflow will allow prediction of transport and transformations of ecologically relevant solutes such as carbon, nitrogen and phosphorus in the spring and river systems in the region.

The ParFlow.CLM model for the SFRB presented in this dissertation was developed using best available information on the basin's physical characteristics and model parameters obtained from various state and federal agencies. However the Global Sensitivity Analysis conducted as a part of this research provides a foundation to design quantitative spatially distributed optimal parameter estimation techniques (such as the Ensemble Kalman Filter) to reduce the uncertainty of model predictions using high frequency streamflow, groundwater level and end member mixing model estimates. In particular seven parameters namely the hydraulic conductivity of the IAS, the hydraulic conductivity and specific storage of the UFAS, maximum LAI for mixed forests, wilting point, and the Manning's coefficient in the confined and unconfined regions were identified to be most sensitive towards ET, streamflow and groundwater

level predictions and require more accurate estimation for future models developed for the basin.

Boundary conditions applied at the four lateral boundaries of the basin in the current model were assumed to be time invariant constant head conditions which allow some groundwater to leave or enter the basin through domain's lateral boundaries. Although these lateral boundaries were located far from the river, and outside the surface watershed, in order to minimize their effects on surface-groundwater interactions, future modeling efforts should evaluate the effects of extending the lateral boundaries (especially the south boundary of the basin), and/or the adoption of time-varying boundary conditions, on model predictions.

Similarly the effect of model grid resolution on simulated hydrologic behavior should be further investigated. The version of ParFlow used in this study required a uniform grid. This, together with the large size of the study domain, required a relatively coarse grid resolution to maintain computational efficiency. The ParFlow model now has the capability to discretize domains using variable grid sizes. Thus the ParFlow.CLM predictions obtained in this study could be compared with a model that incorporates higher resolution grid cells in hydrologically dynamic regions near the land surface, stream networks and high conductivity zones.

Finally, the ParFlow model developed here assumed that overland and streamflow would be well-predicted using the kinematic wave equation and that conduits in the system could be represented by high conductivity porous media networks. Future work should test the sensitivity of model predictions to alternative overland flow physics and alternative conduit flow physics and geometry.

APPENDIX
CHAPTER 4 ADDITIONAL FIGURES

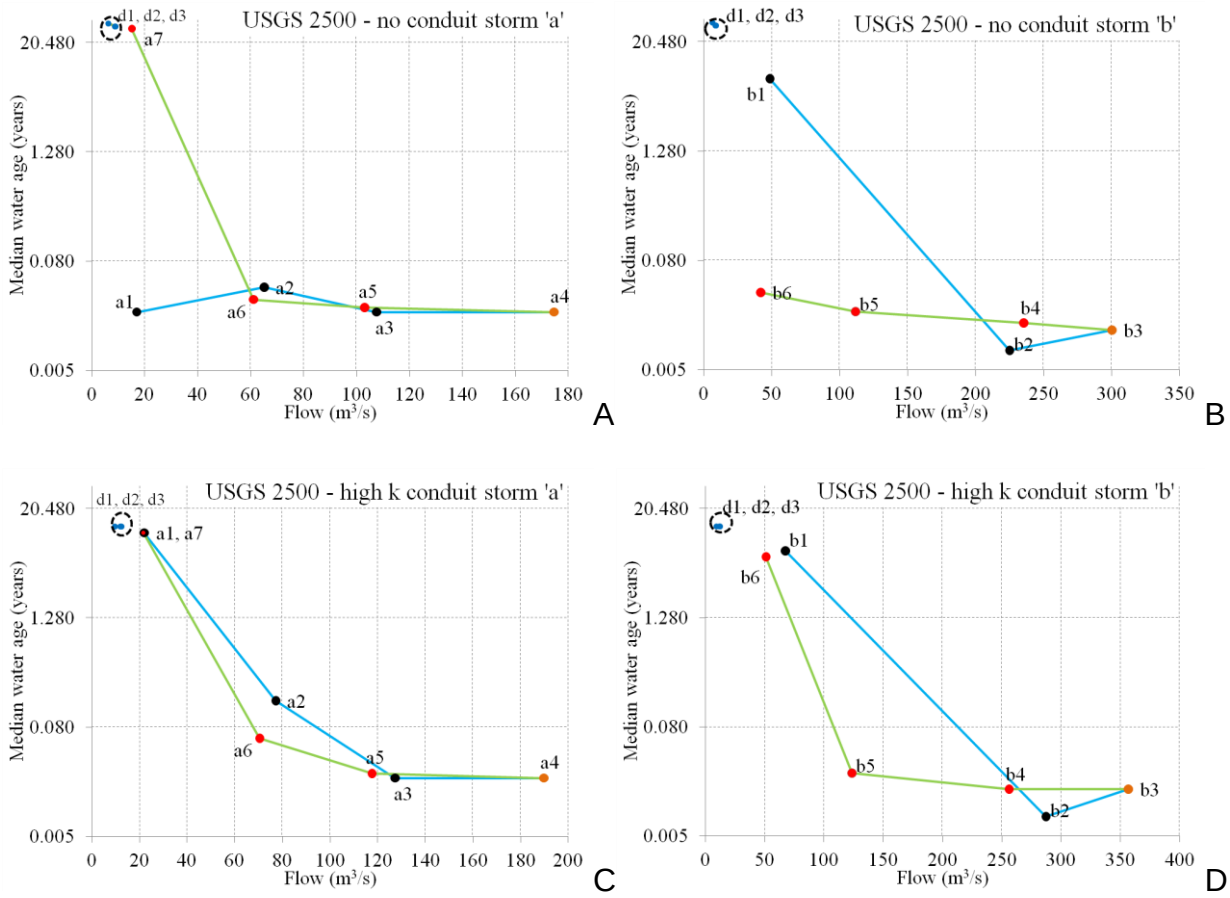

Figure A-1. Water particle median age versus flow for base case model variants. A) No high hydraulic conductivity conduit during storm ‘a’. B) No high hydraulic conductivity conduit during storm ‘b’. C) Higher hydraulic conductivity conduits during storm ‘a’. D) Higher hydraulic conductivity conduits during storm ‘b’. Blue line with black circles present data for the rising limb and green lines with red circles present data for the recession period; value corresponding to storm peak is represented by orange circle. Also shown are the median water ages for the three drought periods (dotted circle on upper left corner of each plot)

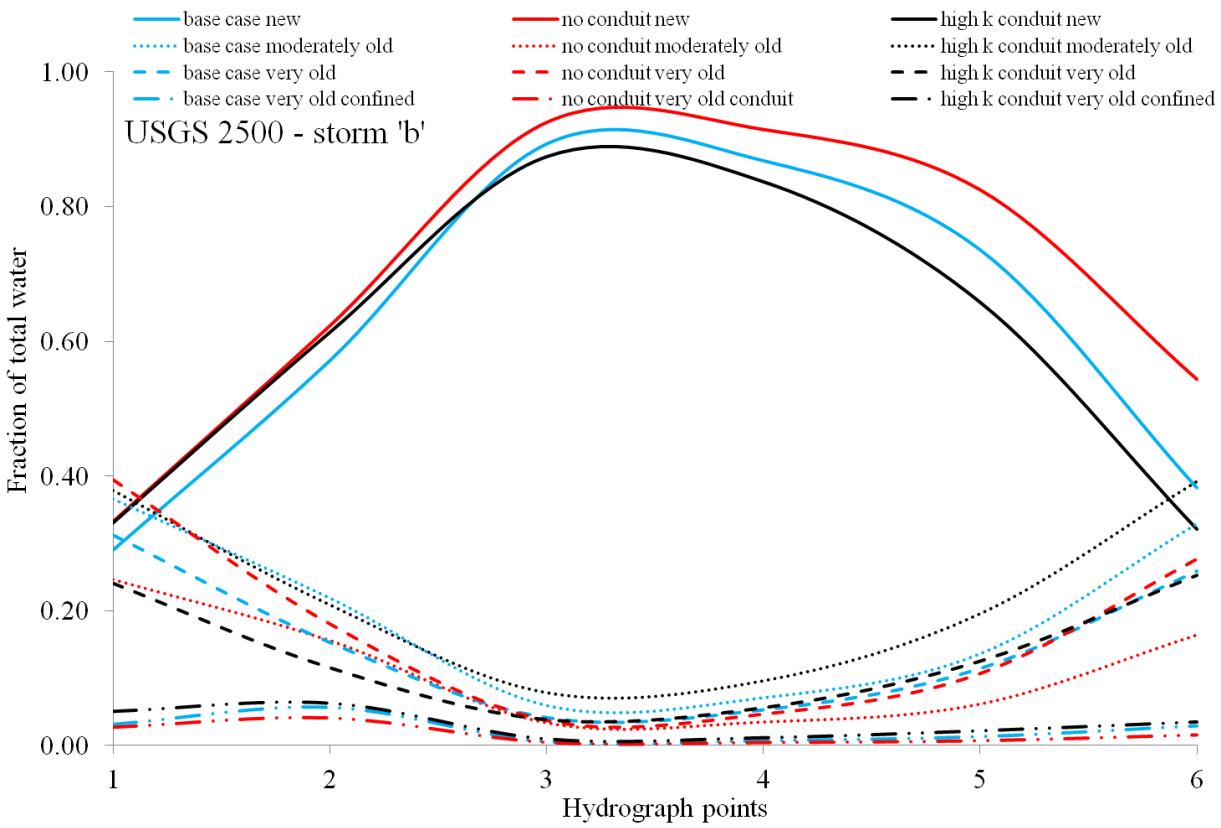

Figure A-2. Temporal dynamics of various sources of water at 2500 during various times within a storm hydrograph for base case and its variants. Variants are “no conduit” (red lines) and “high hydraulic conductivity conduit” (black lines) during storm ‘b’.

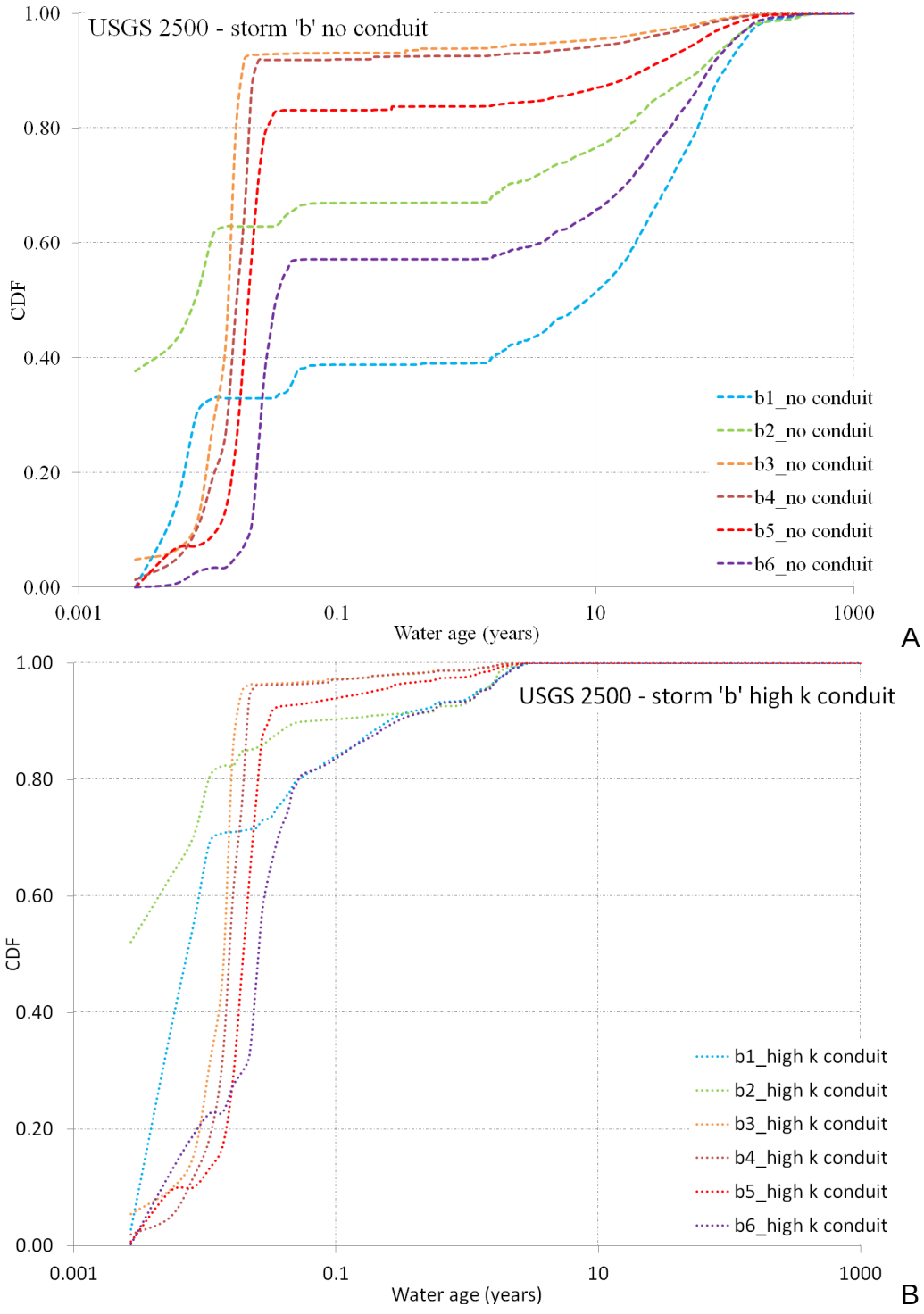

Figure A-3. Water particle age distribution at station 2500 at various points on storm event ‘b’. A) No conduit base case. B) Higher hydraulic conductivity conduit base case.

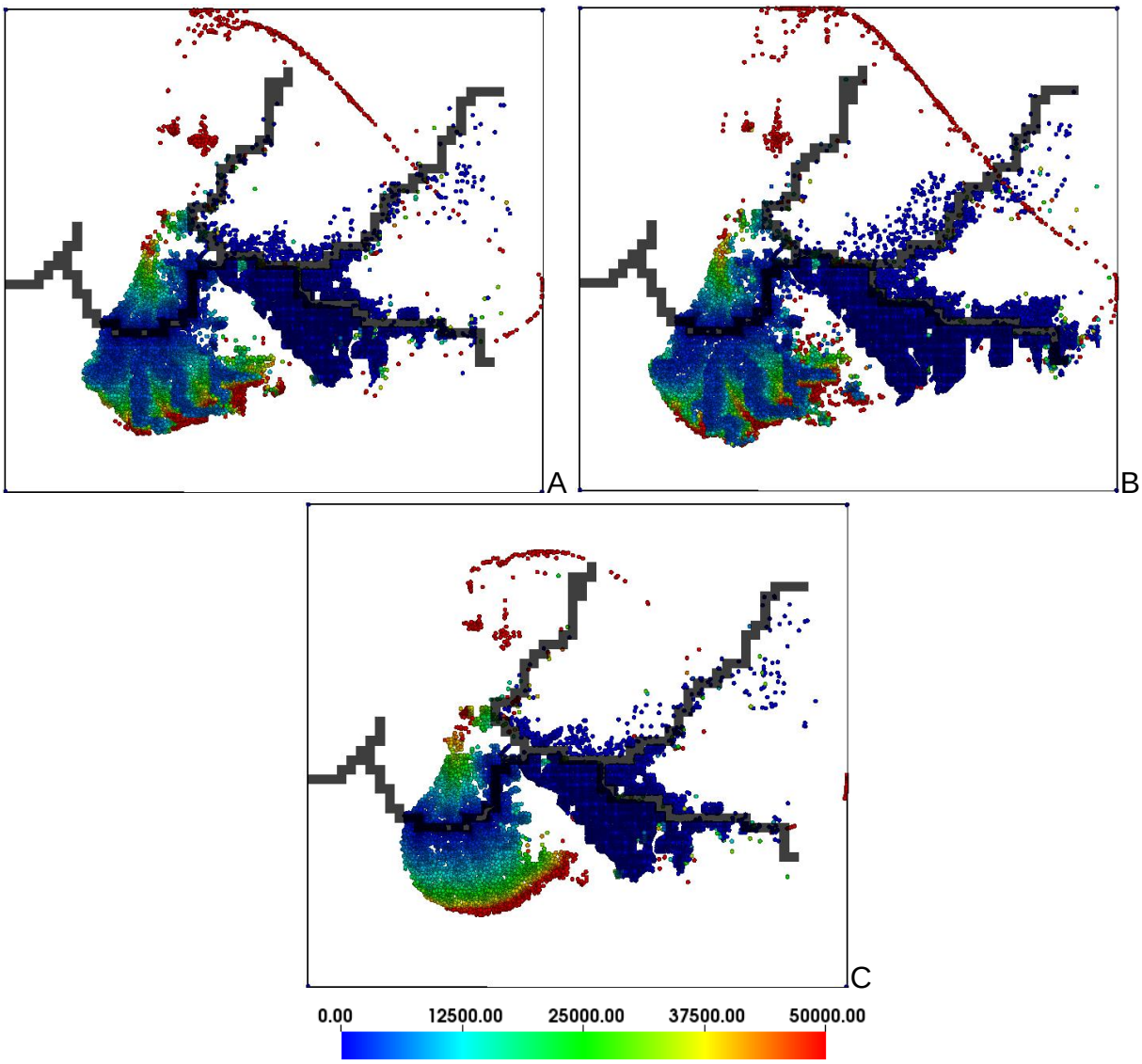

Figure A-4. Spatial extent of water particle source location during peak of storm event ‘b’. A) Basecase. B) Base case with higher hydraulic conductivity conduits. C) Base case with no conduit. The color scheme shows the age (days) of all the particles arriving at station 2500 during storm ‘b’.

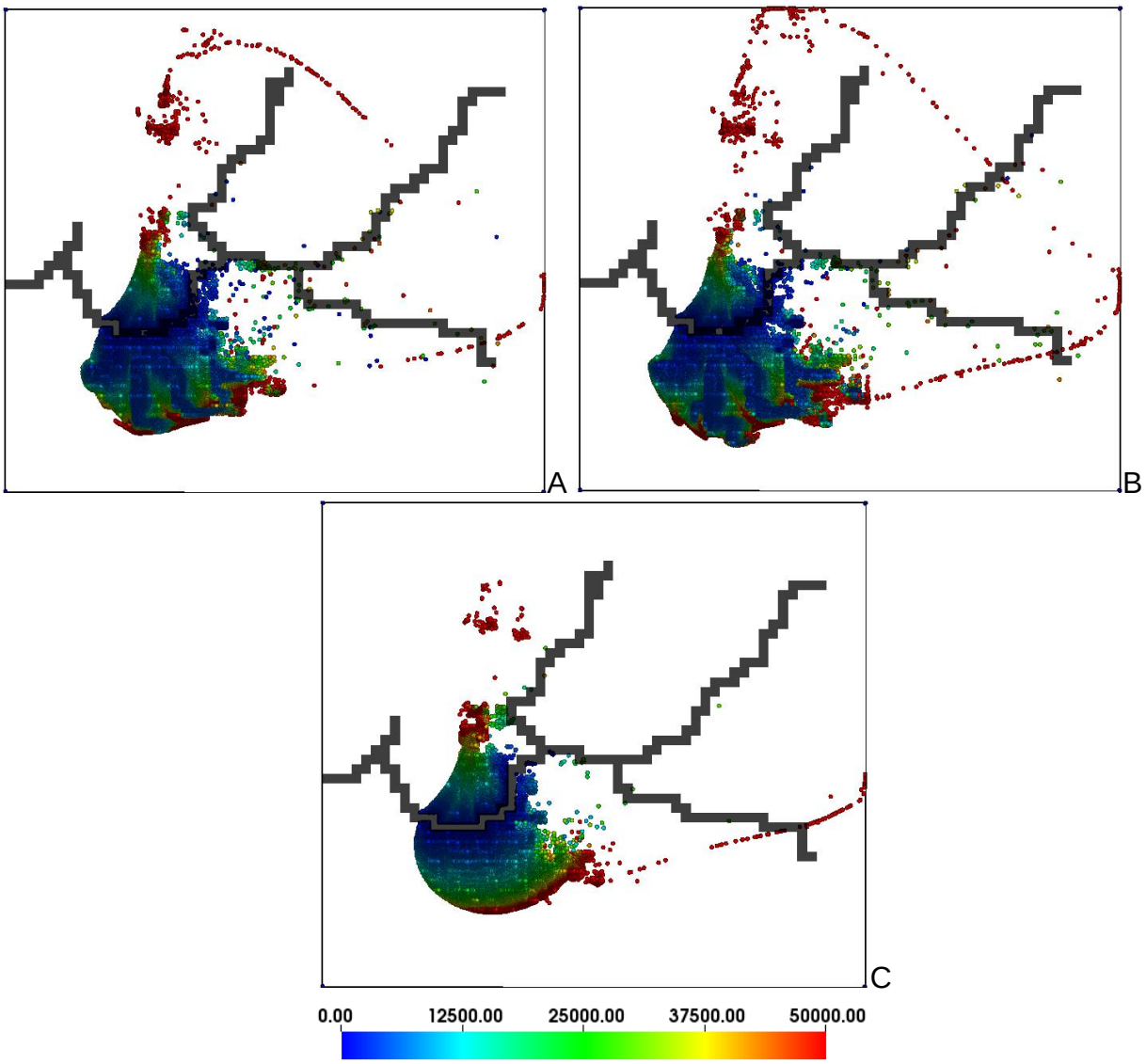

Figure A-5. Spatial extent of water particle source location during drought ‘d3’. A) Basecase. B) Base case with higher hydraulic conductivity conduits. C) Base case with no conduit. The color scheme shows the age (days) of all the particles arriving at station 2500 during drought ‘d3’.

LIST OF REFERENCES

Anderson M.P., Woessner W.W. 1992. Applied groundwater modeling: simulation of flow and advective transport. Academic Press: California; 381.

Ando K., Kostner A., Neuman S.P. 2003. Stochastic continuum modeling of flow and transport in a crystalline rock mass: Fanay-Augeres, France, revisited. *Hydrogeology Journal* 11 : 521-35.

Arthur J.D., Baker A.E., Cichon J.R., Wood H.A.R., Rudin A. 2005. Florida, Aquifer Vulnerability Assessment (FAVA): Contamination potential of Florida's principal aquifer systems. *Florida Geological Survey*; 67 : 1-149.

Ashby S.F., Falgout R.D. 1996. A parallel multigrid preconditioned conjugate gradient algorithm for groundwater flow simulations. *Nuclear Science and Engineering* 124 : 145-59.

Bailly-Comte V., Martin J.B., Screaton E. 2011. Time variant cross correlation to assess residence time of water and implication for hydraulics of a sink-rise karst system. *Water Resources Research* 47: W05547. DOI: doi:10.1029/2010WR009613.

Bailly-Comte V., Martin J.B., Jourde H., Screaton E.J., Pistre S., Langston A. 2010. Water exchange and pressure transfer between conduits and matrix and their influence on hydrodynamics of two karst aquifers with sinking streams. *Journal of Hydrology* 386 : 55-66.

Banks E.W., Simmons C.T., Love A.J., Shand P. 2011. Assessing spatial and temporal connectivity between surface water and groundwater in a regional catchment: Implications for regional scale water quantity and quality. *Journal of Hydrology* 404 : 30-49.

Basu N.B., Jindal P., Schilling K.E., Wolter C.F., Takle E.S. 2012. Evaluation of analytical and numerical approaches for the estimation of groundwater travel time distribution. *Journal of Hydrology* 475 : 65–73.

Beven K.J. 2010. Preferential flows and travel time distributions: defining adequate hypothesis tests for hydrological process models. *Hydrological Processes* 24 : 1537-47.

Beven K., Binley A. 1992. The future of distributed models: model calibration and uncertainty prediction. *Hydrological Processes* 6 : 279-98.

Beven K., Freer J. 2001. Equifinality, data assimilation, and uncertainty estimation in mechanistic modelling of complex environmental systems using the GLUE methodology. *Journal of hydrology* 249 : 11-29.

Beven K. 1993. Prophecy, reality and uncertainty in distributed hydrological modelling. *Advances in Water Resources* 16 : 41-51. DOI: 10.1016/0309-1708(93)90028-E.

Birkel C., Soulsby C., Tetzlaff D., Dunn S., Spezia L. 2012. High-frequency storm event isotope sampling reveals time-variant transit time distributions and influence of diurnal cycles. *Hydrological Processes* 26 : 308-16.

Bolger B.L., Park Y., Unger A.J.A., Sudicky E.A. 2011. Simulating the pre-development hydrologic conditions in the San Joaquin Valley, California. *Journal of Hydrology* 411 : 322-30.

Botter G., Peratoner F., Putti M., Zuliani A., Zonta R., Rinaldo A., Marani M. 2008. Observation and modeling of catchment-scale solute transport in the hydrologic response: A tracer study. *Water Resources Research* 44 : W05409.

Botter G. 2012. Catchment mixing processes and travel time distributions. *Water Resources Research* 48 : W05545. DOI: 10.1029/2011WR011160.

Botter G., Bertuzzo E., Rinaldo A. 2010. Transport in the hydrologic response: Travel time distributions, soil moisture dynamics, and the old water paradox. *Water Resources Research* 46 : W03514. DOI: 10.1029/2009WR008371.

Butscher C., Huggenberger P. 2009. Modeling the temporal variability of karst groundwater vulnerability, with implications for climate change. *Environmental science & technology* 43 : 1665-9.

Campolongo F., Cariboni J., Saltelli A. 2007. An effective screening design for sensitivity analysis of large models. *Environmental Modelling & Software* 22 : 1509-18.

Capell R., Tetzlaff D., Malcolm I.A., Hartley A.J., Soulsby C. 2011. Using hydrochemical tracers to conceptualise hydrological function in a larger scale catchment draining contrasting geologic provinces. *Journal of Hydrology* 408 : 164-77.

Chow V.T., Maidment D.R., Mays L.W. 1988. Applied hydrology. McGraw-Hill: New York; 576.

Christophersen N., Hooper R.P. 1992. Multivariate analysis of stream water chemical data: The use of principal components analysis for the end-member mixing problem. *Water Resources Research* 28 : 99-107.

Cosgrove B.A., Lohmann D., Mitchell K.E., Houser P.R., Wood E.F., Schaake J.C., Robock A., Marshall C., Sheffield J., Duan Q. 2003. Real-time and retrospective forcing in the North American Land Data Assimilation System (NLDAS) project. *Journal of Geophysical Research* 108 : 8842.

Cox M.H., Su G.W., Constantz J. 2007. Heat, chloride, and specific conductance as ground water tracers near streams. *Ground Water* 45 : 187-95.

Dai Y., Zeng X., Dickinson R.E., Baker I., Bonan G.B., Bosilovich M.G., Denning A.S., Dirmeyer P.A., Houser P.R., Niu G. 2003. The common land model. *Bulletin of the American Meteorological Society* 84 : 1013-23.

Darracq A., Destouni G., Persson K., Prieto C., Jarsjö J. 2010. Quantification of advective solute travel times and mass transport through hydrological catchments. *Environmental fluid mechanics* 10 : 103-20.

de Rooij R., Graham W., Maxwell R.M. 2012. A particle-tracking scheme for simulating pathlines in coupled surface-subsurface flows. *Advances in Water Resources* 52 : 7-18.

Desmarais K., Rojstaczer S. 2002. Inferring source waters from measurements of carbonate spring response to storms. *Journal of Hydrology* 260 : 118-34.

Du J., Qian L., Rui H., Zuo T., Zheng D., Xu Y., Xu C. 2012. Assessing the effects of urbanization on annual runoff and flood events using an integrated hydrological modelling system for Qinhuai River basin, China. *Journal of Hydrology* 464-465 : 127-139.

Dunn S., Birkel C., Tetzlaff D., Soulsby C. 2010. Transit time distributions of a conceptual model: their characteristics and sensitivities. *Hydrological Processes* 24 : 1719-29.

Dunn S., Freer J., Weiler M., Kirkby M., Seibert J., Quinn P., Lischeid G., Tetzlaff D., Soulsby C. 2008. Conceptualization in catchment modelling: simply learning? *Hydrological Processes* 22 : 2389-93.

Duriancik L.F., Bucks D., Dobrowolski J.P., Drewes T., Eckles S.D., Jolley L., Kellogg R.L., Lund D., Makuch J.R., O'Neill M.P. 2008. The first five years of the Conservation Effects Assessment Project. *Journal of Soil and Water Conservation* 63 : 185A-97A.

Fenicia F., McDonnell J.J., Savenije H.H. 2008a. Learning from model improvement: On the contribution of complementary data to process understanding. *Water Resources Research* 44 : W06419.

Fenicia F., Savenije H.H., Matgen P., Pfister L. 2008b. Understanding catchment behavior through stepwise model concept improvement. *Water Resources Research* 44 : W01402.

Ferguson I.M., Maxwell R.M. 2010. Role of groundwater in watershed response and land surface feedbacks under climate change. *Water Resources Research* 46 : W00F02.

Florea L.J., Vacher H.L. 2007. Eogenetic karst hydrology: Insights from the 2004 hurricanes, peninsular Florida. *Ground Water* 45 : 439-46.

Foglia L., Hill M., Mehl S., Burlando P. 2009. Sensitivity analysis, calibration, and testing of a distributed hydrological model using error based weighting and one objective function. *Water Resources Research* 45 : W06427. DOI: 10.1029/2008WR007255.

Francone C., Cassardo C., Richiardone R., Confalonieri R. 2012. Sensitivity Analysis and Investigation of the Behaviour of the UTOPIA Land-Surface Process Model: A Case Study for Vineyards in Northern Italy. *Boundary-Layer Meteorology* : 1-12.

Freeze R. A., Harlan R. L. 1969. Blueprint for a physically-based disgitally simulated hydrologic response model. *Journal of Hydrology* 9: 237 – 258.

Fröhlich H.L., Breuer L., Frede H., Huisman J.A., Vaché K.B. 2008. Water source characterization through spatiotemporal patterns of major, minor and trace element stream concentrations in a complex, mesoscale German catchment. *Hydrological Processes* 22 : 2028-43.

Furman A. 2008. Modeling coupled surface-subsurface flow processes: a review. *Vadose Zone* J 7: 741 – 756.

Goderniaux P., Brouyère S., Fowler H.J., Blenkinsop S., Therrien R., Orban P., Dassargues A. 2009. Large scale surface–subsurface hydrological model to assess climate change impacts on groundwater reserves. *Journal of Hydrology* 373 : 122-38.

Graham W.D., McLaughlin D.B. 1991. A stochastic model of solute transport in groundwater: Application to the Borden, Ontario, Tracer Test. *Water Resources Research* 27 : 1345-59.

Graham W., McLaughlin D. 1989. Stochastic analysis of nonstationary subsurface solute transport: 2. Conditional moments*. Water Resources Research* 25 : 2331-55.

Gulley J.D., Martin J.B., Spellman P., Moore P.J., Screaton E.J. 2012. Influence of partial confinement and Holocene river formation on groundwater flow and dissolution in the Florida carbonate platform. *Hydrological Processes* : DOI:10.1002/hyp.9601. DOI: 10.1002/hyp.9601.

Gupta H.V., Sorooshian S., Yapo P.O. 1999. Status of automatic calibration for hydrologic models: Comparison with multilevel expert calibration. *Journal of Hydrologic Engineering* 4 : 135-43.

Hooper R.P., Christophersen N., Peters N.E. 1990. Modelling streamwater chemistry as a mixture of soilwater end-members—An application to the Panola Mountain catchment, Georgia, USA. *Journal of Hydrology* 116 : 321-43.

Hrachowitz M., Soulsby C., Tetzlaff D., Malcolm I., Schoups G. 2010a. Gamma distribution models for transit time estimation in catchments: Physical interpretation of parameters and implications for time-variant transit time assessment. *Water Resources Research* 46 : W10536.

Hrachowitz M., Soulsby C., Tetzlaff D., Speed M. 2010b. Catchment transit times and landscape controls—does scale matter? *Hydrological Processes* 24 : 117-25.

Huntington J.L., Niswonger R.G. 2012. Role of surface water and groundwater interactions on projected summertime streamflow in snow dominated regions: An integrated modeling approach. *Water Resources Research* 48 : W11524.

Jones J.E., Woodward C.S. 2001. Newton–Krylov-multigrid solvers for large-scale, highly heterogeneous, variably saturated flow problems. *Advances in Water Resources* 24 : 763-74.

Jones J.P., Sudicky E.A., McLaren R.G. 2008. Application of a fully-integrated surface-subsurface flow model at the watershed-scale: A case study. *Water Resources Research* 44 : W03407. DOI: 10.1029/2006WR005603.

Katz B. 2004. Sources of nitrate contamination and age of water in large karstic springs of Florida. *Environmental Geology* 46 : 689-706.

Katz B.G., Böhlke J.K., Hornsby H.D. 2001. Timescales for nitrate contamination of spring waters, northern Florida, USA. *Chemical Geology* 179 : 167-86.

Katz B.G., Griffin D.W. 2008. Using chemical and microbiological indicators to track the impacts from the land application of treated municipal wastewater and other sources on groundwater quality in a karstic springs basin. *Environmental Geology* 55 : 801-21.

Kirchner J.W. 2006. Getting the right answers for the right reasons: Linking measurements, analyses, and models to advance the science of hydrology. *Water Resources Research* 42 : W03S04.

Kirchner J.W., Feng X., Neal C. 2001. Catchment-scale advection and dispersion as a mechanism for fractal scaling in stream tracer concentrations. *Journal of Hydrology* 254 : 82-101.

Kirchner J.W., Feng X., Neal C. 2000. Fractal stream chemistry and its implications for contaminant transport in catchments. *Nature* 403 : 524-7.

Kirchner J.W., Feng X., Neal C., Robson A.J. 2004. The fine structure of water-quality dynamics: The (high-frequency) wave of the future. *Hydrological Processes* 18 : 1353-9.

Koeniger P., Leibundgut C., Stichler W. 2009. Spatial and temporal characterisation of stable isotopes in river water as indicators of groundwater contribution and confirmation of modelling results; a study of the Weser river, Germany†. *Isotopes in environmental and health studies* 45 : 289-302.

Kollet S., Cvijanovic I., Schüttemeyer D., Maxwell R., Moene A., Bayer P. 2009. The influence of rain sensible heat, subsurface heat convection and the lower temperature boundary condition on the energy balance at the land surface. *Vadose Zone* J 8 : 846-57.

Kollet S.J., Maxwell R.M. 2008a. Capturing the influence of groundwater dynamics on land surface processes using an integrated, distributed watershed model. *Water Resources Research* 44 : W02402.

Kollet S.J., Maxwell R.M. 2008b. Demonstrating fractal scaling of baseflow residence time distributions using a fully-coupled groundwater and land surface model. *Geophysical Research Letters* 35 : L07402. DOI: 10.1029/2008GL033215.

Kollet S.J., Maxwell R.M. 2006. Integrated surface–groundwater flow modeling: A free-surface overland flow boundary condition in a parallel groundwater flow model. *Advances in Water Resources* 29 : 945-58.

Langston A., Screaton E., Martin J., Bailly-Comte V. 2012. Interactions of diffuse and focused allogenic recharge in an eogenetic karst aquifer (Florida, USA). *Hydrogeology Journal* 20 : 767-81.

Legates D.R., McCabe G.J. 1999. Evaluating the use of “goodness-of-fit” measures in hydrologic and hydroclimatic model validation. *Water Resources Research* 35 : 233-41.

Li Q., Unger A.J.A., Sudicky E.A., Kassenaar D., Wexler E.J., Shikaze S. 2008. Simulating the multi-seasonal response of a large-scale watershed with a 3D physically-based hydrologic model. *Journal of Hydrology* 357 : 317-36.

Linhoss A., Muñoz-Carpena R., Kiker G., Hughes D. 2012. Hydrologic Modeling, Uncertainty, and Sensitivity in the Okavango Basin: Insights for Scenario Assessment: Case Study. *Journal of Hydrologic Engineering* . DOI: 10.1061/(ASCE)HE.1943-5584.0000755.

Loague K., Heppner C.S., Abrams R.H., Carr A.E., VanderKwaak J.E., Ebel B.A. 2005. Further testing of the Integrated Hydrology Model (InHM): event-based simulations for a small rangeland catchment located near Chickasha, Oklahoma. *Hydrological Processes* 19 : 1373-98.

Małoszewski P., Zuber A. 1982. Determining the turnover time of groundwater systems with the aid of environmental tracers: 1. Models and their applicability. *Journal of hydrology* 57 : 207-31.

Maresch W., Walbridge M.R., Kugler D. 2008. Enhancing conservation on agricultural landscapes: A new direction for the Conservation Effects Assessment Project. *Journal of Soil and Water Conservation* 63 : 198A-203A.

Matsubayashi U., Velasquez G.T., Takagi F. 1993. Hydrograph separation and flow analysis by specific electrical conductance of water. *Journal of Hydrology* 152 : 179-99.

Maxwell R.M., Miller N.L. 2005. Development of a coupled land surface and groundwater model. *Journal of Hydrometeorology* 6 : 233-47.

Maxwell R.M., Welty C., Tompson A.F. 2003. Streamline-based simulation of virus transport resulting from long term artificial recharge in a heterogeneous aquifer. *Advances in Water Resources* 26 : 1075-96.

Maxwell R., Kastenberg W. 1999. Stochastic environmental risk analysis: an integrated methodology for predicting cancer risk from contaminated groundwater. *Stochastic Environmental Research and Risk Assessment* 13 : 27-47.

McDonnell J., Sivapalan M., Vaché K., Dunn S., Grant G., Haggerty R., Hinz C., Hooper R., Kirchner J., Roderick M. 2007. Moving beyond heterogeneity and process complexity: A new vision for watershed hydrology. *Water Resources Research* 43 : W07301. DOI: 10.1029/2006WR005467.

McGuire K.J., McDonnell J.J. 2006. A review and evaluation of catchment transit time modeling. *Journal of Hydrology* 330 : 543-63.

McGuire K., McDonnell J., Weiler M., Kendall C., McGlynn B., Welker J., Seibert J. 2005. The role of topography on catchment-scale water residence time. *Water Resources Research* 41 : W05002. DOI: 10.1029/2004WR003657.

McGuire K., Weiler M., McDonnell J. 2007. Integrating tracer experiments with modeling to assess runoff processes and water transit times. *Advances in Water Resources* 30 : 824-37.

McMillan H.K., Clark M.P., Bowden W.B., Duncan M., Woods R.A. 2011. Hydrological field data from a modeller's perspective: Part 1. Diagnostic tests for model structure. *Hydrological Processes* 25 : 511-22.

McMillan H., Tetzlaff D., Clark M., Soulsby C. 2012. Do time-variable tracers aid the evaluation of hydrological model structure? A multimodel approach*. Water Resources Research* 48 : W05501. DOI: 10.1029/2011WR011688.

Meals D.W., Dressing S.A., Davenport T.E. 2010. Lag time in water quality response to best management practices: A review. *Journal of environmental quality* 39 : 85-96.

Meyer B.A., Kincaid T.R., Hazlett T.J. 2008. Modeling Karstic Controls on Watershed-Scale Groundwater Flow in the Floridan Aquifer of North Florida. In Sinkholes and the Engineering and Environmental Impacts of Karst (GSP 183), Yuhr LB, Alexander EC, Beck BF (eds). *ASCE*: VA; 351-361.

Moore P.J., Martin J.B., Screaton E.J. 2009. Geochemical and statistical evidence of recharge, mixing, and controls on spring discharge in an eogenetic karst aquifer. *Journal of Hydrology* 376 : 443-55.

Morris M.D. 1991. Factorial sampling plans for preliminary computational experiments. *Technometrics* 33 : 161-74.

Mueller-Warrant G., Griffith S., Whittaker G., Banowetz G., Pfender W., Garcia T., Giannico G. 2012. Impact of land use patterns and agricultural practices on water quality in the Calapooia River Basin of western Oregon. *Journal of Soil and Water Conservation* 67 : 183-201.

Muñoz-Carpena R., Zajac Z., Kuo Y. 2007. Global sensitivity and uncertainty analyses of the water quality model VFSMOD-W. *Trans.ASABE* 50 : 1719-32.

Nakamura R. 1971. Runoff analysis by electrical conductance of water. *Journal of Hydrology* 14 : 197-212.

Nash J., Sutcliffe J. 1970. River flow forecasting through conceptual models part I—A discussion of principles. *Journal of hydrology* 10 : 282-90.

Nossent J., Bauwens W. 2012. Multi-variable sensitivity and identifiability analysis for a complex environmental model in view of integrated water quantity and water quality modeling. *Water science and technology* 65 : 539-49.

Ogrinc N., Kanduč T., Stichler W., Vreča P. 2008. Spatial and seasonal variations in δ18O and δD values in the River Sava in Slovenia. *Journal of Hydrology* 359 : 303-12.

Osmond D., Meals D., Hoag D., Arabi M., Luloff A., Jennings G., McFarland M., Spooner J., Sharpley A., Line D. 2012. Improving conservation practices programming to protect water quality in agricultural watersheds: Lessons learned from the National Institute of Food and Agriculture–Conservation Effects Assessment Project. *Journal of Soil and Water Conservation* 67 : 122A-7A.

Panagopoulos G., Lambrakis N. 2006. The contribution of time series analysis to the study of the hydrodynamic characteristics of the karst systems: Application on two typical karst aquifers of Greece (Trifilia, Almyros Crete). *Journal of Hydrology* 329 : 368-76.

Pilgrim D.H., Huff D.D., Steele T.D. 1979. Use of specific conductance and contact time relations for separating flow components in storm runoff. *Water Resources Research* 15 : 329-39.

Pollock D.W. 1988. Semianalytical computation of path lines for finite-difference models. *Ground Water* 26 : 743-50.

Rihani J.F., Maxwell R.M., Chow F.K. 2010. Coupling groundwater and land surface processes: Idealized simulations to identify effects of terrain and subsurface heterogeneity on land surface energy fluxes. *Water Resources Research* 46 : W12523. DOI: 10.1029/2010WR009111.

Rinaldo A., Beven K.J., Bertuzzo E., Nicotina L., Davies J., Fiori A., Russo D., Botter G. 2011. Catchment travel time distributions and water flow in soils. *Water Resources Research* 47 : W07537. DOI: 10.1029/2011WR010478.

Ritorto M., Screaton E., Martin J., Moore P. 2009. Relative importance and chemical effects of diffuse and focused recharge in an eogenetic karst aquifer: an example from the unconfined upper Floridan aquifer, USA. *Hydrogeology Journal* 17 : 1687-98.

Roa-García M., Weiler M. 2010. Integrated response and transit time distributions of watersheds by combining hydrograph separation and long-term transit time modeling. *Hydrology and Earth System Sciences* 14 : 1537-49.

Running S.W., Loveland T.R., Pierce L.L. 1994. A vegetation classification logic based on remote sensing for use in global biogeochemical models. *Ambio* 23 : 77-81.

Saltelli A., Ratto M., Tarantola S., Campolongo F. 2005. Sensitivity analysis for chemical models. *Chemical Reviews-Columbus* 105 : 2811-28.

Saltelli A. 1999. Sensitivity analysis: Could better methods be used? *Journal of Geophysical Research: Atmospheres* (1984–2012) 104 : 3789-93.

Saltelli A., Tarantola S., Campolongo F., Ratto M. 2004. Sensitivity analysis in practice: a guide to assessing scientific models. Wiley; 219.

Schneider J.W., Upchurch S.B., Chen J., Cain C. 2008. Simulation of groundwater flow in north central Florida and south-central Georgia. Suwannee River Water Management District. : Live Oak; 92.

Seibert J., McDonnell J.J. 2002. On the dialog between experimentalist and modeler in catchment hydrology: Use of soft data for multicriteria model calibration. *Water Resources Research* 38 : 1241. DOI: 10.1029/2001WR000978.

Sobol I.M. 1993. Sensitivity estimates for nonlinear mathematical models. *Mathematical Modelling and Computational Experiments* 1 : 407-14.

Soulsby C., Dunn S.M. 2003. Towards integrating tracer studies in conceptual rainfall runoff models: recent insights from a sub arctic catchment in the Cairngorm Mountains, Scotland. *Hydrological Processes* 17 : 403-16.

Soulsby C., Tetzlaff D., Dunn S., Waldron S. 2006. Scaling up and out in runoff process understanding: insights from nested experimental catchment studies. *Hydrological Processes* 20 : 2461-5.

Speed M., Tetzlaff D., Soulsby C., Hrachowitz M., Waldron S. 2010. Isotopic and geochemical tracers reveal similarities in transit times in contrasting mesoscale catchments. *Hydrological Processes* 24 : 1211-24.

Srivastava V., Graham W., Maxwell R. 2013a. Geologic and climatic controls on streamflow generation processes in a complex eogenetic karst basin. *Under preparation.*

Srivastava V., Graham W., Carpena R., Maxwell R. 2013b. Global sensitivity analysis of an integrated hydrologic model-insights on geologic and vegetative controls over the hydrologic functioning of a large complex basin. *Under preparation*.

Sudicky E.A., Jones J.P., Park Y.J., Brookfield A.E., Colautti D. 2008. Simulating complex flow and transport dynamics in an integrated surface-subsurface modeling framework. *Geosciences Journal* 12 : 107-22.

Tetzlaff D., Soulsby C., Hrachowitz M., Speed M. 2011. Relative influence of upland and lowland headwaters on the isotope hydrology and transit times of larger catchments. *Journal of Hydrology* 400 : 438-47.

Tripathi N. 2006Spatial water balance of the Suwannee River Basin, Florida: an application of El Niño Southern Oscillation Climatology. University of Florida: Gainesville; 174.

Tsang Y., Tsang C., Hale F., Dverstorp B. 1996. Tracer transport in a stochastic continuum model of fractured media. *Water Resources Research* 32 : 3077-92.

Upchurch S.B. 2007. An introduction to the Cody Escarpment, North-Central Florida. Suwannee River Water Management District: Live Oak, Florida; 16.

Upchurch S., Chen J., Cain C. 2008. Springsheds of the Santa Fe River Basin. Alachua county Department of Enviremental Protection, Gainesville, Fl. Springsheds of the Santa Fe River Basin. Alachua County (Florida) Department of Environmental Protection: Gainesville, FL ; 93.

Vacher H., Mylroie J.E. 2002. Eogenetic karst from the perspective of an equivalent porous medium. *Carbonates and Evaporites* 17 : 182-96.

Van der Velde Y., De Rooij G., Rozemeijer J., Van Geer F., Broers H. 2010. Nitrate response of a lowland catchment: On the relation between stream concentration and travel time distribution dynamics. *Water Resources Research* 46 : W11534. DOI: 10.1029/2010WR009105.

Van Genuchten M.T. 1980. A closed-form equation for predicting the hydraulic conductivity of unsaturated soils. *Soil Science Society of America Journal* 44 : 892-8.

Van Griensven A., Meixner T., Grunwald S., Bishop T., Diluzio M., Srinivasan R. 2006. A global sensitivity analysis tool for the parameters of multi-variable catchment models*. Journal of Hydrology* 324 : 10-23.

VanderKwaak J.E., Loague K. 2001. Hydrologic-Response simulations for the R-5 catchment with a comprehensive physics-based model. *Water Resources Research* 37 : 999-1013.

Water resources associates. 2007. MFL establishment for the upper Santa Fe River. Live Oak; 294.

Werner A.D., Gallagher M.R., Weeks S.W. 2006. Regional-scale, fully coupled modelling of stream–aquifer interaction in a tropical catchment. *Journal of Hydrology* 328 : 497-510.

Yang J. 2011. Convergence and uncertainty analyses in Monte-Carlo based sensitivity analysis. *Environmental Modelling & Software* 26 : 444-57.

Yang J., Liu Y., Yang W., Chen Y. 2012. Multi-objective sensitivity analysis of a fully distributed hydrologic model WetSpa. *Water Resources Management* : 1-20.

BIOGRAPHICAL SKETCH

Vibhava Srivastava was born and grew up in the city of Allahabad, Uttar Pradesh, India. He earned a Bachelor of Technology in agricultural engineering from the Allahabad Agricultural Institute – Deemed University in 2003. In January 2004 he joined the University of Arkansas from where he received a Master of Science in biological and agricultural engineering in August 2006. He joined the University of Florida in August 2006 and received a Doctor of Philosophy in August 2013. He is currently working as Post Doctorate researcher at the Water Institute, University of Florida.